CURRENT LIMITATION IN MERCURY VAPOUR DISCHARGES

by

PETER C. STANGEBY

University College

Michaelmas, 1970

This thesis is submitted in partial fulfilment of the requirements for the Degree of Doctor of Philosophy in the University of Oxford

CURRENT LIMITATION IN MERCURY VAPOUR DISCHARGES

"Lack of experience diminishes our power of taking a comprehensive view of the admitted facts. Hence, those who dwell in intimate association with nature and its phenomena grow more and more able to formulate, as the foundation of their theories, principles such as to admit of a wide and coherent development; while those whom devotion to abstract discussions has rendered unobservant of the facts are too ready to dogmatize on the basis of a few observations".

Aristotle: "De Generatione et Corruptione"
(Book I, Cap.II)

ACKNOWLEDGEMENTS

The author wishes to thank Dr J.E. Allen for his supervision, advice and encouragement during the course of this work. Helpful discussions with various staff members and students at Oxford University are gratefully acknowledged.

The project was financed by Culham Laboratory, UK AE A. Gratitude is expressed to Shell, Canada and N.R.C. of Canada for personnal support.

To Ken Calkin, much appreciation and commendation for his excellent glass blowing.

Finally, the author expresses his gratitude to Mrs Ina Godwin for such careful typing of this thesis, and to his wife for her unfailing understanding and encouragement.

ABSTRACT

This thesis constitutes a study of the current limitation phenomenon of a low pressure arc discharge in mercury vapour.

A new theory is presented which provides a theoretical relation between the D.C. current limit, I_L and the independent discharge parameters of gas density p_0 and tube radius r_0. This theory is based on the fact that arc existence is impossible for values of the lumped parameter (pr) less than a critical value.

If at $I = 0$, $p = p_0$, where p_0 is such that $(p_0 r_0)$ is above the critical value, then by increasing the current to a sufficiently high level (i.e. to $I = I_L$) such a degree of neutral rarefaction is brought about (due to the high level of ionization) that the local p is lowered to the point where (p r) is equal to the critical value.

Similarly a lower current limit is found, for as I is decreased, the wall sheath grows, effectively reducing r to such a point that (p r) reaches the critical value.

Arc existence is only possible between these two limits. The upper and lower limit converge at a certain finite pressure, and below this, no arc existence is possible whatsoever. Proper experimental testing of such a theory, derived from fundamental relations, requires very careful control of the physical variables, especially local neutral density. Accordingly a special discharge tube, 5 metres in length, was constructed and the experimental results obtained therefrom were found to be in excellent agreement with the new theory.

Theoretical predictions of the radial variation of neutral density for all values of I, were confirmed by experimental measurements of

density using the absorption of resonance radiation.

The case of constricted positive column geometry is considered, where a double sheath is formed at the diameter change. It is argued that if the double sheath is followed by a long uniform column, then the current limit I_L, will be that of the smaller diameter tube, even though severe neutral depletion occurs near the double sheath. Experimental evidence is presented in confirmation of this prediction.

Other aspects of the current limit theory are confirmed by Langmuir probe measurements and by heavy particle wall flux measurements using ionization gauges. These latter measurements also shed further light on the unresolved phenomenon of current-sustained pressure effects in the positive column.

In the positive column at high currents, the neutral velocity distribution is found to be no longer Maxwellian (due to selective ionization of fast particles and of those with long flight paths) which leads to the unusual case of a non-Gaussian radiation absorption profile, although the only broadening influence is that due to the Doppler effect. The resultant profiles are computed and experimental results are presented which substantiate the calculations.

The possibility of Hg sputtering by Hg ion bombardment of liquid Hg surfaces on the positive column walls is considered and a possible application to Hg valve technology is suggested.

Measurements of metastable particle densities are presented and related calculations indicate the role of cumulative ionization in low pressure discharges.

The Bohm sheath criterion for ions is generalized to include a number of complications, including that of oblique ion motion relative to the sheath edge. The plasma-sheath boundary is found to be mathematically equivalent to the Mach surface of fluid flow.

C O N T E N T S

Page

C H A P T E R I

I N T R O D U C T I O N

C H A P T E R II

THE POSITIVE COLUMN

C H A P T E R III

REVIEW OF PREVIOUS CURRENT LIMITATION STUDIES AND THE ROLE OF THE PRESENT WORK

CONTENTS
(continued)

Page

CHAPTER IV

PLASMA BOUNDARY AS A MACH NUMBER

CHAPTER V

NEW THEORY FOR D.C. LIMITATION

C O N T E N T S
(continued)

Page

C H A P T E R   V
(continued)

C H A P T E R   VI

EXPERIMENTAL APPARATUS

C H A P T E R   VII

NON-OPTICAL EXPERIMENTAL RESULTS AND DISCUSSION

CONTENTS
(continued)

Page

CHAPTER VIII

OPTICAL MEASUREMENTS AND DISCUSSION

CHAPTER IX

CONCLUSIONS

APPENDIX

CHAPTER I

INTRODUCTION

Gas discharges have had a long and illustrious career in the history of science and technology. This most convenient terrestrial form of the most abundant state in the universe - the plasma state - has been an object of intrinsic interest to physicists for more than a century. Even more significant than its intrinsic interest, however, has been the important role that gas discharges have played in the unravelling of other branches of fundamental physics, e.g. spectroscopy. Indeed the entire edifice of modern physics has been built-up, in no small part, by the discoveries which gas discharge studies have facilitated.

The technological applications of gas discharges have been no less impressive and future prospects are more promising yet. One may think of the various forms of gas discharge lighting, e.g. fluorescent lights and gas lasers, or of Hg rectifier valves which have been essential to the electricity supply industry. In the future lie the exciting possibilities of magnetohydrodynamic power generation and controlled fusion.

Turning our attention away from terrestrial plasmas we may note that earth is set in a universe which is almost entirely in the plasma state. Earth itself is immersed in a tenuous plasma, and is kept alive by a nearby concentration of thermonuclear plasma, the sun, on which man's existence is completely dependent. Many of the phenomena which occur in these extra-terrestrial plasmas can be conveniently studied in gas discharges.

In light of the quintessential role which gas discharges have already played in science and technology, and will inevitably continue to play in the future, it is evident that a complete understanding of gas discharge processes is one of the most worthwhile forms of scientific investigation.

Many of the processes occuring in gas discharges have been thoroughly investigated and are now fairly well understood. There are some exceptions, of course, and the present thesis concerns one such outstanding problem, that of the current limitation of a gas discharge.

In Fig.1 we see the familiar voltage — current characteristics of a gas discharge, extending over many orders of magnitude in voltage and current. The various regimes may be noted; each has been well studied. The interest of the present work focuses on the upper current end of the characteristic. Usually, the characteristic is shown to trail off to infinity in an unspectacular way; however, this is not the case, for it is known that an upper limit to the current of a low pressure discharge exists, at which point the voltage either rises steeply to infinity, or the discharge extinguishes completely.

Such spectacular behaviour is obviously of intrinsic interest, and it also has practical application, for example, in the technology of Hg arc rectifier valves.

The phenomenon was discovered almost half a century ago, Langmuir and Mott-Smith (1924), but despite extensive investigation, has remained an outstanding problem until the present time.

The present work examines the simplest and most fundamental form of the current limit phenomenon, that which occurs in the steady state in a cylindrical vessel, without constriction. Time dependent currents and constricted geometries introduce many other interesting and even visually spectacular phenomena, e.g. double sheaths at constrictions.

In Chapters II and III, previous gas discharge work, especially as it relates to the current limit phenomenon, is reviewed.

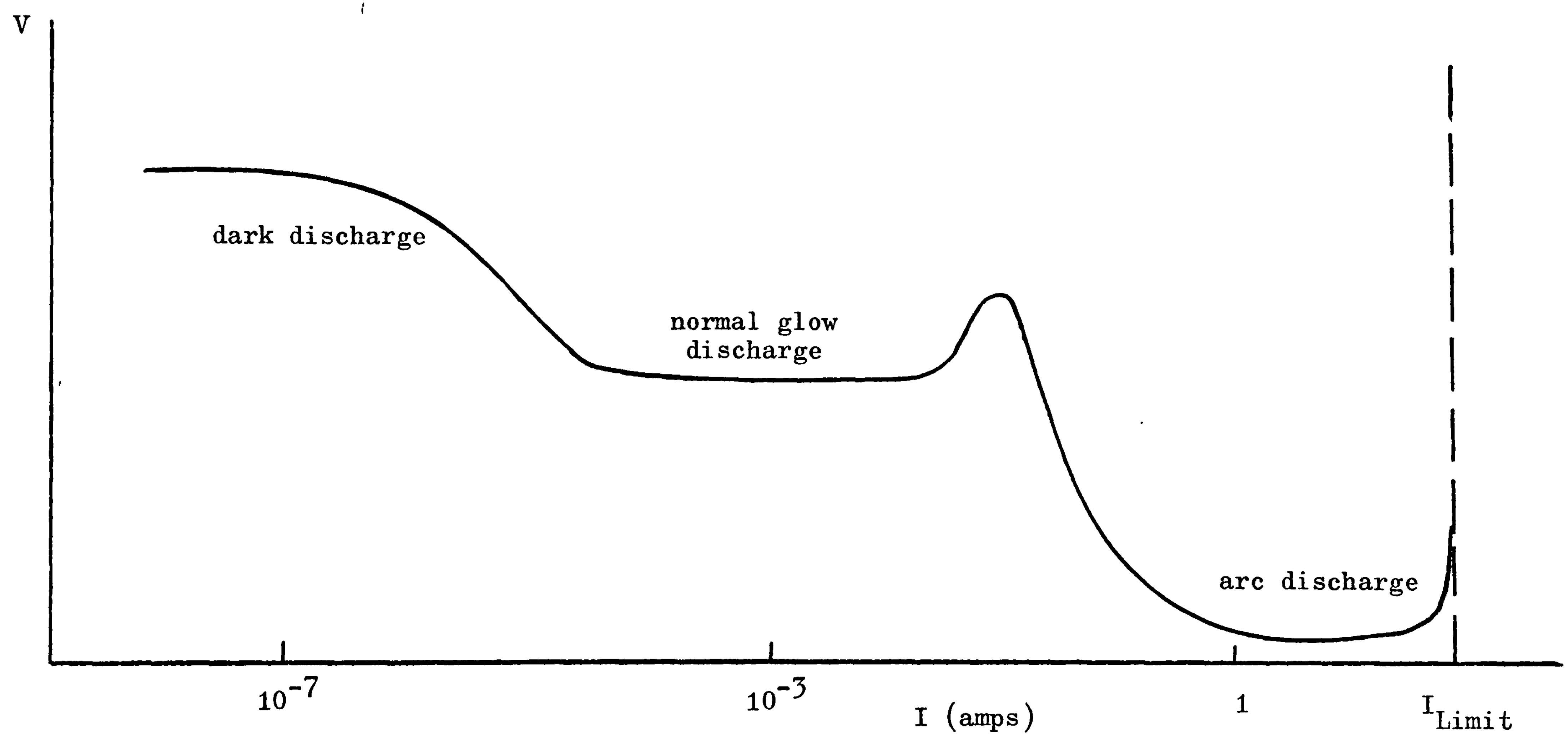

Fig.1
Discharge voltage vs discharge current showing main types of discharge.
I_{Limit} is a function of discharge vapour, pressure, geometry

Chapter IV presents an original analysis of the nature of the wall sheath which occurs in gas discharges.

Chapter V presents a new theory of the current limit effect and predicts the current limit level as a function of the independent gas discharge parameters, viz, the choice of gas, gas pressure p_0 and tube radius r_0. This new theory is based on the observation, Poletaev (1951), that arc existence is impossible for values of $p_0 r_0$ less than a critical value. At the same time, this work uses the current limit theories of Allen and Thonemann (1954) as a basic frame-work.

Hitherto, the upper limit of arc current has been studied, but in Chapter V it is pointed out that a lower current limit exists as well, and this limit is also predicted in terms of the independent discharge parameters.

To thoroughly test the present theory, a special discharge tube, 5 metres in length, has been constructed in which considerable care has been taken to completely control the relevant physical variables. The majority of previous current limitation experimental studies have been of limited quantitative value owing to the great diversity of mutually-interacting phenomena which have occurred simultaneously within the devices. The present apparatus is described in Chapter VI and in Chapter VII, experimental results are presented which completely confirm the new theories.

Also in Chapter VII, other related experimental studies, i.e. Langmuir probe and pressure gauge results, are presented which confirm other aspects of the current limit theories.

Pressure gauge results are reported in Chapter VII which cast further light on the question of current sustained pressure effects.

Variation in neutral density near current limit lies at the heart of the explanation of the current limit phenomenon and, therefore, one of the most important measurements to be made is that of neutral density near current limit. Such measurements, made with a U.V. absorption technique, are reported in Chapter VIII and confirm the neutral variations predicted in Chapter V.

Near current limit, the neutral distribution in the discharge tube is no longer Maxwellian owing to the selective ionization of slow neutrals and of neutrals which have long flight paths. This leads to the unusual situation of a non-Gaussian absorption profile, although the only broadening influence is due to the Doppler effect. The resulting absorption profiles have been computed and are presented in Chapter VIII, also, the corrections for such profiles to the neutral density measurements are made.

Also in Chapter VIII the role of cumulative ionization at low pressures is investigated making use of measurements of the metastable densities.

Portions of this work have been written up for direct publication, and references are given in the relevant sections.

CHAPTER II

THE POSITIVE COLUMN

2.1 THE CLASSICAL THEORY

While the various regions of gas discharges had been identified before this century, a physically detailed picture of the positive column was not provided until the work of I. Langmuir, in the 1920's. From his work and the work of others, the following model of the low pressure positive column emerged: the column is of two more-or-less distinct parts — the 'plasma' (Langmuir's term), in the centre and a 'sheath' near the wall. In the plasma quasineutrality holds, $n_e \approx n_i$, while the sheath is a charged layer (usually positive). The radial potential variation is trough-like, as the electrons see it, and hump-like for the ions. The potential variation in the plasma is small compared to the (usually) large drop in the sheath. At low pressures (say $< 10^{-3}$ torr for Hg) the electrons are very hot, e.g. $T_e = 30{,}000\ ^{\circ}K$, while the ion temperature may be the same as the neutral gas. The ions, however, fall radially outward to the walls under the influence of the radial field. The electrons are mainly contained by the walls of the potential trough, however, a few electrons in the high energy tail of the electron distribution can surmount the wall potential, which in fact is just such as to permit the electron wall flux to equal the ion wall flux, thereby maintaining the charge neutrality of the wall (if the wall is conducting a net current may be drawn at a different wall potential.) The continuous charged particle loss to the wall is compensated by volume ionization by the electrons. An axial electrical field (which constitutes the arc voltage) accelerates the electrons which by colliding elastically with neutrals and the wall sheath achieve a more-or-less Maxwellian distribution.

This 'pre-sheath', of small potential radial variation, within the plasma itself is necessary to sweep out the ions whose temperature is usually quite low.

In the absence of a magnetic field, and provided the drain of high energy electrons to the walls is small then the electrons will obey the Boltzmann relation:

$$n_e = n_o \exp\left(\frac{eV}{kT_e}\right), \qquad \dots (2.1)$$

where V is the radial potential. Within the plasma, equation (2.1) also gives n_i of course.

The sheath thickness is given approximately by the Debye length

$$\lambda_D = \left(\frac{kT_e \varepsilon_o}{n_e e^2}\right)^{\frac{1}{2}} \qquad \dots (2.2)$$

as it can be shown that generally in a medium of mobile charges any electrostatic field will be reduced by the factor $\exp(-x/\lambda_D)$, that is, the plasma can 'shield' itself from an electrostatic field by means of a sheath (the shielding is not complete, thus the small pre-sheath in the plasma itself). For low pressure discharges (10^{-3} torr) of moderate currents (~ 1 A) the sheath thickness is extremely small ($\sim 10^{-3}$ cm) so that the sheath is confined to a very thin layer at the edge of the plasma.

Schottky (1924) considered the case of the charged particle m.f.p's being smaller than the tube radius so that they moved under ambipolar diffusion conditions. He also restricted himself to the plasma region and assumed that the ionization rate was given by Zn, where Z is the number of ionizing collisions/electron/sec. He thus obtained for the cylindrical case;

$$n(r) = n_o J_o \left(r\sqrt{Z/D_a}\right) \qquad \dots (2.3)$$

where n_0 is the density at $r = 0$, J_0 is the zero order Bessel function and D_a is the ambipolar diffusion coefficient.

As $n(r) \geqslant 0$, the boundary condition at $r = r_0$ (the wall) is taken to be $n(r_0) = 0$ so that:

$$n(r) = n_0 \; J_0 \left(\frac{2{\cdot}4048r}{r_0} \right) \qquad \ldots (2.4)$$

also. Hence one must have:

$$\sqrt{\frac{Z}{D_a}} = \frac{2{\cdot}4048}{r_0} \; . \qquad \ldots (2.5)$$

While there are many different models and refinements to positive column theories, they all must provide an equation equivalent to (2.5), generally known as a 'plasma balance equation'. Such equations stipulate the rate of ionization which will be required to 'fit' the plasma column into the given space (r_0). Of course, Z must also be given by the electron temperature and the density of neutral gas, hence a plasma balance equation also gives T_e as a function of r_0 and p_0, gas pressure.

Tonks and Langmuir (1929) have written the classical paper on the positive column. They consider plane, cylindrical and spherical geometries; ionization proportion to electron density or spatially uniform; the ambipolar diffusion or the ion free fall case. They confirm the special case of Schottky.

They set up the plasma equation and solve it by a series method providing the potential $V(s)$ (where $r = s\,f\,(Z)$ and $f(Z)$ is a function of the ionization rate constant, Z). It is found that at a value of $s = s_0$ the plasma solution 'blows-up', that is $\frac{dV}{ds} \rightarrow \infty$. This point is identified with the plasma-sheath boundary as evidently such a large variation in V is incompatible with the assumption of quasineutrality.

This gives s_0, and if one assumes that $r_w = s_0 f(Z)$, where r_w is the wall radius, then one obtains a plasma balance equation (the sheath thickness has been taken as negligible).

The case of the ion free-fall regime is made somewhat difficult by virtue of the fact that the ions at any point are all moving at different radial velocities, reflecting the potential drops from their various points of origin. Thus $n_i(r)$ is represented by an integral with limits $r = 0, r = r$. This awkward point can be eliminated by appropriate approximations, see below.

Tonks and Langmuir provide comprehensive tables of theoretical results giving radial potential variations, the position and potential of the sheath edge, the constants for the plasma balance equation, e.g. for cylindrical geometry, ionization proportional to n_e, free-fall regime:

$$\frac{1 \cdot 092}{r_0} = Z\left(\frac{M_i}{kT_e}\right)^{\frac{1}{2}}, \qquad \dots (2.6)$$

also the ion wall current and the (floating) wall potential.

While their equations provide the basis for the sheath criterion, i.e. the ions always have the same average velocity $\left(\frac{kT_e}{M_i}\right)^{\frac{1}{2}}$ at the sheath edge, they do not in fact explicitly state this point.

Tonks and Langmuir also treated the sheath equations separately and attempted to join the two solutions. However, as a transition region is obviously required, it remained for subsequent refinements, see below, to achieve proper plasma-sheath matching. (This matter of proper matching is of more importance for thick sheaths, and so the plasma solutions of Tonks and Langmuir remain of considerable use for the bulk of many positive columns.)

2.2 SUBSEQUENT REFINEMENTS TO THE CLASSICAL THEORY AND OTHER WORK.

2.2.1 Introduction

Many theories have been produced since the classical paper of Tonks and Langmuir extending their work in various ways. These theories are reviewed very briefly below. In addition certain other areas of positive column work are also reviewed although no attempt to be comprehensive has been made, e.g. the extensive field of oscillations on the positive column has been omitted.

2.2.2 Free-Fall Regime with Ion Velocity Dispersion

Perhaps the most valuable work to be done since Tonks and Langmuir (TL) is the work of Self (1963) and Parker (1963) who have taken the full TL equations (complete with the ion velocity dispersion due to the distribution of ion creation), and without assuming quasineutrality (i.e. no division into plasma and sheath) have solved this equation numerically by computer. This has been done for a range of the parameter λ_D/r_0 and for finite λ_D/r_0 the artificiality of dividing the discharge into plasma and sheath becomes evident when the potential is plotted.

Harrison and Thompson (1959) discovered that the TL plasma equation for plane geometry and ion free-fall could be solved analytically and confirmed the TL series solutions.

Caruso and Cavaliere (1962) by employing an Abel transformation on the TL equation obtained elegant formulations for the plasma and sheath solutions separately for finite λ_D/r_0 , but could not join these solutions without a transition region. Recognizing that the position of the plasma-sheath boundary is somewhat arbitrary for finite λ_D/r_0 , they obtained a formulation for ion wall current which is independent of sheath criteria (see below) or the precise sheath position.

Self (1965) defines asymptotic expansions for both the TL plasma and sheath equations (as TL did for the plasma) in the limit of $\lambda_D/r_0 \to 0$, but no attempt is made to match these solutions properly via a transition zone.

Franklin and Ockendon (1970) have obtained asymptotic solutions, (i.e. for small λ_D/r_0) to the TL equations in the plasma and sheath and matched them via a transition region. The matching is to first order in λ_D/r_0.

2.2.3 Free-Fall Regime with Ion Fluid Model

Woods (1965) has proposed the simplifying assumption that all ions at a given point be considered to have the same velocity, i.e. the ion velocity dispersion is simply ignored and the ions considered to behave as a fluid with a single ion velocity at each point. The ion behaviour is defined by the continuity and momentum equations of fluid flow — and the electron behaviour by the Boltzmann relation, as before. Assuming quasi-neutrality, a single fluid set of equations is obtained, and Woods (neglecting ion pressure, p_i) obtains a plasma solution which agrees to within a few percent with the original TL plasma solution. Kino and Shaw (1966) extend this plasma solution to allow for finite p_i.

Forrest and Franklin (1966) also pursue this model and obtain plasma solutions which allow for magnetic field effects (introducing magnetic field effects to the full TL model was found troublesome), and thus extended the work of Bickerton and von Engel (1956) etc.

Franklin and Ockendon (1970) as with the full TL model, obtain asymptotic solutions (in small λ_D/r_0) both in plasma and sheath using the ion fluid model and match them via a transition region.

2.2.4 Collisional Regime

The work of Schottky (1924) (where the ions suffer collisions on their way to the wall) has been extended by Persson (1962) for the plasma and plane geometry. Persson finds that the unrealistic boundary condition, $n_e = 0$ at the wall, can be avoided when the ion motion is described by a momentum equation containing the non-linear ion inertia term (which Schottky effectively omitted).

Cohen and Kruskal (1965) obtain asymptotic expansions (small λ_D/r_0) for both plasma and sheath and match them. However, they neglected the non-linear ion inertia term, which Friedman (1967) has added to the analysis. Blank (1968) continuing in this way, examines the limitations of assuming spatially uniform transport coefficients.

Friedman and Levi (1967) show that if quasineutrality is not assumed, then the joining of sheath and plasma is quite smooth, even when the ions reach the ambipolar sound speed, where quasineutral solutions 'blow-up'.

2.2.5 Transition Theories

The transitions region between collision-dominated flow and free-fall flow of ions to the wall, is especially amenable to the fluid model where a collision term may be easily inserted and allowed to take on such a range of values as to span the transition. In this vane we have the work of Self and Ewald (1966) who provide only a plasma solution, and also the more complete work of Forrest and Franklin (1968) who assume no quasineutrality and for finite λ_D/r_0 provide complete plasma-sheath solutions, including also the effects of an applied magnetic field. The latter paper also provides calculations $T_e(I)$, the electron temperature as a function of current (as I decreases, n_e does also, thus λ_D

increases making the effective tube radius smaller and thus sending T_e up since T_e varies inversely as r).

2.2.6 The Sheath Criterion

Bohm (1949) by assuming a sharp plasma-sheath boundary and mono-energetic ions showed that the ion velocity at the sheath edge v_{is} must satisfy:

$$\frac{1}{2} M v_{is}^2 \geqslant kT_e \;, \qquad \dots (2.7)$$

if $T_e \gg T_i$. This is a direct consequence of using the Poisson equation to describe the sheath, setting the boundary conditions at the sheath edge:

$$n_e = n_i \qquad \frac{dV}{dx} = 0 \;, \qquad \dots (2.8)$$

and requiring that the sheath potential vary monotonically. Equation (2.7), known as the 'Bohm Criterion' is a highly useful relation, providing convenient calculations of certain column properties, e.g. ion wall current, although when λ_D/r_0 is finite (and therefore sheath-plasma transition region is finite), the applicability of this relation becomes somewhat uncertain, see Caruso and Cavaliere (1962), Auer (1961).

Allen and Thonemann (1954) derive equation (2.7) even more simply than Bohm, by using the boundary conditions:

$$n_e = n_i \qquad \frac{dn_e}{dV} = \frac{dn_i}{dV} \;, \qquad \dots (2.9)$$

and Andrews (1969) has shown the equivalence of the two approaches.

Harrison and Thompson (1959) extend the criterion to the case of a distribution of ion energies at the sheath edge, obtaining:

$$\frac{1}{2} M \langle v_{is}^{-2} \rangle^{-1} \geqslant kT_e \;, \qquad \dots (2.10)$$

which providing the ion velocity distribution at the sheath edge, $f_{is}(v)$, is well behaved, is essentially the same as Bohm. Hall (1962), however, points out that $f_{is}(v)$ must go to zero as $v \to 0$ sufficiently rapidly, or equation (2.10) does not hold and a more complex formulation is needed.

Sheath criteria in the presence of various complicating factors have been provided: Allen et al (1963) in the presence of a magnetic field; Bertotti et al (1965) in the presence of oscillations; Andrews (1970) for a growing sheath; Andrews and Varey (1970b(when the wall potential is small, c.f. kT_e/e; Friedman and Levi (1970) when a net current passes through the sheath; Stangeby and Allen (1970a) and Andrews and Stangeby (1970) when the ions enter the sheath obliquely.

2.2.7 Electron Distribution and the Langmuir Paradox

Langmuir established that the electron distribution in the positive column was approximately Maxwellian thus presenting a paradox; how can the distribution be Maxwellian when high energy electrons are lost to the wall, and tail regenerating collisions are rare? There was some suggestion, Gabor (1952) etc. that low frequency oscillations might account for tail regeneration, but it has now been established, Crawford and Self (1965), on the basis of Langmuir probe work, Klarfeld (1937), Howe (1953) (and Rayment and Twiddy (1968)) that the paradox is unreal, i.e. the high energy tail is missing and Langmuir's original work was not sufficiently accurate to establish this. (Actually the depletion is of high energy electrons moving normal to the wall sheath — longitudinally moving electrons are only removed if they are scattered into the normal direction.) One thus can appreciate the dangers in using an assumed Maxwellian electron distribution to calculate various excitation and ionization rates, especially if the rate is sensitive to the tail electrons, as is often the case.

2.2.8 Experimental Confirmation of Theories

Much experimental evidence has been provided over the last forty years which confirms in broad outline, positive column theory. Especially one might consider the early work of Tonks and Langmuir (1929), Killian (1930) and Klarfeld (1941). Electron distribution across the column, for example, has been measured by Irish and Bryant (1964) with a microwave technique, and recently Goldan (1970) has confirmed the theory of the collisionless sheath by measuring the potential variation with an electron beam.

2.2.9 Similarity Relations

From the work of Klarfeld (1941), Francis (1960), Hoyaux and Gans (1959) and Hoyaux (1970) we obtain the interesting and useful similarity relations for the positive column. The related variables are:

$$p_o r_o \quad \text{and} \quad T_e$$

$$\frac{r_o^2 n_e}{I} \quad \text{and} \quad T_e$$

$$E r_o \quad \text{and} \quad T_e \ ,$$

where E is the longitudinal voltage gradient. Various combinations are therefore also possible, e.g. E/p_o and $p_o r_o$ etc. The above-mentioned works provide both a theoretical basis for the relations and supporting experimental evidence.

2.2.10 Cumulative Effects

In order to calculate many processes in the positive column, one must know whether or not to allow for cumulative effects, e.g. ionization from a metastable level. The contribution of cumulative ionization to the total, for Hg columns has been considered by Klarfeld (1941), Howe (1953) and Forrest and Franklin (1969). For low enough currents and pressures, cumulative ionization is a negligible contribution but the precise levels of I and p at which it becomes appreciable is difficult to establish. In section 6.6.3, experimental evidence is presented which indicates that the transition may not occur at levels of I and p, quite as low as the theoretical predictions of Forrest and Franklin (1969).

Fabrikant et al (1938) have considered cumulative excitation of the 7^3S_1 level in a low pressure Hg discharge.

2.3 THE DOUBLE SHEATH IN THE POSITIVE COLUMN

When the cross section of a low pressure discharge is abruptly reduced by a constriction, such as the grid in a rectifier valve, an electrical double layer, a double sheath (d.s) is observed to form over the cathode side of the constriction opening, Langmuir and Mott-Smith (1924). The light emission on the anode side of the d.s. is usually enhanced over that of the cathode side. This d.s. is similar in structure to the cathode d.s. (Langmuir (1929)) except that it is free to move and balloon out into the cathode plasma, forming a 'sac', Hoyaux and Williams (1967).

The d.s. is characterized by a thin region of high field, at each end the potential gradient is nearly zero, although as with the wall sheath, a small potential gradient may extend for some distance into the adjacent plasmas. The d.s. potential step is characterized by a curvature d^2V/dx^2 which must change sign from positive to negative, and thus by Poisson's equation:

$$\frac{d^2V}{dx^2} = -\rho ,$$

the net charge density must change sign also. Thus a double layer of opposite charges is present - a 'double sheath'.

Langmuir and Mott-Smith (1924) and Langmuir (1932) explain the formation of the d.s. using the assumption that the ratio β of electron drift current to random current density is constant along the length of the arc. Now, since it is evident that the total drift current must be constant in the two sections, the ratio of the drift current densities must be inversely proportional to the ratio of cross sectional areas, thus also the random current densities. Since the latter are linearly related to the electron densities (temperature assumed constant) then the density in the constricted section is greater than in the non-constricted. Such adjacent co-existance of different electron densities would indicate the formation of a potential drop at the constriction entrance. The discharge confines this drop to a thin region thus forming a d.s. If the cathode plasma is not able to feed enough randomized electrons into the constriction region to maintain the high electron density required, then the potential of the d.s. may grow until the electrons accelerated into the constriction cause ionization there. Also, by ballooning out into a sac, the d.s. will be able to gather more randomized electrons into the constriction.

It was Langmuir (1929) who first derived the ratio of the electron current j_e and the ion current j_i (oppositely directed) across a d.s., viz:

$$j_e/j_i = (M/m)^{\frac{1}{2}} , \qquad \dots (2.11)$$

ignoring initial velocities (he also provides a more complex equation taking initial velocities into account).

Sena and Taube (1956), Crawford and Freeston (1963) and Wasserrab (1964) present a different explanation for the d.s. From the similarity relation between T_e and p_0r_0, one notes that T_e in the smaller diameter region must be greater than in the larger diameter.

To control the net random flux of electrons across the transition plane, a d.s. must form so as to reduce the flux from the smaller diameter region. For zero net current it is then easily shown that the d.s. potential drop, ΔU is given by:

$$\Delta U = \frac{k}{e}\left(T_2 - T_1 + \bar{T}\,\ell n\,(n_2/\,n_1\,)\right) \qquad \ldots (2.12)$$

where subscripts 1 and 2 refer to cathode and anode regions respectively and $T_1 < \bar{T} < T_2$.

Von Ardenne (1956), Demirkhanov (1962), and Kistemaker (1965) explain the d.s. potential drop on a somewhat different basis again. Their interest is primarily in the plasma sac as an ion source, and so they emphasize the ionization occurring within the sac. The d.s. voltage drop then is such as to create enough extra ionization within the sac as to compensate for the increased particle losses over the d.s. (i.e. ions falling into the cathode plasma). Further in this vane we have Quigley (1968) and Andrews (1969).

Thus, there are more than enough explanations for the formation of a d.s., in fact the situation is made confused by the abundance, and one is not sure what parameters define which variables. In Section 5.5 a new attempt is made to define a comprehensive and consistent model of the d.s., incorporating all the information currently available.

Schönhuber (1957, 1963) has carried out experimental work on the d.s. measuring ΔU as a function of p_0, r_2: r_1, j etc. Crawford and Freeston (1963), Hoyaux and Williams (1967) and Hoyaux and Kettani (1968) have examined the electron velocity distribution in the plasma sac, and into the anode column. Crawford and Freeston (1963) find that the accelerated 'bump' on the electron distribution (resulting from acceleration over the d.s.), decays via ordinary electron neutral collisions. Hoyaux et al, in pulsed work confirm this except when the pulse is made very rapid in which case a 'fast randomization' occurs in the sac. This is interpreted as a kind of beam-plasma interaction.

Andrews (1969) and Andrews and Allen (1970) have made an extensive study of the criteria for the formation of the double sheath. In this, they have extended the work of Langmuir (1929) by including four sorts of particles within the double sheath: electrons and ions from both the cathode and anode plasmas. (Langmuir neglected cathode plasma ions and anode plasma electrons.) Among the most interesting results we have the following:

(a) The distribution function of anode plasma ions at the upper sheath edge must be such that:

$$\left\langle \left(\frac{1}{2} M \, v_i^2 / eV_s \right)^{-1} \right\rangle^{-1} > \frac{1}{2} \frac{kT_e}{eV_s} , \qquad \ldots (2.13)$$

where V_s is the d.s. voltage drop.

(b) The distribution function of cathode plasma ions at the lower sheath edge must be such that:

$$\left\langle \left(\frac{1}{2} m \, v_e^2 / eV_s \right)^{-1} \right\rangle^{-1} > \frac{1}{2} \frac{kT_i}{eV_s} . \qquad \ldots (2.14)$$

(These results are reminiscent of the Bohm wall sheath criterion as expressed by Harrison and Thompson (1959).)

(c) The distribution function of anode plasma ions at the upper sheath edge, f_i , must satisfy:

$$f_i = 0 \quad \text{as} \quad v_i \to 0 .$$

(d) The distribution function of cathode plasma electrons at the lower sheath edge, f_e , must satisfy:

$$f_e = 0 \quad \text{as} \quad v_e \to 0 .$$

(These last two results are similar to the conclusions of Hall (1962) in connection with the wall sheath criterion of Harrison and Thompson (1959.)

(e) The Langmuir relation $j_e/j_i = \sqrt{M/m}$ is now modified to

$$j_e/j_i = \alpha \sqrt{M/m} \qquad \dots (2.15)$$

where α may depart substantially from unity, e.g. for monoenergetic cathode plasma electrons and anode plasma ions, and for $kT_i/eV_s = 0 \cdot 01$ and $kT_e/eV_s = 0 \cdot 5$, then $\alpha = 0 \cdot 21$.

CHAPTER III

REVIEW OF PREVIOUS CURRENT LIMITATION STUDIES AND THE ROLE OF THE PRESENT WORK

Current limitation work dates back almost half a century to the first observations of Langmuir and Mott-Smith (1924). Much of the interest in the phenomenon has been manifested by electrical engineers concerned with the operation of Hg arc values. Whenever the work has been done with devices of engineering application, firm conclusions have been difficult owing to the great variety of interacting phenomena which occur simultaneously within these engineering devices (also, Hg valve work almost always involves the further complexities of time-dependent phenomena). Perhaps it is for this reason, that despite the considerable attention which has been directed onto current limitation phenomena, the matter has not been finally resolved.

While the present thesis concerns the steady state current limit, for completeness sake, a.c. current limitation work will also be briefly reviewed.

Langmuir and Mott-Smith (1924) working with a low pressure Hg arc observed that when the current was raised to a certain rather sharply defined critical value, the voltage across the tube rose suddenly to several hundred volts and violent electrical surges were produced which caused sparks. This critical current was smaller for small pressures.

Tonks (1937) proposed several effects as possible causes of current limitation:

(a) longitudinal pressure gradient;

(b) double sheaths formed at constrictions;

(c) transverse pressure gradient;

(d) magnetic effects (self-pinch).

It is suggested that the pressure gradients (a), (c) might occasionally be sufficiently severe to induce a local gas rarefaction and cause the arc to revert to a vacuum mode. No mechanism is involved to explain how current limiting effects can be caused by a pinch. (Indeed the work of Timofeyev (1955, 56, 59) and Leontovich and Osovets (1957) indicate that self-pinch may extend arc existance.)

Kenty (1938) observes that current surges cause the local gas density to be depleted due to clean-up of ions to the walls, and current limiting effects are then observed. This tends to confirm the idea that neutral depletion is the important mechanism.

Klarfeld and Poletaev (1939) observe that near the constriction of an arc, gas rarefaction is observed which they attribute to gas blow-out (i.e. transfer of longitudinal momentum from the electrons accelerated through the d.s., to the neutral atoms). They attribute current limitation to gas rarefaction caused by this gas blow-out. (It is one of the conclusions of the present work that since gas blow-out is not necessarily present, even with a d.s., it cannot be the general explanation of current limitation — nevertheless, this work again emphasizes the importance of neutral depletion.)

Poletaev (1951) made a highly important contribution to the explanation of the phenomenon by noting that oomplete gas rarefaction is not necessary to bring about instability, but only depletion to a certain critical level. (This work is more extensively reviewed in section 5.2.2.)

The first attempt to construct a quantitative theory of current limitation for the most basic case of d.c. operation, no d.s., no self-magnetic effects, no gas blow-out, no longitudinal density gradients, is due to Allen and Thonemann (1954), who relate the current limit level to the basic discharge parameters. As this work constitutes the basis for a new current model presented in this thesis, it will be reviewed in some detail.

The ion current to the wall is:

$$I_w = e\, n_s\, \alpha\, v_B \,, \qquad \ldots (3.1)$$

where:
- n_s = charge density at sheath edge,
- α = constant of order one (to account for distributed ionization),
- $v_B = \sqrt{kT_e/M}$, the Bohm speed,
- M = ion mass.

The random current density at the sheath edge is

$$I_{iR} = e\, n_s\, (kT_e/2\pi m)^{\frac{1}{2}} \qquad \ldots (3.2)$$

where: m = electron mass. Hence:

$$I_{iR} = (M/2\pi m)^{\frac{1}{2}}\, I_w/\alpha \qquad \ldots (3.3)$$

and thus the tube current is

$$I = \left(\frac{\beta\gamma}{\alpha}\right)(M/2\pi m)^{\frac{1}{2}}\, I_w\, \pi r_0^2 \,, \qquad \ldots (3.4)$$

where:
- β = ratio of drift to random electron current density (assumed a constant of order one).
- r_0 = tube radius,
- γ = ratio of electron density averaged across the tube to the density at the sheath edge, Andrews (1968).

Current limitation is considered to occur when the level of ionization reaches such an extreme level, that all the neutrals leaving the wall, are ionized before making even one transit, i.e. at current limit:

$$I_w \to e\, \nu_0$$

where: ν_0 = neutral flux emitted by the walls.

Thus the current limit is:

$$I_{A.T.} = \left(\frac{\beta\gamma}{\alpha}\right)\left(M/2\pi m\right)^{\frac{1}{2}} \nu_0 \, e \, \pi \, r_0^2 \,. \qquad \ldots (3.5)$$

If the walls are covered with temperature controlled Hg, then ν_0 is firmly established. In other cases, it may be necessary to measure ν_0, see Section 7.3.

Experimental evidence is presented which indicates the approximate validity of equation (3.5) over the pressure range measured. This model is further extended by Thonemann (1955), Allen and Coville (1961), Allen, Boschi and Magistrelli (1961, 1963) and Caruso and Cavaliere (1964). The present work, while based on equation (3.4), is essentially a different model, see Section 5.3.

Allen and Coville (1961) present experimental evidence again confirming qualitatively, the neutral depletion near current limitation. This work is extended and put on a quantitative basis in section 8.

Experimental work on Hg arc values of engineering application is presented by Hull and Elder (1934, 1942), Fetz (1940), Fetz and Haug (1950), Granovskii et al (1945, 1946a, 1946b, 1947), Wasserrab (1950), Steiner and Strecker (1960), Timofeyev (1964), Harrison et al (1965), Fraser et al (1965), Quigley (1968), Sander and de Villier (1969) Andersson et al (1970). The complexity of the interacting phenomena present in these devices makes interpretation very difficult, and any theories are usually phenomenalogical.

Carlqvist and Jacobsen (1964) apply current limiting explanations to the phenomena of solar flares and solar currents,

Ware et al (1967) seeks to explain current limitation for the d.s. case by invoking plasma diode instability theories. The analogy obviously fails if no d.s. is present (as in the most general case) or when there is only a single diameter change or even when there is a diameter reduction then an increase - for no d.s. forms at the anode end diameter change. Other objections to this theory are made by Stangeby (1968).

Torvén (1968) extends the gas-clean up work of Kenty (1938) and by measuring the neutral density depletion spectroscopically, further substantiates the vital role of the neutral density.

Aitken and Sander (1968) also measuring neutral density spectroscopically observe the neutral depletion near the d.s. of a pulsed Hg arc value. They make the interesting observation, as did Kenty (1938) that full neutral depletion is not necessary to cause instability or limitation - but only reduction to the level predicted by Poletaev (1951). This work, in a specialized situation where quantitative theories would be highly difficult - again confirms the important role of neutral density.

Steady state current limit results are presented by Andersson et al (1969) but for a device which is closely akin to an engineering Hg valve, and thus, the interpretation is open to question.

Torvén (1969) has presented a highly interesting theory for current limitation which may apply to the special case of current limitation by a d.s. This theory is based on the Poletaev (1951) prescription that neutral density cannot be depleted below a critical level for stable arc existence. (This in fact is the same basis for the theory of Stangeby and Allen (1970b) and of this thesis.) However, even in the presence of a d.s. evidence is presented, section 7.1.4, that current limitation is not necessarily caused by the d.s. - and so it still remains to establish the general cause of the current limit phenomenon.

The accumulated evidence therefore is in favour of current limitation due to neutral density depletion to the Poletaev level. The exact cause and nature of this depletion may be complex, especially in the case of engineering devices where the neutral density is likely to be distorted by:

(a) enhanced Hg emission from the cathode spot;
(b) vacuum pumping effects;
(c) longitudinal density gradients;
(d) gas blow-out at a d.s.;
(e) enhanced ionization near a d.s.;
(f) self-magnetic effects.

As none of these complications are necessary for the observation of current limitation, it is evident that the most basic theory of current limitation must be independent of such effects. Such a theory is presented in section 5.3. Experimentally, the aim of fundamental current limit studies must also be to avoid these complications - and such a programme is undertaken herein, see sections 6 and 7.1.

CHAPTER IV

PLASMA BOUNDARY AS A MACH SURFACE

4.1 INTRODUCTION

In Bohm's (1949) derivation of the sheath criterion, as in all subsequent refinements, the ion motion at the sheath edge is assumed to be normal to the boundary. In the positive column this is never so, for the ions in falling to the wall, also acquire some longitudinal velocity from the axial field, and thus enter the sheath obliguely. What effect this has on the sheath criterion is a question of interest.

This matter is examined below where the fluid equations for both ions and electrons are employed and the sheath criterion is developed in the presence of oblique motion relative to the boundary. In the collisionless, ionization free case, the charged particle equations combine to the familiar, Woods (1961), compressible neutral fluid equation and the plasma boundary can be identified with the Mach surface of neutral flow. This work has been reported elsewhere, Stangeby and Allen (1970a), Andrews and Stangeby (1970).

4.2 BASIC EQUATIONS

Consider the continuity equations for ions and electrons:

$$\frac{\partial \rho_{i,e}}{\partial t} + \vec{\nabla} \cdot (\rho_{i,e} \vec{v}_{i,e}) = C_{i,e} \qquad \ldots (4.1)$$

where the subscripts i and e refer to ions and electrons respectively.

$\rho_{i,e} = m_{i,e} n_{i,e}$, mass density ;

$m_{i,e}$ = particle mass ;

$n_{i,e}$ = particle density ;

$\vec{v}_{i,e}$ = flow velocity

$C_{i,e}$ = mass density creation rate.

Also consider the momentum equations for no magnetic field:

$$\rho_{i,e}\, d\frac{\vec{v}_{i,e}}{dt} = q_{i,e}\,\vec{E} - \vec{\nabla}\cdot\vec{\vec{P}}_{i,e} - \vec{M}_{i,e}\ , \qquad \ldots\ (4.2)$$

where:

$q_{i,e} = \pm\, e\, n_{i,e}$, charge density;

$\vec{E}$ = electrical field ;

$\vec{\vec{P}}_{i,e}$ = pressure tensor ;

$\vec{M}_{i,e}$ = momentum transfer rate by collision.

The ion and electron equations may be conveniently combined to form a pair of one fluid equations if quasineutrality is assumed. The assumption of quasineutrality insures the formation of a precise plasma sheath boundary, see Friedman and Levi (1967), otherwise the full Poisson equation is used and the plasma-sheath transition is smooth. We define, after Davies (1966):

$$\rho = n_i m_i + n_e m_e = n(m_i + m_e) = nm$$

$$m = m_i + m_e$$

$$\rho\vec{v} = m_i n_i \vec{v}_i + m_e n_e \vec{v}_e$$

thus: $$\vec{v} = (m_i\vec{v}_i + m_e\vec{v}_e)/m\ .$$

$$C = C_i + C_e$$

$$\vec{M} = \vec{M}_i + \vec{M}_e$$

$$\vec{\vec{P}} = \vec{\vec{P}}_i + \vec{\vec{P}}_e\ ,$$

so that the new continuity and momentum equations become:

$$\frac{\partial\rho}{\partial t} + \vec{\nabla}\cdot(\rho\vec{v}) = C \qquad \ldots\ (4.3)$$

$$\rho\,\frac{d\vec{v}}{dt} = -\,\vec{\nabla}\cdot\vec{\vec{P}} - \vec{M} \qquad \ldots\ (4.4)$$

The momentum equation may be re-written, using a vector identity,

$$\rho\,\frac{\partial\vec{v}}{\partial t} + \rho\,\vec{\nabla}(\tfrac{1}{2}V^2) - \rho\,\vec{v}\times\vec{\omega} = -\,\vec{\nabla}\cdot\vec{\vec{P}} - \vec{M} \qquad \ldots\ (4.5)$$

where $\vec{\omega} = \vec{\nabla}\times\vec{v}$, the fluid rotation. The following assumptions are made:

(a) steady state, $\frac{\partial}{\partial t} \to 0$;

(b) direct ionization by electron impact to create singly charged species , $C = \lambda n m_1 + \lambda n m_2 = \lambda \rho$.

(c) irrotational flow, $\vec{\omega} = 0$, see Woods (1965). Flow which originates from an irrotational region, e.g. $\vec{v}$ = constant, will always be irrotational (Stoke's theorem).

(d) $\vec{M}_{i,e} = n m_{i,e} (\nu_{i,e} + \lambda) \vec{v}_{i,e}$ where $\nu_{i,e}$ is the momentum-transferring collisional frequency and the term $n m_{i,e} \lambda \vec{v}_{i,e}$ is employed to approximately correct for the assumption that all charged particles are born with the local flow velocity. Momentum $m_{i,e} \vec{v}_{i,e}$ must be 'robbed' from the acceleration field $\vec{E}$ each time a new charged particle is created and accelerated to $\vec{v}_{i,e}$.

(e) The pressure tensors can be reduced to scalars, $p_{i,e} = nkT_{i,e}$. Also, the assumption of adiabatic flow is made, $p_{i,e} \propto n^{\gamma_{i,e}}$ where $\gamma_{i,e}$ are specific heat ratios (the isothermal case is simply regained by setting $\gamma_i = \gamma_e = 1$. This is equivalent to using the Boltzmann relation for the electrons instead of continuity and momentum equations, the case treated by Stangeby and Allen (1970)). Thus:

$$\vec{\nabla} \cdot \vec{\vec{P}} \to a^2 \vec{\nabla} \rho ,$$

where: $$a^2 = (\gamma_e kT_e + \gamma_i kT_i)/(m_i + m_e).$$

With these assumptions, the fluid equations become:

$$\vec{\nabla} \cdot (\rho \vec{v}) = \lambda \rho \qquad \ldots (4.6)$$

$$\rho \vec{\nabla}(\tfrac{1}{2} v^2) = - a^2 \vec{\nabla} \rho - \alpha \rho \vec{v} + \beta \vec{J}, \qquad \ldots (4.7)$$

where we define, after Davies (1966):

$$\alpha = (m_i \nu_i + m_e \nu_e)/m + \lambda$$

$$\beta = \frac{m_i m_e}{em} (\nu_e - \nu_i)$$

$$\vec{J} = en (\vec{v}_i - \vec{v}_e)$$

A sixth assumption is made:

(f) $\vec{J}$ can be neglected. Usually, the sheath is assumed to draw no current, $\vec{v}_i = \vec{v}_e$, then $\vec{J} = 0$. Even if current is drawn, it may be shown that $\beta \vec{J} \ll \alpha\, \rho\vec{v}$. Taking the extreme case of $\lambda = 0$, and $\vec{v}_e = 0$, $\vec{v}_i = a$, one finds that:

$$\beta \vec{J} / \alpha\, \rho\vec{v} = 0\left(\frac{m_e}{m_i}\right) ;$$

in the more realistic case of $\vec{v}_i \approx \vec{v}_e$, the ratio is further reduced by the factor $(\vec{v}_i - \vec{v}_e)/(\vec{v}_i + \vec{v}_e)$. The sheath criterion, see below, is thus unaffected by the drawing of a modest sheath current (provided there is an external current supply as: $C_i/m_i = C_e/m_e$).

4.3 COLLISIONLESS CASE

If one neglects ionization and collisional effects, then the basic equations of the flow are:

$$\vec{\nabla} \cdot (\rho\, \vec{v}) = 0 \qquad \ldots (4.8)$$

$$\rho\vec{v}\, (\tfrac{1}{2}\, v^2) = -\, a^2\, \vec{\nabla} \rho \qquad \ldots (4.9)$$

$$\vec{\omega} = \vec{\nabla} \times \vec{v} = 0\ . \qquad \ldots (4.10)$$

Since $\vec{\omega} = 0$, one is free to define a velocity potential such that

$$\vec{v} = -\, \vec{\nabla} \varphi \qquad \ldots (4.11)$$

and the equations (4.8) - (4.9) may be combined to give the single equation:

$$\nabla^2 \varphi = \frac{1}{2a^2}\, \vec{\nabla}\varphi \cdot \vec{\nabla}(\vec{\nabla}\varphi \cdot \vec{\nabla}\varphi) \qquad \ldots (4.12)$$

which completely defines the flow. Equation (4.12) may be recognized, see Woods (1961), as the equation for inviscid, steady-state, irrotational, compressible, potential fluid flow with a interpreted as a sound speed, and thus all mathematical results of the latter theory may be appropriated to describe the ion fluid motion.

For example, Stangeby and Allen (1971b), have considered the case of a probe immersed in a plasma where the ions are flowing (say towards a wall) and solved equation (4.12) with the appropriate boundary conditions by a method similar to the Rayleigh-Jansen method for ordinary fluid flow past a body.

In the present context we wish to utilize the concept of the Mach surface. In a region of supersonic flow, $v > a$, a Mach surface is such that the fluid velocity component normal to the surface is equal to the sound speed a. It is possible to identify a plasma-sheath boundary as a closed Mach surface. To do so it must be shown that:

(i) a plasma-sheath boundary can only occur on a closed Mach surface, i.e. a necessary condition for sheath formation is that the normal velocity component be a.

(ii) If a closed Mach surface exists the plasma solution blows up on it, that is, a sheath forms at this surface, i.e. a sufficient condition for sheath formation is that the normal velocity component reaches a.

These conditions are considered in turn:

(i) Necessary Condition

This condition is established directly from compressible fluid flow theory. At a plasma-sheath boundary the plasma solution can no longer be extended using step-by-step integration of the differential equations, i.e. the plasma and sheath solutions are analytically different. From Courant and Friedrichs (1948, p.55) "Whenever the flow in two adjacent regions is described by expressions which are analytically different then the two regions are necessarily separated by a characteristic", i.e. a Mach surface.

(ii) Sufficient Condition

Consider any simple contour C in two-dimensional configuration space (two dimensions will be considered for simplicity), and the variable pair (p,s) where s is measured along C and p normally to C. We wish to show that if $C = C_m$, a closed Mach line, then $\frac{\partial q_p}{\partial p} \to \infty$ everywhere on C_m, i.e. the plasma solution blows up on C_m. (Where $\vec{q} \equiv \vec{v}$ has been used for consistency with the work of Stangeby and Allen (1970).)

The differential equations are written in terms of (p,s) by considering Fig.2. Equation (4.9). the momentum equation becomes:

$$q_p \frac{\partial q_p}{\partial p} + q_s \frac{\partial q_s}{\partial p} = - \frac{a^2}{n} \frac{\partial n}{\partial p} , \qquad \ldots (4.13)$$

$$q_p \frac{\partial q_p}{\partial s} + q_s \frac{\partial q_s}{\partial s} = - \frac{a^2}{n} \frac{\partial n}{\partial s} . \qquad \ldots (4.14)$$

Equation (4.8), the continuity equation becomes:

$$\frac{\partial (nq_p)}{\partial p} + \frac{\partial (nq_s)}{\partial s} + \frac{nq_p}{R(s)} = 0 , \qquad \ldots (4.15)$$

where $R(s)$ is the radius of curvature of C at s. Equation (4.15) is obtained by considering the net flux out of the elemental region shown in Fig.(2). The irrotationality condition, equation (4.10) becomes:

$$\frac{\partial q_p}{\partial s} - \frac{\partial q_s}{\partial p} - \frac{q_s}{R(s)} = 0. \qquad \ldots (4.16)$$

Combining equations (4.13) to (4.16):

$$\frac{\partial q_p}{\partial p}\left(1 - \frac{q_p^2}{a^2}\right) + \frac{q_p}{R(s)}\left(1 + \frac{q_s^2}{a^2}\right) + \frac{\partial q_s}{\partial s}\left(1 - \frac{q_s^2}{a^2}\right) - \frac{2q_p q_s}{a^2} \frac{\partial q_p}{\partial s} = 0 . \qquad \ldots (4.17)$$

Now if $C = C_m$ then $q_p = - a$ and $\partial q_p/\partial s = 0$, hence:

$$\lim_{q_p \to -a} \left\{ \frac{(1 - q_p^2/a^2)}{(1 + q_s^2/a^2)} \frac{\partial q_p}{\partial p} \right\} - \frac{a}{R(s)} + \frac{(1 - q_s^2/a^2)}{(1 + q_s^2/a^2)} \frac{\partial q_s}{\partial s} = 0 . \qquad \ldots (4.18)$$

Multiply equation (4.18) by ds and integrate around C_m. The following two properties of contour integration may be noted:

(i) $\oint \left\{ 1/R(s) \right\} ds = 2\pi$ for any closed contour;

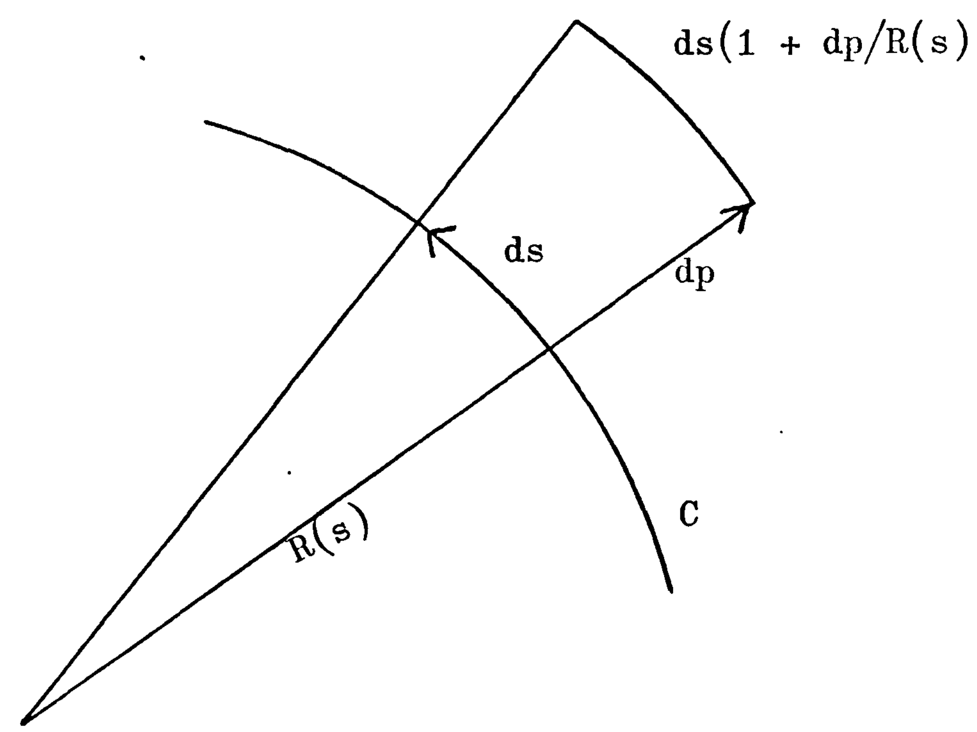

Fig.2
Diagram defining p,s and R(s)

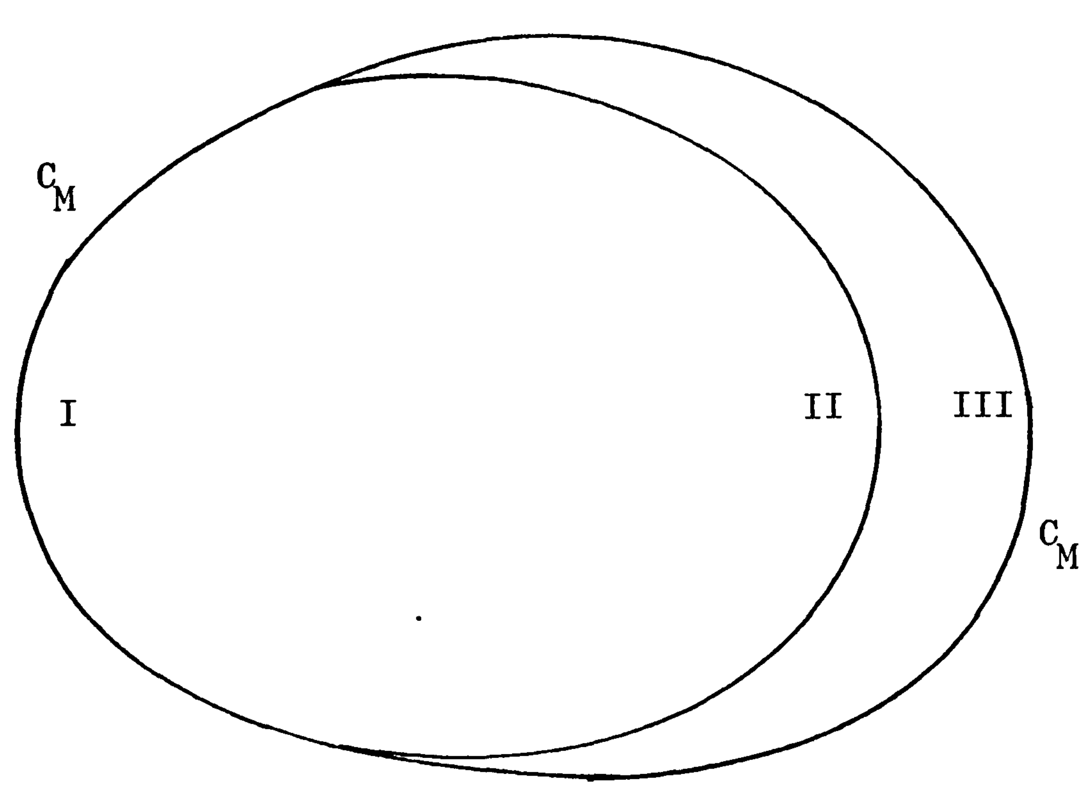

Fig.3
Diagram to show that $\partial q_p/\partial p \to \infty$ on all of C_M

(ii) $\oint f(y)(\partial y/\partial s)\, ds = 0$ for any closed contour and y a physical variable defined on the contour.

(Strictly, these results are valid for simple closed Jordan curves.)

Thus one obtains:

$$\lim_{q_p \to -a} \oint_{C_m} \frac{(1 - q_p^2/a^2)}{(1 + q_s^2/a^2)} \frac{\partial q_p}{\partial p}\, ds = 2\pi a\,, \qquad \ldots (4.19)$$

hence $\partial q_p/\partial p \to \infty$ on some portion at least of C_m.

It may be shown that $\partial q_p/\partial p \to \infty$ on all of C_m as follows. Consider C_m as shown in Fig.3, where on portion I $\partial q_p/\partial p \to \infty$ but does not do so on portion III. Now there must exist a curve such as portion II on which $\partial q_p/\partial p \to \infty$ in order to close the sheath formed by portion I. Since portion II is a sheath, then $q_p = -a$ here as well (from the necessity condition).

Set:

$$f = \lim_{q_p = -a} \frac{1}{a} \frac{(1 - q_p^2/a^2)}{(1 + q_s^2/a^2)} \frac{\partial q_p}{\partial p}\,,$$

then:

$$\int_I f ds + \int_{II} f ds - \int_I \frac{ds}{R} - \int_{II} \frac{ds}{R} = 0\,, \qquad \ldots (4.19a)$$

$$\int_I f ds + \int_{III} f ds - \int_I \frac{ds}{R} - \int_{III} \frac{ds}{R} = 0\,. \qquad \ldots (4.19b)$$

Subtracting equation (4.19b) from equation (4.19a):

$$\int_{II} f ds - \int_{III} f ds - \int_{II} \frac{ds}{R} + \int_{III} \frac{ds}{R} = 0\,.$$

Now:

$$\int_I \frac{ds}{R} + \int_{II} \frac{ds}{R} = \int_I \frac{ds}{R} + \int_{III} \frac{ds}{R} = 2\pi\,,$$

thus:

$$\int_{II} \frac{ds}{R} = \int_{III} \frac{ds}{R} \quad ,$$

and

$$\int_{II} f ds = \int_{III} f ds \ .$$

However, on portion III $\partial q_p / \partial p \not\to \infty$ hence:

$$\int_{II} f ds = 0,$$

and since f is the same sign everywhere on C_m, then on portion II $\partial q_p/\partial p \not\to \infty$ in contradiction to the above. If portion I expands to occupy all of C_m then this contradiction is avoided.

The possibility of multiple segments where $\partial q_p / \partial p \not\to \infty$ is treated similarly, each segment being considered in turn.

Thus one concludes that a necessary and sufficient condition for sheath formation is that the plasma fields should accelerate the ions until their velocity normal to the sheath is equal to a independent of the ion velocity component tangential to the sheath.

At the sheath edge (returning to the $\vec{v}$ notation)

$$\frac{m_e v_{esp} + m_i v_{isp}}{m_e + m_i} = a = \left(\frac{\gamma_e kT_e + \gamma_i kT_i}{m_e + m_i} \right)^{\frac{1}{2}} \qquad \ldots (4.20)$$

where v_{esp} and v_{isp} are the electron and ion flow velocities normal to the plasma-sheath boundary, at the sheath boundary.

The criterion of Bohm (1949) can be regained from equation (4.20) by taking:

(a) zero net current, $v_{esp} = v_{isp}$;

(b) $T_i = 0$;

(c) $\gamma_e = 1$, isothermal electrons (Boltzmann relation applicable).

(d) $m_e \ll m_i$, then:

$$v_{isp} = \sqrt{\frac{kT_e}{m_i}} \; . \qquad \ldots (4.21)$$

4.4 COLLISIONAL CASE

In the presence of ionization and collisions, the conclusions of section 4.3 are uneffected as may now be shown. The flow equations are

$$\vec{\nabla} \cdot (\rho\vec{v}) = \lambda\rho \qquad \ldots (4.21)$$

$$\rho\vec{v}(\tfrac{1}{2} v^2) = - a^2 \vec{\nabla}\rho - \alpha \rho\vec{v} \qquad \ldots (4.22)$$

$$\vec{\omega} = \vec{\nabla} \times \vec{v} = 0 \; . \qquad \ldots (4.23)$$

One can readily show that this leads to the equivalent of equation (4.18):

$$\frac{\partial q_p}{\partial p}\left(1 - \frac{q_p^2}{a^2}\right) + \frac{q_p}{R(s)}\left(1 + \frac{q_s^2}{a^2}\right) + \frac{\partial q_s}{\partial s}\left(1 - \frac{q_s^2}{a^2}\right)$$
$$- 2\,\frac{q_p q_s}{a^2}\,\frac{\partial q_p}{\partial s} - \lambda - \alpha\,\frac{(q_p^2 + q_s^2)}{a^2} = 0 \; , \qquad \ldots (4.24)$$

and the equivalent of equation (4.19) is:

$$\lim_{q_p \to -a} \oint_{C_m} \frac{(1 - q_p^2/a^2)}{(1 + q_s^2/a^2)}\,\frac{\partial q_p}{\partial p}\, ds = 2\pi a + \lambda \oint_{C_m} \frac{ds}{(1 + q_s^2/a^2)} + \alpha \oint_{C_m} ds \; .$$
$$\ldots (4.25)$$

In general, the right-hand side of equation (4.25) is positive so that the argument proceeds as in section 4.3, and the same conclusions are applicable. (One may note that the assumptions on the nature of the ionization process, $C = \lambda\, m\, n$, may also be removed without effecting the conclusion. Then the second term on the right-handside of equation (4.25) becomes:

$$\oint \frac{C(s)}{mn(s)}\,\frac{ds}{(1 + q_s^2/a^2)} \; ,$$

which is obviously still positive.)

In terms of the velocity potential we now have:

$$\nabla^2\varphi = \frac{1}{2a^2}\vec{\nabla}\varphi\cdot\vec{\nabla}(\vec{\nabla}\varphi\cdot\vec{\nabla}\varphi) + \lambda + \frac{\alpha}{a^2}(\vec{\nabla}\varphi\cdot\vec{\nabla}\varphi) \quad .. \quad (4.26)$$

As the additional two terms are less than second order, the nature of this second order, non-linear partial differential equation (as to whether it be elliptic, parabolic or hyperbolic) is uneffected and the characteristic surface remains as before, although now one may prefer to use this purely mathematical term rather than 'Mach surface'.

4.5 CONCLUSIONS

In any plasma (i.e. wherever quasineutrality holds), the fields must accelerate the charged particles until at the sheath edge:

$$\frac{m_e v_{esp} + m_i v_{isp}}{m_e + m_i} = \sqrt{\frac{\gamma_e kT_e + \gamma_i kT_i}{m_e + m_i}},$$

where terms are defined as before. This is irrespective of:

(a) tangential flow components;

(b) net current collection by the sheath;

(c) collisional effects in the plasma;

(d) the presence and nature of ionization effects in the plasma;

(e) whether charged particle behaviour is adiabatic or isothermal;

(f) temperature ratios.

CHAPTER V

NEW THEORY FOR D.C. LIMITATION

5.1 INTRODUCTION

In the simplest discharge situation, i.e. that of unconstricted geometry and d.c. operation, it would seem evident that the Allen-Thonemann limit, I_{AT}, (section III) certainly constitutes an upper limit to the current (assuming, of course, the independence of ν_0 and $\gamma\beta/\alpha$ on current). However, it turns out to be the case that an effect not considered by Allen and Thonemann intervenes to limit the current before I_{AT} is reached.

In the Allen-Thonemann model, at current limitation all neutrals emitted from the wall are ionized and return to the wall as ions. This may be objected to, Stangeby (1968), on the grounds of the limited ionizing ability of the electrons. This limited ionizing ability is due to three factors:

(a) even if all the electrons possess an energy corresponding to the maximum in the ionization cross-section of the neutral, the m.f.p. of the neutral for ionization, λ, may still be greater than r_0 since for finite I, the electron density n_e is finite;

(b) some neutrals are emitted almost tangentially to the wall and therefore have such short flight paths that their probability of ionization is low;

(c) in any case, ionization in the discharge is a statistical phenomenon, and for any finite n_e there will always be some neutrals which traverse even the tube diameter without being ionized.

The electrons will always reach the limit of their ionizing ability before the condition $I_i/e = \nu_0$ is reached. However it will be found that high pressures correspond to high current limits, as before, so that as p becomes large, λ becomes increasingly smaller and the condition $I_i/e = \nu_0$ is approached asymptotically, i.e. the current limit I_L approaches I_{AT} asymptotically for large p.

An earlier attempt, Stangeby (1968), to transform the foregoing observations into a quantitative theory proved unsatisfactory. As the electron distribution at current limitation is probably substantially non-Maxwellian, any calculation of λ based on an assumed electron distribution, will be suspect. The key to the problem lies in exploiting the long known fact, Poletaev (1951), that existence of the positive column is only possible for values of neutral pressure p and tube radius r such that $pr > C_1$ some critical value. This key is suggested by the work of Torvén (1969) who attempts to explain current limitation as being due to double sheaths. In sections 5.5 and 7.1 it is concluded that the double sheath is not the cause of current limitation and so it remains to apply the Poletaev prescription properly. This is undertaken in sections 5.3 and 5.4.

Briefly, current limitation comes about as follows: the starting pressure, p_0, is fixed and I is raised causing neutral depletion. This depletion constitutes an effective decrease in p, i.e. $p = p(I)$, effectively, and when $p(I)r_0 = C_1$, limitation occurs. This constitutes the upper limit to I; in section 5.4 it is observed that as I decreases to small values, the wall sheath grows causing decrease in r, i.e. $r = r(I)$ effectively, and when $p_0 r(I) = C_1$ limitation occurs. This constitutes the lower limit to I.

5.2 THE POLETAEV PRESCRIPTION FOR STABLE EXISTENCE OF THE COLUMN

5.2.1 Qualitative Reason for Critical pr

The effect of the finite ionization ability of the electrons on the arc characteristics may be seen by the following qualitative argument. The ion loss per unit length is :

$$2\pi r \; n_s \, \alpha \, v_B \qquad \ldots (5.1)$$

while ion production is:

$$\pi r^2 \, \bar{n}_e n \; f(T_e) \qquad \ldots (5.2)$$

where n is the neutral density and $f(T_e)$ is a function of the electron temperature and the ionization cross section of the neutral. From equations (5.1) and (5.2) one obtains the plasma balance equation, relating T_e and nr :

$$\frac{2\,\alpha}{\gamma}\sqrt{\frac{k}{M}}\;\frac{T_e^{\frac{1}{2}}}{f(T_e)} = nr \; . \qquad \ldots (5.3)$$

Due to the finite ionization cross section, $f(T_e)$ has a maximum and hence a minimum exists to possible values of the parameter nr for stable existance of the positive column. In the foregoing it has been assumed that n and r are parameters which may be specified independent of current.

5.2.2 Poletaev's Work Reviewed

Poletaev (1951) first presented a quantitative analysis of the fore-going. From the Tonks-Langmuir theory of the positive column we have the plasma balance equation, see equation (2.6)

$$Z = \frac{1{\cdot}092}{r}\sqrt{\frac{kT_e}{M}} \qquad \ldots (5.4)$$

where Z is the electron ionization rate.

The ionization rate is also given by:

$$Z = \int_{\varepsilon_i}^{\infty} s_e(\varepsilon) p \left(\frac{2\varepsilon}{m}\right)^{\frac{1}{2}} N(\varepsilon) \, d\varepsilon, \qquad \ldots (5.5)$$

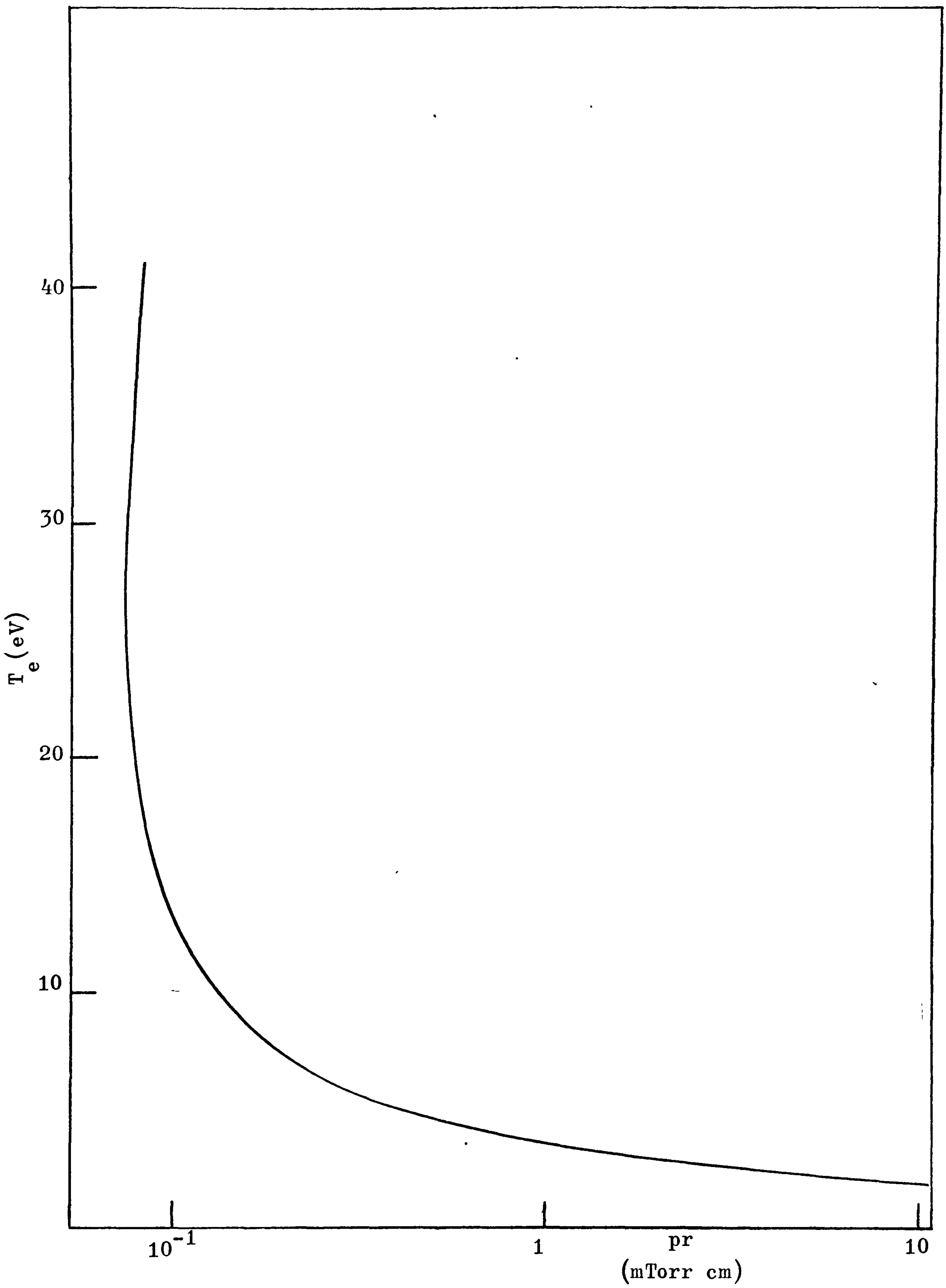

Fig.4
T_e vs pr showing the minimum value of (pr) for which arc existance is possible

where $s_e(\varepsilon)$ is the ionization efficiency for an electron of energy ε, $N(\varepsilon)$ is the normalized electron energy distribution and ε_i is the ionization threshold energy, see von Engel (1965).

Poletaev assumed a Maxwellian electron distribution:

$$N(\varepsilon)d\varepsilon = \frac{2}{\sqrt{\pi}}\left(\frac{\varepsilon}{\varepsilon_m}\right)^{\frac{1}{2}} \exp\left(-\frac{\varepsilon}{\varepsilon_m}\right) d\left(\frac{\varepsilon}{\varepsilon_m}\right), \qquad \ldots (5.6)$$

where $\varepsilon_m = kT_e$ and for $s_e(\varepsilon)$ he used a mathematical approximation to the experimental data of Bleakney (1930) for Hg:

$$s_e(\varepsilon) = 0{\cdot}525\ (\varepsilon - \varepsilon_i) \exp\left(-\frac{(\varepsilon - \varepsilon_{max})}{(\varepsilon_{max} - \varepsilon_i)}\right), \qquad \ldots (5.7)$$

where $\varepsilon_i = 10{\cdot}39$ eV and $\varepsilon_{max} = 50$ eV, and the numerical constant holds if all ε are in eV. This approximation for $s_e(\varepsilon)$ has the virtue of being integrable in equation (5.5) and one may obtain finally:

$$pr = 7{\cdot}6 \times 10^{-5} \exp\left(\frac{\varepsilon_i}{\varepsilon_m}\right) \frac{(1 + \beta\,\varepsilon_m)^3}{1 + \varepsilon_m(\frac{2}{\varepsilon_i} + \beta)}, \qquad \ldots (5.8)$$

where $\beta \equiv 1/(\varepsilon_{max} - \varepsilon_i)$ and pr is in units cm torr. Equation (5.8) provides T_e as a function of pr, shown in Fig.4. The critical value of pr as reported by Poletaev is:

$$(pr)_{min} = C_1 = 0{\cdot}079 \text{ cm mTorr},$$

for Hg. In fact this appears to be slightly in error as equation (5.8) actually gives $C_1 = 0{\cdot}077$ cm mTorr.

Poletaev also supplies the experimental value of $C_1 = 0.11$ cm mTorr for Hg. He endeavours to reduce the discrepancy between the two figures (which is considerably greater for other gases) by correcting the electron distribution for drift effects. Thus he uses the drift Maxwellian distribution

$$N(\varepsilon)d\varepsilon = \frac{1}{2\sqrt{\pi}}\ \frac{1}{\varepsilon_m\Gamma^{\frac{1}{2}}} \exp -\left(\frac{\varepsilon}{\varepsilon_m} + \Gamma\right) \left\{ \exp\left[2\left(\frac{\Gamma\varepsilon}{\varepsilon_m}\right)^{\frac{1}{2}}\right] - \exp\left[-2\left(\frac{\Gamma\varepsilon}{\varepsilon_m}\right)^{\frac{1}{2}}\right]\right\} d\varepsilon, \qquad \ldots (5.9)$$

where $\Gamma \equiv \varepsilon_D/\varepsilon_m$, $\varepsilon_D = \frac{1}{2} mu^2$ and u is the drift velocity. (The notation of Forrest (1967) has been employed.) In this way Poletaev finds that $C_1 = 0{\cdot}086$ cm mTorr for $\Gamma = 1/16$ and $C_1 = 0.098$ cm mTorr for $\Gamma = 6{\cdot}25$. Evidently drift effects are not sufficient to account for the discrepancy (especially as the latter drift value is unrealistically high).

5.2.3 Calculations of C_1 and T_e at Critical pr

There are four objections which may be made to the theoretical value of C_1 obtained by Poletaev for Hg:

(a) In the extreme conditions corresponding to $pr \simeq C_1$, the column structure is unlikely to correspond to the theory of Tonks-Langmuir. Hence the numerical value $1{\cdot}092$ in equation (5.4) (i.e. $\sqrt{2}\, s_0$ in the notation of Tonks-Langmuir) is likely to be in error.

(b) The electron distribution at current limit is depleted of electrons due to excitation and ionization.

(c) The ionization efficiency curve of Bleakney (1930), to which equation (5.7) is only an approximation, is itself only approximately correct compared to the more accurate data of Nottingham (1939).

(d) No account is taken of the loss rate of Hg^{++} ions (which reach the sheath edge with speeds $\sqrt{2}$ times greater than Hg^{+} ions) despite the fact that the ionization cross section for Hg^{++} starts at 29 eV. There is spectroscopic evidence, see Allen and Thonemann (1954), that in these extreme conditions even Hg^{+++} is present in some quantity.

To gain some quantitative measure of the effect that these errors have on the calculation of $(pr)_{min}$ and T_{e_c} (the temperature at $(pr)_{min}$) a number of computations were made with the aid of a computer.

In the case of $\Gamma = 0$, we have by combining equations (5.4), (5.5) and (5.6):

$$pr = 1{\cdot}092\left(\frac{\pi m}{8M}\right)^{\frac{1}{2}} \quad \varepsilon_m^2 \left\{1/\int_{\varepsilon_i}^{\infty} S_e(\varepsilon)\ \varepsilon\ \exp\left(-\varepsilon/\varepsilon_m\right)\ d\varepsilon\right\} \quad \ldots (5.10)$$

and for $\Gamma \neq 0$, by combining equations (5.4), (5.5) and (5.9):

$$pr = 1{\cdot}092\left(\frac{2\pi m}{M}\right)^{\frac{1}{2}} \Gamma^{\frac{1}{2}} e_m^{\frac{3}{2}} \times \left\{1/\int_{\varepsilon_i}^{\infty} S_e(\varepsilon)\varepsilon^{\frac{1}{2}} \exp\left(-\left(\frac{\varepsilon}{\varepsilon_m}+\Gamma\right)\right)\left[\exp\left(2\left(\frac{\Gamma\varepsilon}{\varepsilon_m}\right)^{\frac{1}{2}}\right) - \exp\left(-2\left(\frac{\Gamma\varepsilon}{\varepsilon_m}\right)^{\frac{1}{2}}\right)\right] d\varepsilon\right\} \quad \ldots (5.11)$$

To compare the effect of using Poletaev's approximation to $S_e(\varepsilon)$ with Nottingham's $S_e(\varepsilon)$, both were inserted in equation (5.10) and the computation taken to $\varepsilon = 300$ eV. Result:

TABLE 1

EFFECT OF DIFFERENT CROSS SECTIONS ON CRITICAL CONSTANTS

	Poletaev $S_e(\varepsilon)$	Nottingham $S_e(\varepsilon)$
T_{e_c}	28 eV	29 eV
C_1	0·077 cm mTorr	0·075 cm mTorr

Conclusion: this error introduces only a slight effect.

To study the effect of ignoring high energy electron depletion, the integration of equation (5.10) was taken to 100 eV and 300 eV. (Nottingham's $S_e(\varepsilon)$). Result:

TABLE 2

EFFECT OF ELECTRON DEPLETION ON CRITICAL CONSTANTS

	With Tail	Without Tail
T_{e_c}	29 eV	22.5 eV
C_1	0·075	0·0825

Conclusion: as population depletion is doubtlessly operative well before 100 eV (a 100 eV electron must travel 5 meters in a 0·2 V/cm field without suffering an energy-loosing collision) it seems that the neglect of high energy electron depletion introduces considerable error to the calculation of C_1 and T_{e_c}.

To study the effect of drift on the calculation, equation (5.11) was used with Nottingham's data and the integration taken to $\varepsilon = 100$ eV and $\varepsilon = 300$ eV. The variation of T_{e_c} and C_1 with Γ are given in Figs.5 and 6. Again, the effect of drift is considerable. It may be noted that the variation of C_1 with Γ is the opposite to that stated by Poletaev, who unfortunately provides no details of his calculation.

As to the structural differences between the positive column as treated by Tonks and Langmuir, and that of the column near $(pr)_{min}$, objection (a), the most obvious way to estimate this error is to do Langmuir probe studies of the column near $(pr)_{min}$. The interpretation of the probe characteristics in these extreme conditions is difficult, nevertheless results reported in section 7.2 indicate that charged particle density radial variation is less near $(pr)_{min}$ than in Tonks-Langmuir. This implies that charged particle production relative to loss is improved over the Tonks-Langmuir model, and the structural constant 1·092 in equation 5.4 is too large. Unfortunately this moves the theoretical value of $(pr)_{min}$ farther from the experimental value.

5.2.4 Alternative Theories of $(pr)_{min}$

Although the discrepancy between the theoretical and experimental values of C_1 for Hg is readily explicable in terms of the approximations in the theory, the discrepancies for the inert gases, as reported by Poletaev, see Table 3, are considerably greater. This may be due to the experimental difficulties in controlling inert gas pressure under these extreme discharge conditions. Even controlling Hg pressure is difficult in these circumstances although here temperature controlled Hg condensing surfaces may be used in an attempt to achieve uniformity.

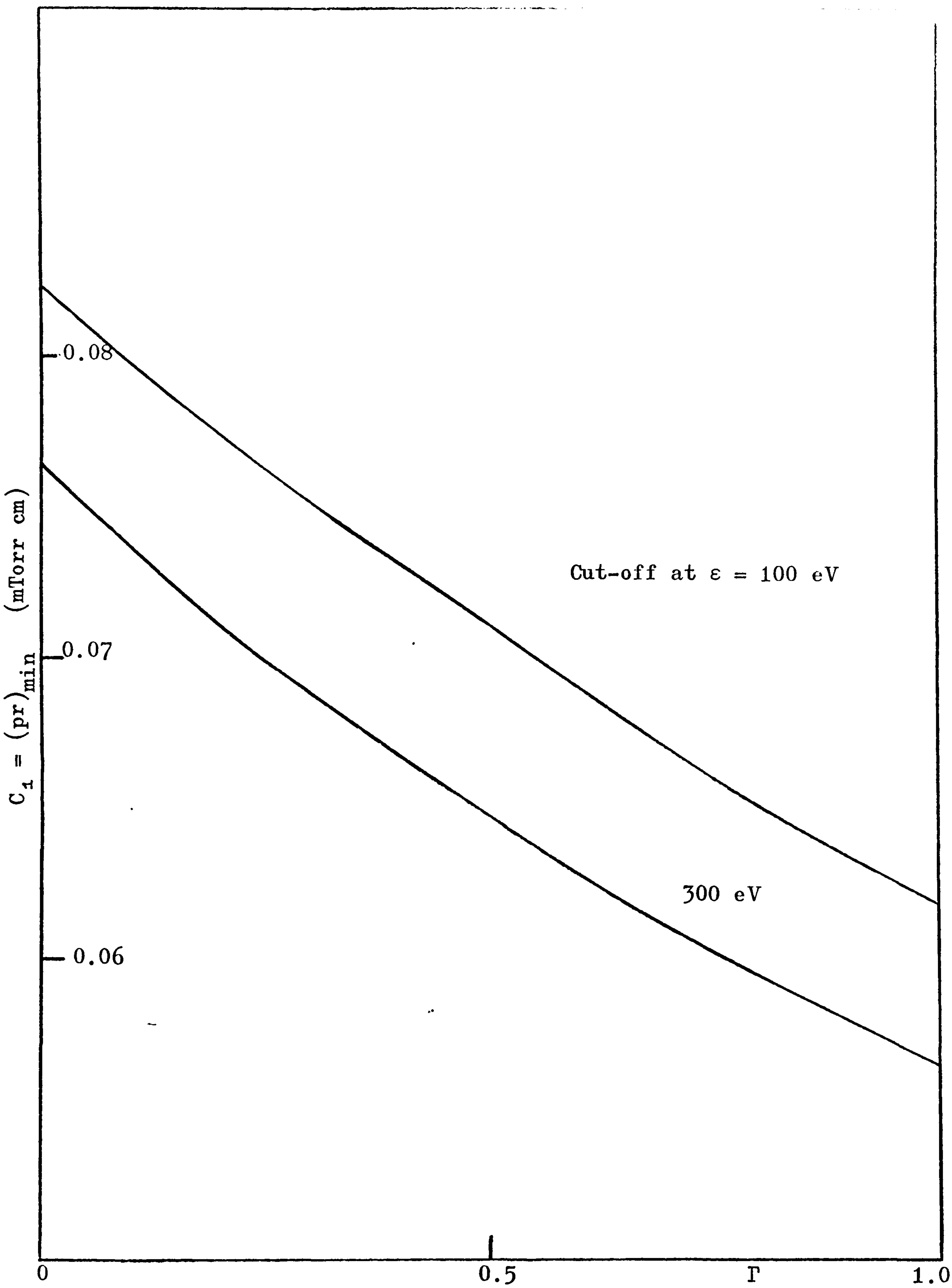

Fig.5

C_1, the calculated critical Potetaev parameter, as a function of Γ, the electron drift parameter. ($\Gamma^{\frac{1}{2}} = v_D/\bar{c}$)

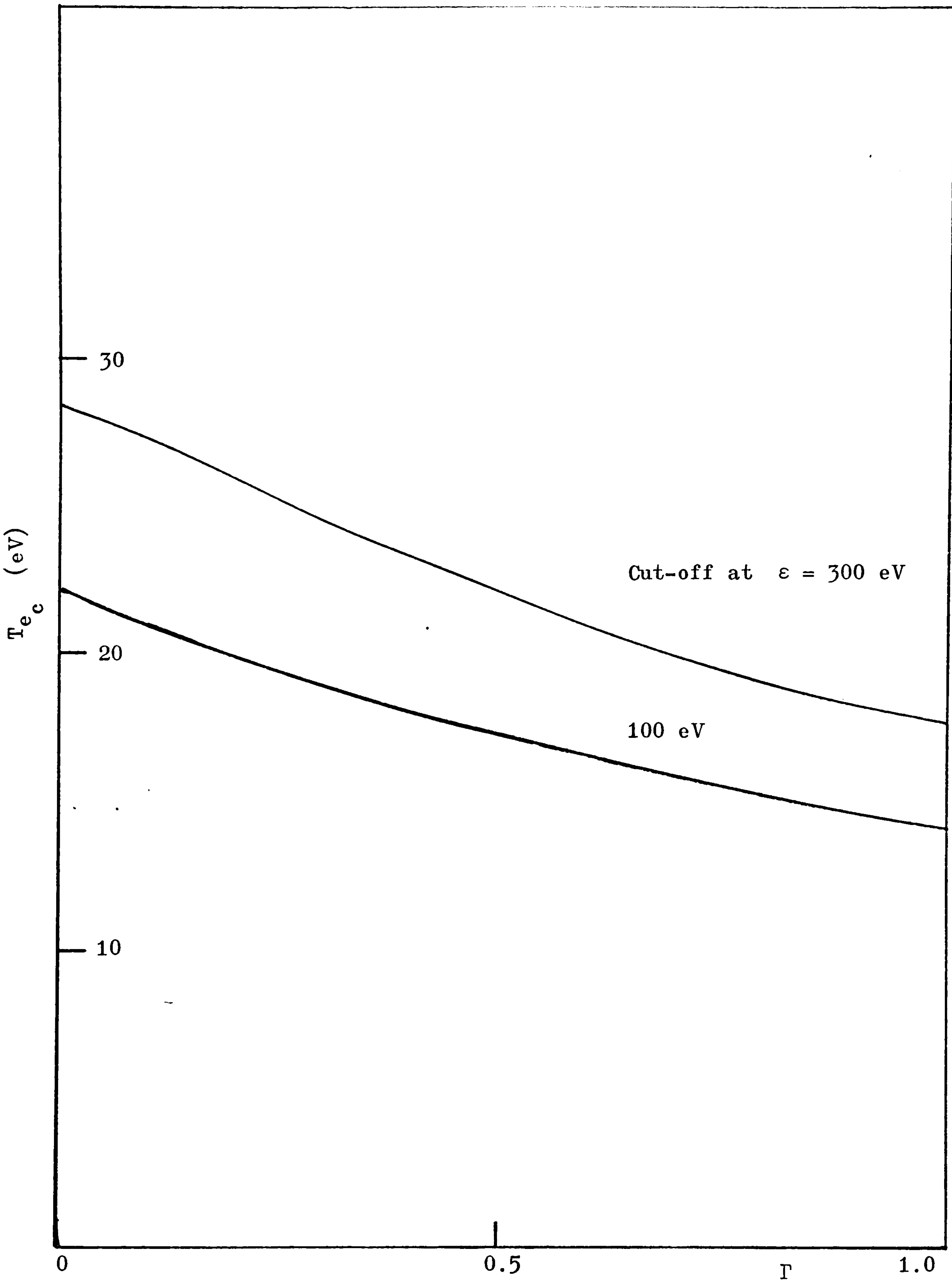

Fig.6 .

T_{e_c} , the calculated electron temperature at the critical Poletaev point, as a function of Γ, the electron drift parameter. ($\Gamma^{\frac{1}{2}} = v_D/\bar{c}$)

TABLE 3

POLETAEV'S VALUES OF $\bar{C}_1$ (Units of cm mTorr)

GAS	K	Ar	Ne	He
C_1 theory	0·21	0·27	1·56	8·66
C_1 experimental	0·48	4·8	15·0	50

Accordingly it must be allowed that some other mechanism may intervene before the electrons reach the peak of their ionizing ability. This question can probably only be resolved by doing very careful measurements of C_1 for the inert gases - under well controlled neutral density conditions. Two possible alternate mechanisms are discussed briefly in sections 5.2.4(a) and 5.2.4(b).

(a) Effect of Instabilities

Near $pr = C_1$, $\beta \approx 1$, that is the electrons are approaching that unstable region where their drift velocity is near their thermal velocity. The resultant beam-plasma interaction probably results in a considerable investment by the discharge in oscillation energy. Indeed increased fluctuations have been observed in this region see Section 7.1. It may be that the level of oscillations becomes unstable near $pr = C_1$, robbing the electrons of the kinetic energy they need to meet ionization requirements. Increasing the voltage gradient may only result in increased investment in fluctuation power density, not in an increase in the ionizing ability of the electrons. In these circumstances stable positive column existance is impossible.

(b) Wall Loss of Ions

In any discharge there is gas clean-up, see Kenty (1938) etc., due to the ions being pounded into the wall. In Hg the sheath voltage drop is $\sim 6\ kT_e/e$. In d.c. discharges this gradual clean-up normally plays no role provided the gas can be replaced, e.g. from a nearby Hg reservoir. In closed-off lamps of course the rate of gas clean-up often governs the lamp life-time.

Near $pr = C_1$, T_e may be quite large and the ions strike the walls with ~ 100 eV energy. In these circumstances the clean-up rate may well be higher than normal and a slight fluctuation in the local T_e could send the discharge into instability if the increased neutral depletion is not immediately compensated.

5.2.5 Conclusions

Poletaev has established the experimental fact that stable positive column existance is impossible for $pr < C_1$. The reason for this effect has not been absolutely established, but is probably due to the finite ionizing ability of the electrons. In light of the uncertainties in calculating C_1, in the remainder of this work the experimental value of C_1 is used:

$$(pr)_{min} = C_1 = 0{\cdot}11 \text{ cm mTorr} \qquad \ldots (5.12)$$

or in terms of neutral density ($T = 0^oC$) :

$$(nr)_{min} = C_1 = 3{\cdot}9 \times 10^{16} \text{ m}^{-2} \qquad \ldots (5.13)$$

5.3 UPPER CURRENT LIMIT IN THE UNCONSTRICTED POSITIVE COLUMN

5.3.1 Outline of Theory

One of the most important relations to be established by any current limitation theory, is the relation of the current limit, I_L, and the neutral pressure p_o and tube radius r_o. The Poletaev prescription as originally established is current-independent and hence supplies no current limit theory directly. However, the neutral density in the positive column is not constant. It is not only a function of the 'base-pressure' p_o but is also a function of the current due to neutral depletion by ionization.

Consider the discharge current to be low and n_o such that $n_o r_o > C_1$. If the current is sufficiently small, there is little ionization and the neutral density in the discharge volume corresponds to n_0. As the current is raised, the level of ionization increases and the neutral density in the discharge volume is depleted. We see that $n = n(I)$ effectively. Since stable column existance is only possible for $nr_0 > C_1$ where n is the actual neutral density in the column, then when $n(I) = C_1/r_0$ the current will limit.

Of course $n = n(p_0)$, as well, so that by means of the Poletaev prescription we have the basis of a current limit theory:

$$n(p_0\ , I_L) = C_1/r_0\ .$$

Since the neutral density will also be a function of radius, in the presence of ionization, $n = n(p_0, r, I)$, the current limit prescription will be taken to be:

$$\bar{n}(p_0\ , I_L) = C_1/r_0 \qquad \ldots\ (5.14)$$

where $\bar{n}$ is the density averaged across the column.

Conceptually, the most straight-forward way to calculate $n(p_0\ , I\ , r)$ would be to relate I to n_e via equations (3.2) and (3.4) then calculate the depletion of the neutrals emitted from the wall assuming an electron energy distribution and knowing n_e and the neutral ionization cross section. This procedure however is subject to large errors due to uncertainties in the form of the electron distribution, $f_e(v_e)$, near current limit. One wishes to avoid any calculation which depends on assumptions about the electron energy distributions.

This problem can be circumvented by working with λ , the m.f.p. for the neutral for ionization and calculating:

(a) $I_i(\lambda)$, the ion wall current as a function of λ .

(b) The relation between I_i and I, where I is the arc current. This is given by Allen and Thonemann, see equation (3.4). (The assumptions involved in equation (3.4) are such that this equation must be verified experimentally - see Section 7.3.) Thus $I(\lambda)$ is obtained.

(c) $n(p_0, r, \lambda)$, the neutral density as a function of base pressure p_0 i.e. the neutral emission rate from the walls - (again one must verify experimentally that in actual discharge conditions the wall emission rate is still given by the pressure p_0, see Section 7.3), radius and neutral m.f.p.

By combining these relations one may eliminate λ and find $n(p_0, r, I)$. In this way the calculation $\lambda(n_e, f_e(\vec{v}_e))$ is never made.

5.3.2 Calculation of Current as a Function of Neutral M.F.P.

Of course $\lambda = \lambda(v_N)$, where v_N is the particular neutral speed, and a calculation based on the distribution of neutral speeds is straightforward in principle, see section 5.3.6, but for simplicity this is avoided here and it is assumed that all the neutrals move with their average speed $\bar{c}$. Also $\lambda = \lambda(r)$, but again for simplicity it shall be assumed that λ is constant across the discharge, i.e. λ is effectively averaged over the cross section. This latter assumption is less serious near current limit than elsewhere owing to the flattening in the radial electron density profile here.

To calculate $I_i(\lambda)$ consider the flux of neutral particles at an element of wall surface in the absence of a discharge. The emitted (or received) flux density according to the cosine law is:

$$\int_{\theta=0}^{\pi/2} \int_{\varphi=0}^{2\pi} \bar{c} \cos\theta \, n_0 \, \frac{d\Omega(\theta,\varphi)}{4\pi} \qquad \ldots (5.15)$$

where θ and φ are the normal and azimuthal angle respectively and the elemental solid angle is:

$$d\Omega(\theta,\varphi) = \sin\theta \, d\theta \, d\varphi \qquad \ldots (5.16)$$

By integration over θ and φ the total emitted flux density is:

$$\nu_0 = \tfrac{1}{4} n_0 \bar{c} \ . \qquad \ldots (5.17)$$

In the presence of a discharge the received flux density is modified due to ionization. We assume that the neutrals are in a 'free-fall' regime as are the ions, i.e. the neutrals follow rectilinear trajectories, see Appendix I. We shall also assume that the emitted flux of neutrals is still given by $\nu_0 = \frac{1}{4} n_0 \bar{c}$, where n_0 is the neutral density in the absence of ionization (it should be emphasized that this latter assumption should be verified experimentally in any given device - see Section 7.3). Therefore each elemental contribution to the received neutral flux density is depleted by the factor $\exp(- \ell(\theta,\varphi)/\lambda)$ where $\ell(\theta,\varphi)$ is the distance from the reception point to the emission point at angle (θ,φ), see Fig.7. From Fig.7 it is easily shown that for cylindrical geometry:

$$\ell(\theta,\varphi) = \frac{2r_0 \cos\theta}{\cos^2\theta + \sin^2\theta \sin^2\varphi} \ . \qquad \ldots (5.18)$$

Hence the total received flux density at a wall point in the presence of ionization is:

$$\iint \bar{c} \cos\theta \ \exp\left\{- \frac{2r_0 \cos\theta}{\lambda(\cos^2\theta + \sin^2\theta \sin^2\varphi)}\right\} n_0 \frac{d\Omega}{4\pi} \ \ldots (5.19)$$

Now we must have conservation of heavy particles in the discharge volume, hence $I_i(\lambda)$ must be:

$$I_i(\lambda) = \tfrac{1}{4} \bar{c} \, n_0 \frac{e}{\pi} \int_{\theta=0}^{\pi/2} \int_{\varphi'=0}^{2\pi} \sin\theta \cos\theta (1 - \exp(-\ell(\theta,\varphi)/\lambda)) d\theta \, d\varphi \qquad \ldots (5.20)$$

where equation (5.16) has been used.

The integral has been obtained numerically on the Oxford KDF9 computer and is given in Fig.8. Note the abscissa is $I_i/\nu_0 e$ but since we have:

$$I = (\gamma\beta/\alpha) \sqrt{\frac{M}{2\pi m}} \, I_i \, \pi r_0^2 \qquad \ldots (5.21)$$

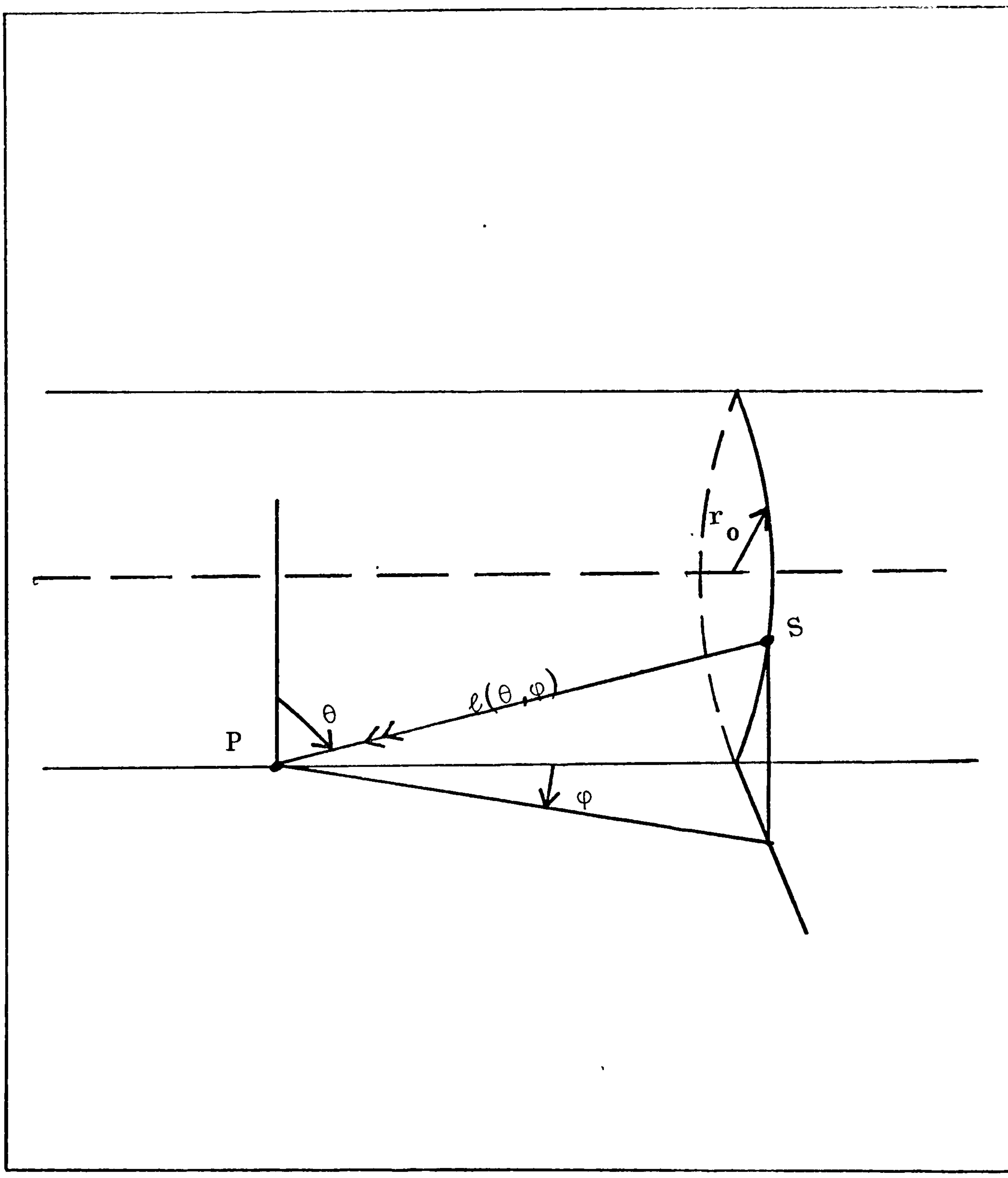

Fig.7

Construction diagram to calculate neutral flux received at wall point P, emitted by wall point S

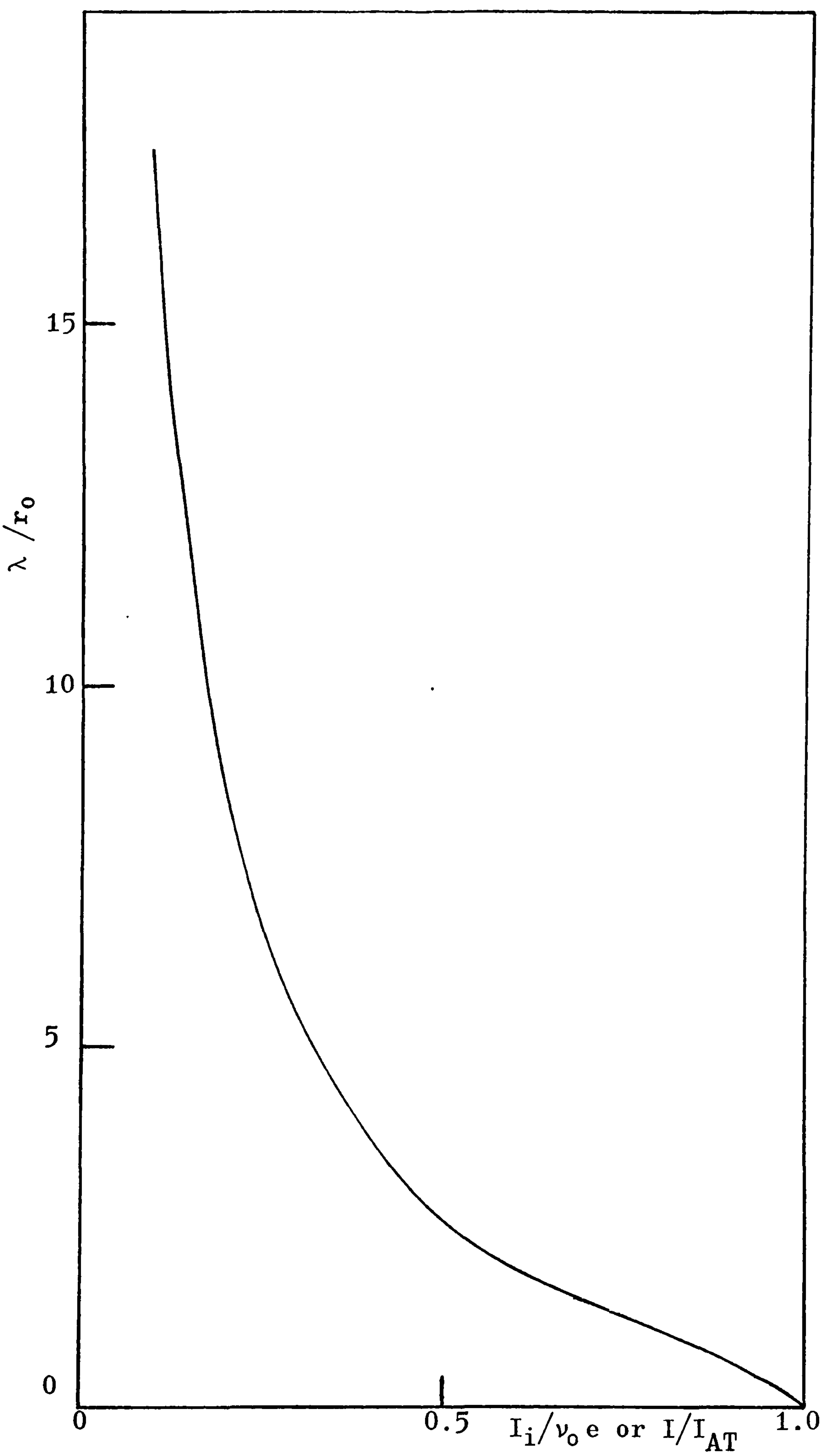

Fig.8

Neutral m.f.p. for ionization, λ, as a function of normalized ion wall current or as a function of normalized arc current and

$$I_{AT} = (\gamma\beta/\alpha) \sqrt{\frac{M}{2\pi m}} \; \nu_o \, e\pi \, r_o^2 \; , \qquad \ldots (5.22)$$

see equations (3.4) and (3.5), then the abscissa may also be written I/I_{AT}, that is we have obtained the required functional relationship $I(\lambda)$.

Note that the Allen-Thonemann limitation occurs when $I_i = \frac{1}{4} n_o \bar{c} e$, i.e. when $\lambda \to 0$, whereas now current limitation occurs for finite λ.

5.3.3 Neutral Density Distribution in the Discharge

It remains to calculate $n(r, p_o, \lambda)$. The solution will be formulated in two equivalent ways for convenience in numerically integrating:

(i) Consider Fig.9. In the absence of a discharge, the elemental area dA_s at point S on the wall emits:

$$\bar{c} \cos\psi \, n_o \frac{d\,\Omega(\psi,\xi)}{4\pi} \, d\,A_s \; , \qquad \ldots (5.23)$$

neutrals/sec. into the elemental cone $d\Omega\,(\psi,\xi)$ where ψ and ξ are the normal and azimuthal angles at S. Hence the flux density across the elemental surface at P viz:

$$d\,Ap = y^2 \, d\,\Omega\,(\psi,\xi) \; , \qquad \ldots (5.24)$$

is:

$$\bar{c} \, \frac{\cos\psi \; n_o}{4\pi \cdot y^2} \, dA_s \quad \text{particles/cm}^2\text{/ sec,} \qquad \ldots (5.25)$$

where $y = |SP|$. This contribution to the density at P is therefore:

$$dn(r,\lambda,p_o) = \frac{n_o \cos\psi}{4\pi y^2} \; dA_s \; . \qquad \ldots (5.26)$$

In the presence of a discharge this is modified as before to

$$dn(r,\lambda,p_o) = \frac{n_o}{4\pi y^2} \, e^{-y/\lambda} \cos\psi \;\; dA_s \; . \qquad \ldots (5.27)$$

From Fig.9, and employing the dotted line construction shown, one may establish the relations:

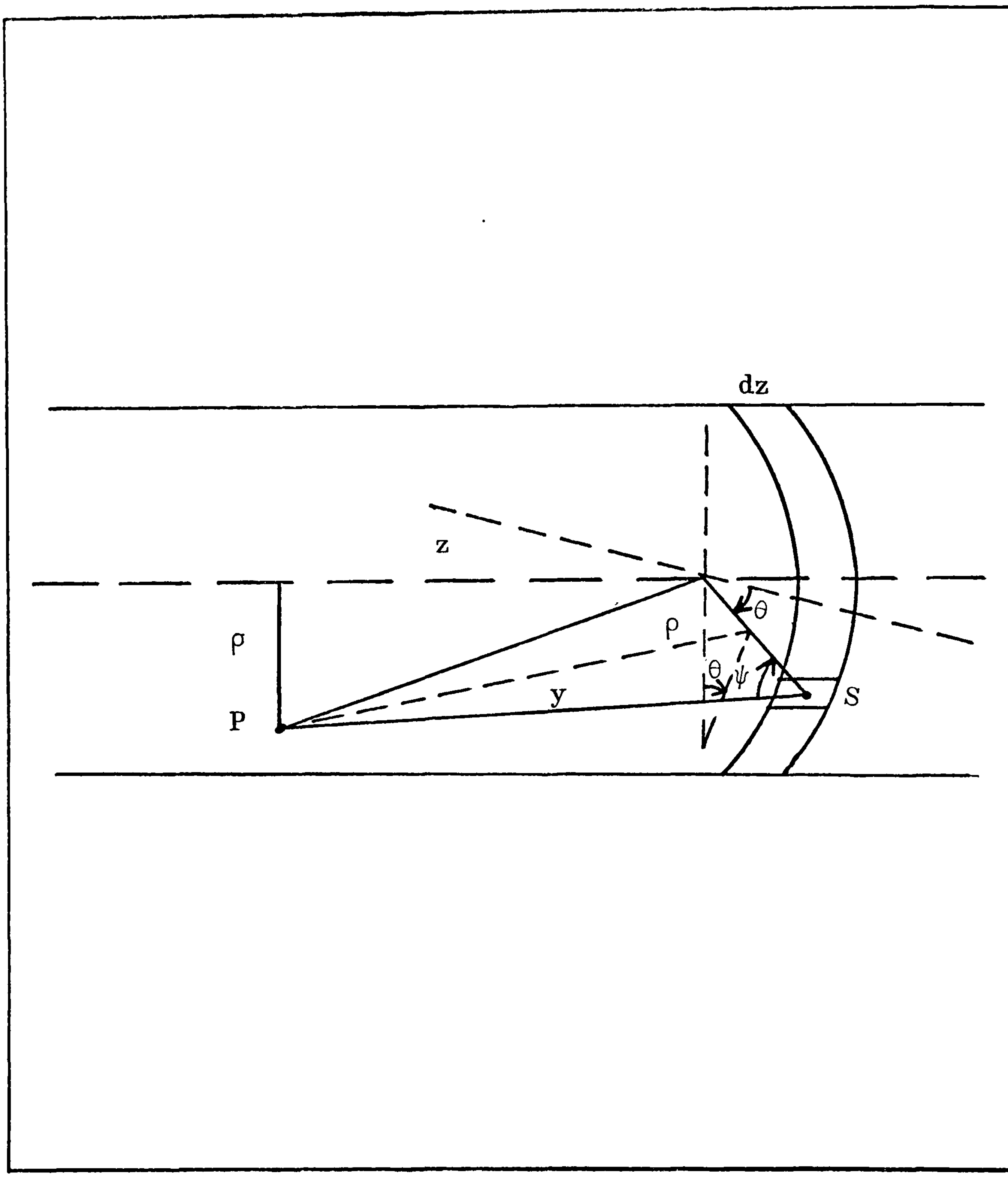

Fig.9

Construction diagram to calculate $n(\rho,\rho_o,\lambda)$, the neutral density at point P. Contributions to the density at point P, emitted by the wall surface element at point S are reduced by the factor $\exp(-y/\lambda)$

$$r_0 = y\cos\psi + r\sin\theta\ , \qquad \ldots (5.28)$$

$$y^2 = r_0^2 + r^2 + z^2 - 2\, r_0 r \sin\theta\ , \qquad \ldots (5.29)$$

$$d\,A_s = r_0\, d\theta\, dz\ . \qquad \ldots (5.30)$$

By using these relations and normalizing with $\rho = r/r_0$, $x = z/r_0$ one obtains:

$$n(p_0,\lambda,\rho) = \frac{n_0}{\pi}\int_{x=0}^{\infty}\int_{\theta=-\pi/2}^{+\pi/2} \frac{(1-\rho\sin\theta)\exp\left[-\left(\frac{r_0}{\lambda}\right)\left(1+\rho^2+x^2-2\rho\sin\theta\right)^{\frac{1}{2}}\right]}{(1+\rho^2+x^2-2\rho\sin\theta)^{\frac{3}{2}}}\, dx\, d\theta\ . \qquad \ldots (5.31)$$

One may note that for $\lambda \to 0$, $n(\rho) \to n_0$ for all ρ as required.

This integral has been obtained by numerical integration and is shown in Fig.10. For $\rho \approx 1$ it is found that convergence is slow and for this reason an equivalent derivation for $n(\lambda,\rho,p_0)$ is given next.

(ii) In the absence of a discharge for any point P in the discharge volume the portion of the neutral density at P which arrived via the elemental solid angle $d\,\Omega(\eta,\zeta)$ is:

$$n_0\,\frac{d\,\Omega(\eta,\zeta)}{4\pi}\ , \qquad \ldots (5.32)$$

and P is the origin for η,ζ. In the presence of a discharge this becomes, as before:

$$n_0\,\frac{d\Omega(\eta,\zeta)}{4\pi}\, e^{-\ell_{PW}(\eta,\zeta)/\lambda} \qquad \ldots (5.33)$$

where $\ell_{PW}(\eta,\zeta)$ is the distance from P to the wall at angle (η,ζ).

Hence:

$$n_p = n(\lambda,p_0,\rho) = \int_{\eta=0}^{\pi}\int_{\zeta=0}^{2\pi} n_0\,\frac{d\Omega(\eta,\zeta)}{4\pi}\, e^{-\ell_{PW}(\eta,\zeta)/\lambda}\ . \qquad \ldots (5.34)$$

From considering Fig.11, one may obtain:

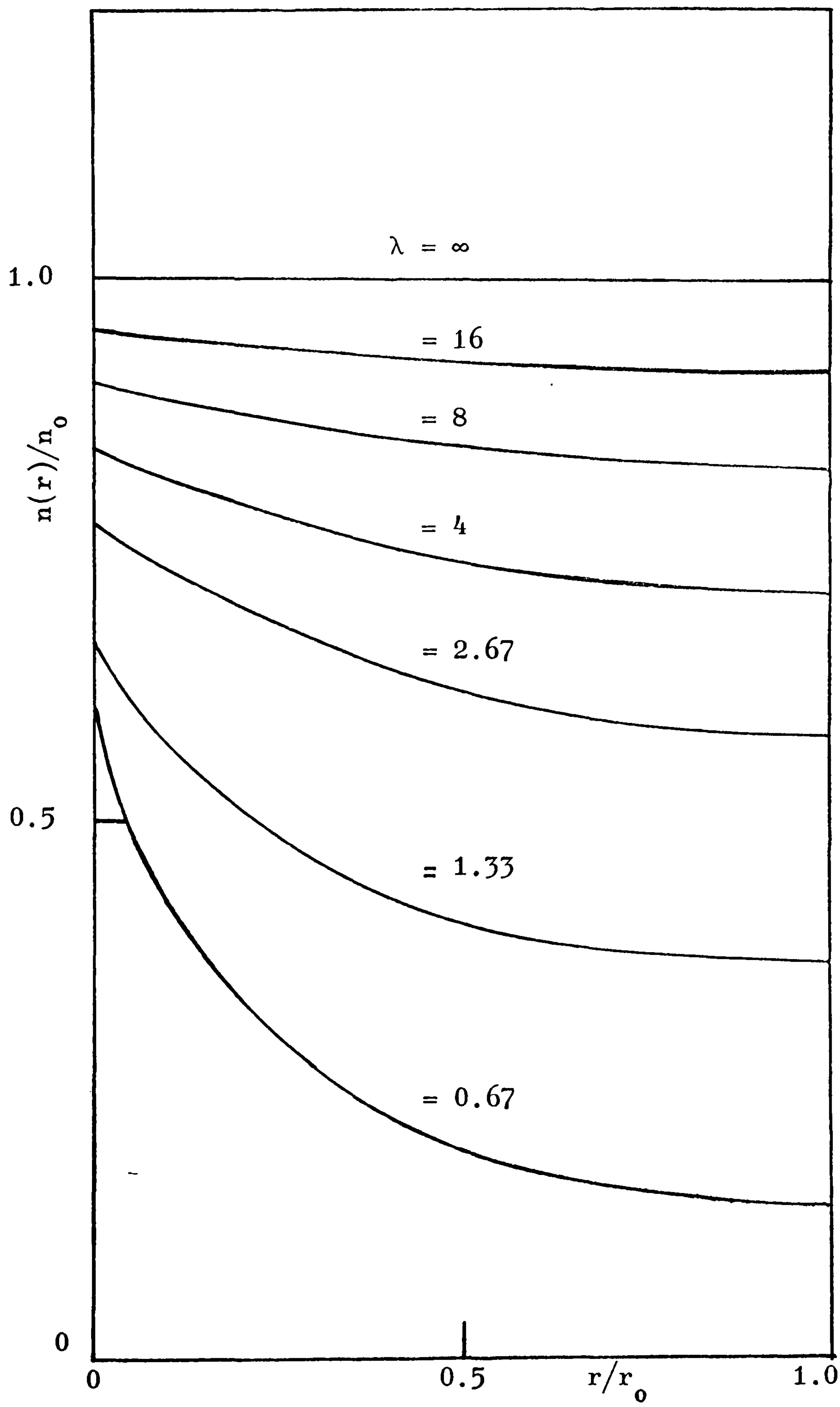

Fig.10

Radial neutral density profiles for various values of λ, the neutral m.f.p. for ionization

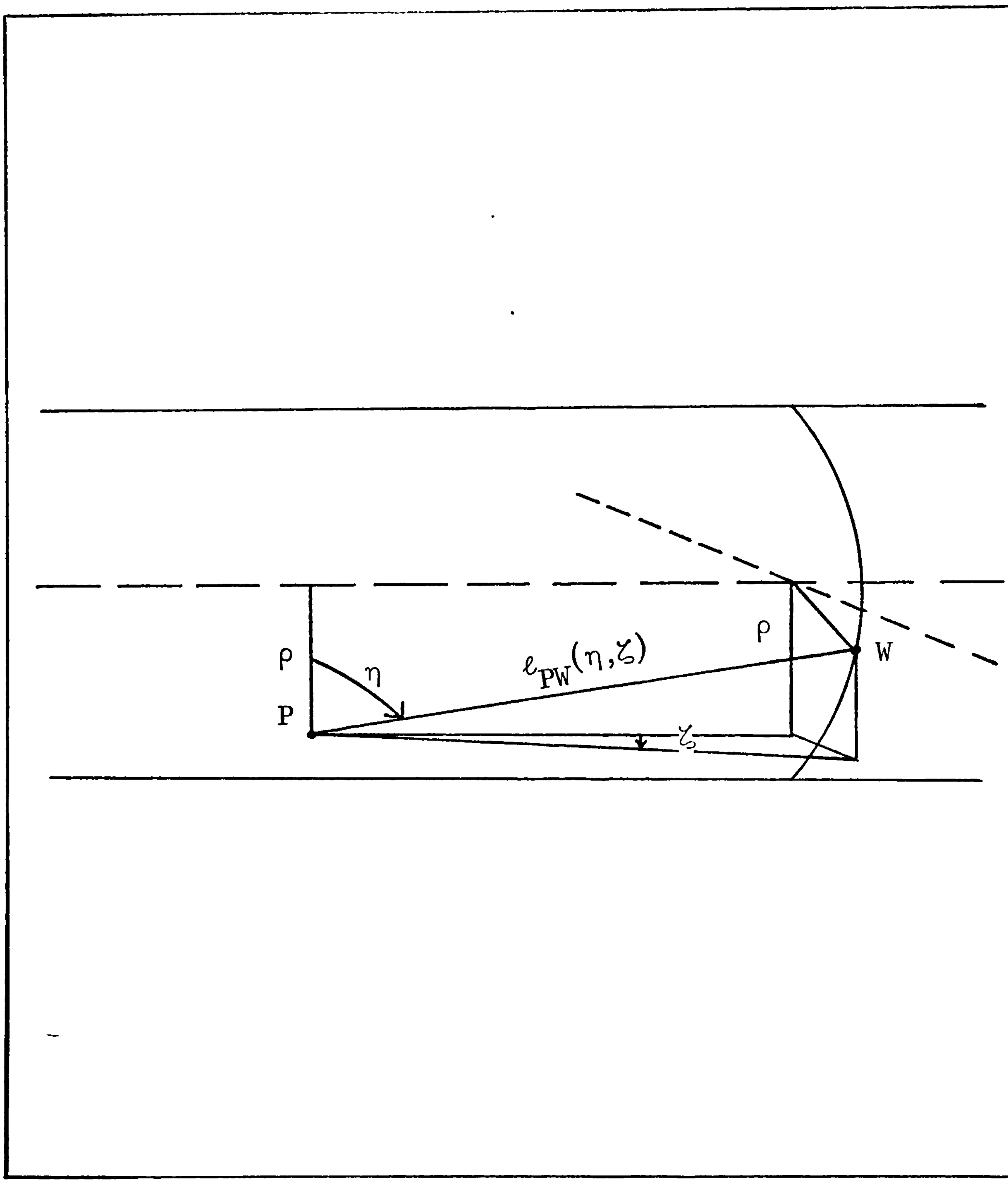

Fig.11

Construction diagram to calculate $\ell_{PW}(\eta,\zeta)$, the distance from any volume point P to wall point W at angle (η,ζ)

$$\frac{\ell_{PW}(\eta,\zeta)}{r_0} = \frac{\rho \cos\eta + \sqrt{\rho^2\cos^2\eta - (1-\rho^2)(\sin^2\eta \sin^2\zeta - 1)}}{1 - \sin^2\eta \sin^2\zeta} \quad \ldots (5.35)$$

If P is just at the wall, i.e. $\rho \simeq 1$, then half the particles arrive at P directly from the wall without attenuation and the remainder as per equation (5.35), hence:

$$n(\rho = 1,\lambda, p_0) = \frac{1}{2} n_0 + \int_{\eta=0}^{\pi/2} \int_{\zeta=0}^{2\pi} n_0 \frac{d\Omega}{4\pi} e^{-\ell(\eta,\zeta)/\lambda} , \quad \ldots (5.36)$$

and now

$$\ell(\eta,\zeta) = \frac{2r_0 \cos\eta}{\cos^2\eta + \sin^2\eta \sin^2\zeta} \quad \ldots (5.37)$$

as in equation (5.18).

The values of $n(\rho = 1,\lambda,p_0)$ obtained numerically provide the $\rho = 1$ points in Fig.10.

5.3.4 Current Limit

From the values of $n(\rho,r,\lambda)$ one obtains the average neutral density across the discharge:

$$\bar{n}(\lambda,p_0) = \frac{1}{\pi}\int_0^1 n(\lambda,\rho,p_0)\, 2\pi\rho d\rho \quad \ldots (5.38)$$

which is given in Table 4.

TABLE 4

AVERAGE NEUTRAL DENSITY V.S. NEUTRAL m.f.p.

λ/r_0	∞	16	8	4	2.67	2	1.33	1	0.67
$\bar{n}(\lambda/r_0)/n_0$	1	0.940	0.874	0.763	0.679	0.608	0.496	0.418	0.311

Now having the relations $\bar{n}(\lambda,p_0)$ and $I(\lambda)$ one readily obtains $\bar{n}(I,p_0)$. The current limit I_L is such that $\bar{n}(I_L,p_0) = C_1/r_0$ and one thereby obtains the required current limitation prediction $I_L(p_0,r_0)$ shown in Fig.12. From this figure one may observe that the current

Fig.12

Current limit vs Hg vapour pressure. Straight line is the Allen-Thonemann current limit. Curved lines are given by the new theory and tend asymptotically to I_{AT} for large p_o

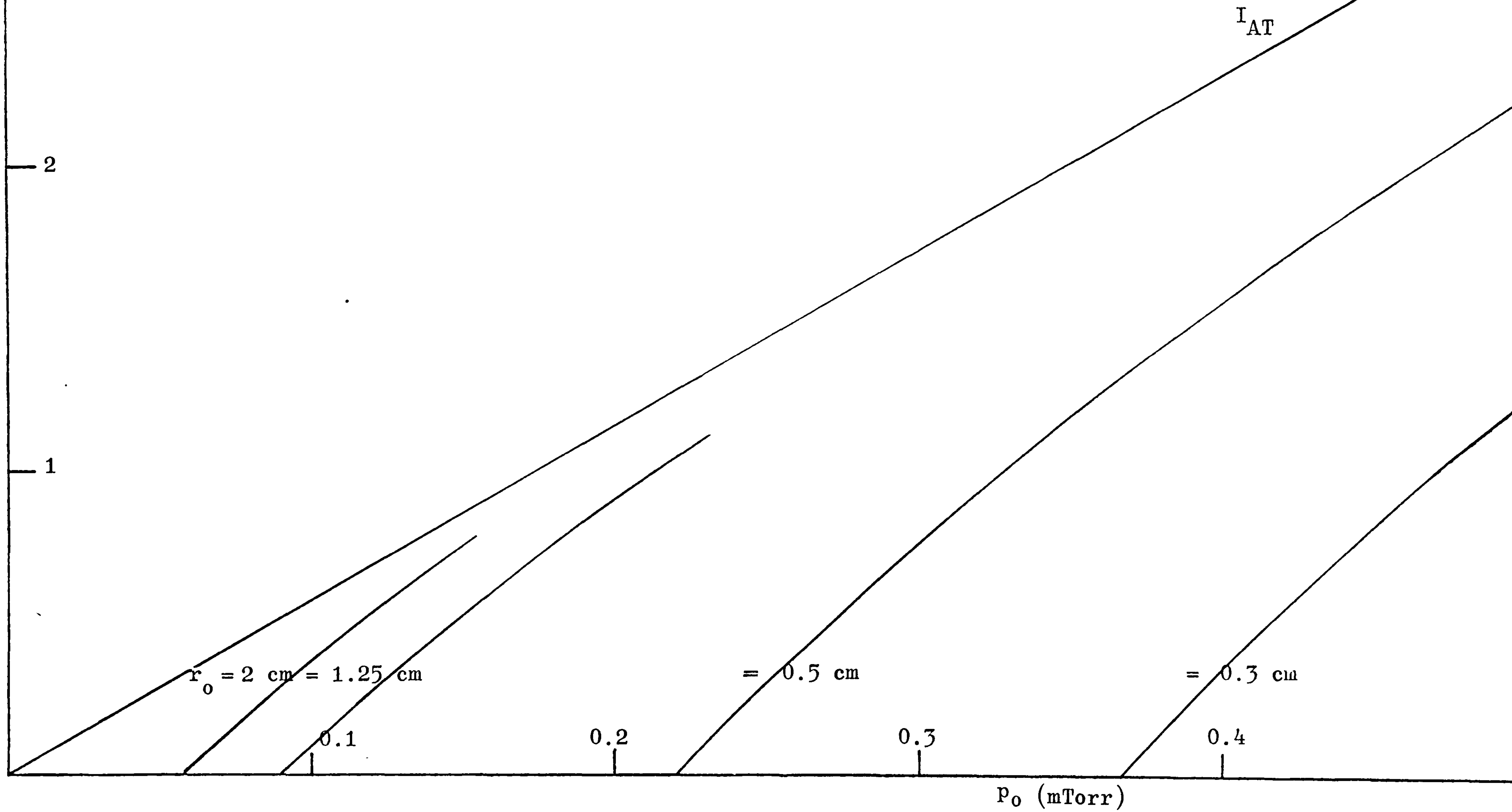

limit falls to zero at finite p_0, and approaches I_{AT} asymptotically for large p_0. The point of contact of each curve with the abscessa is always at $p_0 r_0 = C_1$ of course.

A plot of $\lambda(I_L)$, vs I_L see Fig.13, reveals that:

$$\left(\frac{I_L}{\pi r_0^2}\right) \lambda(I_L) = \text{constant} , \qquad \ldots (5.39)$$

which is to be expected as

$$\lambda\,(I_L) = \frac{\bar{c}}{\bar{n}_e \langle v_e Q \rangle_{max}} , \qquad \ldots (5.40)$$

where $\langle v_e Q \rangle_{max}$ is the neutral ionization coefficient corresponding to maximum ionization efficiency and:

$$I_L = \pi\, r_0^2\, \bar{n}_e\, e\, \beta \sqrt{\frac{kT_{e_L}}{2\pi\, m}} \qquad \ldots (5.41)$$

see equations (3.2) and (3.4), (T_{e_L} must be interpreted as an effective temperature). Thus:

$$\left(\frac{I_L}{\pi r_0^2}\right) \lambda(I_L) = \frac{e\,\beta\sqrt{\frac{kT_{e_L}}{2\pi\, m}}}{\langle v_e Q \rangle_{max}}\, \bar{c} \, . \qquad \ldots (5.42)$$

The fact that Fig.13 is a straight line merely amounts to an internal consistancy verification, and a check that the numerical integrations have been pursued to sufficient accuracy.

5.3.5 A Similarity Relation

R.N. Franklin (1970) has suggested that a similarity relation may hold for $I_L(p_0, r_0)$. Indeed it proves to be the case that I_L/r_0 and $n_0 r_0$ (or $p_0 r_0$) are the similarity variables, see Fig.14. This may be proved as follows: four equations have been used to give $I_L(n_0, r_0)$:

$$I_{i_L} = \frac{1}{4}\, \bar{c}\, n_0\, \frac{e}{\pi} \iint d\theta d\varphi \sin\theta \cos\theta \left[1 - \exp\left\{-\left(\frac{r_0}{\lambda_L}\right)\left(\frac{2 \cos\theta}{\cos^2\theta + \sin^2\theta \sin^2\varphi}\right)\right\}\right] \qquad \ldots (5.43)$$

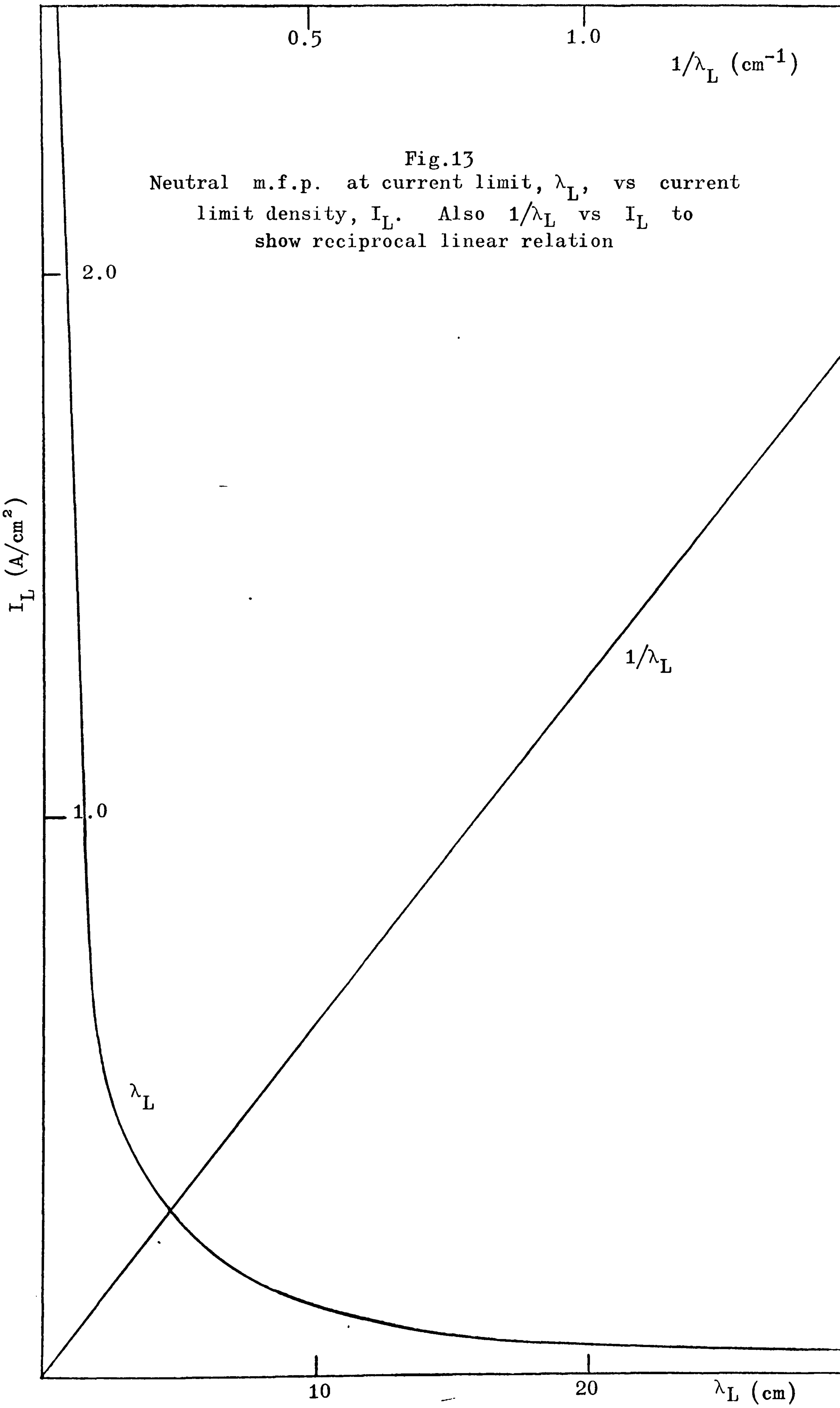

Fig.13
Neutral m.f.p. at current limit, λ_L, vs current limit density, I_L. Also $1/\lambda_L$ vs I_L to show reciprocal linear relation

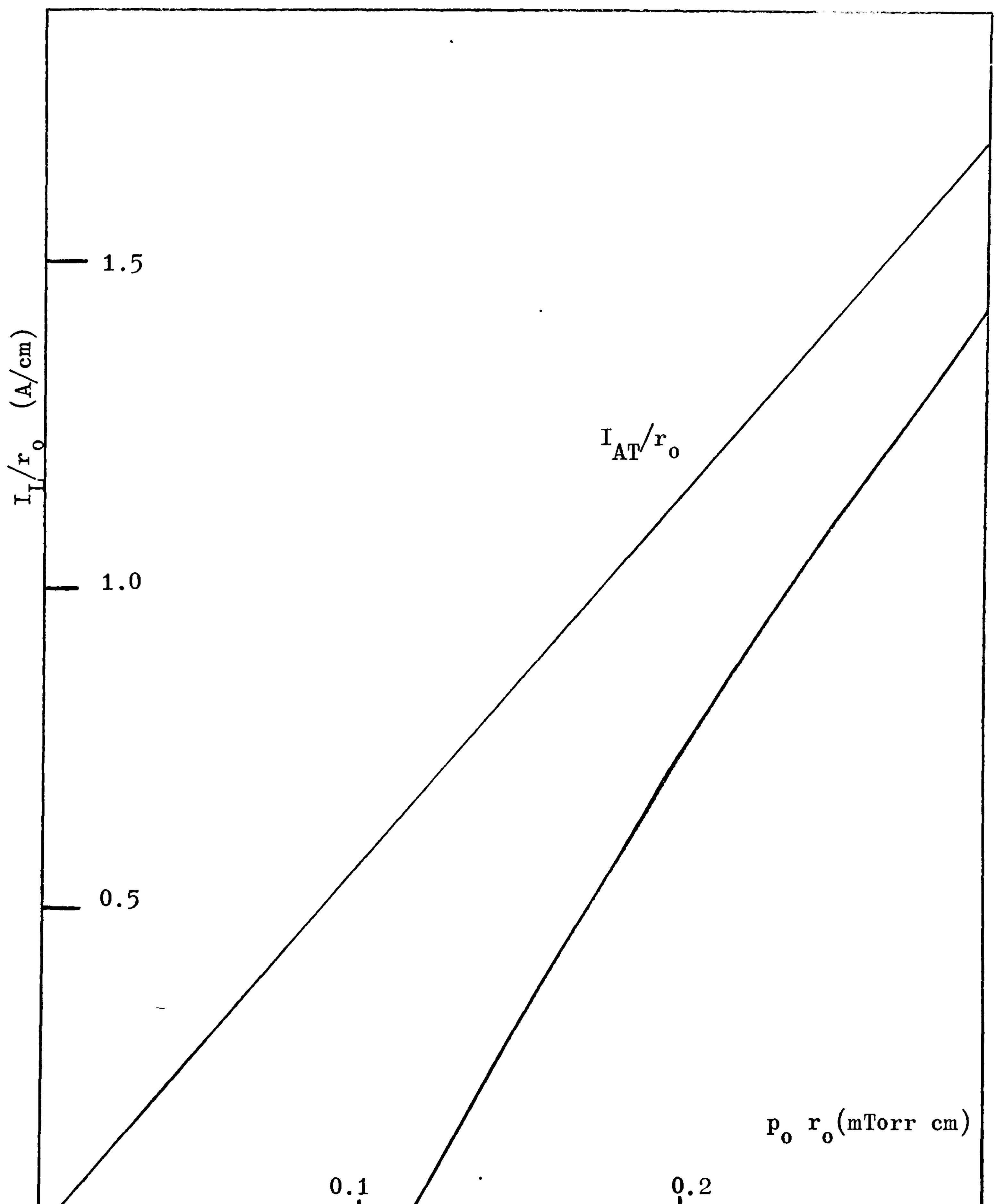

Fig.14
I_L/r_o vs $p_o r_o$, similarity relation
for upper branch current limit

$$I_L = \left(\frac{\gamma\beta}{\alpha}\right)\sqrt{\frac{M}{2\pi m}}\,\pi\, r_o^2\, I_{i_L} \qquad \ldots (5.44)$$

$$\bar{n}_L = \frac{n_o}{\pi^2}\iiint \frac{d\rho\, dx\, d\theta\, 2\pi\rho\,(1 - \rho\sin\theta)\exp\left[-\left(\frac{r_o}{\lambda_L}\right)\left(1 + \rho^2 + x^2 - 2\rho\sin\theta\right)^{\frac{1}{2}}\right]}{(1 + \rho^2 + x^2 - 2\rho\sin\theta)^{\frac{3}{2}}} \qquad \ldots (5.45)$$

$$\bar{n}_L = C_1 / r_o\ . \qquad \ldots (5.46)$$

From equation (5.43)

$$I_{i_L} = n_o\, f(r_o/\lambda_L), \qquad \ldots (5.47)$$

where f is a function of r_o/λ_L only. From equations (5.44) and (5.47)

$$I_L/r_o = r_o n_o \sqrt{\frac{M}{2\pi m}}\;\frac{\pi}{4}\,\bar{c}\; f(r_o/\lambda_L), \qquad \ldots (5.48)$$

so that:

$$(I_L/r_o) = (r_o n_o)\, g\, (r_o/\lambda_L)\ , \qquad \ldots (5.49)$$

and g is a function of r_o/λ_L only.

From equation (5.45):

$$\bar{n}_L = n_o\, h(r_o/\lambda_L)\ , \qquad \ldots (5.50)$$

with h a function of r_o/λ_L only. Combining (5.46) and (5.50):

$$h(r_o/\lambda_L) = C_1/(n_o r_o)\ , \qquad \ldots . (5.51)$$

hence:

$$r_o/\lambda_L = h^{-1}\left[\frac{C_1}{(r_o n_o)}\right], \qquad \ldots (5.52)$$

and from (5.49):

$$r_o/\lambda_L = g^{-1}\left[\frac{(I_L/r_o)}{(r_o\, n_o)}\right]\ , \qquad \ldots (5.53)$$

so that from (5.52) and (5.53):

$$(I_L/r_o) = (r_o n_o)\; g\left\{h^{-1}\left[\frac{C_1}{(r_o n_o)}\right]\right\} \qquad \ldots (5.54)$$

5.3.6 Extension of Theory to Case of Velocity Dependent Neutral M.F.P.

In reality λ , the m.f.p. of a neutral for ionization, is a function of the neutrals' speed and the neutrals obey a Maxwellian distribution of speeds (in the absence of ionization). The velocity dependence is linear so that we are free to define λ' such that:

$$\lambda = \lambda' \; v/\bar{c} \qquad \ldots (5.55)$$

where v is the particular neutral speed and $\bar{c}$ is the r.m.s. neutral speed.

The neutral flux density received at an element of wall surface in the absence of a discharge is:

$$\frac{1}{2\pi\bar{c}^3} n_o \int_{\eta=0}^{\pi/2} \int_{\zeta=0}^{2\pi} \int_{v=0}^{\infty} v \cos\eta \; v^2 \, e^{-v^2/\bar{c}^2} \sin\eta \; dv \, d\eta \, d\zeta \; , \qquad \ldots (5.56)$$

according to Maxwell. Thus as before the ion wall current must be

$$I_i/\tfrac{1}{4} n_o \bar{c} e = \frac{2}{\pi} \int\int\int \sin\eta \cos\eta \; v^3 e^{-v^2} \left(1 - e^{-\ell(\eta,\zeta)/\lambda' v}\right) dv \, d\eta \, d\zeta \; , \qquad \ldots (5.57)$$

where $v \equiv v/\bar{c}$ and $\ell(\eta,\zeta)$ is as in equation (5.37):

$$\ell(\eta,\zeta) = \frac{2r_o \cos\eta}{\cos^2\eta + \sin^2\eta \, \sin^2\zeta} \; . \qquad \ldots (5.58)$$

In a parallel fashion we may obtain the neutral density at volume point P :

$$n(\lambda', \rho, p_o) = \pi^{-\frac{3}{2}} n_o \int_{v=0}^{\infty} \int_{\theta=0}^{\pi} \int_{\varphi=0}^{2\pi} v^2 e^{-v^2} \; e^{-\ell_{PW}(\theta,\varphi)/\lambda' v} \sin\theta \; dv \, d\theta \, d\varphi \; , \qquad \ldots (5.59)$$

where $\ell_{PW}(\theta,\varphi)$ is the same as in equation (5.35).

In practice, of course, the calculation of integrals (5.57) and (5.59) would be very expensive on computer time, and so they are merely set forth here without carrying the computations to completion.

5.4 LOWER CURRENT LIMIT IN THE UN-CONSTRICTED COLUMN

5.4.1 Introduction

The wall sheath thickness is of the order of the Debye length:

$$\lambda_D = \left(\frac{\varepsilon_o \, kT_e}{n_e e^2} \right)^{\frac{1}{2}}$$

As $n_e \propto I$, it is obvious that for small currents the wall sheath will grow to occupy a larger portion of the discharge volume. As the plasma is the principle region of arc current conduction, the effective radius of the discharge is seen to be dependent on I i.e. $r = r(I)$ effectively.

The situation is completely parallel to that of section 5.3, only now by decreasing the current the point is reached where $r(I_L) = C_1/p_o$ resulting in current limitation. Now p is no longer a function of current as the ionization level is so low, just as in section 5.3, $r = r_o$, independent of current, because the sheath was so thin.

Unfortunately, for these larger $\alpha \equiv \sqrt{2}(\lambda_D/r_o)$, (notation of Self, (1963)), the division of the column into sheath and plasma becomes increasingly artificial. No longer is there a plasma region with very little radial variation of potential and a sharply defined sheath containing most of the potential drop. Instead the potential variation comes to be spread over most of the radius. In these circumstances it is most sensible to solve the full Poisson equation for all r and this has been done numerically by Self (1963) for plane geometry, Parker (1963) for cylindrical geometry, see also Franklin and Ockendon (1970).

5.4.2 Simple Theory

As a first attempt at a theory for this lower current limit, we shall assume, despite the foregoing, a sharp division of the column into plasma and sheath. Our limitation prescription is:

$$r(I_L) = C_1/n_0 \ , \qquad \dots (5.61)$$

and it remains to find $r(I)$.

This effective radius of conduction must be given by:

$$r(I_L) = r_0 - C_2 \lambda_D \qquad \dots (5.62)$$

where C_2, a constant, gives the thickness of the sheath in Debye lengths. This equation is indeed a crude estimation, for not only is there no sharp plasma-sheath distinction, but C_2 itself is a function of λ_D . (That is, while there is no unique definition of the plasma-sheath boundary for finite α , one may arbitrarily choose one, see Self (1963), having done so, one discovers that C_2 itself is dependent on α.) Fortunately this dependence is slight, Self finds $9 < C_2 < 20$ for a large range of α, with the smaller values corresponding to $\alpha \sim 0{\cdot}1$. Accordingly we shall make the estimation that $C_2 \simeq 9$, a constant.

For a Maxwellian electron distribution:

$$\lambda_D = \left(\frac{\varepsilon_0 k T_e}{n_e \ e^2}\right)^{\frac{1}{2}} \ . \qquad \dots (5.63)$$

In the present case $f_L(\vec{v}_e)$, the electron distribution near current limit, is probably fairly non-Maxwellian, nevertheless it is assumed that $f_L(\vec{v}_e)$ is independent of r_0, n_0,etc, hence at current limit

$$\lambda_D^2 \ n_e = C_3 \ , \qquad \dots (5.64)$$

with C_3 a constant.

From equations (3.2) and (3.4) we have:

$$I = C_4 \ n_e \ r^2 \ , \qquad \dots (5.65)$$

where

$$C_4 = \beta \sqrt{\frac{kT_e}{2\pi m}} \ \pi \ e \ , \qquad \dots (5.66)$$

and T_e will have to be interpreted as an effective temperature; β is assumed to be a constant here as in the high current case.

Combining equations (5.61, 62, 64 and 65) gives the explicit formula for the lower current limit:

$$I_L(n_o, r_o) = \frac{C_1^2\, C_2^2\, C_3\, C_4}{(r_o n_o - C_1)^2} \;. \qquad \ldots (5.67)$$

For Hg we take the estimates $\beta \approx 1$, $Te_L \approx 10$ eV, and obtain:

$$C_3 \approx 5.5 \times 10^8 \text{ m}^{-1} \qquad \ldots (5.68)$$

$$C_4 \approx 2{\cdot}7 \times 10^{-13} \text{ amp m}^{-1} \;. \qquad \ldots (5.69)$$

For $r_0 = 5$ mm and $12{\cdot}5$ mm, the upper and lower current branches are shown in Fig.15. No attempt has been made to establish theoretical values for the transition between the two branches owing to the uncertainty in the constants.

This simple theory while containing several approximations gives surprisingly good agreement with experiment, see section 7.1. In light of the uncertainty in C_2 alone, which effects I_L as C_2^2, the close agreement must be considered fortuitous.

5.4.3 Refined Theory

The approximations involved in the constant C_2 may be removed but at the price of sacrificing the simplicity of equation (5.67). Equation (5.62) giving $r_{eff}(\alpha)$ may be replaced with a numerical relation obtained from the full calculated profiles of Parker (1963) etc. The procedure is as follows: from the calculated $n_e(r)/n_e(o)$ profiles $r_{eff}(\alpha)$ is obtained:

$$\pi \left(\frac{r_{eff}(\alpha)}{r_o}\right)^2 = \int_0^1 2\pi\rho\, \frac{n_e(\rho)}{n_e(o)}\, d\rho \qquad \ldots (5.70)$$

$$\rho = r/r_o$$

From equations (5.63) and (5.65) one finds that:

$$I = \beta \sqrt{\frac{kT_e}{2\pi m}}\; \pi e\; 2\, \frac{\varepsilon_o k T_e}{e^2}\, \frac{1}{\alpha^2} \left(\frac{r_{eff}(\alpha)}{r_o}\right)^2 . \qquad \ldots (5.71)$$

Fig.15a
Upper and lower current limit lines as a function of Hg bath temperature for $r_0 = 1{\cdot}25$ cm (theory). Arc existance is only possible within the two 'arms'

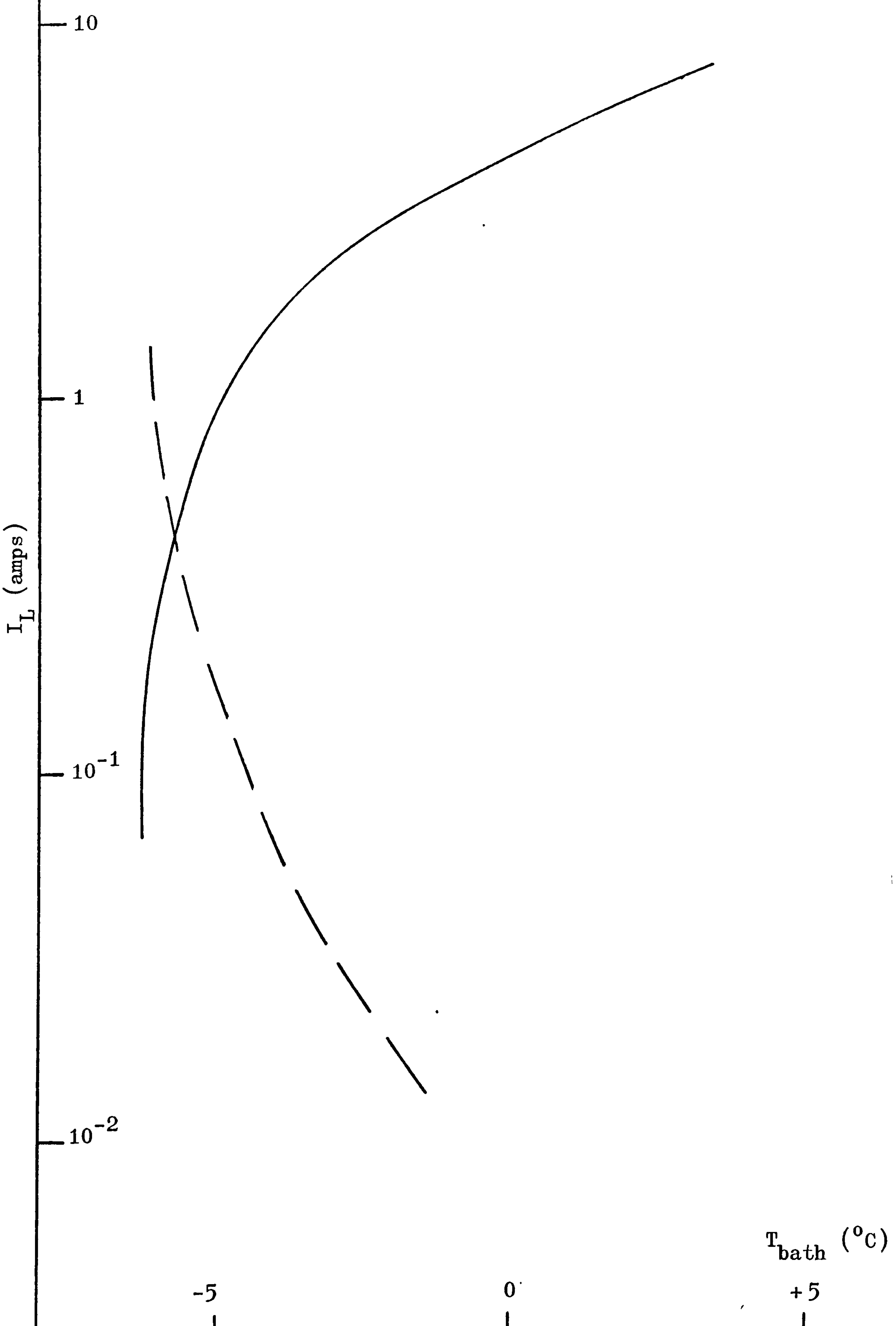

Fig.15b
Upper and lower current limit lines as a function of Hg bath temperature for r_o = 0.5 cm (theory). Arc existance is only possible within the two 'arms'

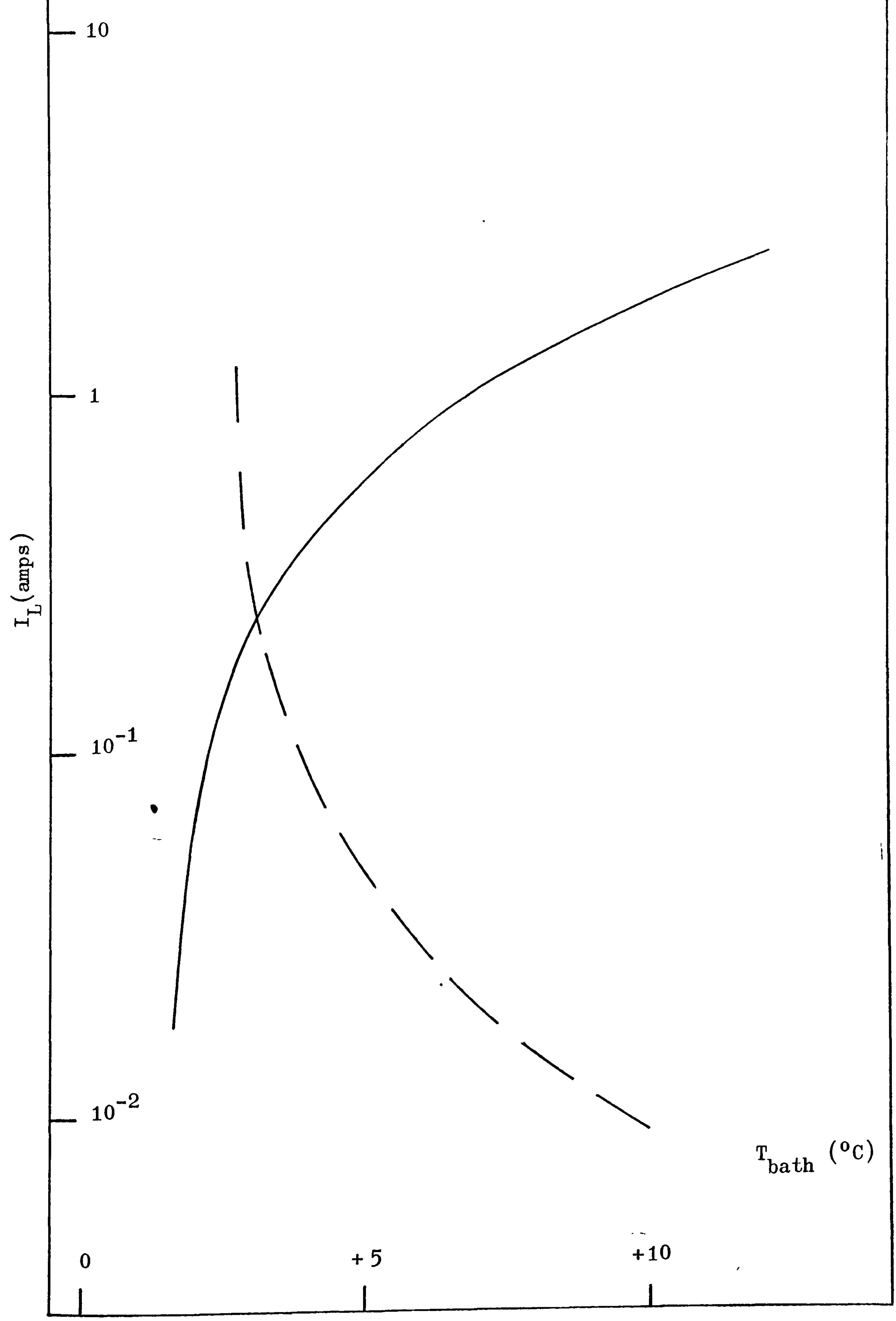

Thus from the two relations $I(\alpha)$ and $r_{eff}(\alpha)/r_0$ one eliminates α (much as λ was eliminated in the high current theory) to obtain $r_{eff}(I)/r_0$. Current limit I_L is such that:

$$\frac{r_{eff}(I_L)}{r_0} = \frac{C_1}{n_0 r_0} \quad \ldots (5.72)$$

Parker (1963) in fact has already calculated $r_{eff}(\alpha)/r_0$ as he presents figures for:

$$\frac{\bar{n}_e}{n_{eo}} = \frac{1}{\frac{1}{2}\, r_0^2\, n_{eo}} \int_0^{r_0} n_e(r)\, r\, dr \quad \ldots (5.73)$$

as a function of α (his parameter $\beta = (2/1\cdot092)\alpha^{-1}$) and obviously

$$\left(\frac{r_{eff}(\alpha)}{r_0}\right)^2 = \frac{\bar{n}_e}{n_{eo}} \quad \ldots (5.74)$$

The relation $r_{eff}(\alpha)$ is given in Fig.16. (In obtaining r_{eff} one must use the electron density throughout, since the electrons are the principle means of conduction. For larger α of course, charge neutrality is no longer even approximately valid - see Forrest and Franklin (1968)).

From equation (5.71) and Fig.16, one obtains $I(\alpha)$, shown in Fig.17. Again it has been assumed that $\beta = 1$, $T_{e_L} = 10$ eV, thus:

$$\beta \sqrt{\frac{kT_e}{2\pi m}}\, \pi e\, 2\, \frac{\varepsilon_0 k T_e}{e^2} = 3\cdot02 \times 10^{-4} \text{ amps.} \quad \ldots (5.75)$$

From Figs.16 and 17 one obtains $\dfrac{r_{eff}(I)}{r_0}$ shown in Fig.18. For high currents the effective radius approaches $\sqrt{2h_0}\, r_0$ as in the Tonks-Langmuir theory.

From equation (5.72) and Fig.18, one obtains the current limit curve $I_L(n_0, r_0)$. This is shown in Fig.19 together with the result from equation (5.67).

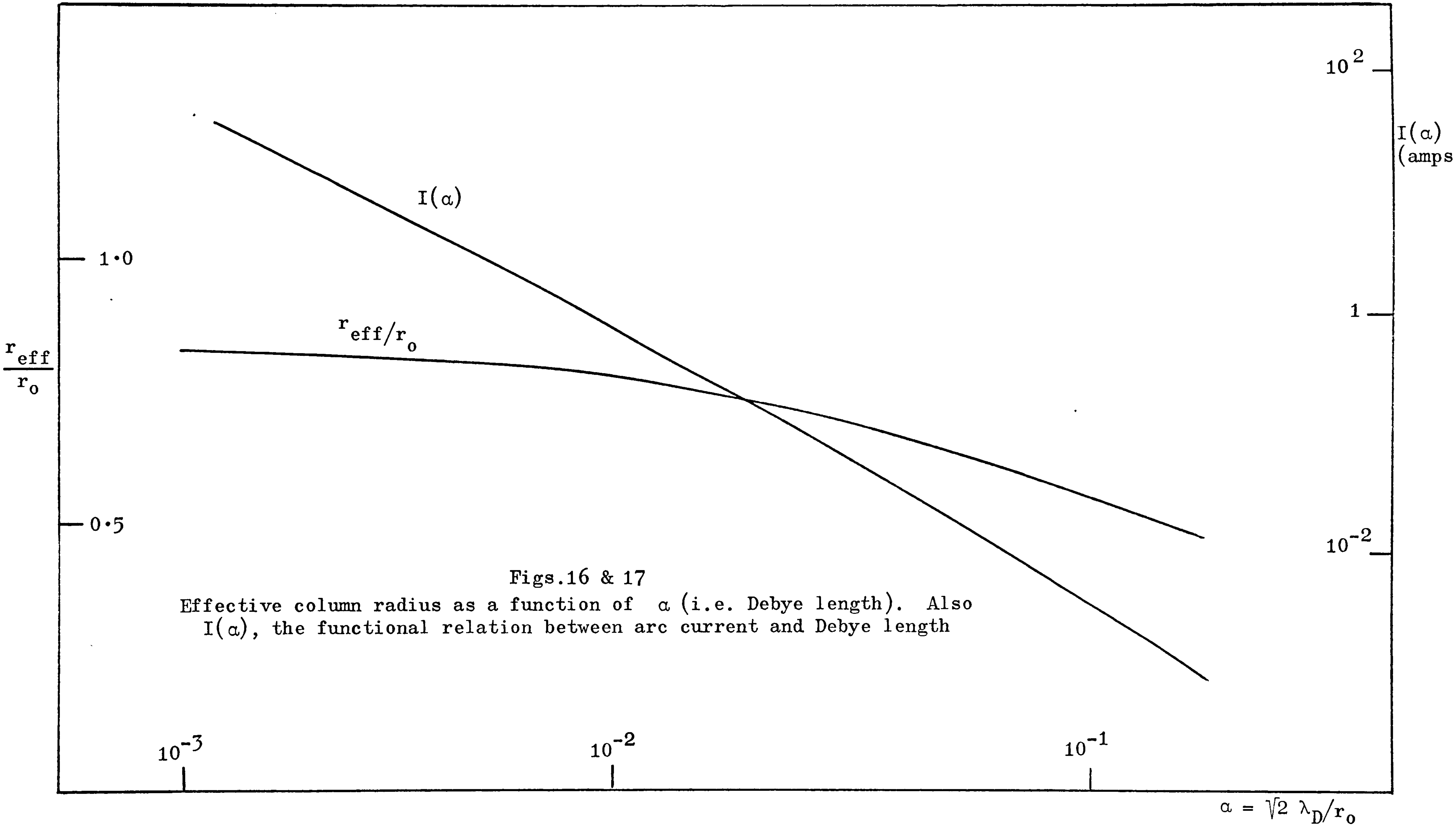

Figs.16 & 17
Effective column radius as a function of α (i.e. Debye length). Also $I(\alpha)$, the functional relation between arc current and Debye length

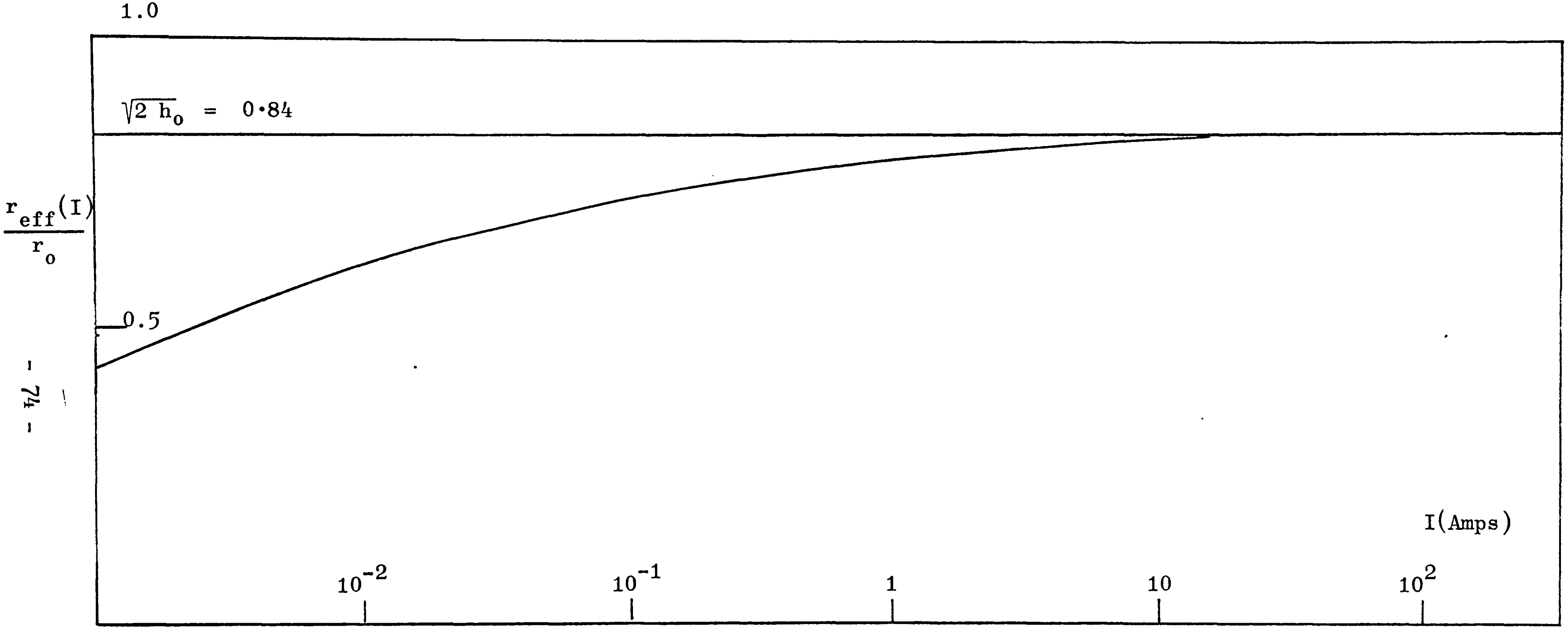

Fig.18
Effective column radius as a function of current. Small currents correspond to thick wall sheaths and hence to smaller column radii

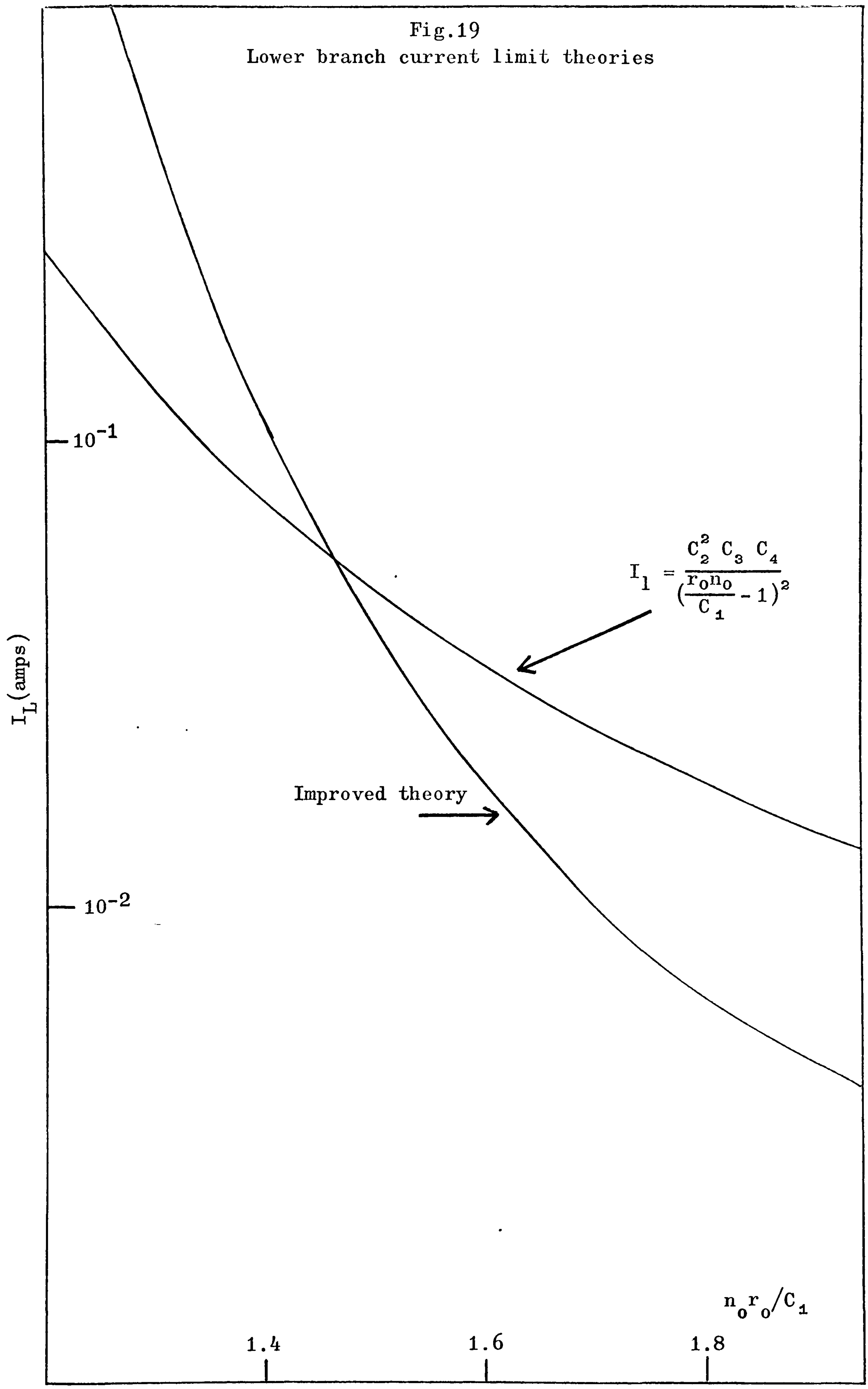
Fig.19
Lower branch current limit theories
I_L(amps)
10^{-1}
10^{-2}
$I_1 = \frac{C_2^2\ C_3\ C_4}{(\frac{r_o n_o}{C_1} - 1)^2}$
Improved theory
$n_o r_o / C_1$
1.4
1.6
1.8

The foregoing analysis amounts to a calculation of $C_2(I)$ to replace the constant value assumed in the simple theory. It may be observed that $C_1 = C_1(I)$ as well. It will be recalled, section 5.2.3, that C_1 contains the structural factor $S_0 = 0{\cdot}7722$ obtained from the Tonks-Langmuir theory. In this regime of large α, S_0 is no longer constant but $S_0 = S_0(\alpha)$ as shown by Self (1963), thus $S_0 = S_0(I)$, thus $C_1 = C_1(I)$.

In principle $C_1(I)$ may be calculated using the work of Self (adapted to the cylindrical case), however it will be recalled, section 5.2.3, that even when S_0 is a constant, the precise calculation of C_1 is not possible.

In light of the many difficulties in calculating the C_i properly, it is concluded that the simple theory provides as adequate a picture as is likely to be available. Partial refinements probably do not warrant the effort.

5.5 CURRENT LIMITATION IN THE CONSTRICTED COLUMN

5.5.1 The Double Sheath at a Constriction

While published literature on this subject is very extensive, see section 2.3, a comprehensive and consistent physical picture, even on a qualitative basis, is still not available. It is intended to formulate such a qualitative description in this section, by combining observations made by previous authors in a fully consistent way. No attempt at quantitative accuracy is made at this stage.

The discussion shall be limited to the case of the double sheath which is observed to form when an abrupt reduction is made in the positive column radius of a low pressure discharge, see Fig.20a — thus the work of Poletaev and Klarfeld (1939), Schönhuber (1957), Crawford and

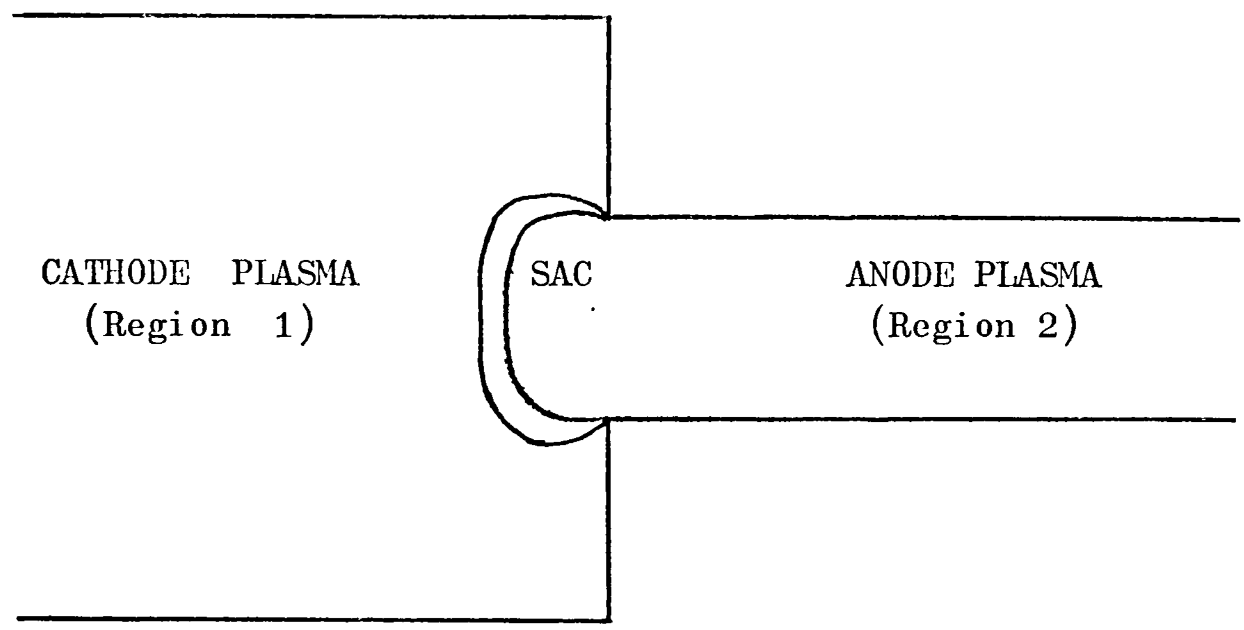

Fig.20a
Double sheath formed at simple constriction

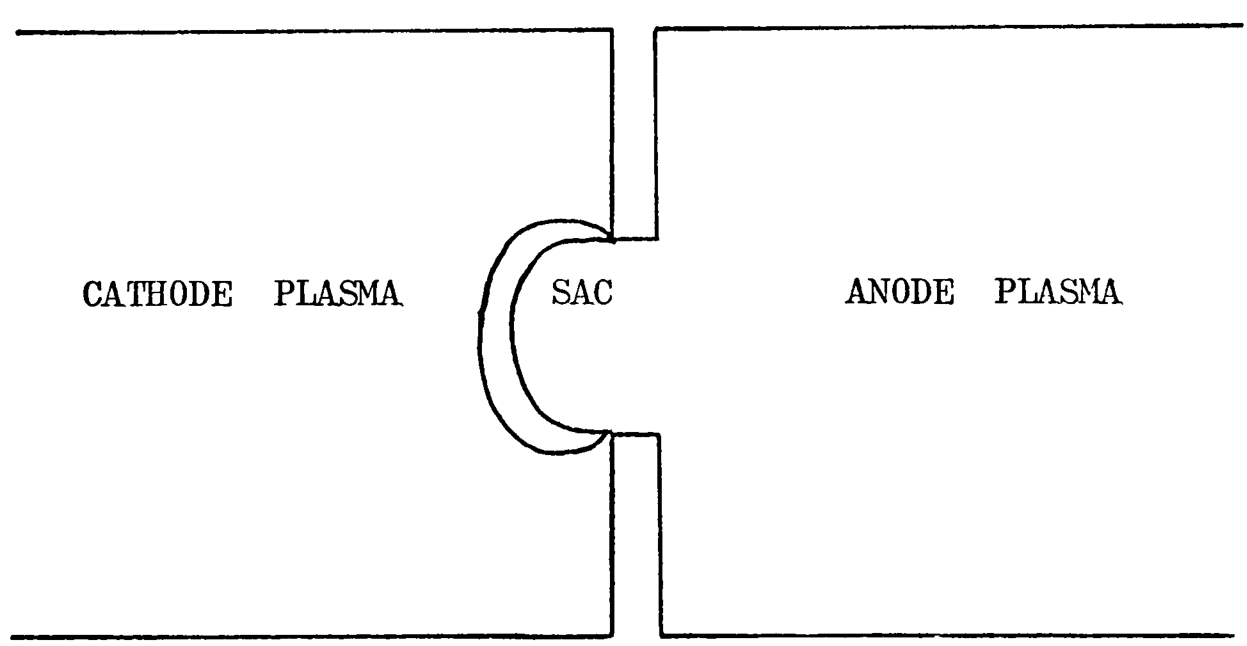

Fig.20b
Double sheath formed at constriction
of Hg arc rectifier type

Freeston (1963, and Andersson et al (1969). We shall not consider the more complex case of double sheaths which form in arc rectifier valves, i.e. where the constriction depth is comparable to the radius, see Fig.20b. This case is more complex as there are three different plasmas mutually interacting, i.e. the anode and cathode plasma, and the highly luminous sac plasma just at the constriction, nor shall we consider the double sheath near the cathode which is not part of the positive column proper. Also excluded are striations in a column of uniform cross-section, which are thought to be a form of double sheath, Schönhuber (1957), Emeleus and Breslin (1968).

We may consider five questions of basic interest in this problem:

(1) Why does a d.s. form?

(2) What is the relation between V_{ds} (the double sheath voltage drop) and the four independent variables $p_0, r_1, r_2, \bar{I}$?

(3) Why does the d.s. bulge out into a 'sac' (Hoyaux (1965))?

(4) What is the relation between the size of the bulge and the four independent variables?

(5) What role does such a d.s. play in the current limit phenomenon of a constricted tube?

These questions are dealt with in turn.

5.5.2 The Cause of a Double Sheath

It is important to emphasize that there are two independent reasons for d.s. formation, and two distinct criteria must be satisfied simultaneously. The two requirements are termed:

(a) T_e/ ionization level requirements;

(b) n_e /current requirements;

described as follows.

(a) T_e / ionization Level Requirements

T_e is a monotonically decreasing function of pr, hence $T_2 > T_1$. However, half the electrons in region 2 (at least within one electron m.f.p. of the constriction) came from region 1 - thus these latter must be abruptly accelerated to make up the difference, i.e. very roughly $V_{ds} \approx \frac{k}{e} (T_2 - T_1)$. In addition there are increased ion losses from region 2 over and above that which corresponds to a tube or radius r_2 viz, the ion losses over the d.s. itself. That is, a d.s. first forms just to make up the ΔT_e but to have a self-consistent d.s., Andrews (1969), there will have to be extra ion losses just to satisfy d.s. existence criteria. The result is that extra electron acceleration is required, i.e.

$$V_{ds} \approx \frac{k}{e} (T_2 - T_1) + V', \qquad \ldots (5.76)$$

with V' some extra drop.

(b) n_e/Current Requirements

As $I_1 = I_2$ and $I \propto r^2 n_e$, then $n_2 > n_1$. For the adjacent co-existance of different n_e, a d.s. must form to reduce electron losses from region 2 (as in a semi-conductor junction) - in fact there must be a net electron drift in the opposite direction, from region 1 to 2, constituting the tube current. If electrons arrive at both sides of the d.s. with random velocities (this is not strictly true, Andrews (1969), however we only want to establish functional relations) then:

$$I = \left[\tfrac{1}{4} n_1 \bar{v}_1 - \tfrac{1}{4} n_2 \bar{v}_2 \, e^{-eV_{ds}/kT_e} \right] \pi r_2^2 \qquad \ldots (5.77)$$

where $\bar{v}_1$ and $\bar{v}_2$ are average random electron velocities in regions 1 and 2, and no bulge is assumed at present.

5.5.3 Relation between V_{ds} and p_0, r_1, r_2, I

We have:

$$V_{ds} \approx \frac{k}{e} (T_2 - T_1) + V' \qquad \ldots (5.78)$$

where

$$V' = V'(n_2, T_2) . \qquad \ldots (5.79)$$

Also, from the low pressure discharge similarity relations:

$$T_e = T_e(p_o , r) , \qquad \ldots (5.80)$$

$$n_e = n_e(I, r, p_o), \qquad \ldots (5.81)$$

thus:

$$V_{ds} = \frac{k}{e}\left[T_e(p_o, r_2) - T_e(p_o, r_1)\right] + V'\left[n_e(I, r_2, p_o), \; T_e(p_o, r_2)\right] \qquad \ldots (5.82)$$

which gives a relation between V_{ds} and r_1, r_2, I, p_o. However, at the same time we must satisfy:

$$I = \left[\tfrac{1}{4}\, n_e(I, r_1, p_o)\, \bar{v}_e\Big(T_e(p_o , r_1)\Big) - \tfrac{1}{4} n_e(I, r_2, p_o)\, \bar{v}_e\Big(T_e(p_o, r_2)\Big) \times e^{-e\, V_{ds}/kT_e(p_o, r_2)}\right] \pi\, r_2^2 \qquad \ldots (5.83)$$

which also gives a relation between V_{ds} and r_1, r_2, I, p_o. Obviously equations (5.82) and (5.83) cannot be satisfied simultaneously in general which leads us to the third question.

5.5.4 Cause of d.s. Bulge

In order to satisfy both T_e/ionization requirements and n_e/I requirements simultaneously, the discharge must vary some other factor. Distorting the d.s. out into a sac is a way of achieving this.

5.5.5 Relation between Bulge magnitude and V_{ds}, I, r_1, r_2, p_o

Assume a bulge factor B which expresses the linear magnitude of the bulge:

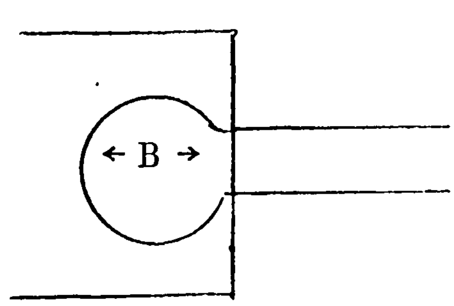

thus the surface area of the sac $\propto B^2$, volume $\propto B^3$.

For T_e/ionization requirements, V' is effected as the ion loss rate over the d.s. goes as B^2, while creation rate in the sac goes as B^3, i.e.

$$V' = V(n_2, T_2, B) \quad , \qquad \ldots (5.84)$$

thus:

$$V_{ds} = \frac{k}{e}\left[T_e(p_o, r_2) - T_e(p_o, r_1)\right] + V'(n(I, r_2, p_o), T_e(p_o, r_2) \ , B) \qquad \ldots (5.85)$$

The n_e/I requirements are effected depending on whether or not the accelerated electrons are fast randomized in the sac by beam-plasma interactions, Hoyaux and Williams (1967), or by collisional effects, Crawford and Freeston (1963).

If randomization is not fast, then electrons travelling thus

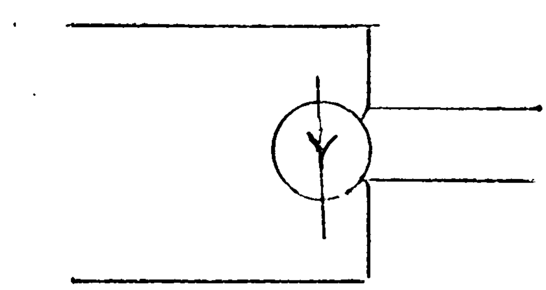

will probably pass right through the sac (the electron m.f.p. at 1 mTorr is $\sim$ 5 cm) and not contribute to I. If fast randomization occurs, then all electrons crossing the d.s. will contribute to I.

Assuming slow randomization then equation (5.83) remains as before and gives:

$$V_{ds}(I, r_1, r_2, p_o) \ .$$

Then B takes on such a value as to satisfy equation (5.85) consistent with this value of V_{ds}.

If randomization is fast then in equation (5.83), the term $\pi r_2^2 \rightarrow B^2$, thus B and V_{ds} take up such values as to satisfy the two equations simultaneously. One thereby relates B and V_{ds} and also obtains:

$$B(p_o, r_1, r_2, I) \quad .$$

Needless to say, the actual computation of any of these quantities would be extremely difficult. The aim here has been merely to outline the functional relationship between all the variables.

5.5.6 Effect of the d.s. on Current Limitation

Current limitation of the arc will be established by whichever limit is the lower, that due to the d.s., or that due to the long column of radius r_2, i.e. as per section 5.3.

While neutral depletion in the d.s. region may be more severe than in the long column (due to the additional ion loss over the d.s.), there are two strong reasons why the current limit may nevertheless be established by the long column.

(1) The sac has the ability to grow thus reducing ion losses relative to ion creation, whereas the column geometry is fixed.

(2) The electron distribution in the column at current limit is unable to rise much above an effective electron temperature of ≈ 10 eV (this is because higher electron energies can only be gained by the electrons travelling a long distance down the tube and thereby risking energy loss by inelastic collisions with neutrals) whereas many of the sac electrons gained their energy in a short distance, i.e. the d.s. thickness and, depending on n_e/I requirements, may have a fairly high energy $\simeq 10-50$ eV. This latter electron distribution is much more sharply peaked than the former, and hence a more efficient ionizing distribution. (In fact it has been proposed, Andrews and Varey (1970a), that such an electron distribution, with electrons in a selected energy range, may be highly efficient for chemical syntheses in the arc, or in selectively populating high energy levels for lasers.) In the formula to calculate $(pr)_{min}$, equation (5.5), one may observe that a sharply peaked electron energy distribution will correspond to a lower $(pr)_{min}$ than will the broader Maxwellian distribution.

Thus, semi-quantitatively, we have for the column:

$$\text{ion loss rate} \approx 2\pi\, r_2\, n_s \sqrt{\frac{kT_e}{M}}\,, \qquad \ldots (5.86)$$

$$\text{ion creation rate} \approx \pi\, r_2^2\, n_g \bar{n}_e\, g\,[f_c(\varepsilon)] \qquad \ldots (5.87)$$

where $f_c(\varepsilon)$ is the electron energy distribution in the column, and $g[f_c(\varepsilon)]$ gives the ionization rate. Thus we have:

$$\bar{n}_g\, r_2 \approx 2\sqrt{\frac{k}{M}}\; \frac{T_2^{\frac{1}{2}}}{g[f_c(\varepsilon)]} \qquad \ldots (5.88)$$

and current limitation in the column occurs when the current causes so much neutral depletion that $\bar{n}_g$ is reduced to the point of making :

$$\bar{n}_g(I_L) r_2 \approx 2\sqrt{\frac{k}{M}}\; \frac{T_{2_L}^{\frac{1}{2}}}{g[f_{c_L}(\varepsilon)]} \qquad \ldots (5.89)$$

and $f_{c_L}(\varepsilon)$ corresponds to $T_{2_L} \approx 10$ eV.

In the sac:

$$\text{ion loss rate} \approx 4\pi\, B^2\, n_s \sqrt{\frac{kT_e}{M}}\,, \qquad \ldots (5.90)$$

$$\text{ion creation rate} \approx \frac{4}{3}\pi B^3 \bar{n}_e\, \bar{n}_g\, g[f_s(\varepsilon)]\,, \qquad \ldots (5.91)$$

where $f_s(\varepsilon)$ is the electron energy distribution in the sac (and no attempt has been made to incorporate proper d.s. ion velocity criteria). Balance gives:

$$\bar{n}_g(I)\, B \approx 3\sqrt{\frac{k}{M}}\; \frac{T_e^{\frac{1}{2}}}{g[f_s(\varepsilon)]}\,. \qquad \ldots (5.92)$$

Now current limitation in the sac may be avoided to a certain degree by B growing as $\bar{n}_g(I)$ decreases - although there may be some limit to this as very large B may be unstable or energetically unfavourable and at any rate we must have $B < r_1$.

More importantly $g[f_{s_L}(\varepsilon)]$ is almost certainly greater than $g[f_{c_L}(\varepsilon)]$ and hence the current limit prescription for the sac is not as severe as for the column, i.e.

$$(pr)_{min_{column}} > (pr)_{min_{sac}} .$$

5.5.7 Complications at the Double Sheath

In certain experimental conditions complications may occur which lead to current limitation by the d.s. instead of by the column, despite the foregoing.

(a) If the anode region is not a sink for neutrals then the electrophoretic effect, Kenty (1938), whereby neutrals move towards the anode due to elastic collisions with electrons, will be replaced by a neutral density gradient build-up towards the anode, Torvén (1968). In this case $\bar{n}_g(I,p)$, where p is the local neutral pressure, may stay above C_1/r_0 in the column and current limitation at the sac will occur first. This may be happening in the experiments of Andersson et al (1969), and makes the interpretation of their results difficult. This unnecessary inhomogeneity should be avoided, at least for the purpose of studying basic processes.

(b) Gas blow-out at the d.s. may occur, Tonks (1937), Andrews (1969). That is the electron flow across the d.s. in some circumstances may result in the removal of sac neutrals, not by ionization, but simply by momentum transfer. This increased neutral depletion in the sac could bring about current limiting conditions here before they occur in the column.

To estimate this latter effect, consider the results reported in section 8.1, for:

$$r_2 = 5 \text{ mm} \quad , \quad p_0 \doteq 0{\cdot}5 \text{ mTorr} \quad , \quad I_L \approx 2\text{A}.$$

Following Andrews (1969) we note that the total momentum gained per second by electrons crossing the d.s. is:

$$M_e = (m\ v_e)\ I_{e/e} \ ,$$

where:

$$v_e = (2\ eV_{ds}/m)^{\frac{1}{2}} .$$

At $p_o = 0 \cdot 5$ mTorr, the m.f.p. of the electrons for momentum transfer is ~ 10 cm, Crawford and Kino (1961), so that about 5% of this momentum is transferred to the neutrals in the sac region. The effective pressure $p_e \approx \dfrac{0 \cdot 05 \, M_e}{\pi \, r_2^2}$ is found to be $p_e \approx 0.014$ N/m^2 assuming $V_{ds} \approx 10$ V. The restoring force for neutrals $p_o = 0 \cdot 5$ mTorr = $0 \cdot 067$ N/m^2 so that even at these relatively low values of I_L, neutral blow-out is starting to be effective. Andrews (1969), similarly finds that in the higher I,p studies of deVilliers (1968) $p_e \approx p_o$ and also depletion on the cathode side of the d.s. due to ion-neutral collisions is a comparable effect.

5.5.8 Conclusion

In the simplest case of no gas blow-out and well controlled vapour conditions it seems probable that the double sheath does not cause current limitation. The calculation of $(pr)_{min}$ for the sac region cannot be accomplished with any precision, so that ultimately the matter must be established experimentally, see section 7.1.4.

In the presence of inhomogeneities, Andersson et al (1969), it may be that current limitation does occur at the double sheath in which case the theory of current limitation at the d.s., Torvén (1969), may be applicable, although adequate theoretical analysis of this situation is probably unobtainable.

CHAPTER VI

EXPERIMENTAL APPARATUS

6.1 INTRODUCTION

The aim in the design of the experimental discharge tube was to achieve such a level of control over the physical variables that a proper experimental verification of the current limit theory of Chapter V would be possible.

Considerable interest in the current limitation phenomenon has been shown by electrical engineers over the decades, as Hg rectifier valves operate at such pressures as to encounter this effect. However, their research is usually done in a configuration approximating that of a valve. This configuration is remarkably ill-suited for the study of the basic processes involved, as so many interconnected phenomena are occurring simultaneously.

In a valve, where the arc length is of the order of the tube diameter, one is always close to the Hg cathode spot. This spot is highly disruptive of Hg vapour conditions, as a spray of Hg droplets is thrown off from the spot, Quigley (1968) etc. To a certain degree, the spray may be confined by placing an umbrella directly over the spot, but even so disruption occurs; de Villiers and Sander (1969), for example, encountered this disruptive effect in their time dependent limitation studies.

Flow effects resulting from vacuum pumping may disrupt vapour conditions. Very high current levels cause heating and play havoc with the vapour conditions.

In a short discharge, the electrons are not fully Maxwellianized - they still 'remember' their fall over the d.s. at the cathode, see, e.g.

Rayment and Twiddy (1968). In fact, for the positive column to be truly independent of the electrode regions, the discharge must be several metres long, thus concludes Crawford and Self (1965), for only then is the 'average electron' more likely to be lost to the column wall, than to the anode (Hg vapour and $p_0 \simeq 1$ mTorr, assumed).

At sharp bends in the low pressure discharge, double sheaths may form to aid current continuity. As such sheaths have an uncertain effect on the current limit phenomenon, they should be avoided. At any rate, double sheaths are a known source of fluctuations and discharge noise, Crawford and Self (1965), and their effect on current limitation. is uncertain.

The double sheath at a constriction, of course, may have quite considerable disruptive effects on the discharge, see section 5.5, and in the simplest case it should be avoided if one wishes to obtain an experimental arrangement approximating the positive column theory of section 5.3 and 5.4.

Most discharge vessels employ an anode which does not behave as a neutral sink, e.g. Andersson et al (1969) in which case a neutral density gradient builds up towards the anode, Kenty (1938), Torvén (1968) etc. This constitutes a further disruptive influence on neutral density conditions.

As the current limit I_L is so sensitive to the local neutral density it is apparent that the latter must be very carefully controlled if readily interpretable results are to be obtained.

6.2 DISCHARGE TUBE DESIGN

In Fig.21 an overall view of the vessel is given. The construction is entirely of glass and quartz throughout, O-rings or greased joints have been avoided.

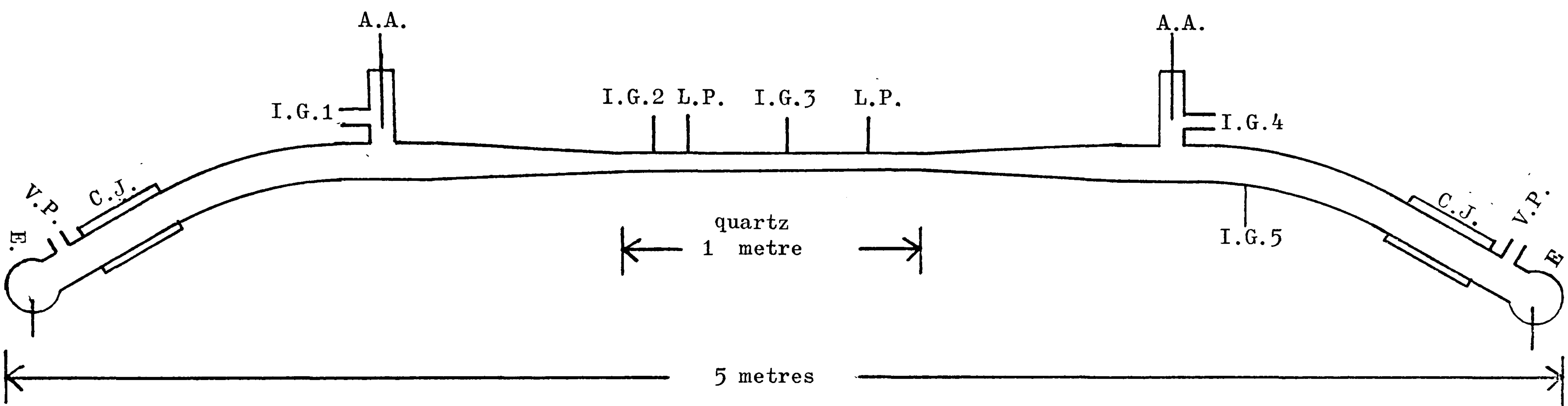

Fig.21
Discharge tube. E, electrode; V.P., to vacuum pump; C.J., cooling jacket; I.G., ion gauges; A.A., auxiliary anode; L.P., Langmuir probe

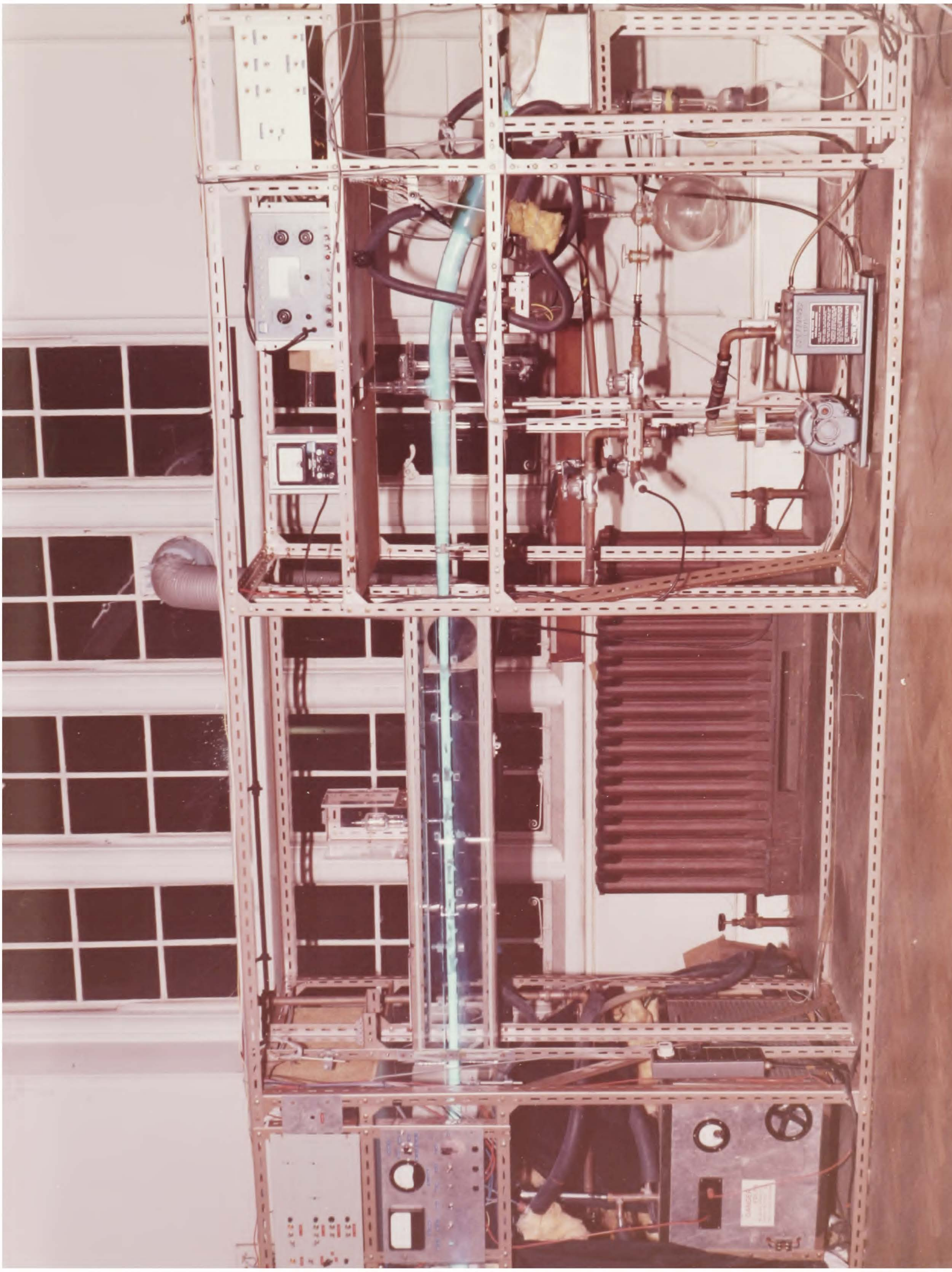

Plate 1
View of discharge apparatus in operation

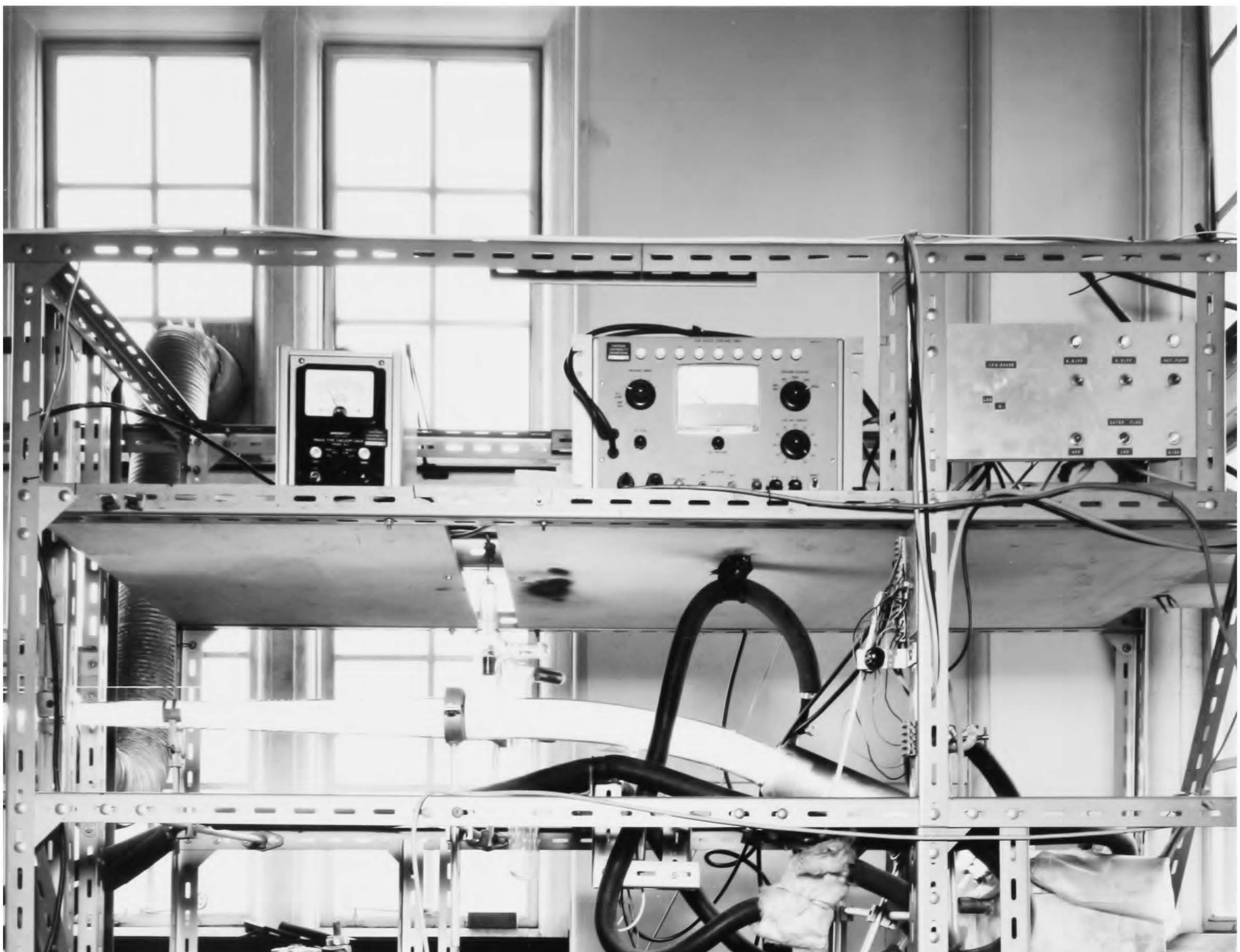

Plate 2
Close-up of discharge apparatus showing
one end in greater detail

The vessel, 5 metres in length, is symmetrical and the discharge may be run in either direction. The end electrodes, shown in Fig.22, are Hg pools with tungsten pins, 2 mm in diameter, to anchor the cathode spot (an unanchored spot is a known source of discharge noise). The entire cathode bulb is immersed in a bath of circulating coolant, the coolant flows over the top of the bulb. Only by such direct electrode cooling will the electrode heating be kept from disrupting vapour conditions in the experimental region.

Over the electrode is a tantalum disc umbrella of such a size and position as to block the Hg droplet spray from entering the positive column. An auxilliary arc of up to 5 amps may be run to the umbrella if this is needed to stabilize the cathode spot, also for low main arc currents, an auxilliary current must be run to keep the spot alive.

The tungsten rod striker was found to be ineffective for helping to initiate the discharge, but an externally applied tesla coil was usually quite sufficient (supplemented with a hot-air blower on the bulb, if necessary).

Just into the positive column, at both ends, are the pumping ports to the 17 l/sec. glass Hg diffusion pumps (water cooled). Each diffusion pump is backed by a 5 litre glass reservoir which acts as a backing vessel if one wishes to switch off the rotary pump (an Edwards ED75, 1·25 l/sec). The pressure in the backing spheres is monitored with Edwards GSC2 Pirani gauges. Just before the rotary pump are anti-vibration bellows and a cold trap to keep Hg from contaminating the rotary pump. From the reservoirs on, the system is entirely of glass without grease, and therefore the attainment of good vacuum is comparatively easy, i.e. pressure of residual gas $< 10^{-6}$ torr. In the event of water coolant failure, the diffusion pumps are automatically switched off.

Fig.22
Electrode assembly (full scale)

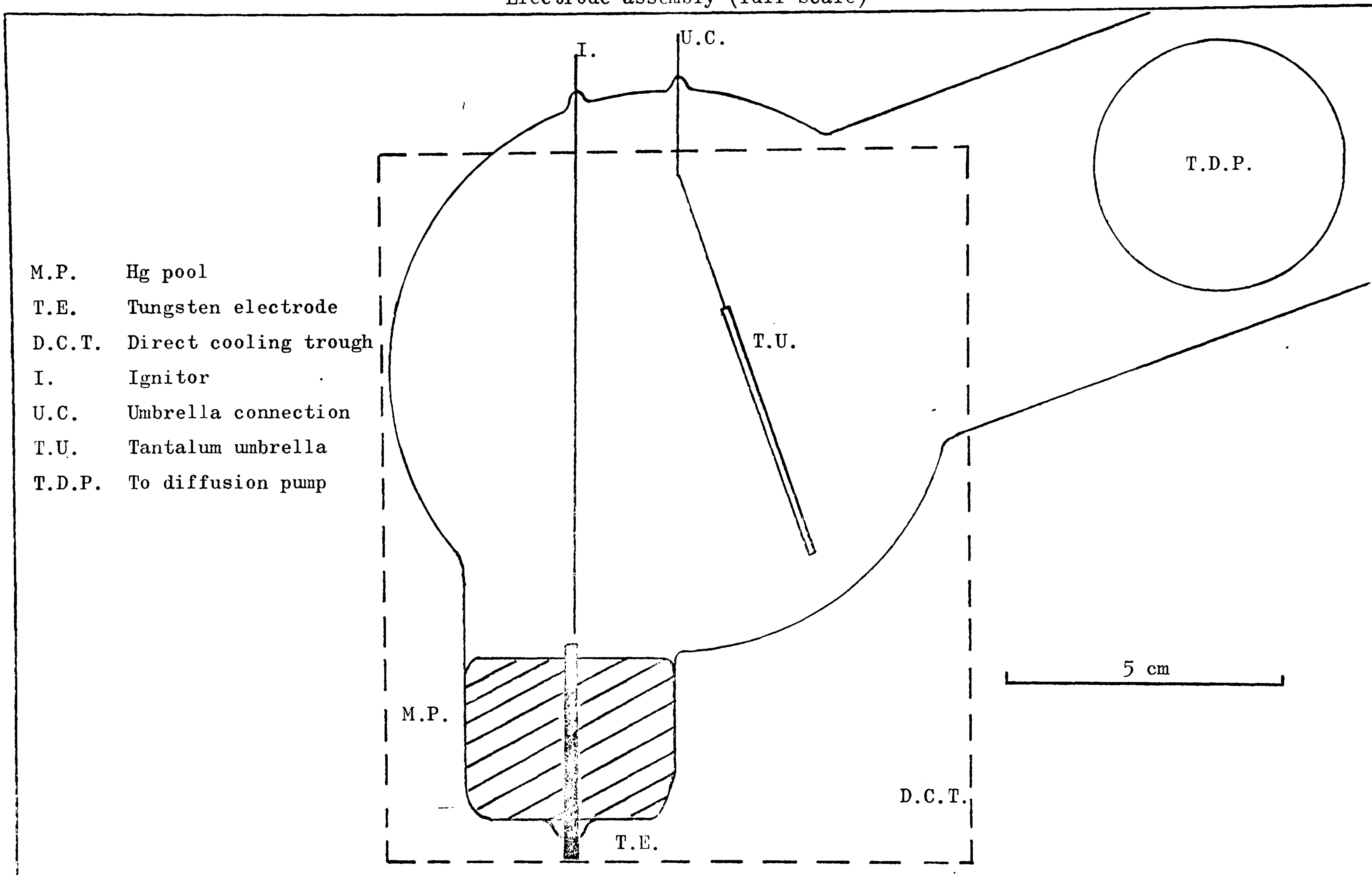

The end regions, with their pressure-disrupting effects, are separated from the central experimental region by 30 cm long, cooling jackets. The coolant through the jackets is temperature controlled and Hg is induced to condense on the discharge walls inside the jackets. In this way neutral density conditions in the central region are established independently of electrode effects (at least, the jackets can control vapour conditions in the central region provided that the electrode regions are not allowed to become excessively hot). In this way, positive column conditions may be varied independently of electrode conditions, and one may verify that current limitation is not due to electrode region effects, i.e. it is a genuine positive column phenomenon. Excess condensed Hg runs down the gentle slope (20^{o} from the horizontal) into the electrode pools.

Even in fairly good vacuum conditions liquid Hg is known to develop a surface oxide layer which reduces its vapour pressure. However, the Hg condensed on the jacket walls is subject to ion bombardment during the discharge, and remains clean. Liquid Hg elsewhere in the system and not subject to such bombardment was found to develop a crust.

Having such a Hg condensing region at the anode ends means that the neutral density gradients are avoided and a flow of Hg vapour takes place instead. One result is that the anode Hg pool gradually fills up.

It is important, of course, that temperature controlled jackets be placed between each Hg diffusion pump and the central region, as the Hg in the pumps is at least at a pressure corresponding to tap water temperature.

After each jacket, the tube is bent gradually, 20^{o} in 20 cm, in order to avoid double sheaths.

Next are openings, see Fig.21, leading to ionization gauges, which with the Mullard WPS3 unit, read in the range 10^{-3} torr to 10^{-11} torr. The main tube is 62 mm in diameter with walls 2 mm thick. The opening to these gauges is of large diameter, 36 mm diameter. The gauge heads are protected from the discharge with nickel screen inserts.

Also at this opening are auxiliary anodes, hollow cylinders of tantalum on tungsten pins through the glass wall. These auxiliary anodes facilitate the striking of the arc all the way to the anode pool.

One of the principal intended diagnostics was neutral density measurement by absorption of the 2537Å Hg resonance line, see Chapter VIII. As this U.V. line is not transmitted by pyrex, a quartz tube is necessary. It is too expensive to construct the entire discharge vessel of quartz, so just the central region is made of spectrosil quartz. (Thermal Syndicate Ltd) one metre in length. The quartz is 25 mm I/D with walls 1.6 mm thick. The quartz region is made smaller than the pyrex region in order that current limitation will be sure to occur where it can be observed. (At the design stage it was not certain that as current limit was approached, conditions would remain completely uniform along the tube.) Furthermore, it is convenient to keep the power density low at the jackets in order that the condensed Hg not be heated by the discharge energy dissipation.

A further advantage to having the condensing jackets of larger diameter than the current-limiting region is that the tendency for unipolar arcs to form on the Hg droplets and the probability of Hg sputtering by ion bombardment to occur is substantially reduced, see sections 7.1.1 and 7.1.2.

The spectrosil quartz is of higher optical quality than the more standard vitreosil (substantially less striae).

The transition in diameter must be accomplished very smoothly and gradually in order to avoid the formation of a double sheath with its attendant complications, see section 5.5. In the case of the 25 mm diameter central region, the tapers are 60 cm long, and for the central diameter of 10 mm the tapers are 73 cm long.

The resultant length of 5 metres for the whole tube has the added advantage that the electron distribution in the central region should be quite independent of electrode effects, Crawford and Self (1965).

The different central tube replacements will be further discussed in Chapter VII, on experimental results.

6.3 AUXILIARY APPARATUS

The circulating coolant circuit is shown in Fig.23. Two refrigerators are employed in series, a 0·75 and a 0·5 H.P. water cooled condensing unit. The coolant is an antifreeze-water mixture. The refrigerators operate continuously and when the temperature falls below the level set on the electrical contact thermometer, the electrical hot water heater switches on. The reservoir ensures that temperature wobble is tolerably small, i.e. less than $0 \cdot 2^{o}$C. The flow of coolant to the two jackets is adjusted so that both are at the same temperature when the arc is running.

The D.C. supply circuit is shown in Fig.24. The main source is a 250 V, 30 A battery, but for starting, a 3000 V rectified source is available. It was found easiest to strike the arc progressively down the tube via the auxiliary anodes, which were then shut off. Manipulation of the arc with a hand magnet also facilitated in striking this rather long arc. Running voltage was around 100 volts anode-to-cathode.

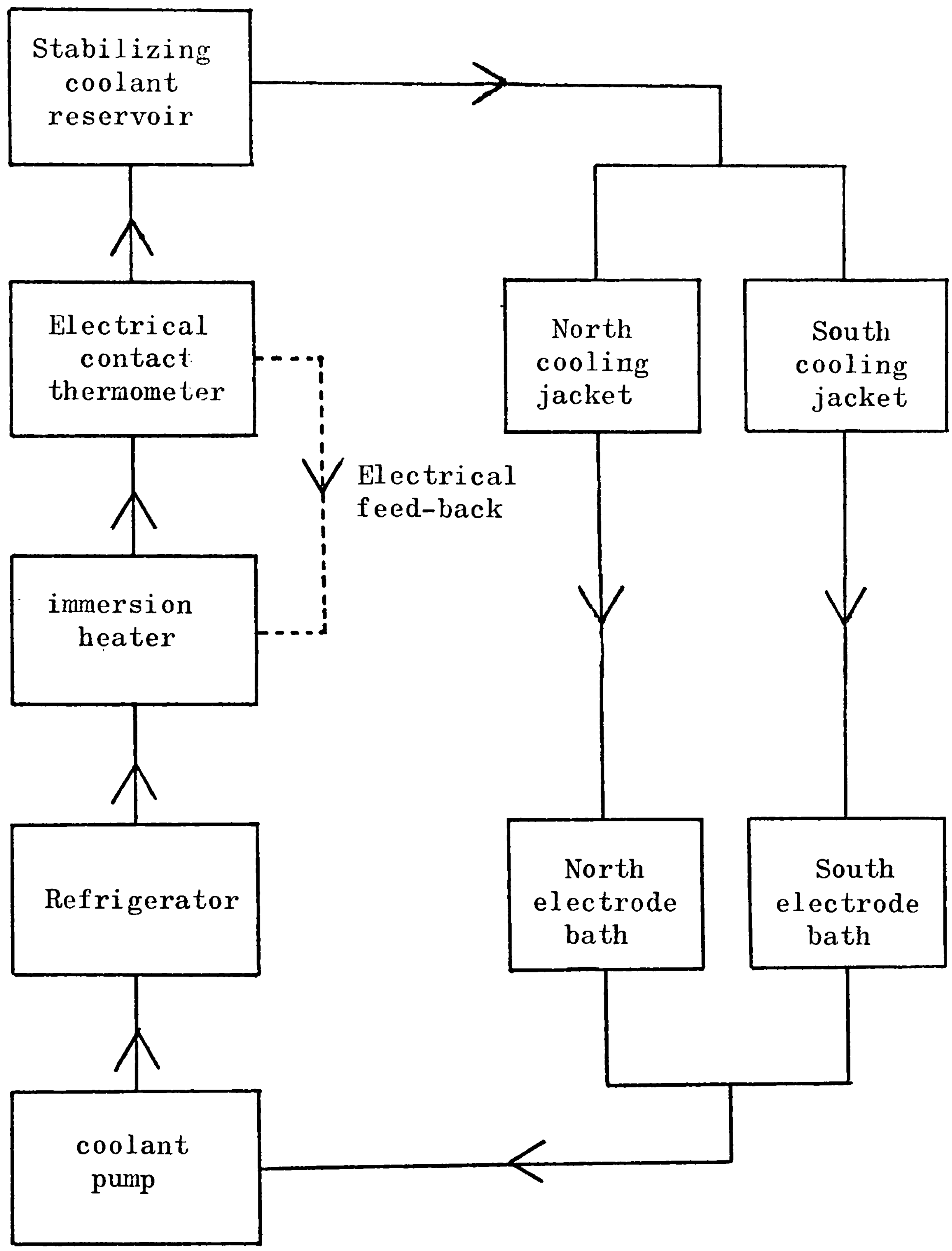

Fig.23
Coolant circuit for main discharge temperature control

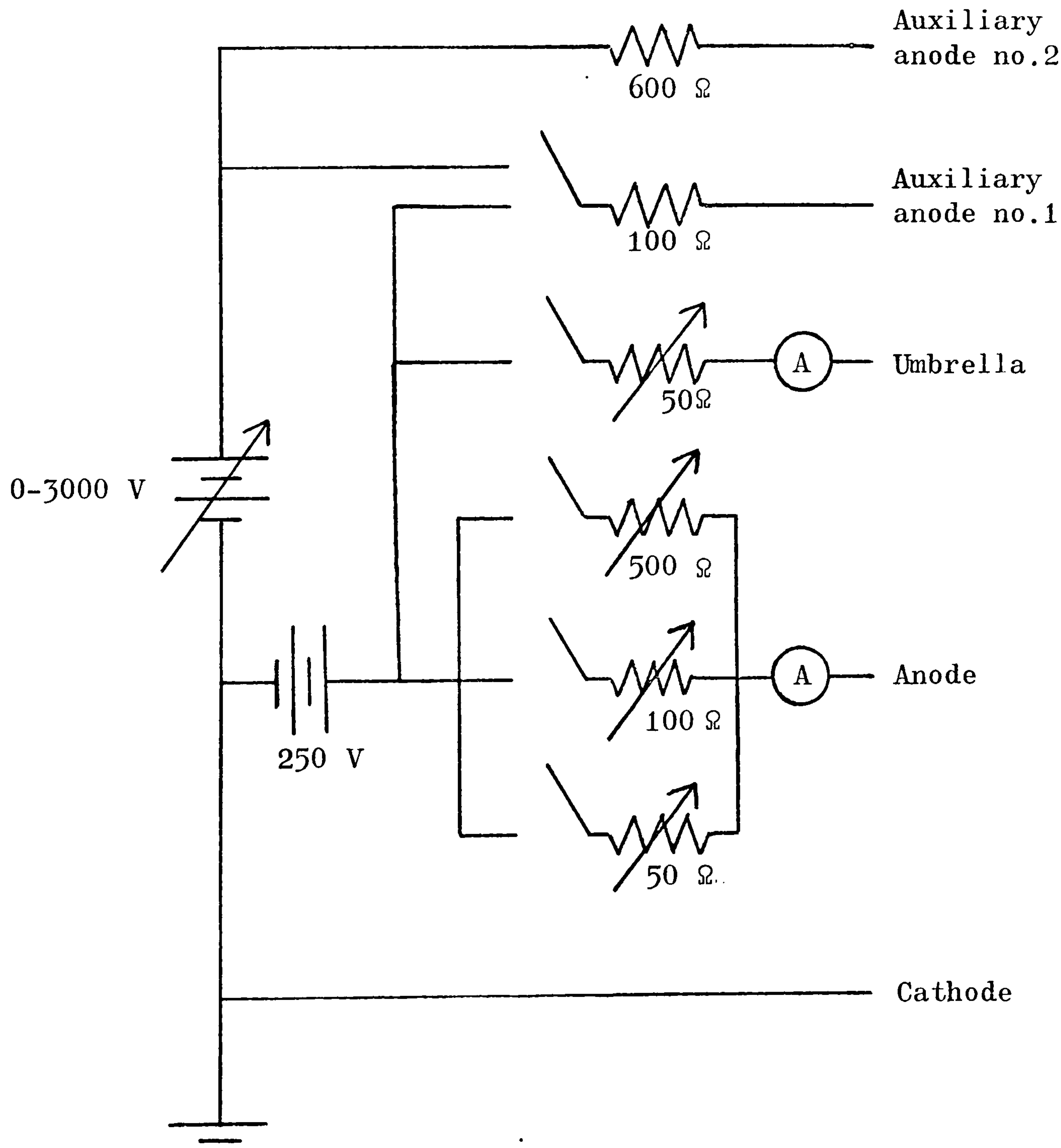

Fig.24

D.C. arc supply with 250 V battery supply for continuous operation and a 0-3000 V rectified D.C. supply to facilitate starting

The U.V. light transmitted through the quartz is harmful to the eyes and also produces ozone. For these reasons, the quartz section was surrounded with a glass box and the ozone pumped away with an extraction fan.

Elements of diagnostic apparatus will be discussed in the relevant experimental sections.

CHAPTER VII

NON-OPTICAL EXPERIMENTAL RESULTS AND DISCUSSION

7.1 CURRENT LIMIT RESULTS

7.1.1 25 mm Tube with Extra Hg Reservoirs

In Fig.25 is shown the first tube to be employed. Graded seals connect the quartz and the main pyrex vessel. In light of the difficulties reported by Allen et al (1963) in obtaining reproducible current limit results it was decided to incorporate extra liquid Hg reservoirs in the central region, hence the two larger Hg reservoirs at each end, and the ten small pips along the length. It was also thought that these extra Hg deposits in the central region would be necessary to fully control Hg vapour conditions in the quartz region as recent work, Rosa and Allen (1970), had indicated that the end jackets might not in fact fully control the Hg neutral pressure in the central region. (This latter matter is dealt with more fully in section 7.3, and it is concluded that for the present apparatus, at least, the end jackets do exercise complete control.) Connections for probes and ionization gauges are discussed in sections 7.2 and 7.3.

Current limitation could be obtained either by increasing the current for a fixed pressure, or decreasing the bath temperature, and thereby the neutral pressure, for a fixed current. In either case reproducible results were only obtained if current limitation was approached very gradually. It appeared that the discharge was only marginally stable near current limitation and small perturbations could send it into instability. In practice it was found that lowering the bath temperature very slowly for fixed I was most convenient and all results reported were obtained this way.

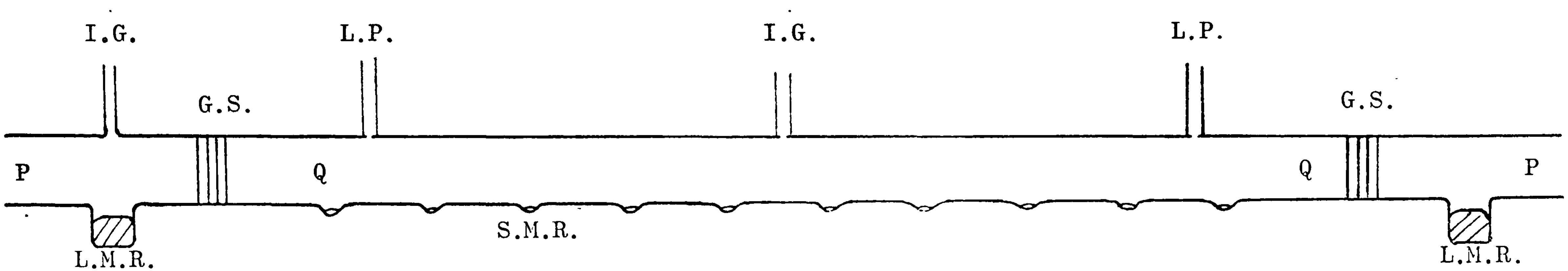

Fig.25
First 25 mm diameter quartz tube. P., pyrex; Q., quartz; I.G., ion gauge; L.M.R., large Hg reservoir; S.M.R., small Hg reservoir; G.S., graded seal; L.P., Langmuir probe

There were no indications of double sheaths if current limit was approached gradually. Double sheaths could be induced to form by large, abrupt increases in current, or by blowing cold air against the outside of the quartz.

The onset of current limitation was characterized by either the complete extinction of the arc (leaving only the auxiliary arc to the umbrella) or the arc voltage would commence to rise extremely rapidly, and it was impossible to decrease the series resistance quickly enough to maintain the current constant. The latter tended to be the case for higher currents (>1 A).

Even upon entering this unstable regime there was still no visual evidence of double sheath formation, although certain regions such as the anode taper became extremely hot to the touch, indicating large local voltage drops.

If an auxiliary arc had been maintained up to the first auxiliary anode, then at extinction, this arc remained, indicating that current limitation was occurring in the smaller diameter region, as expected.

At first, experiments were attempted with Hg deposited in the two large pips and in the 10 small ones. The quartz region was immersed in a trough of coolant which was connected to a refrigerator, pump and temperature controling circuit similar to that for the end jackets, see section 6.3. Although considerable care was taken to keep the coolant temperature uniform throughout the trough, current limit results for this arrangement were perplexing: there was no current limit at all! Despite the attempts to fully control the liquid Hg temperature on the inside of the quartz, it was evident that the current was removing neutrals from the wall, effectively increasing the neutral pressure and thereby current limitation was never reached. It was finally established that unless the coolant flow pattern around the tube is extremely constant in time, the condensed Hg near the end of the cooled region, is subject to inadequate temperature control. When the current is off, liquid Hg deposits just at the edge of the cooled region. When the current is turned on, the temperature of this region becomes intermediate between that of the fully cooled tube and the uncooled region. This Hg soon evaporates and re-deposits in the fully controlled area. If however, the flow pattern is varying with time, equilibrium is never established. This problem is avoided in the completely closed end jackets where the coolant flow pattern is steady.

A further complication was the formation of unipolar arcs, when the Hg deposit on the wall were very extensive. Sharp flashes of light could be seen from various parts of the thin Hg film on the quartz. The effect of these arc spots on vapour conditions is uncertain.

By taking very great care, the open trough flow could be rendered adequate, see section 7.1.2, however it was at this time that it was discovered that these central Hg deposits were unnecessary either for obtaining reproducible results or for controlling the neutral pressure in the central region independent of current (this latter matter is discussed in section 7.3). Accordingly, the cooling trough was removed and the pips emptied of Hg (the Hg surface in the two large end pips was too far from the discharge and an oxide film had covered the surface lowering its vapour pressure and thus rendering it useless for pressure control anyway).

With pressure conditions established solely by the end jacket, see section 7.3, the results shown in Fig.26 were obtained. The agreement with theory is very satisfactory.

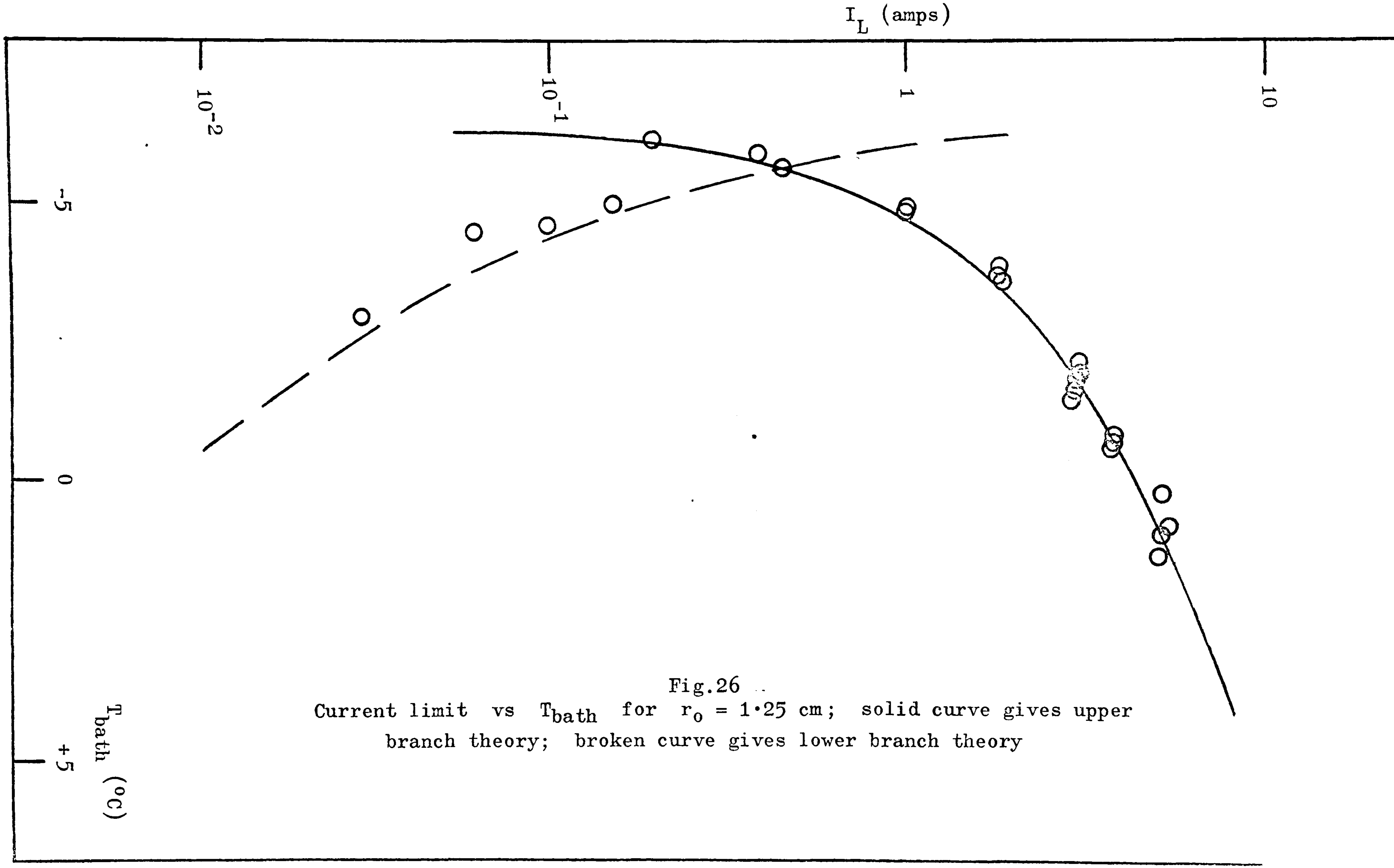

Fig.26

Current limit vs T_{bath} for $r_o = 1{\cdot}25$ cm; solid curve gives upper branch theory; broken curve gives lower branch theory

The temperature uncertainty is about $\pm 0{\cdot}5^oC$, owing to thermometer errors, inhomogeneities in the coolant flow, uncertainties in the temperature drop across the jacket walls, etc. The experimental scatter, also about $\pm 0{\cdot}5^oC$, spans the theoretical curve. The theoretical values for n_0 in equation (5.38) were converted to Hg condensing temperatures using the data of the Handbook of Physics and Chemistry, 47th edition.

7.1.2 10 mm Tube without Constrictions

(a) Results

Theory, section 5.3, indicates that the current limit is a strong function of tube radius. Accordingly, a pyrex tube of internal diameter 10 mm, wall thickness 1 mm, was inserted in the central region. Both tapers were extended at the same pitch to make this possible.

Again there was no evidence of double sheath formation; the current limiting process appeared to be occurring uniformly along the length of the positive column. The results shown in Fig.27 are again in very good agreement with the theory and indicate that the current limit scales with radius as predicted. Running the discharge in either direction, as before had no effect on I_L .

(b) Irrelevance of Wall Temperature

As the central region becomes fairly warm, especially at the higher current densities in this smaller tube, it was thought worthwhile to see if the tube wall temperature, T_w, effects the current limit (in the absence of liquid Hg deposits in the central region, the neutral density is supposed to be established by the end jackets solely). Accordingly, a temperature controlled cooling trough was placed around the central section and the T_w varied (T_w had to be maintained above the cooling jacket temperature of course, to avoid Hg condensation).

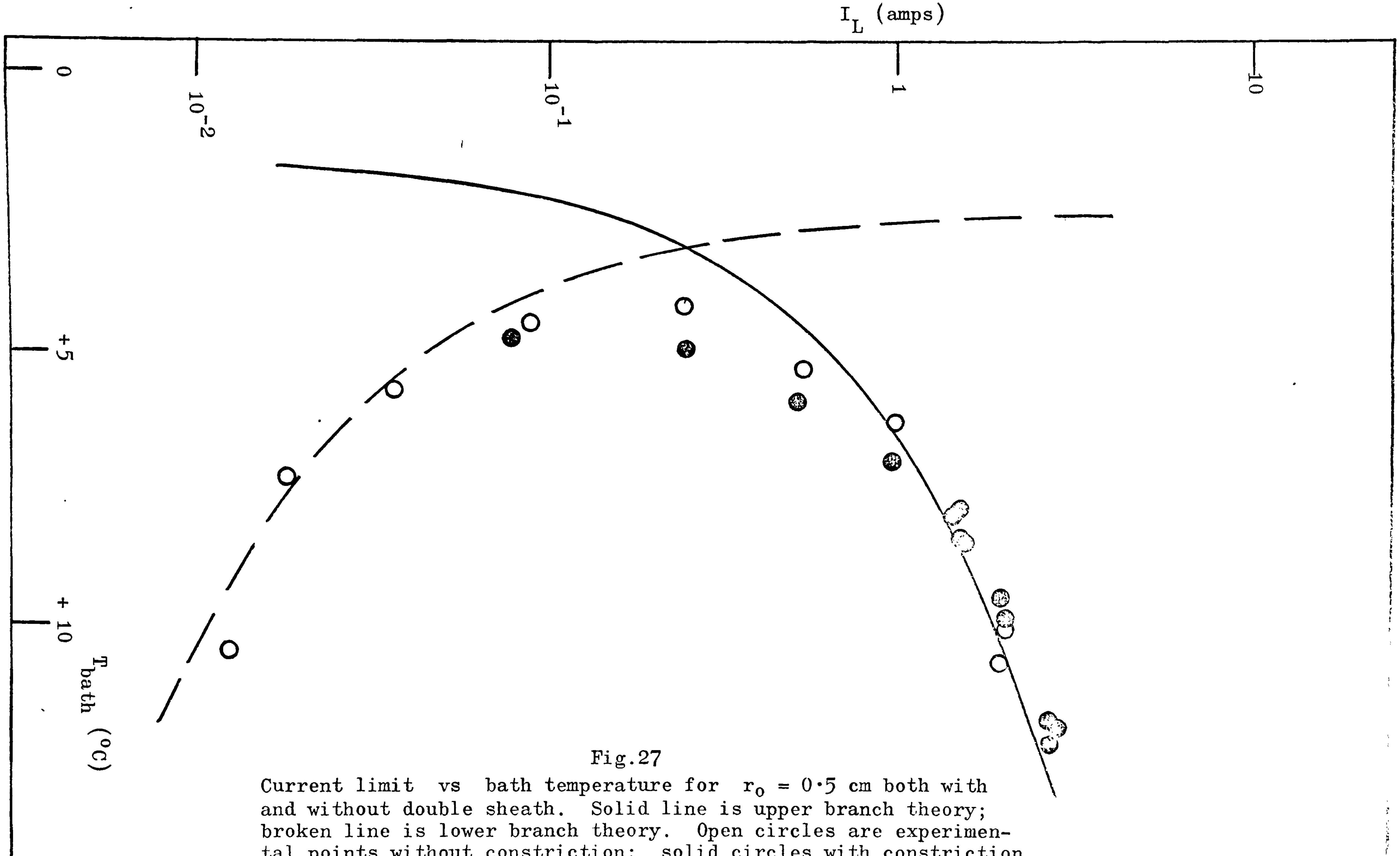

Fig.27
Current limit vs bath temperature for $r_0 = 0{\cdot}5$ cm both with and without double sheath. Solid line is upper branch theory; broken line is lower branch theory. Open circles are experimental points without constriction; solid circles, with constriction

The results, given in Table (5) for $I_L = 1{\cdot}0$ A indicate the irrelevance of the wall temperature. This accords with ion gauge pressure results, see section 7.3.

TABLE 5

IRRELEVANCE OF WALL TEMPERATURE TO CURRENT LIMIT

Jacket T at I_L	$T_{central}$
+ 7 °C	+ 12 °C
+ 7 °C	+ 20 °C
+ 7.1 °C	+ 29 °C
+ 7 °C	+ 50 °C

(c) Hg Sputtering by Ion Bombardment and a Possible Application to Hg Valves

It is well known that when ions bombard a solid, neutral atoms of the solid are sputtered off. One notes the distinction between heating the solid by bombardment such that individual atoms of the solid are sublimated (or evaporated) in a statistical way and sputtering which involves a more direct interaction between the incoming ion and the ejected neutral.

If the ions striking the Hg on the discharge walls are causing sputtering then any attempt to control the neutral emission rate from the liquid Hg by controlling the Hg temperature (as via the jackets or troughs) will be ineffectual. Unfortunately, there appears to be no data on sputtering from liquid Hg (presumably due to the complications in distinguishing sputtered from evaporated neutrals). It is difficult even to theoretically estimate the sputtering rate for ions with energies < 100 eV, as here the rate falls off very rapidly, see e.g. Askerov and Sena (1969).

Accordingly it was decided to try and obtain some information on this effect in the following way: an ion gauge for measuring neutral pressure was connected to the centre of the 10 mm tube. Near the opening to the gauge, Hg was deposited over a localized area by placing liquid nitrogen on the outside of the pyrex just at that point. A very long cooling trough was then placed around the tube. In this way the Hg had a tendency to condense just near the centre of the trough, i.e. near the already established deposit, and the pressure control difficulties mentioned in section 7.1.1 were avoided. Even so it was necessary to take care to make the cooling flow homogeneous. The Hg deposit was also small enough, that unipolar arcs were probably not present.

In this situation the current limit was measured as a function of jacket and trough temperatures, also the pressure reading was noted at I_L.

With $I = 1A$, and the jacket temperature just about current limiting, it was found necessary to lower the central trough temperature about 1·5 °C below the usual current limiting temperature, before the current in fact limited. The pressure gauge, however, indicated a temperature of about + 7 °C, i.e. current limiting.

The implication of the foregoing is that sputtering <u>is</u> occurring and maintaining the neutral gas density above that given by the liquid Hg temperature. Unfortunately, owing to the uncertainties in the actual wall temperature, due to trough cooling inhomogeneities and the large heat dissipation at this current density, this conclusion should be modified: if sputtering does occur it is producing $\lesssim$ 10% of thermal emission.

The ion flux, according to equation (3.4) is about

$$3 \times 10^{16} \text{ ions/cm}^2\text{/sec},$$

and the neutral emission rate, $\nu_0 = \frac{1}{4} n_0 \bar{c}$ is about:

$$6 \times 10^{16} \text{ particles/cm}^2\text{/sec.}$$

Thus the sputtering rate per ion is less that 0·2, (this is for ions of energy

$$\sim 6 \frac{kT_{e_L}}{e} \simeq 60 \text{ eV}).$$

Askerov and Sena (1969) report sputtering yields of low energy Hg^+ ions on various metals (but not on Hg). They find that their data can be fitted by:

$$S = k(E - E_0)^3 \qquad \ldots (7.1)$$

where S is the sputtering.yield;
E is the ion energy in eV;
E_0 is the threshold sputtering energy in eV.

Extrapolating their data for Hg indicates that for Hg, $E_0 \sim 1$ eV, so that approximately $S = kE^3$ and one can see how rapidly S varies with E. Using Askerov and Sena's value of k for Au (which, of the metals tested, appears closest in sputtering properties to Hg) gives a value of $S \simeq 0.06$ for $E = 60$ eV. Considering the considerable uncertainties involved, this would appear to confirm the experimental findings of $S \lesssim 0{\cdot}2$.

From this we may conclude that sputtering is unlikely to be effecting the neutral emission rate from the Hg on the jacket walls, where the ion wall current density is considerably less than in the central region. Had the discharge diameter been the same throughout, it is less certain that the jackets would have exercised proper pressure control.

If this sputtering is genuine, and experiments at higher current densities and better temperature control are needed to establish this, then there may be an application to Hg rectifier valve problems. Here, the current is time dependent, obviously, and the base pressure must be kept below a level where arc-back in the reverse cycle will occur, see, e.g. Quigley (1968). This base pressure is so low that current limitation can be a problem. If the walls of the narrow sections were coated with temperature controlled liquid Hg (perhaps a difficulty due to the extremely high power densities) then during the forward conduction cycle, Hg neutrals would be sputtered from the walls, effectively increasing the neutral pressure and avoiding current limit. During the reverse cycle the pressure would immediately (i.e. in a neutral flight time) return to the base pressure and arc-back would be avoided as before.

As the electron temperature near valve constrictions is very high, the wall-directed ion velocities are presumably very high as well and since S increases very rapidly with ion energy, quite high sputtering yields may be possible in such devices. Indeed, it might even be the case that the current limit would be raised by <u>lowering</u> the base pressure, if by so doing the electron temperature was raised sufficiently.

7.1.3 <u>25 mm Tube Without Reservoirs</u>

The Hg pips on the first 25 mm tube constituted a distortion of the cylindrical geometry; to verify that this distortion was inconsequential, a completely cylindrical, pip-free, 25 mm quartz tube was installed, and the results were found to be as before. In fact the points in Fig.26 are a mixture of results from the two tubes.

The first 25 mm tube had gradually become extensively covered with Hg stains. Presumably these stains are imbedded Hg atoms which were impelled into the quartz lattice as ions after falling through the wall sheath. They were not easily removed by heating with a torch as liquid Hg would be. These atoms are far more firmly bound to the wall that are adsorbed atoms, and presumably play no role in a D.C. discharge except to constitute a long range gas clean-up, which is easily replaced in the present apparatus.

To verify that these imbedded atoms are not playing a role in the D.C. discharge mechanism, the current limit of this new, clean tube was compared with that of the stained one, and the results were found to be the same.

7.1.4 10 mm Tube with Constriction

In section 5.5.8 it was postulated that a double sheath would not effect the current limit if it was followed by a long, uniform, positive column of the smaller diameter. To test this hypothesis, the gradual taper at the cathode end of the 10 mm tube was replaced by an abrupt constriction, $r_1 : r_2$ = 12.5 mm :5 mm. In this situation, a prominent double sheath was observed for all pressures and currents, see Fig.20(a). It was observed to change shape to a certain degree as current limit was approached, but as the D.S. boundary is somewhat diffuse it is difficult to make quantitative visual observations.

The current limit results, shown in Fig.27, indicate that there is essentially no difference in I_L , with or without the D.S., confirming the hypothesis of section 5.5.8.

Running the discharge in the opposite direction put the abrupt constriction at the anode end. In this case there was no D.S. anywhere (visual observation) and nothing very unusual occurred at the constriction.

7.2 LANGMUIR PROBE RESULTS

7.2.1 Introduction

The charged particle properties in a low pressure discharge may be established in principle using Langmuir probes. In practice there are often complications which make the interpretation of the probe characteristics difficult and reduce the probe's usefulness.

In the positive column, the radial flow of ions to the walls has been shown by Stangeby and Allen (1971b) to distort the fields about a cylindrical probe such that the resultant errors in density measurements, for example, are of the same order as the theoretical radial variation of density (as per e.g. Tonks-Langmuir). In addition, near current limit there is evidence that the electron drift speed is comparable with the electron random speed. What precise effect this has on the probe characteristic is uncertain but it is probably appreciable.

Fortunately, from the view-point of current limitation work, the most interesting probe measurement is the ion wall current and this use of the probe is fairly free of objections. If a flat-faced probe is placed flush with the tube wall and biased so as to receive the ion current which would have arrived there in the probe's absence, then complications should be at a minimum. In any other position the distortions to the positive column potential distribution will be appreciable, and while the effect of these distortions for the cylindrical or spherical probe is calculable, Stangeby and Allen (1971b), for the flat probe, see Varey (1970), a full calculation would be very difficult (for example, the potential distribution varies in a two-dimensional way around the tip of a flat-faced probe, i.e. edge effects are important).

In section 7.2.3, ion wall current measurements are discussed. While other measurements are open to the objections aforementioned, they are still of some qualitative interest and are presented in section 7.2.4.

7.2.2 Structure and Position of Probes

The Langmuir probes were of flat-faced tungsten wire, 0·3 mm. in diameter, jacketed with thin quartz tubing, wall $\approx$ 0·1 mm. The probes were mounted in a housing, see Fig.28(a), which permitted their movement

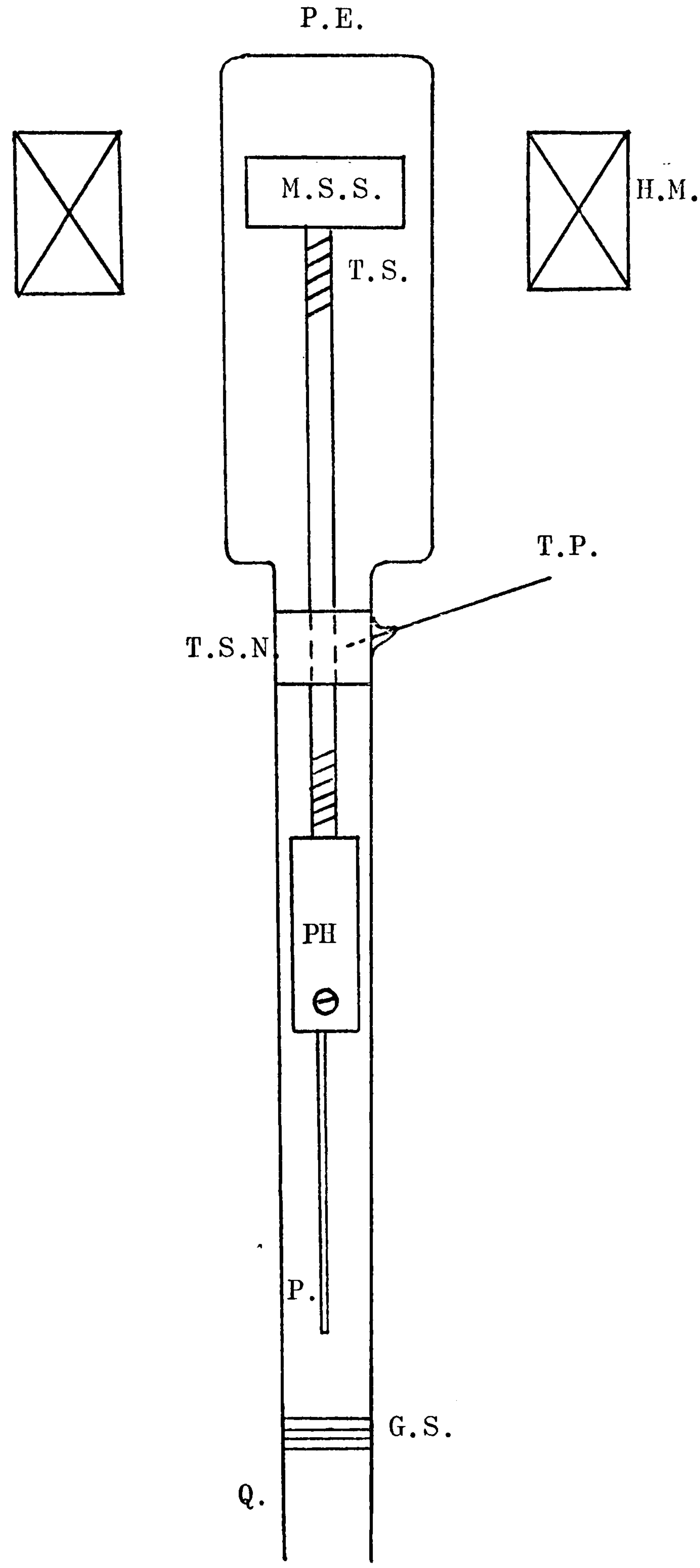

Fig.28a

Moveable Langmuir probe housing. P.E., pyrex envelope; H.M., hand magnet; M.S.S, magnetic stainless steel cylinder; T.S., threaded shaft; T.S.N., threaded stainless steel nut; T.P., tungsten pin; P.H., probe holder; P., probe; G.S., graded seal; Q., quartz.

across the diameter of the column. The housing is entirely of glass joined to the quartz by graded seals. Motion up and down is accomplished with an externally applied magnet which engages the magnetic stainless steel slug at the top of the threaded shaft. By exerting sufficient torque the shaft will move relative to the fixed nut. Electrical connection is via the shaft and nut to a tungsten pin in the glass wall of the housing.

The probe face is parallel to the longitudinal axis of the column.

The probes were mounted only on the 25 mm quartz tubes. On the first tube, the holes through the column wall are shown in Fig.28(b), and on the second tube, in Fig.28(c). As the probe openings on the first tube are smaller, most of the results reported were taken with this tube. In reporting specific results, the position of the probe along the length of the column is not given because longitudinal position appeared to be irrelevant.

The current-voltage characteristics were obtained with a standard circuit and points plotted manually.

7.2.3 Ion Wall Current and $(\gamma\beta/\alpha)$

In the theory of current limitation given in section 5.3, and also in the theory of Allen and Thonemann, one derives the relation between ion wall current density I_i and arc current I.

$$I = (\beta\gamma/\alpha)\sqrt{\frac{M}{2\pi m}}\; I_i \,\pi r_0^2 \,, \qquad \ldots (7.2)$$

and it is postulated that $(\beta\gamma/\alpha)$ is a constant, independent of current. Furthermore, in arriving at equation (7.2), T_e was cancelled from denominator and numerator, and since the electron distribution at current limit is not Maxwellian, the cancellation of these effective temperatures (which may be different) may be invalid.

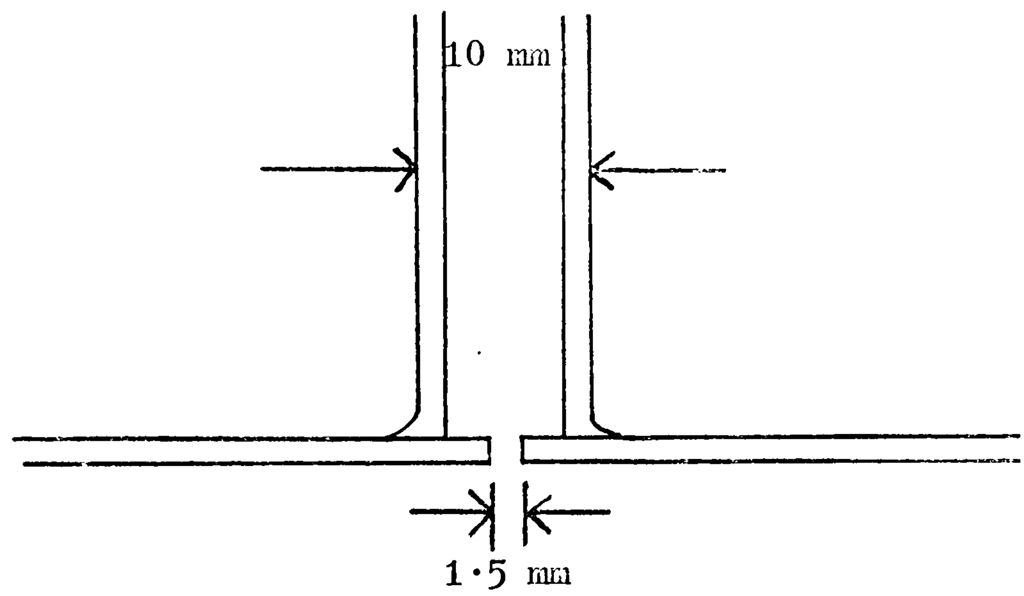

Fig.28b
Probe opening on first 25 mm diameter quartz tube

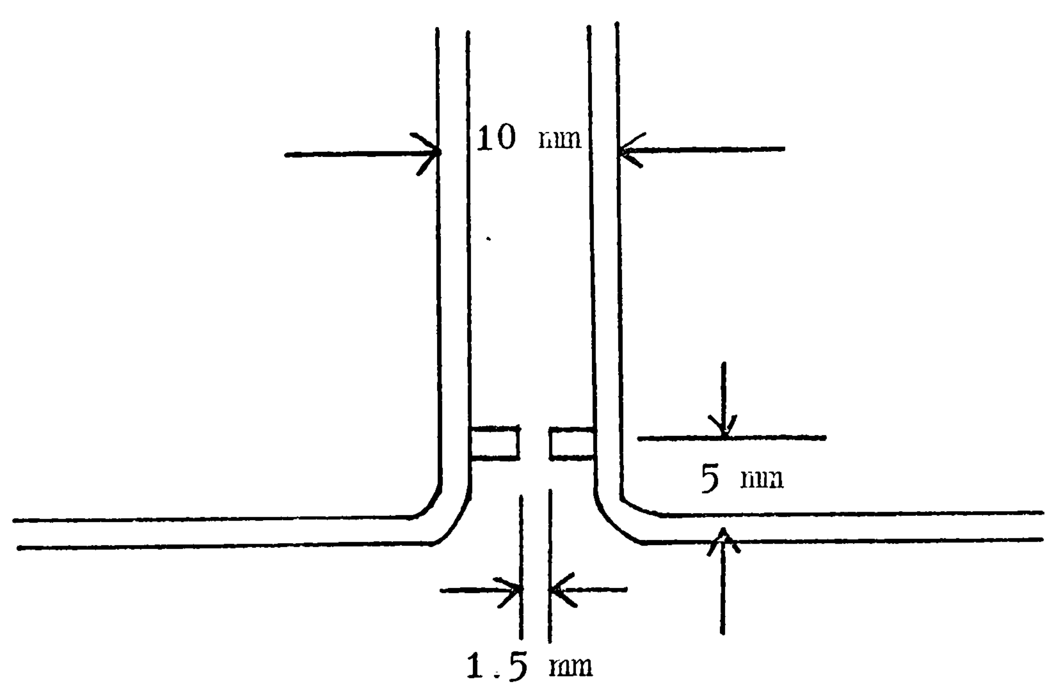

Fig.28c
Probe opening on second 25 mm diameter quartz tube,

Since this equation is fundamental to the entire theory it should be verified experimentally. To establish α, β, γ separately, is difficult to do with precision as it necessitates probe measurements in the column where distortions due to anisotropies are present. Fortunately the verification of equation (7.2) requires only the measurement of I_i with a probe flush with the wall, and of I.

Measurements were made as follows: the probe face was positioned by eye to be near the column edge and the ion collection part of the characteristic taken, an example is given in Fig.29. As the ion collection characteristic is not horizontal, the straight line portion is extrapolated back to the floating potential and the ion current read at this point. Thus in Fig.29, the ion current is read as 6.6 μA.

As it is difficult to judge the plasma edge by eye, the probe is then moved inward (or outward) and the process repeated for different positions. The values of I_i vs radial position are given in Fig.30 for I = 5 A. The ion wall current is taken to be at the intersection of the extrapolated straight line segments, point A in Fig.30, and the error in I_i is taken to be:

$$\Delta I_i = I_B - I_C .$$

In this way one may obtain the relation between I_i and I, shown in Fig.31. The solid line is given by equation (7.2) with $(\gamma\beta/\alpha) = 1$. It is evident that over the current range investigated the relation between ion wall current density and arc current is given by:

$$I = \sqrt{\frac{M}{2\pi m}}\, I_i \pi r_o^2 , \qquad \ldots (7.3)$$

to within experimental error.

The measurements shown in Fig.31 were obtained with a probe positioned half-way along the first tube and for pressures near current

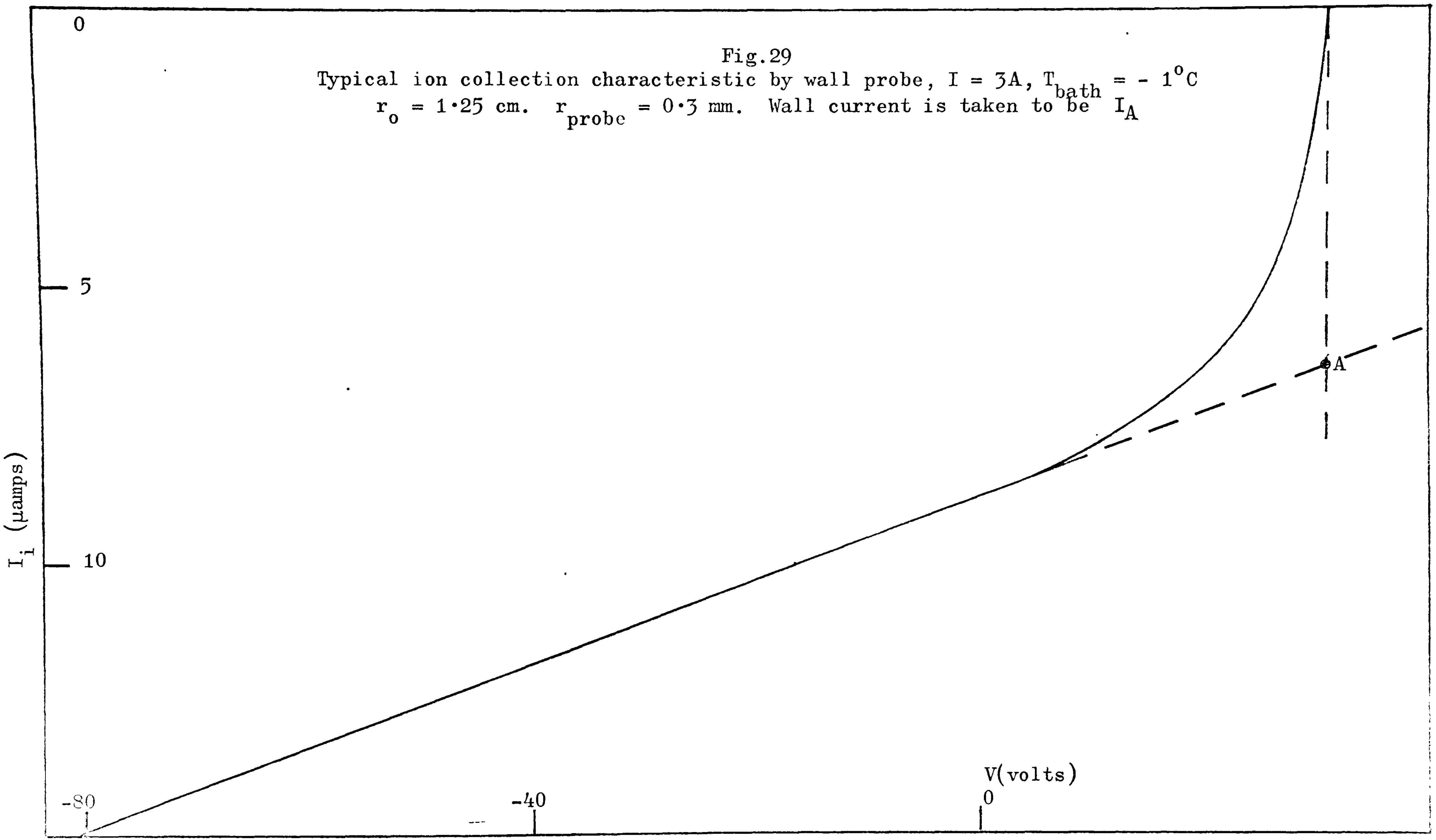

Fig.29
Typical ion collection characteristic by wall probe, $I = 3A$, $T_{bath} = -1^{o}C$
$r_o = 1{\cdot}25$ cm. $r_{probe} = 0{\cdot}3$ mm. Wall current is taken to be I_A

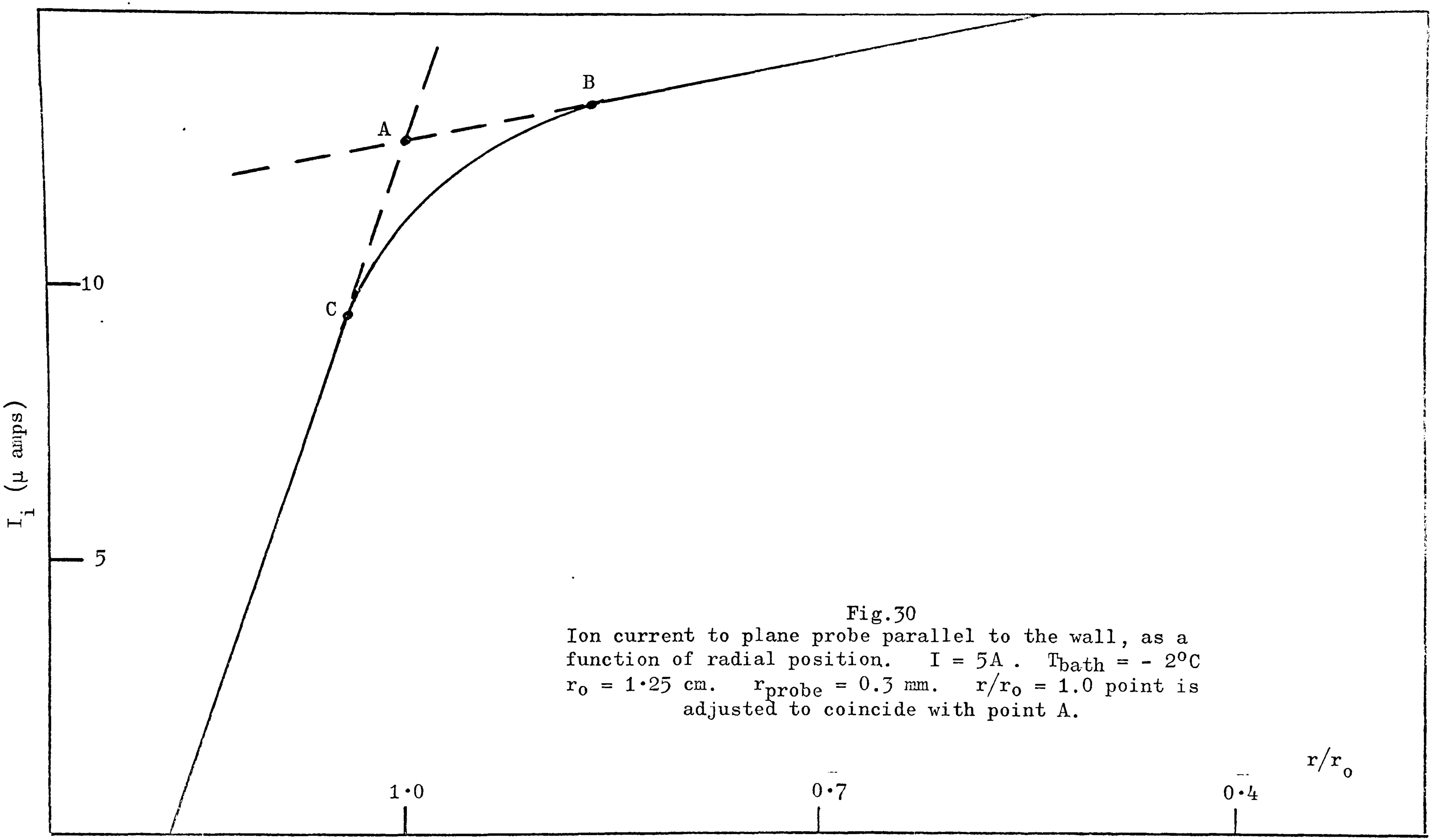

Fig.30
Ion current to plane probe parallel to the wall, as a function of radial position. $I = 5A$. $T_{bath} = -2^oC$ $r_o = 1{\cdot}25$ cm. $r_{probe} = 0.3$ mm. $r/r_o = 1.0$ point is adjusted to coincide with point A.

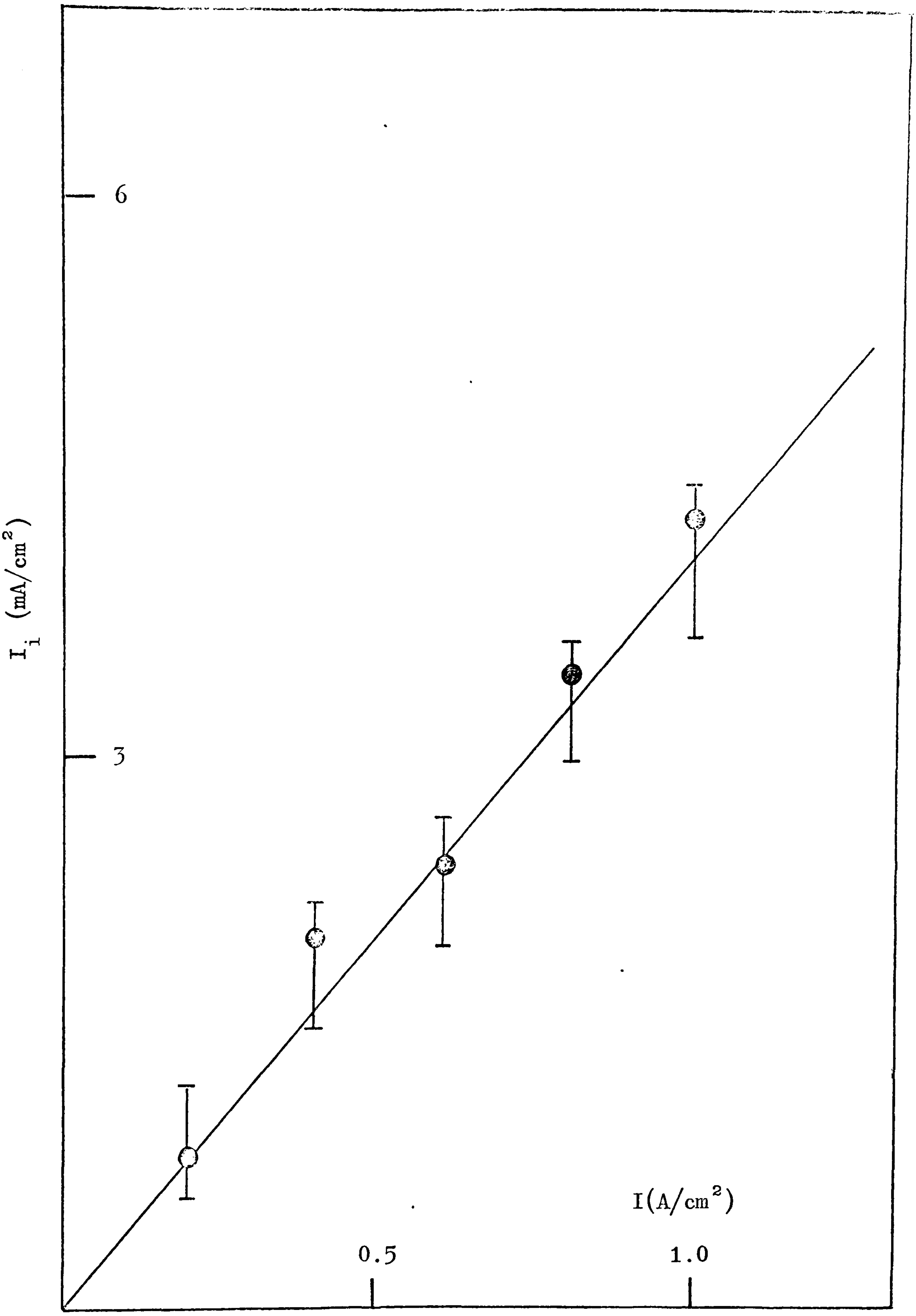

Fig.31

Ion wall current vs tube current near current limit. Solid line is $I_i = (\alpha/\gamma\beta)(2\pi m/M)^{\frac{1}{2}} I$ with $(\alpha/\gamma\beta) = 1$. Points are from a planar wall probe.

limiting. In fact it was found that a probe located near one end of the second quartz tube gave essentially identical results, thus indicating that the size of the probe hole is not too critical and conditions are longitudinally homogeneous. The variation of I_i with bath temperature is slight within a few ^{o}C of the limiting temperature, T_L, while at about $10^{o}C$ above T_L, I_i has increased by about 20%.

7.2.4 Electron Temperature

With the probe at the column edge and I = 4 A, the two electron characteristics shown in Fig.32 were obtained. The effect on the electron distribution as current limit is approached may be seen qualitatively from this figure. The electron 'temperature' (as taken from the slope of the main straight line segment) increases from 3·2 eV to 7 eV, but the log plot is straight over a shorter segment, indicating the non-Maxwellian nature of the electron distribution near current limit.

In some log plots, e.g. Fig.33, one may be able to discern two or even three straight line segments, indicating several different 'temperatures'. As the probe is measuring only the 'perpendicular temperature' as distinct from the 'longitudinal temperature', this distortion is presumably due more to the depletion effects of excitation and ionization than to electron drift effects.

From Fig.32 one may note that the large departure from linearity for the characteristic near current limit makes the error in the electron saturation current, and hence n_e, very large. It is for this reason that separate estimates of α and β would be too crude to be of much value. The parameter γ may be estimated from Fig.30, and assuming that $n_e \propto I_i$, one obtains $\alpha \approx 1{\cdot}2$ compared to the Tonks-Langmuir $\gamma = 2\, h_o \exp(\eta_o) = 2.22$, i.e. the radial density distribution is much

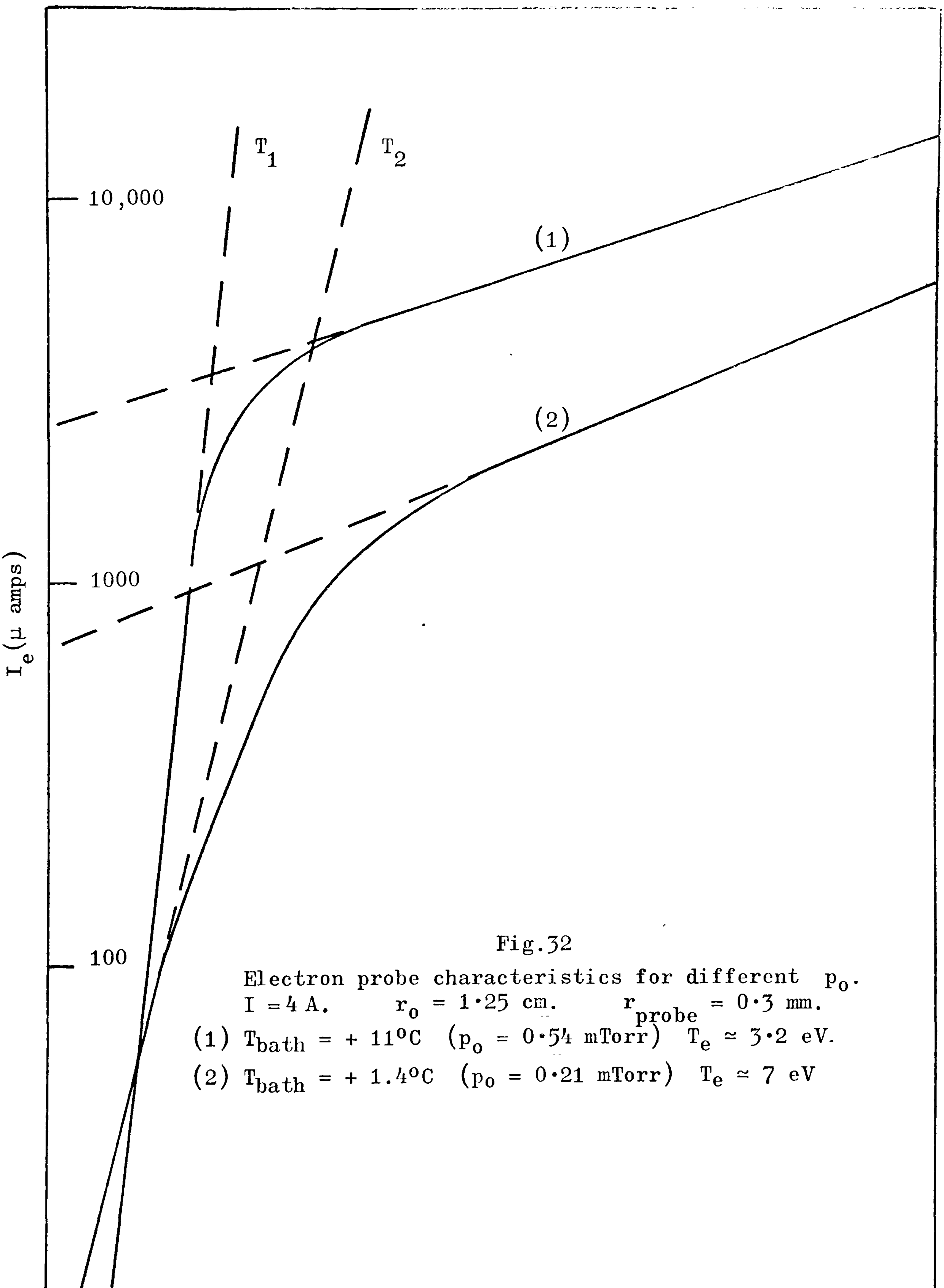

Fig.32
Electron probe characteristics for different p_o.
$I = 4$ A. $r_o = 1{\cdot}25$ cm. $r_{probe} = 0{\cdot}3$ mm.
(1) $T_{bath} = +11^oC$ ($p_o = 0{\cdot}54$ mTorr) $T_e \simeq 3{\cdot}2$ eV.
(2) $T_{bath} = +1.4^oC$ ($p_o = 0{\cdot}21$ mTorr) $T_e \simeq 7$ eV

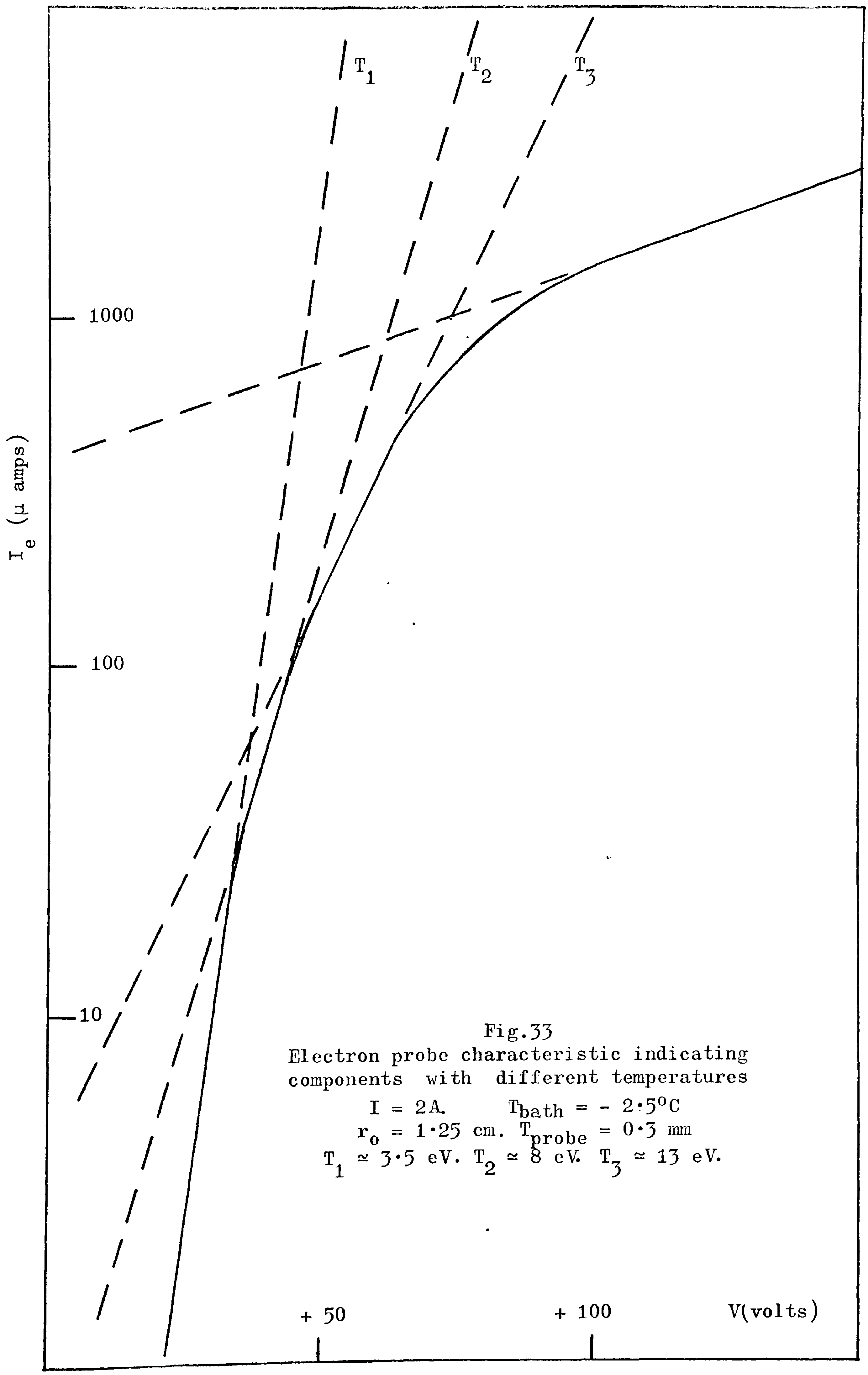

Fig.33
Electron probe characteristic indicating components with different temperatures
$I = 2A.$ $T_{bath} = -2{\cdot}5^oC$
$r_o = 1{\cdot}25$ cm. $T_{probe} = 0{\cdot}3$ mm
$T_1 \simeq 3{\cdot}5$ eV. $T_2 \simeq 8$ eV. $T_3 \simeq 13$ eV.

flatter near current limit than in the normal column. In fact, the distribution would be even flatter than shown, if ion flow corrections were made, Stangeby and Allen (1971b).

As the electron distribution is not Maxwellian there is no proper way to show how T_e varies with I or p. However, to gain some qualitative picture one might either plot the '$\bar{T}_e$' as obtained from the initial slope of the single probe characteristic or one might use two single probes as a double probe. In either case one is obtaining the 'temperature' of the high energy electrons which is presumably some measure of the average electron energy, i.e. the true effective temperature.

A typical double probe characteristic is shown in Fig.34. The experimental conditions are: second 25 mm tube, 1st probe at 61 cm from cathode taper, 2nd probe at 101 cm from cathode taper, both probes at the wall, $I = 3A$, $T_{Bath} = 0^oC$.

For the positive column far from current limit, see, e.g. Klarfeld (1941), T_e is not a function of current. In Fig.35, T_e is plotted vs I for $T_{Bath} = 0^oC$, results obtained from double probe characteristics, and one can see that T_e is a function of I near current limit. This occurs because the effective pressure is not independent of I, and $T_e(pr)$.

Of course for a given current, T_e is still a function of p and this relation is shown in Fig.36 both with double probe and single probe (initial slope) results. The theoretical curve for T_e vs p, taken from the theoretical calculations of section 5.2.3, is shown also, but a direct comparison between theory and experiment is not possible as the experimental T_e is only an indication of the true effective T_e, and effective pressures would have to be used instead of p_o .

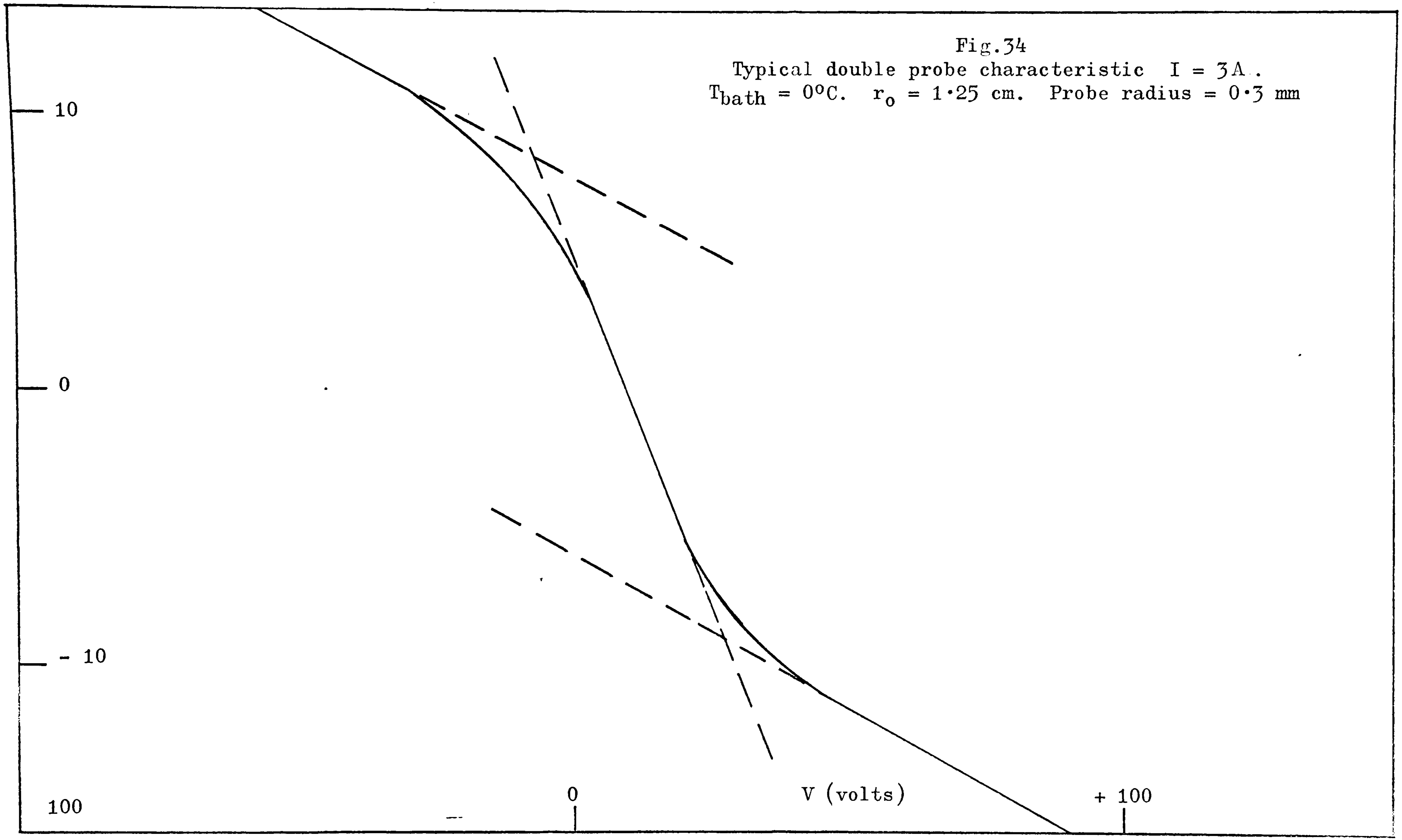

Fig.34
Typical double probe characteristic I = 3A.
$T_{bath} = 0^{o}C$. $r_o = 1{\cdot}25$ cm. Probe radius = 0·3 mm

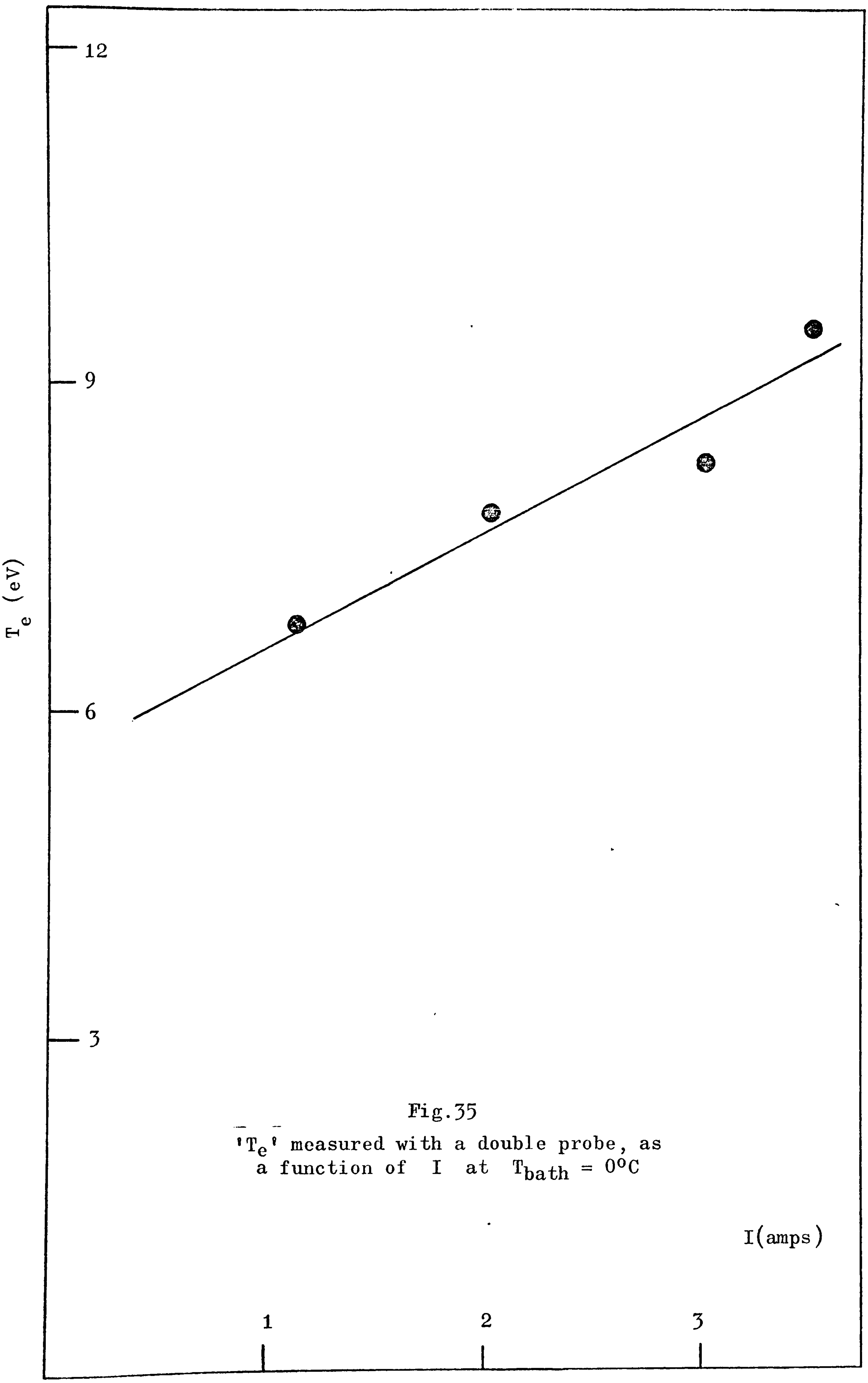

Fig.35

'$\bar{T}_e$' measured with a double probe, as a function of $\bar{I}$ at $T_{bath} = 0^oC$

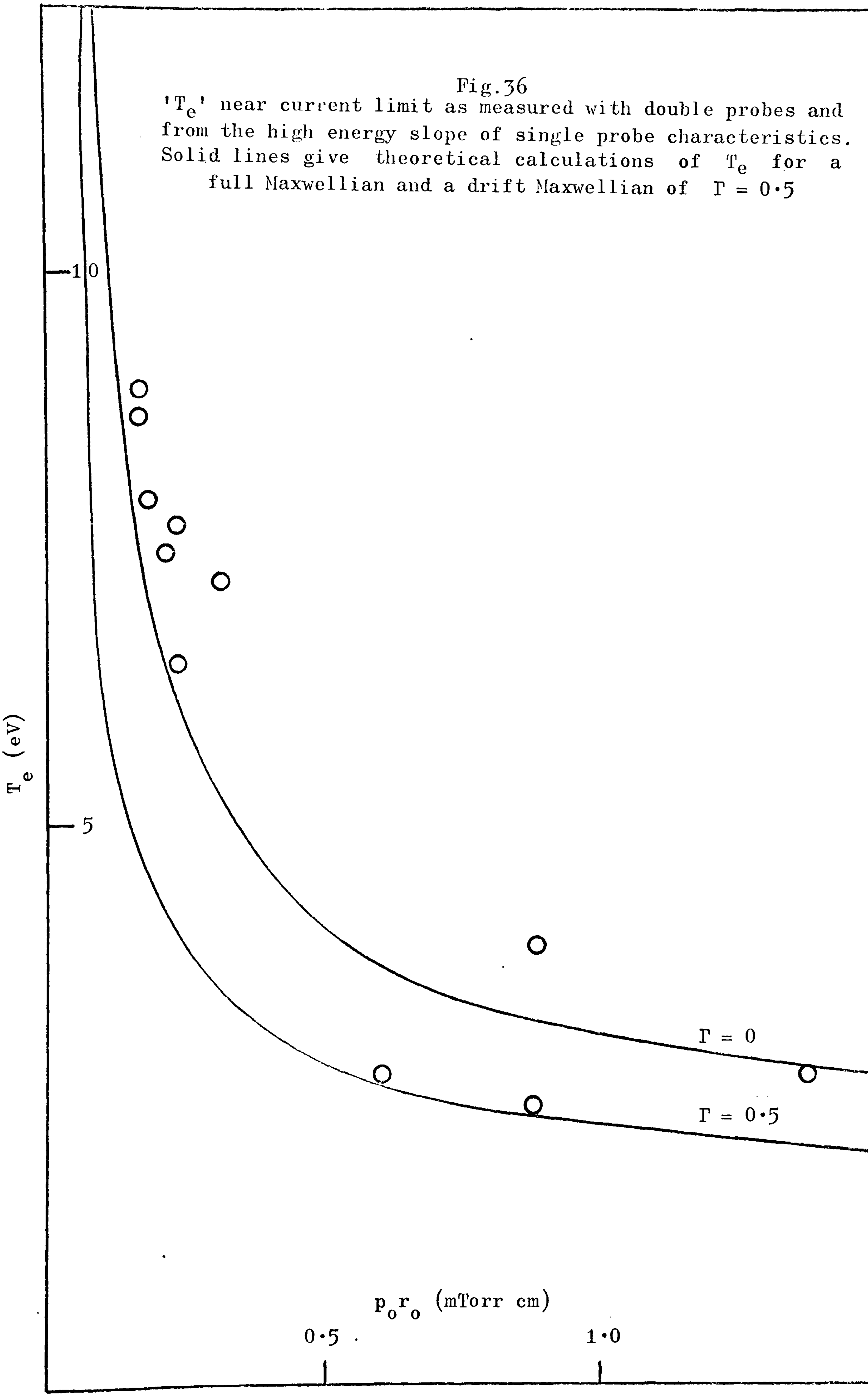

Fig.36
'T_e' near current limit as measured with double probes and from the high energy slope of single probe characteristics. Solid lines give theoretical calculations of T_e for a full Maxwellian and a drift Maxwellian of $\Gamma = 0{\cdot}5$

7.3 PRESSURE GAUGE MEASUREMENTS

7.3.1 Introduction

In the theory of section 5, it is assumed that the neutral flux from the tube wall in the presence of the discharge is still given by ν_0, the neutral flux from the temperature controlled liquid Hg surfaces. If it turns out that the flux from the walls is current dependent, $\nu = \nu(I)$, then this can be incorporated in the theory of section 5, but the theory is then more complicated of course. In any event, the flux of neutrals from the wall in the experimental region should be measured to establish this matter conclusively.

If the discharge wall is completely covered with temperature controlled liquid Hg, then the wall flux is always ν_0, and ν_0 is given by the wall temperature only. In practice, it can be inconvenient to cover all the walls with Hg, see section 7.1. In equilibrium, the neutral emission from a dry wall is simply equal to the received flux, i.e. unlike the wet wall, there is no independent means of establishing ν. There is thus the possibility that $\nu_{dry} \neq \nu_0$, but that $\nu_{dry} = \nu(I)$.

For high currents and pressures when one is near the Allen-Thonemann regime where $\nu_0 \sim I_i/e$ one may consider the reasoning of Allen et al (1963): the flux to the walls is almost purely of ions; the ion current is likely to be a function of arc current only and therefore longitudinally uniform; hence the flux to the dry wall is the same as to the wet wall; thus the flux to the dry wall is $\sim \nu_0$, and in equilibrium this gives the dry wall emission rate.

Whether this reasoning is still valid in the presence of the large longitudinal density gradients which build up towards a non-condensing anode, is open to question. Certainly, when one is not near the $\nu_0 \sim I_i/e$ regime, this argument cannot be relied on.

In the present apparatus, pains have been taken to avoid the longitudinal neutral gradients, see Chapter VI, however recent work, Rosa and Allen (R. & A.) (1970), has indicated that $\nu_{dry} = \nu(I)$ even when a condensing region is present at the anode end.

Experimentally, R. & A. have found that the readings of ionization (pressure) gauges located in the dry regions, increased with I (it is reasoned that gauge readings are proportional to the flux of heavy particles into the gauge opening). Now, there are two pressure effects - an anisotropic effect (due to the longitudinal flow of neutrals from cathode to anode, i.e. a pumping effect) indicated by increased readings on gauges facing into the flow - and an isotropic effect, which should increase readings on gauges whose openings are parallel to the flow (R. & A. did not in fact employ such gauges on their apparatus, see Fig.38). The anisotropic effect is simple enough to understand - it replaces the longitudinal neutral gradient to the solid anode; this is the electrophoretic effect. Also, this effect does not directly concern the present current limitation work, as only the neutral flux to and from the walls, i.e. the random flux is of interest.

The observed isotropic effect is thus of primary interest. R. & A. present the following physical argument for the isotropic effect: for higher currents, the dry wall temperature increases; thus the neutrals in the dry region have a higher average speed; 'when the neutral flow comes to a hotter region, the neutral-wall collision frequency increases and with it the frictional force due to the presence of the wall. As a consequence, the neutral drift speed is slowed down and for the sake of mass conservation, the gas density rises'. By similar reasoning an enhanced effect is predicted if the tube diameter is gradually tapered from one cross-section to another 'when the radius decreases the frictional drag due to the presence of the wall goes up while the tube cross-section does down. If the mass flux is to be conserved then the gas density must increase'.

The implication of all this is quite serious for the present current limitation work and so it was decided to do further experimental work on the question, specifically to discover if ν increases with wall temperature T_W, and with decrease in r_0. Results are presented in section 7.3.2, and indicate that these predictions are not correct.

7.3.2 Pressure Gauge Experiments

On the present apparatus, five gauges were employed, see Fig.21. Gauges 1 and 4 may be observed to have large openings, i.e. about 4 cm going down to 2·5 cm, while gauges 2, 3 and 5, have small openings, i.e. about 1·5 to 2·0 mm. In all cases the gauge openings are parallel to the longitudinal neutral flow and therefore should give a measure of the flux of heavy particles to the dry wall (which, in equilibrium, is the flux from the dry walls). i.e. these gauges should measure any isotropic effect.

Variations of the gauge readings with I are given in Figs.39. As may be seen, the isotropic effect in the large diameter regions is confirmed, and is of approximately the same magnitude as reported by (R. & A. (1970)).

Somewhat surprisingly, gauges 2 and 3 in the smaller diameter section far from indicating an enhanced effect due to decrease in r_0, show no isotropic effect at all, i.e. the gauge readings indicate that $\nu \simeq \nu_0$ independent of current, at least for pressures of $p \lesssim 0{\cdot}3$ mTorr (where all the present current limitation work has been done). At higher pressures, however, the central gauges indicate the isotropic effect as well.

It was thought that since the end gauges 1 and 4 had large openings and the central gauges 2 and 3, small openings, that the size of the gauge entrance might be relevant. For this reason gauge 5, of small opening, was installed in the end region and as it indicated essentially the same effects as gauge 4, it was concluded that this factor is irrelevant.

To further investigate this phenomenon, the apparatus of (R. & A.), see Fig.38 was put back into operation. In addition an extra gauge was installed in the central region of their tube, see Fig.38, of small opening facing parallel to the flow. This gauge directly indicated the isotropic effect, whereas the end gauge measurements reported by (R. & A.) had to be averaged to give the isotropic effect. Again, the evidence for an enhanced random flux was obtained.

To test the relevance of the wall temperature, T_w, heating tapes were wrapped around the central region and it was well lagged so that T_w could be set uniformly at any desired value, independent of I. With I = 5A throughout the run, the central gauge reading was observed as T_w ranged from $\sim + 30^oC$ to $+ 220^oC$, (a range far greater than that which naturally occurs if T_w is set by I and ambient, unlagged, conditions). There was essentially no change in the gauge reading whatsoever as T_w varied from $+ 30^oC$ to $+ 220^oC$

7.3.3 Conclusions

(a) Experimental evidence of the existence of a current sustained isotropic pressure effect is obtained, generally confirming the experimental results of Rosa and Allen (1970).

(b) The negative result of the experiment in which wall temperature was varied independent of I, seems to indicate that the theory of Rosa and Allen, in which T_w plays the basic role, is in error.

(c) At the present time no alternative theoretical explanation is evident to this author, although it may be that variations in electron temperature with changing parameters, such as T_W, may be of some importance. The matter remains an open question and further experimental work, including measurements of T_e and neutral gas density (by U.V. absorption, for example) are in order.

(d) Changes in tube diameter undoubtedly introduce considerable complications to an already uncertain model, and for the present it will be taken as an experimental fact that $\nu = \nu_0$ independent of I in the quartz region of the present apparatus. While neutral flow suffers a greater drag force when r_0 decreases, it may be that increased electron drift and temperature in the smaller diameter tube, compensates for the increased drag. For purposes of current limitation predictions, it may be necessary to measure ν in the particular device employed (an easy experimental measurement, using an ionization gauge) and the experimental $\nu(I)$ is then inserted in the theory of section 5.3.

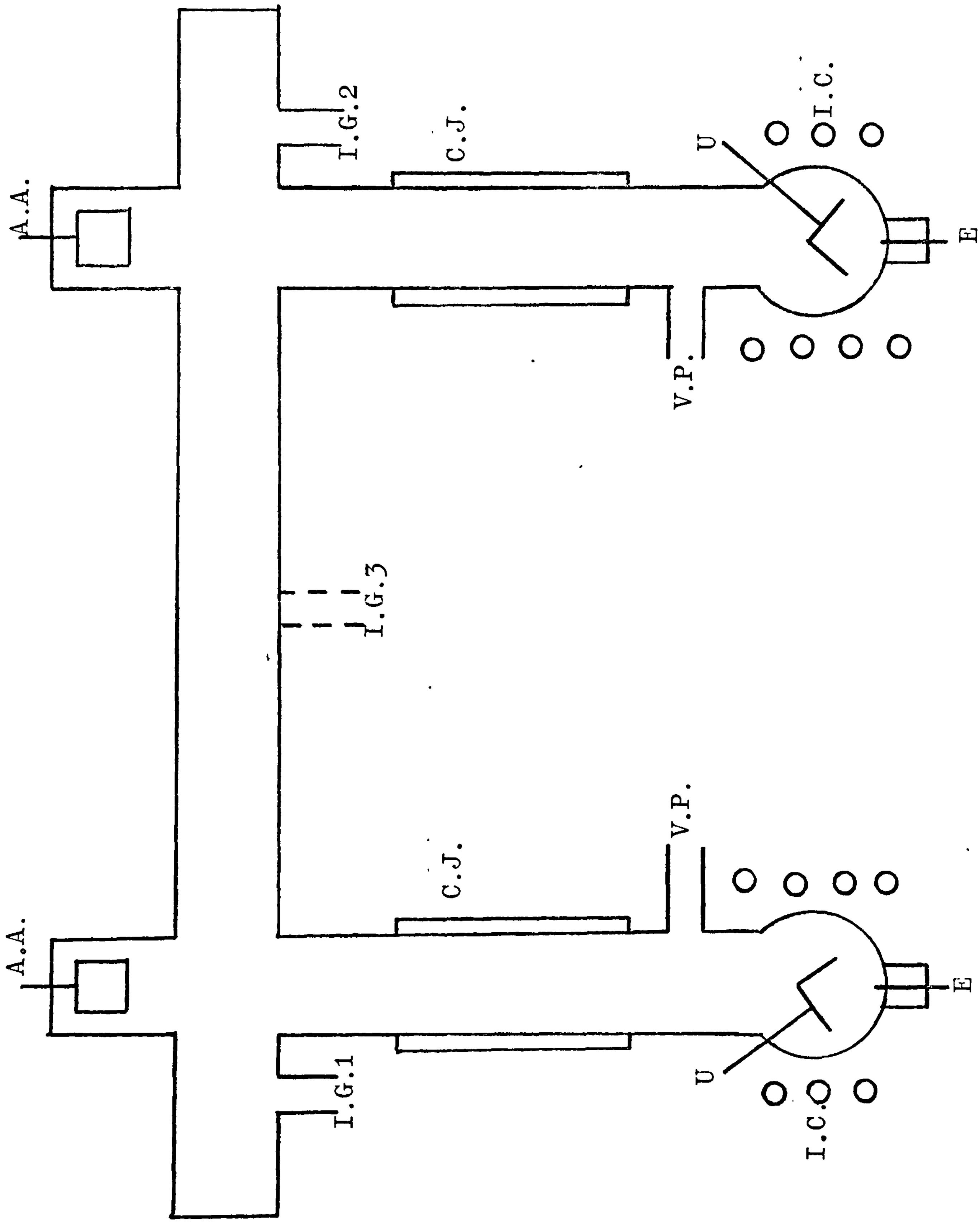

Fig.38
Discharge tube originally used by Rosa and Allen (1970) and altered for the present work by the addition of I.G.3, ion gauge no.3. E., electrode; I.C., indirect electrode cooling via an oil bath; U., umbrella; V.P., to vacuum pump; C.J., cooling jacket; I.G., ion gauges; A.A., auxiliary anode

Fig.39a

Current sustained pressure effect (isotropic). p_0 = 0·15 mTorr

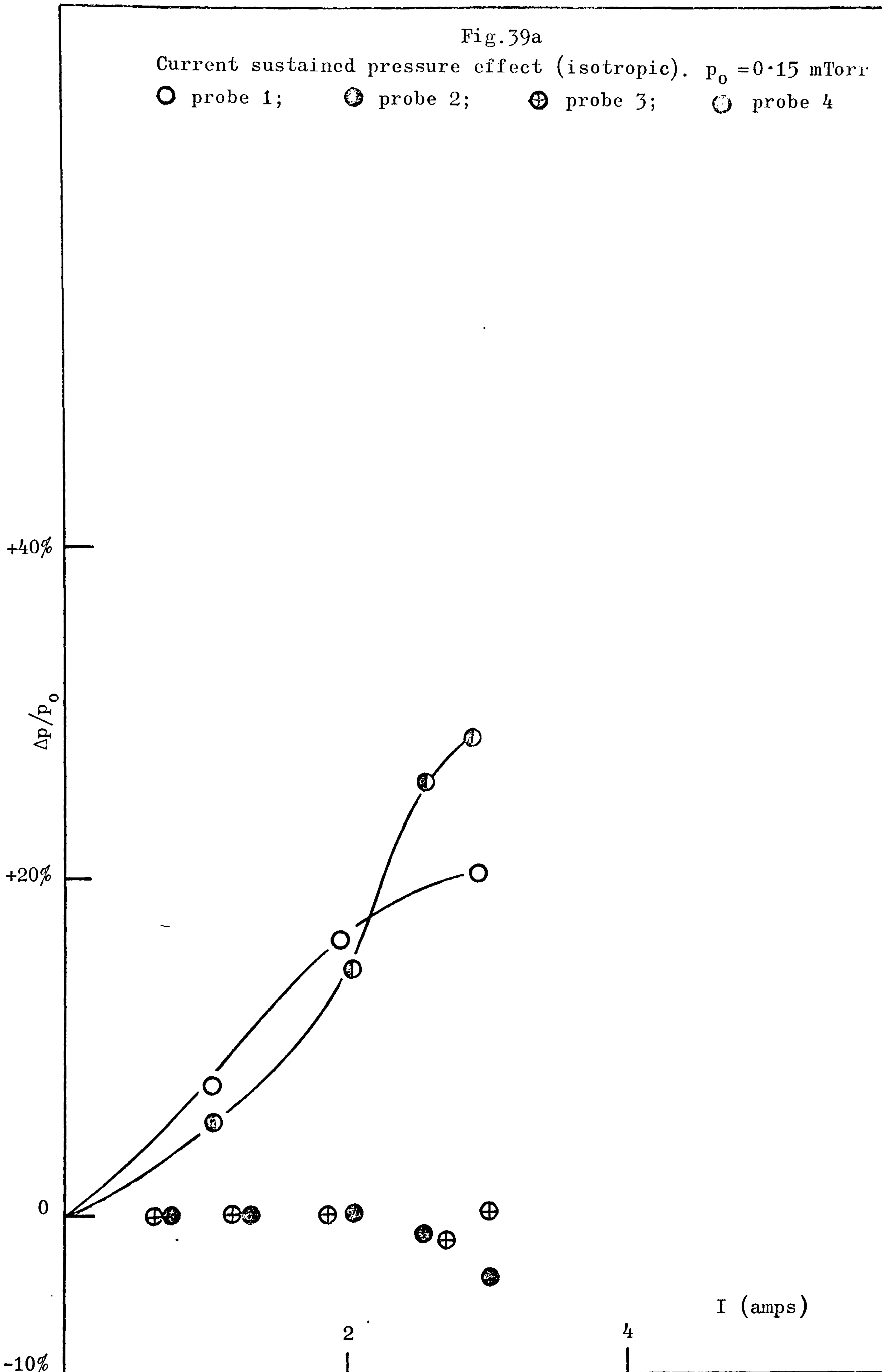

Fig.39b
As in Fig.39a but p_o = 0·2 mTorr

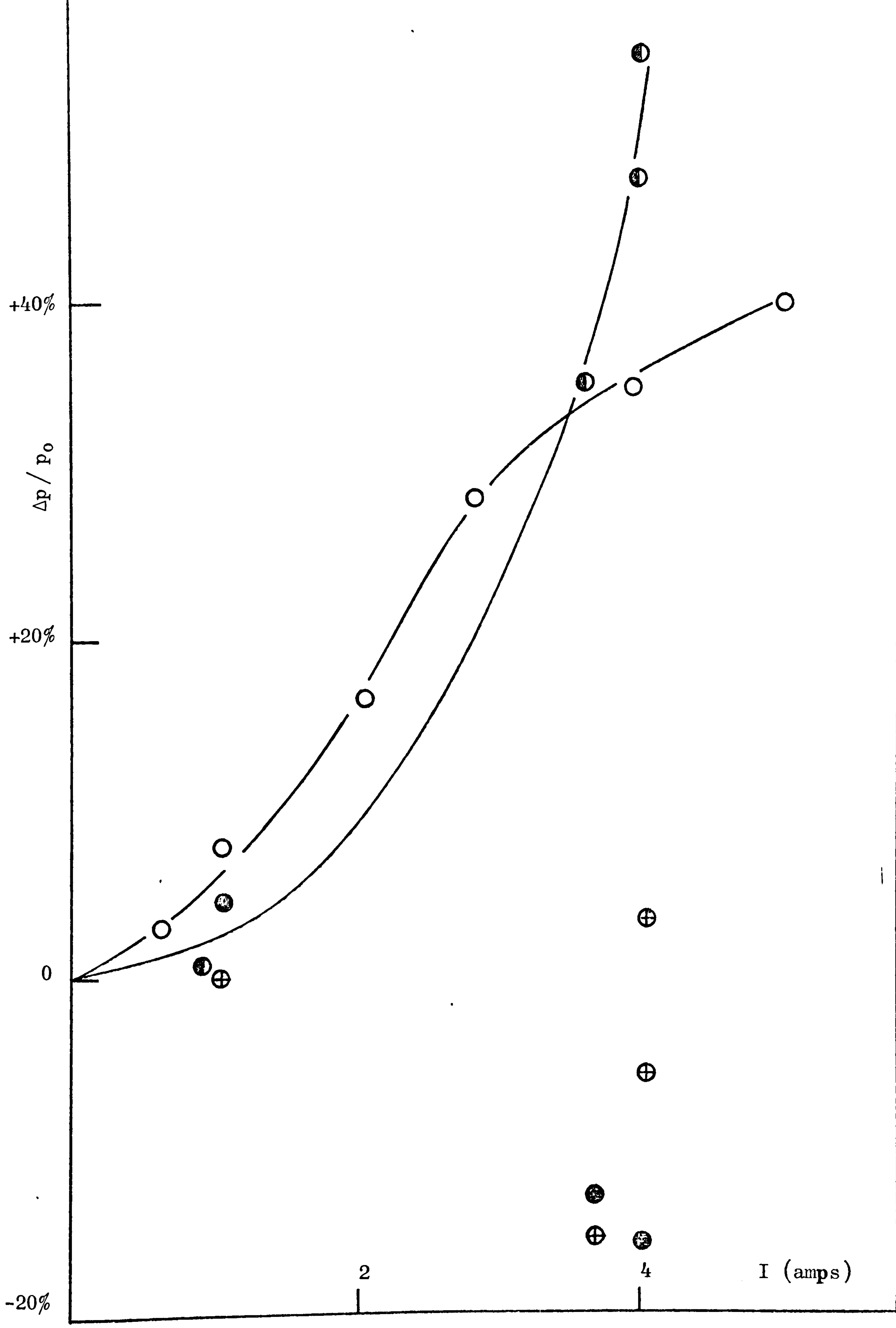

Fig.39c
As in Fig.39a but p_o = 0·3 mTorr

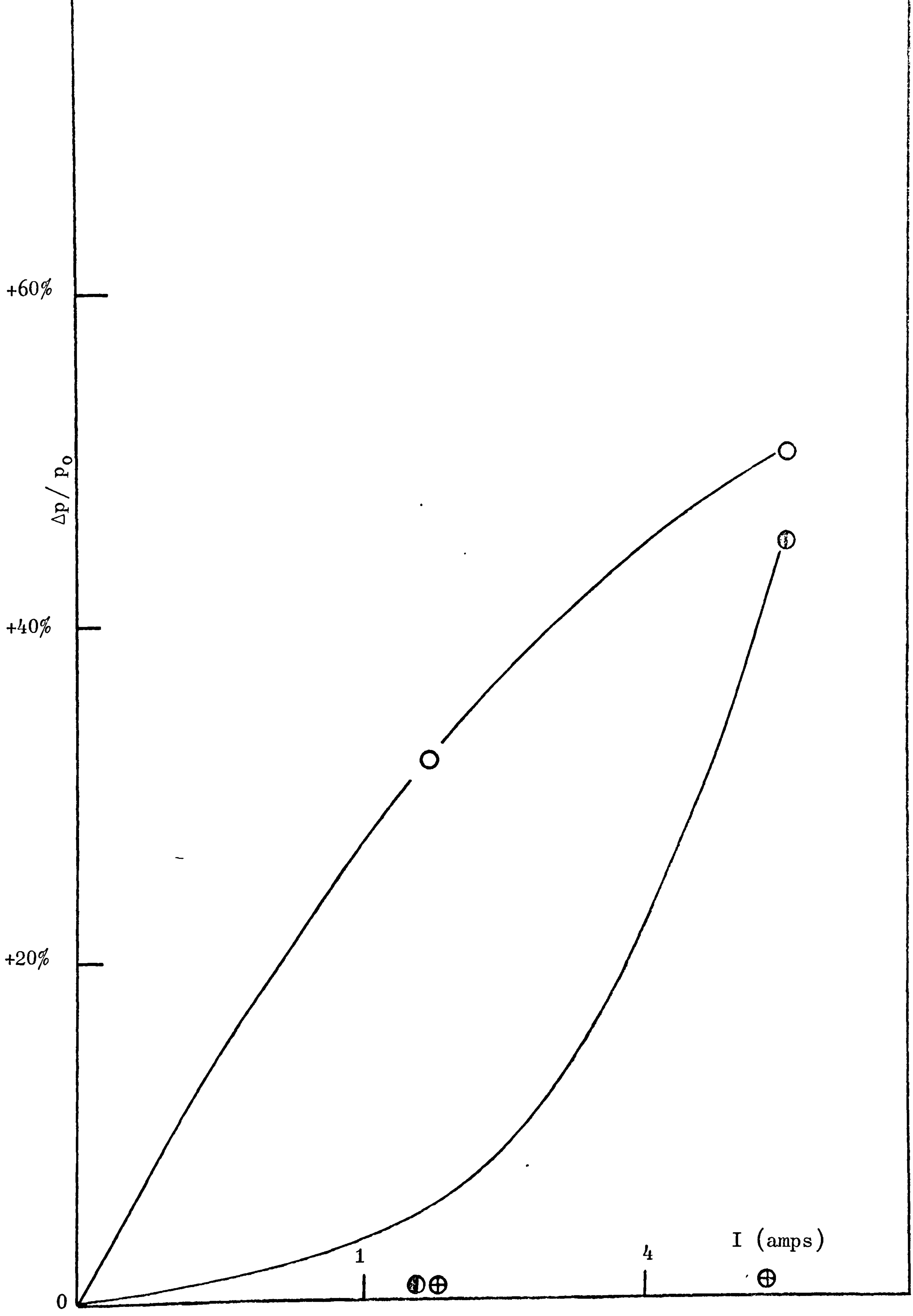

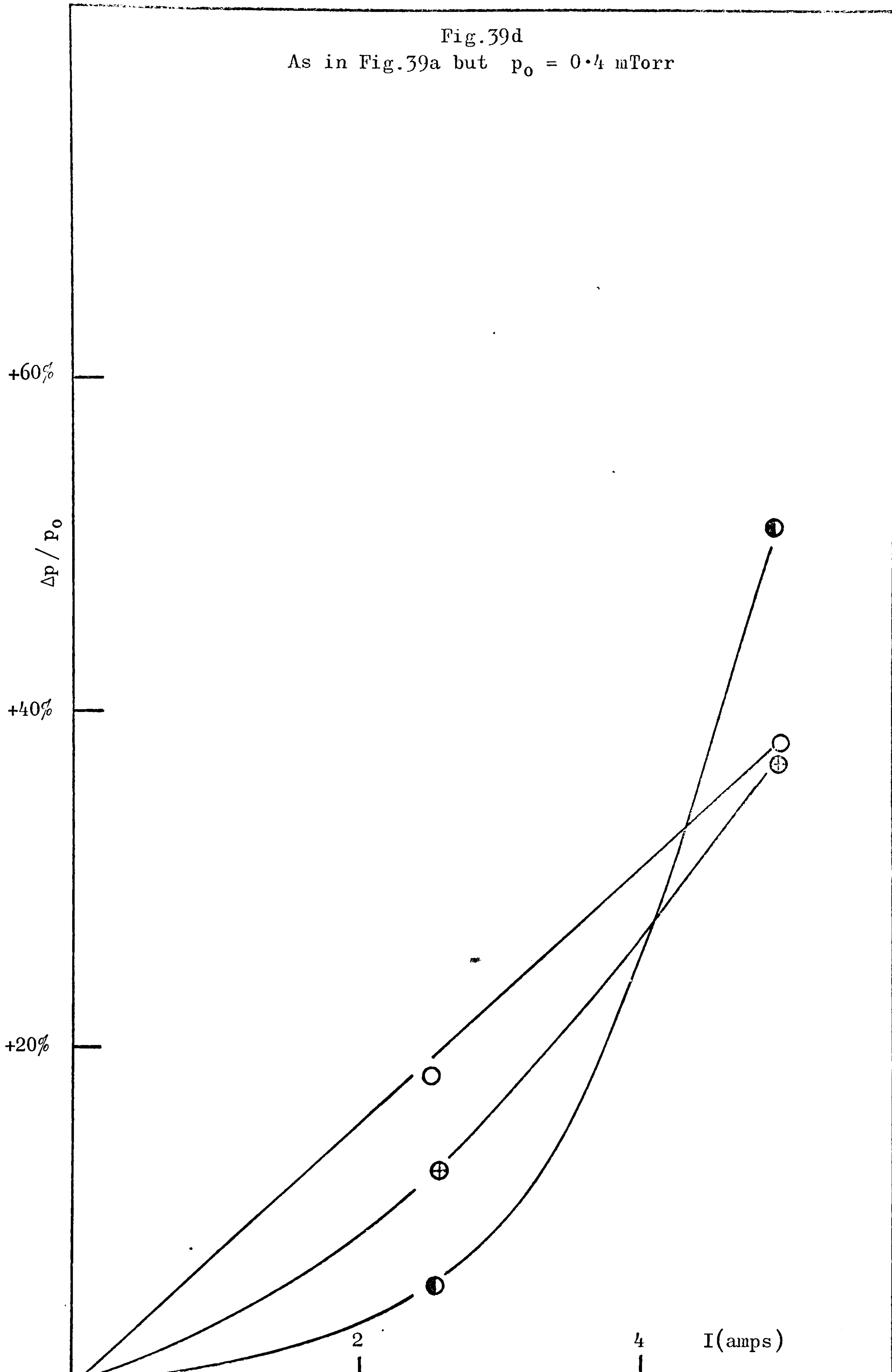

Fig.39d
As in Fig.39a but p_o = 0·4 mTorr
+60%
+40%
+20%
0
$\Delta p / p_o$
2
4
I(amps)

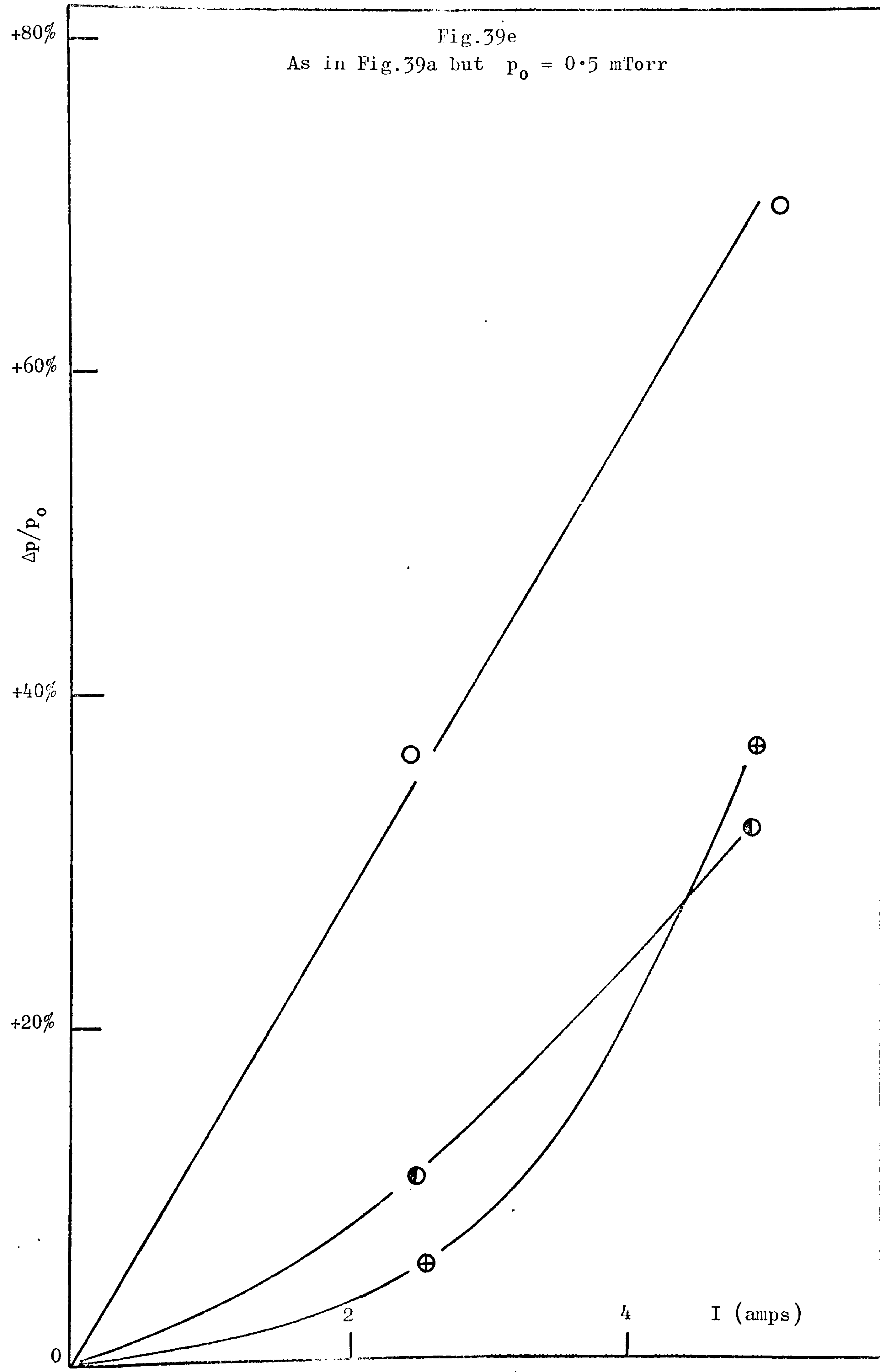
Fig.39e
As in Fig.39a but p_o = 0·5 mTorr
+80%
+60%
+40%
+20%
0
$\Delta p/p_o$
2
4
I (amps)

CHAPTER VIII

OPTICAL MEASUREMENTS AND DISCUSSION

8.1 INTRODUCTION

As the neutral density plays such a fundamental role in the phenomenon of current limitation, it was thought worthwhile to experimentally test the theory of section 5.3.3, which predicts the neutral density as a function of p_0, r_0 and I.

In the normal low pressure positive column, Klarfeld (1941) has estimated that cumulative ionization via the Hg metastable state 6^3P_0 and 6^3P_2 for $p_0 < 1$ mTorr, to be negligible for all I. Whether this continues to be true when the column is near limitation is an important question and so measurements of metastable densities in this regime were also undertaken.

There are many techniques for measuring the neutral density within a plasma but unfortunately most methods result in the disturbance of the plasma, effecting to an unknown degree the neutral density to be measured. Optical methods and certain other techniques can be non-disruptive; while these latter methods are incapable of providing local measurements they are to be preferred on the former grounds.

An optical method of some interest is an interferometric technique for measuring Nf, the product of neutral density N and oscillator strength f. This method called the Rozhdestvenskii (1912) hook method has been reviewed by Meroz (1960), Foster (1964) and Marlow (1965). It is concluded, Stangeby (1968), that this method is only sensitive to the measurement of Hg neutral density via the 2537 Å line, for neutral pressures greater than a few mTorr (for a single pass and path length $\simeq 1$ cm).

Measurement of particle density by the absorption of a beam of resonance radiation has been recognized by several experimenters to be the optimum method, thus Allen and Coville (1961), Torvén (1965), Hamberger (1966).

Its application has been mainly to the measurement of excited state populations, thus Fabrikant et al (1937), Yokoyama (1959), Hamberger (1961, 1966), Koedam and Kruithof (1962, 1963), Coulter et al (1963), Nodwell and Robinson (1965), Mitchell and Twiddy (1967), etc., but also to ground state populations, thus Allen and Coville (1961) Clark and Fairchild (1964), Torvén (1965), Egorov et al (1965), Gibbs and Hull (1967), Kreye (1967), Riley and Hall (1967), Bleekrode (1967), Aitkens and Sander (1968), etc.

Resonance radiation physics is extensively reviewed by Mitchell and Zemansky (1961).

The local emission and absorption line profile in a low pressure discharge is governed by Doppler broadening, and thus if the neutral velocity distribution is Maxwellian, the profile is Gaussian (the total emission line may well be influenced by self-absorption effects, see below). In the column near current limitation, the neutral distribution is no longer Maxwellian due to selective ionization of slow particles and of particles which have long flight paths. This leads to the rather unusual situation of a non-Gaussian local emisssion profile, i.e. emissivity, and more important for the technique of neutral density measurement, to a non-Gaussian absorption profile. The profile in these circumstances has been calculated in section 8.5, and the corrections to the results assuming a Gaussian profile are given.

8.2 DENSITY MEASUREMENT BY RESONANCE RADIATION ABSORPTION

The absorption coefficient $k(\nu)$ is defined by the equation:

$$\frac{dI(\nu,x)}{dx} = - k(\nu)\ I(\nu,x)\ , \qquad \ldots (8.1)$$

where $I(\nu,x)$ is the intensity of a parallel beam of light passing through a quantity of absorbing gas, of frequency ν at a distance x from the point of entry.

Consider this beam being attenuated by atomic absorption from a normal state of population N to an excited state of population N'; the beam is reinforced by induced emission (spontaneous emission being isotropic contributes negligibly to the parallel beam and is neglected here). Then

$$d[I(\nu,x)\ \delta\nu] = \delta\ N'(\nu)dx\ h\nu\ B_{21}$$

$$- \delta\ N(\nu)dx\ h\nu\ B_{12}\ \frac{I(\nu,x)}{4\ \pi} \qquad \ldots (8.2)$$

where:

$$N' = \int \delta\ N'(\nu)d\nu$$

and:

$$N = \int \delta\ N(\nu)d\nu\ .$$

B_{21}, B_{12} are the Einstein coefficients related by:

$$B_{21}/B_{12} = g_1/g_2\ , \qquad \ldots (8.3)$$

and

$$B_{12} = \frac{c^2}{2\ h\nu^3\ \tau}\ g_2/g_1 \qquad \ldots (8.4)$$

where g_1 and g_2 are the statistical weights of the normal and excited states respectively, τ is the lifetime of the excited state. Equation (8.2) may be written as

$$- \frac{1}{I(\nu,x)}\ \frac{dI(\nu,x)}{dx}\ \delta\nu = \frac{h\nu}{4\pi}\left(B_{12}\ \delta\ N(\nu) - B_{21}\ \delta N'(\nu)\right) \ldots (8.5)$$

and using equations (8.1) and (8.4) and integrating over all frequencies gives:

$$\int k(\nu)d\nu = \frac{\lambda_0^2\ g_2}{8\pi\ g_1}\ \frac{N}{\tau}\left(1 - \frac{g_1}{g_2}\frac{N'}{N}\right) \qquad \ldots (8.6)$$

where it has been assumed that $k(\nu)$ is a sharp function of frequency centred at ν_0 i.e. $k(\nu)$ corresponds to a 'line' at ν_0 (or λ_0).

Torvén (1965) has shown that for the type of discharge concerned with here $g_2 N \gg g_1 N'$, i.e. stimulated emission is negligible, so that in the following we may use $f\tau = (mc^2\lambda_0 g_2)/(8\pi e^2 g_1)$ to give:

$$\int k(\nu)d\nu = \frac{\pi e^2}{mc} Nf . \qquad \ldots (8.9)$$

The precise form of $k(\nu)$ is dependent on the broadening mechanisms operative in the plasma. Confining our interest to the Hg 2537 Å line originating in a low pressure (10^{-3} Torr) discharge, we may conclude that Doppler broadening is the only significant contribution to $k(\nu)$: the natural width $\Delta\nu_N$ is given by:

$$\Delta\nu_N = \frac{1}{2\pi\tau} , \qquad \ldots (8.10)$$

where $\tau = 10^{-7}$ sec. for this line, Blamont (1951), thus $\Delta\nu_N \simeq 10^6$ sec^{-1}. The Doppler width $\Delta\nu_D$, Mitchell and Zemansky (1961), is given by:

$$\Delta\nu_D = 2\sqrt{2 \ \ell n \ 2}\ \frac{\nu_0}{c}\left(\frac{kT}{M}\right)^{\frac{1}{2}} , \qquad \ldots (8.11)$$

where T = temperature of the gas (Maxwellian distribution assumed)
M = mass of Hg atom.

At room temperature this gives:

$$\Delta\nu_D = 10^9 \text{ sec}^{-1}$$

or

$$\Delta\nu_D = 10^{-3} \text{ Å}.$$

The Stark width $\Delta\nu_S$ may be estimated as follows: the local fields in a plasma are given approximately by:

$$E = e/\langle r^2\rangle \qquad \ldots (8.12)$$

where $\langle r^2\rangle$ is the average distance squared to the nearest charged particle, i.e. $n_e^{\frac{2}{3}}$; using the quadratic Stark effect displacement for Hg, see Hindmarsh (1967),

$$\Delta\nu_S = 8{\cdot}9 \times 10^{-3} E^2 , \qquad \ldots (8.13)$$

we obtain:

$$\Delta\nu_S \approx 20 \text{ sec}^{-1}.$$

The effect of collisional broadening may be estimated by the Lorentz half-breadth $\Delta\nu_L$ given by:

$$\Delta\nu_L = Z/\pi \;, \qquad \ldots (8.14)$$

where Z is the number of broadening collisions/sec/atom. At $p = 10^{-3}$Torr, estimating $Z < 10^4 \text{sec}^{-1}$ (using the neutral-neutral collision frequency, Crawford and Kino (1961)), thus $\Delta\nu_L < 10^4 \text{ sec}^{-1}$.

Therefore, assuming an absorption coefficient given by Doppler broadening and a Maxwellian distribution of absorbing atoms one can show that, see Mitchell and Zemansky (1961), also section 8.5,

$$k(\nu) = k_o \exp - [2(\nu - \nu_o)\sqrt{\ell n2}/\Delta\nu_D]^2 \qquad \ldots (8.15)$$

and k_o can be calculated from equation (8.9),

$$k_o = \frac{2}{\Delta\nu_D}\sqrt{\frac{\ell n2}{\pi}}\;\frac{\pi e^2}{mc}\,Nf \;. \qquad \ldots (8.16)$$

This preceeding development has been for a single absorption line. The Hg 2537Å line is in fact composed of five hyperfine components each separated by about 10^{-2}Å and of intensity ratios 19 : 29 : 24 : 15 : 13. Since each component has a width of only 10^{-3}Å, it is a valid approximation to consider each line separately and to write:

$$k_i(\nu) = k_o a_i \exp - \left[2(\nu - \nu_{oi})\sqrt{\ell n2}/\Delta\nu_D\right]^2 \quad i = 1,2,3,4,5, \qquad \ldots (8.17)$$

where the a_i are the appropriate weights (which we shall take to be 0·2 for all components).

The line emitted by the lamp (and absorbed by the discharge) shall be assumed to be Gaussian, but we shall allow for this emitted line to have a different width than the absorption line of the discharge:

$$\alpha \equiv \frac{\text{emission line breadth}}{\text{absorption line breadth}}$$

hence:

$$I(\nu,0) = I_o \exp - (\omega/\alpha)^2 \qquad \ldots (8.18)$$

for each component, where:

$$\omega \equiv 2(\nu - \nu_o)\sqrt{\ell n2}/\Delta\nu_D \;. \qquad \ldots (8.19)$$

Now, integrating equation (8.1) gives:

$$I(\nu,x) = I_0\left[\exp - (\omega/\alpha)^2\right] \exp\,(-k(\nu)x), \qquad \ldots (8.20)$$

and integrating over all frequencies one obtains the absorption, $A(\alpha,\beta)$, given by:

$A(\alpha,\beta)$ = intensity absorbed / intensity

$$= \frac{\int_{-\infty}^{+\infty} e^{-(\omega/\alpha)^2}\left(1 - e^{-\beta\, e^{-\omega^2}}\right) d\omega}{\int_{-\infty}^{+\infty} e^{-(\omega/\alpha)^2}\, d\omega}, \qquad \ldots (8.21)$$

where $\beta = 0{\cdot}2\ k_0\ell$ and ℓ is the total length of absorbing gas. Values of $A(\alpha,\beta)$ obtained by numerical integration on a computer are shown in Fig.41, (it was found that the values of $A(\alpha,\beta)$ given by Mitchell and Zemansky are very slightly in error, usually $< 1\%$).

Value of β: in the present experimental situation the range of ℓ and N are given by:

$$0{\cdot}6 < \ell < 2{\cdot}4 \text{ cm},$$
$$3 \times 10^{12} < N < 2 \times 10^{13} \text{ cm}^{-3},$$

and from equation (8.16) with $T = 303^oK$:

$$\beta = 0{\cdot}2\ k_0\ell = 1{\cdot}16 \times 10^{-13} N\ell \qquad \ldots (8.22)$$

hence:

$$0{\cdot}3 < \beta < 6$$

From the graphs of $A(\alpha,\beta)$ one can see that the absorption technique is fairly sensitive over this range of β, and it is this fact which makes the technique the optimum one for the present experiment. Value of α: by examining the graph of $A(\alpha,\beta)$ vs β one can see that the sensitivity, $\partial A/\partial\beta$ is a monotonically decreasing function of α. Hence the lowest possible α obtainable is to be desired. In practice $\alpha = 1$ is the practical lower limit, see section (8.3); Table 6 gives some impression of the sensitivity as a function of α and β.

Fig.41

$T(\alpha,\beta)$. Theoretical transmission curves for Gaussian profiles. $\beta = 0{\cdot}2$ $\quad k_0\ell = 1{\cdot}16 \times 10^{-13}\ N\ell$ for Hg.

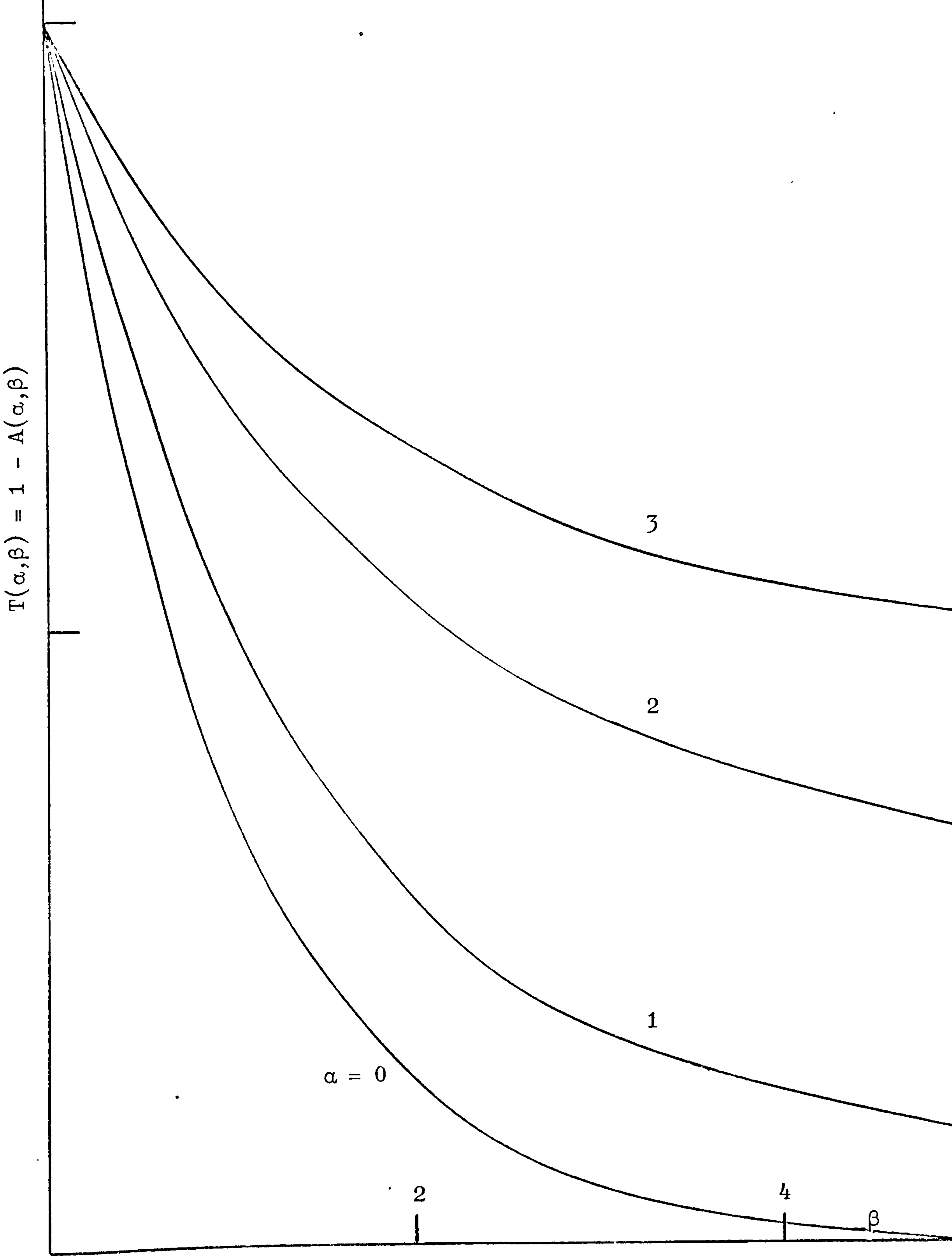

TABLE 6

ERROR IN β CAUSED BY A 5% UNCERTAINTY IN T (= 1-A)

	α=	1	2	3
β =	1	8%	16%	25%
	4	3%	12%	17%

8.3 OPTICAL APPARATUS

8.3.1 General

The optical arrangement is shown schematically in Fig.42.

Since the 2537Å line from the lamp is at the same wavelength as the more intense radiation from the discharge itself, the most convenient way to distinguish the two signals, is by phase sensitive detection. The 2537Å radiation from the lamp, is passed through a mechanical chopper (typically 130 Hz), into a U.V. monochromator (Hilger and Watts, model 186 with adaptor D183, vitreous silica 60^{o} prism) and thence into a photomultiplier, p.m. The signal from the p.m. was amplified 10 or 100 times and passed into the phase sensitive detector, p.s.d. The reference signal for the p.s.d. was obtained from a photodiode which looked at a small light bulb through the mechanical chopper. The two chopped signals, as viewed on a dual beam oscilloscope, were brought into phase by adjusting the position of the photodiode relative to the U.V. lamp and chopper. The output from the p.s.d. was integrated and the D/C level read from a voltmeter. This voltmeter reading gave a measure of the transmission of the lamp signal independent of the 2537Å radiation eminating from the discharge.

The light path from the chopper to the monochromator was collimated to give a beam diameter of 1 mm. The collimation and the general positioning of the elements was such as to maximize the lamp signal relative to the

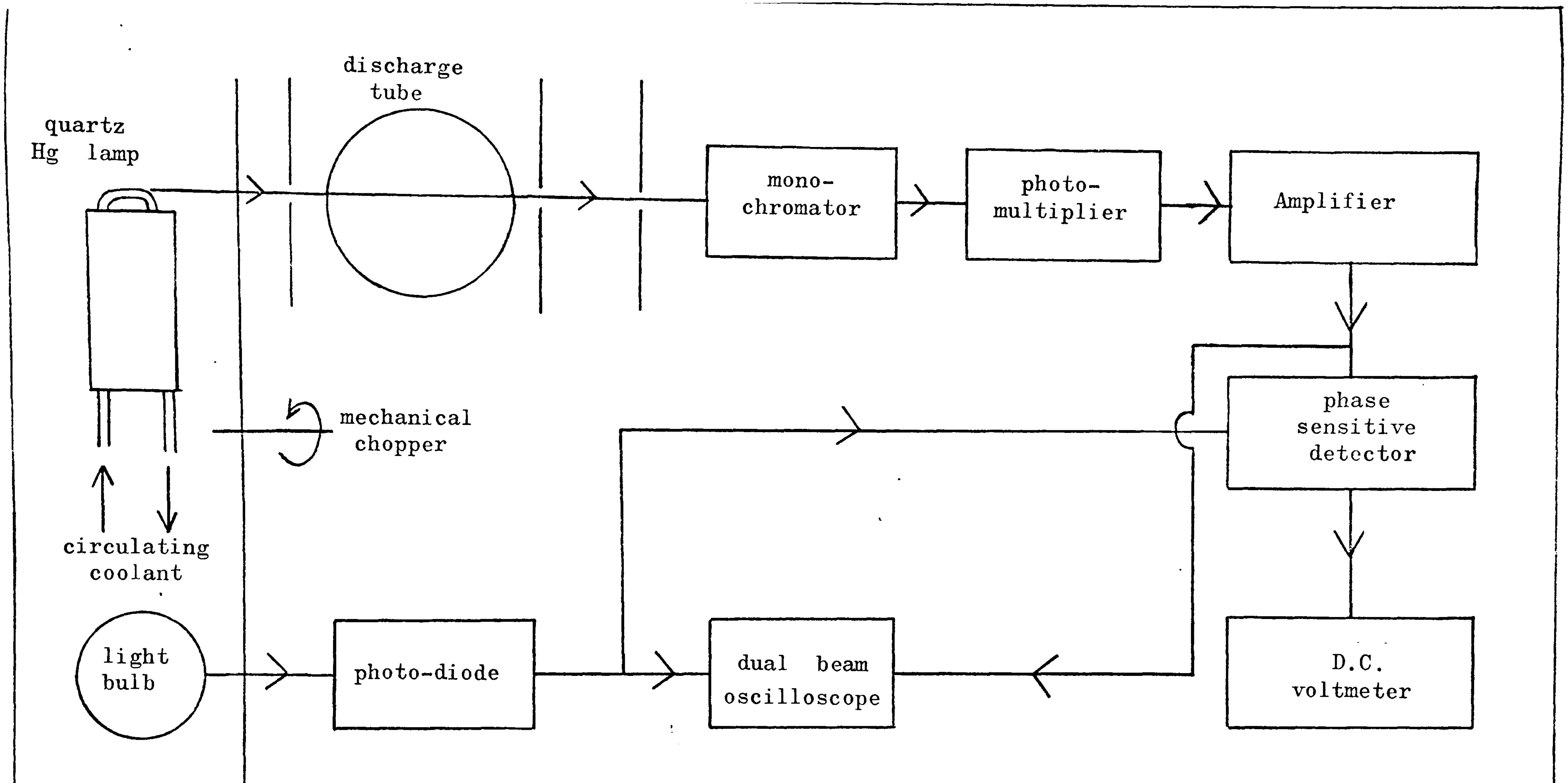

Fig.42
Schematic diagram of optical arrangement for neutral and metastable density measurements

discharge light output. In this way it was found that the D/C level from the discharge was typically only an order of magnitude greater than the A/C lamp output, and thus the risk of saturating the p.m. with the D/C signal was minimized. No lenses were employed.

In the present set-up, one has the option of obtaining values of the neutral density from the transmission measurements and using the theoretical values of $A(\alpha,\beta)$ if the α of the lamp is known, or one can simply calibrate the transmission against known neutral densities if the lamp α is unknown. In the arrangement of Allen and Coville (1961), where the discharge light is used as its own lamp (via a mirror), calibration is impossible and the value of α is uncertain due to self-absorption, see section 8.3.3(a).

The lamp, chopper, collimators and monochromator were mounted on an adjustable table, which could be raised or lowered so as to obtain transmissions through different cross-sections of the tube, with a view to doing an Abel inversion to obtain $N(r)$.

Mechanical vibrations, especially from the chopper, were found to be troublesome and it was necessary to reduce these vibrations as much as possible.

The width of the monochromator slits was not critical as the 2537Å line is so much more intense than any line nearby. A moderately strong line ~ 2650Å (tentatively identified as the cluster of neon lines around 2650Å - the lamp had a partial filling of neon, see section 8.3.3), was easily avoided.

The photomultiplier employed was an RCA-IP28, 9-stage, U.V. transmitting tube. The circuit diagram is given in Fig.43. For stability and the elimination of stray effects, the entire circuit is mounted within the p.m. housing and the signal taken out by coaxial cable. The risk

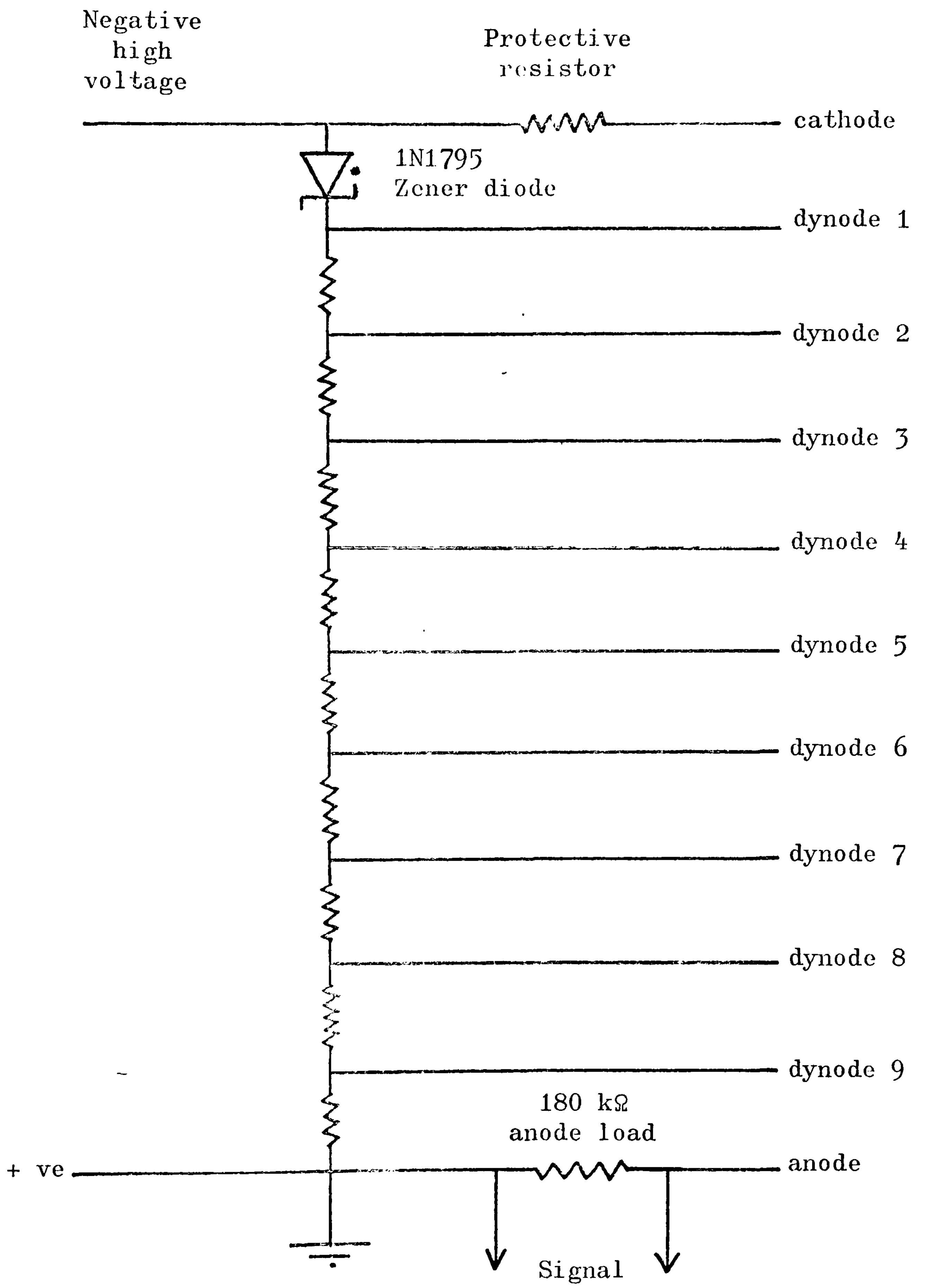

Fig.43
Circuit diagram for photomultiplier supply. All resistors are 100 kΩ high stability except anode load

of high anode currents from the discharge D/C 2537Å emission rendering the p.m. circuit response non-linear was avoided firstly by suppressing this D/C level by good collimation, and secondly by using the auxiliary $100\times$ amplifier shown in Fig.42. In this way the p.m. chain current, ~ 1 mA, was well above even the D/C anode current, $< 1\ \mu$A, and the further $100 \times$ amplification brought the signal up to a convenient level, ~ 0.3 V. Therefore it was unnecessary to make the p.m. circuit extremely linear as would be necessary if a small A/C signal was superimposed on an extremely powerful D/C level.

8.3.2 The Phase Sensitive Detector

A schematic diagram of a p.s.d. is shown in Fig.44 and its operation will be briefly summarized: the reference signal causes the 2-way switch to shunt the signal alternatively between R_1 and R_2. In effect the signal, $V_S f_2(t)$ is multiplied by a square-wave $f_1(t)$:

$$f_1(t) = \sin \omega t + \tfrac{1}{3} \sin 3\,\omega t + \frac{1}{5} \sin 5\,\omega t + \ldots \qquad \ldots (8.23)$$

where ω is the frequency of the reference signal, thus:

$$\overline{V_1 - V_2} = V_S \frac{1}{T} \int_0^T f_1 f_2 \, dt \qquad \ldots (8.24)$$

where $\overline{V_1 - V_2}$ is the time integrated signal averaged for time T (averaging may be accomplished with capacitors strapped between outputs and earth). It is evident that if T is sufficiently long then only those components of $V_S f_2(t)$ which are at the same frequency and phase as the reference signal will contribute to the D/C output (odd harmonics of ω in $V_S f_2(t)$ are passed as well, of course).

For finite T there will be a passband of frequencies $\Delta\omega$ about ω given by $\Delta\omega \sim 1/T$. In the present work, the time constant of the integrator is:

$$\begin{aligned} T &= RC \\ &= 1\ \text{k}\Omega \times 5000\ \mu\text{F} \\ &= 5\ \text{sec} \end{aligned}$$

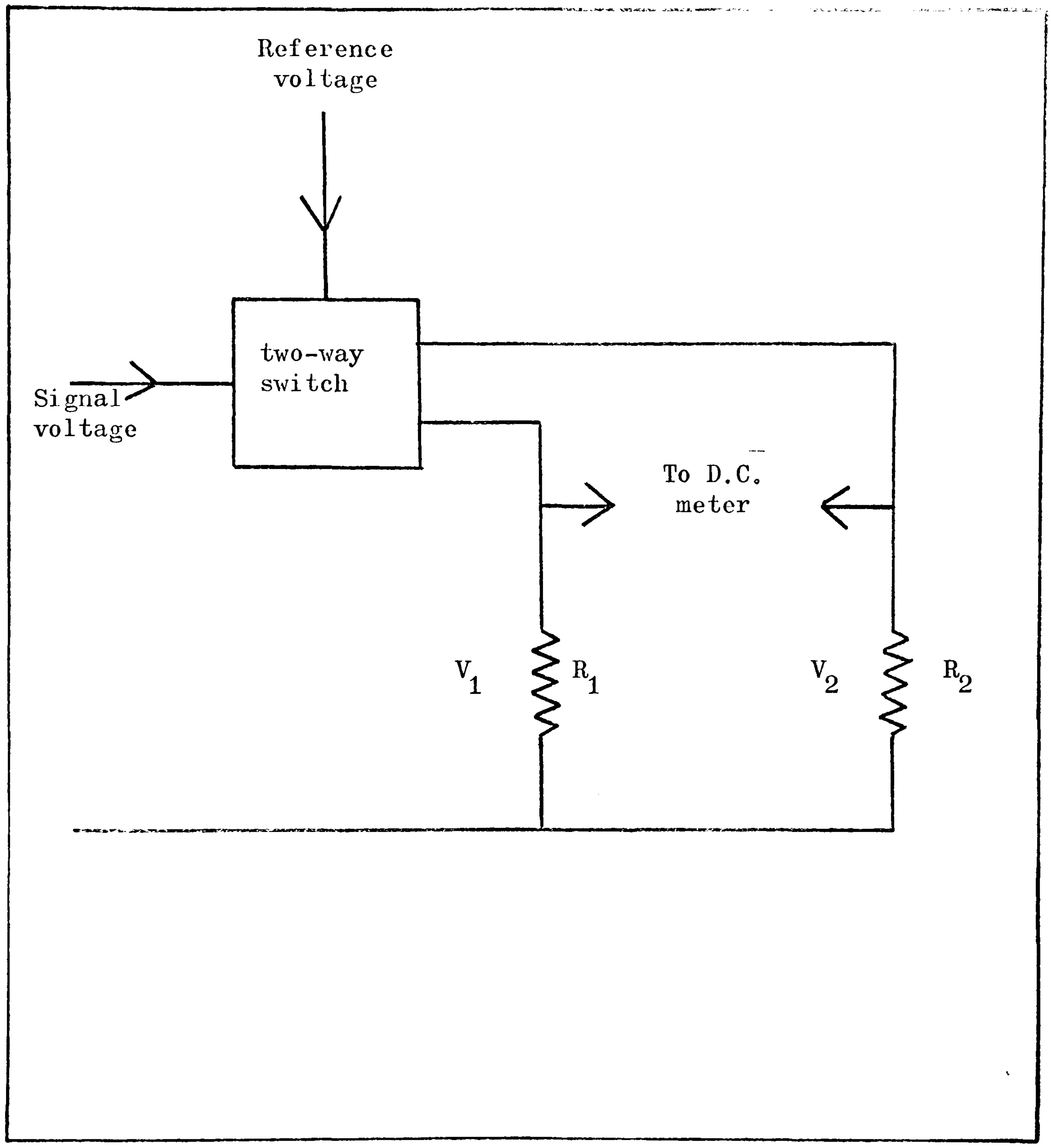

Fig.44
Schematic diagram of phase sensitive detector

hence the passband for noise transmission, $\Delta\omega \sim {}^{1}/_{5}$ Hz, is quite narrow.

The p.s.d. employed was a Brookdeal PP313A, 3 Hz to 300 kHz.

8.3.3(a) Lamp

A convenient source of 2537Å radiation is a simple D/C discharge lamp, that is, a sealed-off quartz vessel with hollow electrodes and a filling of a few mm pressure of permanent gas and some Hg droplets. Unfortunately, such a source tends to produce a line which is self-reversed due to re-absorption of 2537Å light within the lamp itself. The reason for this is as follows:

The photons at the wings of the emission line tend to pass right out of the lamp without being re-absorbed, as the absorption coefficient at the wings is very small. The photons near the centre of the line, are re-absorbed within the lamp as the absorption coefficient is large here. If the atom re-emitted this absorbed photon with just the same Doppler shift as before, then there would be no net effect, but of course, the atom having just absorbed a photon with a small Doppler shift, i.e. a photon near the line centre, will have a tendency to re-emit the photon in the same direction as the atom velocity, i.e. with a large Doppler shift. Thus the net result of re-absorption within the lamp is to transfer photons from the centre of the line to the wings, i.e. the resultant line emitted by the lamp is self-reversed (or at least self-broadened).

The process of self-reversal is often attributed to an assumed layer of cold non-emitting, absorbing, vapour around the emitting core, but this explanation fails to emphasise the net photon transfer from centre to wings, and furthermore, the self-reversal can obviously occur even if the whole lamp is excited homogeneously, see Hearn (1963, 1964).

Now, a self reversed line cannot be used for the absorption work contemplated here, because the transmission of such a line is always near 1,

Fig.45
Quartz Hg U.V. lamp with partial filling of 4 Torr of neon

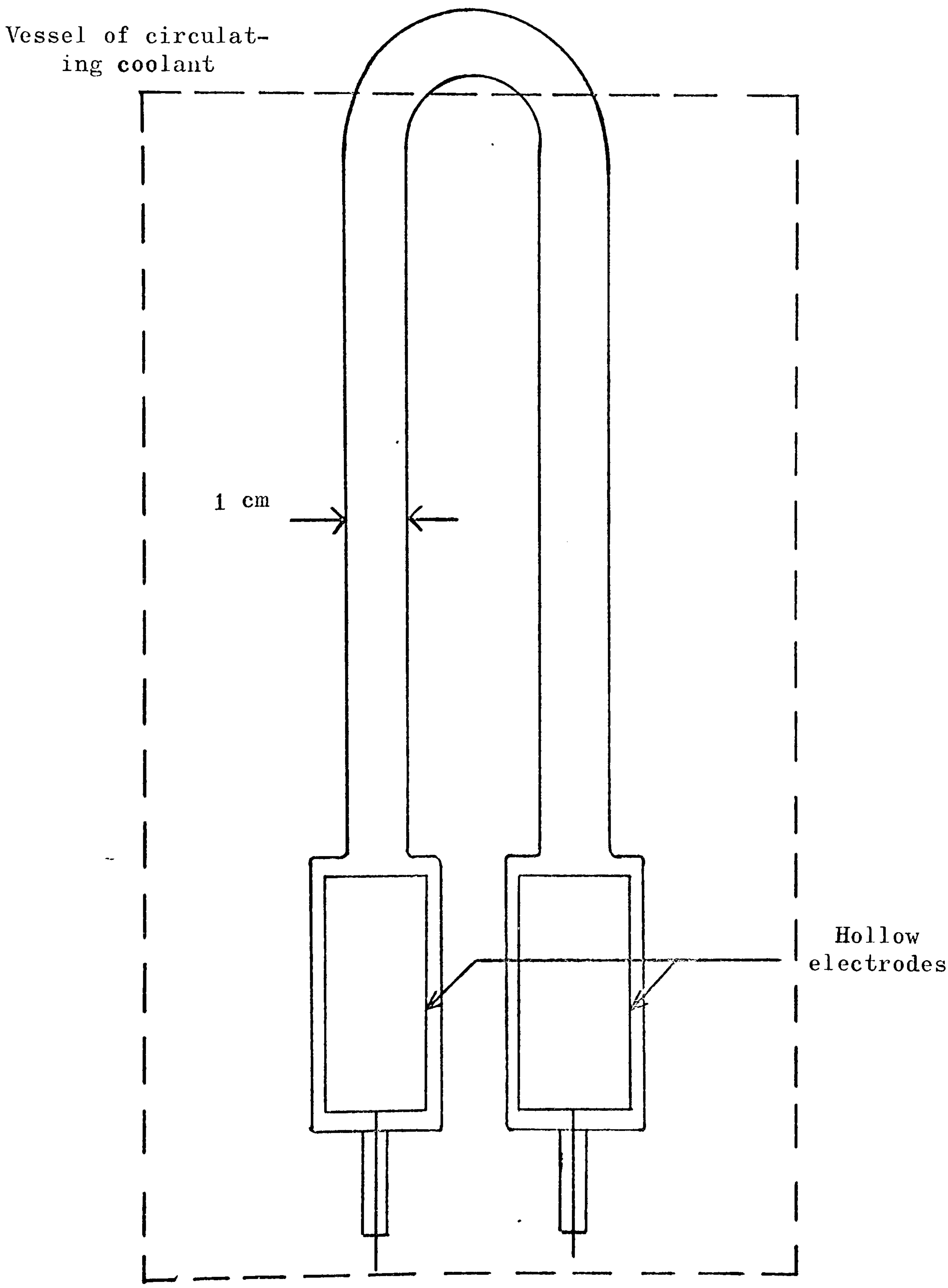

and shows therefore no sensitivity to the sort of changes in neutral density expected in the present work. Furthermore, such a line, being non-Gaussian, does not correspond to the theory providing $A(\alpha,\beta)$.

If such a lamp were cooled, i.e. the Hg density lowered, so severely that even the photons at the line centre had small probability of being re-absorbed in the lamp, then the intensity would be far too low to be useful.

In practice, a compromise can be accepted and the lamp cooled to such a degree that instead of actual reversal taking place, the top of the Gaussian profile becomes blunted and the resultant profile is practically equivalent to a Gaussian but with a larger half-width. In this way, one can continue to use the parameter α and the values of $A(\alpha,\beta)$. There are three ways to establish what α will be for this self-broadened line:

(a) Measure the line profile with a high dispersion spectrometer and a Fabry-Perot etalon.

(b) Calculate the value of α for the lamp.

(c) Estimate α by measuring $A(\alpha,\beta)$ for known β (i.e. known neutral densities).

The first method has not been attempted in the present work for lack of equipment. The second method, that of calculating α is discussed in section 8.3.3(b). The third method is the easiest in practice, but of course once the system has been calibrated, i.e. A vs β obtained, then α is only of academic interest, as one may then use the calibration curve directly.

The complications of self-broadened lines could be avoided either if a 2537Å laser were available or if a resonance lamp could be made sufficiently powerful. A resonance lamp is a vessel of Hg vapour which is illuminated by a powerful, but strongly self-broadened Hg arc lamp.

The line re-radiated by the resonance lamp will not be at all self-broadened if its Hg pressure is kept sufficiently low - but of course this results in low intensity.

For the present experiment a special quartz lamp was produced by Thermal Syndicate Ltd, see Fig.45. The lamp is filled with 4 Torr neon (as a carrier gas) and a few drops of Hg. The lamp is similar to a standard one with 1 Torr argon and 18 Torr neon filling, but the lower pressure carrier gas was decided on to reduce pressure broadening. At 18 Torr of neon, the 2537 Å line is 15% broader than the Doppler width, while at 4 Torr the effect should be ~ 1%, Mitchell and Zemansky (1961). The lamp is normally rated at 120 mA, but to narrow the profile it was usually run at 10 mA. It was cooled, usually at + 20°C, by a circulating bath of temperature controlled coolant (the system is similar to that of the coolant circuit and control for the discharge tube, see section 6.3).

At these low currents, ~ 10 mA, the light output tended to wobble and this was substantially reduced by using a current-stabilized power supply.

With $T_{Lamp} = +\ 20^{o}C$ and $I_{Lamp} = 10$ mA a value of $\alpha = 1{\cdot}4 \pm 0{\cdot}1$ was found. As can be seen from the graphs of $A(\alpha,\beta)$, this line gives quite adequate sensitivity for the neutral density variations expected.

8.3.3(b) Calculation of the Lamp Line Profile (α)

If in the lamp $\beta \gtrsim 1$, then re-absorption of photons becomes important and the problem is one of radiation transfer. This process is a highly complex one as there is generally a correlation between the direction of the absorbed and re-emitted photon, also the frequency distribution of the re-emitted photons is dependent on the absorption profile in a complicated way. (Collisions while the atom is excited remove both of these complexities, but a collisionless regime is considered here).

The problem of radiation transfer and the resultant emitted line profile has been treated quite extensively and we may consider for example, the work of Hearn (1963, 1964).

Hearn (1963) employed a model in which the photons were completely re-distributed in space and frequency on each absorption, i.e. re-emission is considered to be isotropic and also the local re-emitted profile is assumed to be given solely by Doppler broadening, independent of the frequency distribution of the absorbed photons. He considered slab geometry and with the aid of a computer solved the system of related equations. In the 1964 paper, he removed the assumption of complete re-distribution in frequency space.

The chief result of interest in the present context is the computed total emission profile as viewed normally to the slab, for Hearn's results confirm the experimental fact that even when $\beta \sim 4$, the emitted line is not self-inverted, but only self-broadened. The 1964 results show that removing the assumption of re-distribution in frequency space effects the profiles less than 10%. While this model is still approximate and valid for slab geometry rather than the cylindrical geometry of the lamp employed, it is interesting to compare Hearn's calculated profile, and Gaussian profiles. For the lamp operating at $T \simeq +20^{o}C$ and with diameter $D \simeq 1$ cm, we may employ Hearn's profile for $\tau = 2$ ($\tau = \frac{1}{2} \times 1.16 \times 10^{-13}$ N D) which is shown in Fig.46 along with various Gaussians. As may be seen, the agreement between the calculated profile and the $\alpha = 1{\cdot}4$ Gaussian is quite reasonable, in agreement with the experimentally established $\alpha = 1{\cdot}4 \pm 1$.

It is difficult to appreciate the physical processes in a model so complex as Hearn's, and it is interesting to note that a far simpler and intuitive model gives a profile with essentially the same half-width: consider slab geometry and the simplifying assumption that photons are

Fig.46

Comparison of Hearn's calculated emission profile for $\beta = 4$ (broken line) with various Gaussians ($e^{-\omega^2/\alpha^2}$)

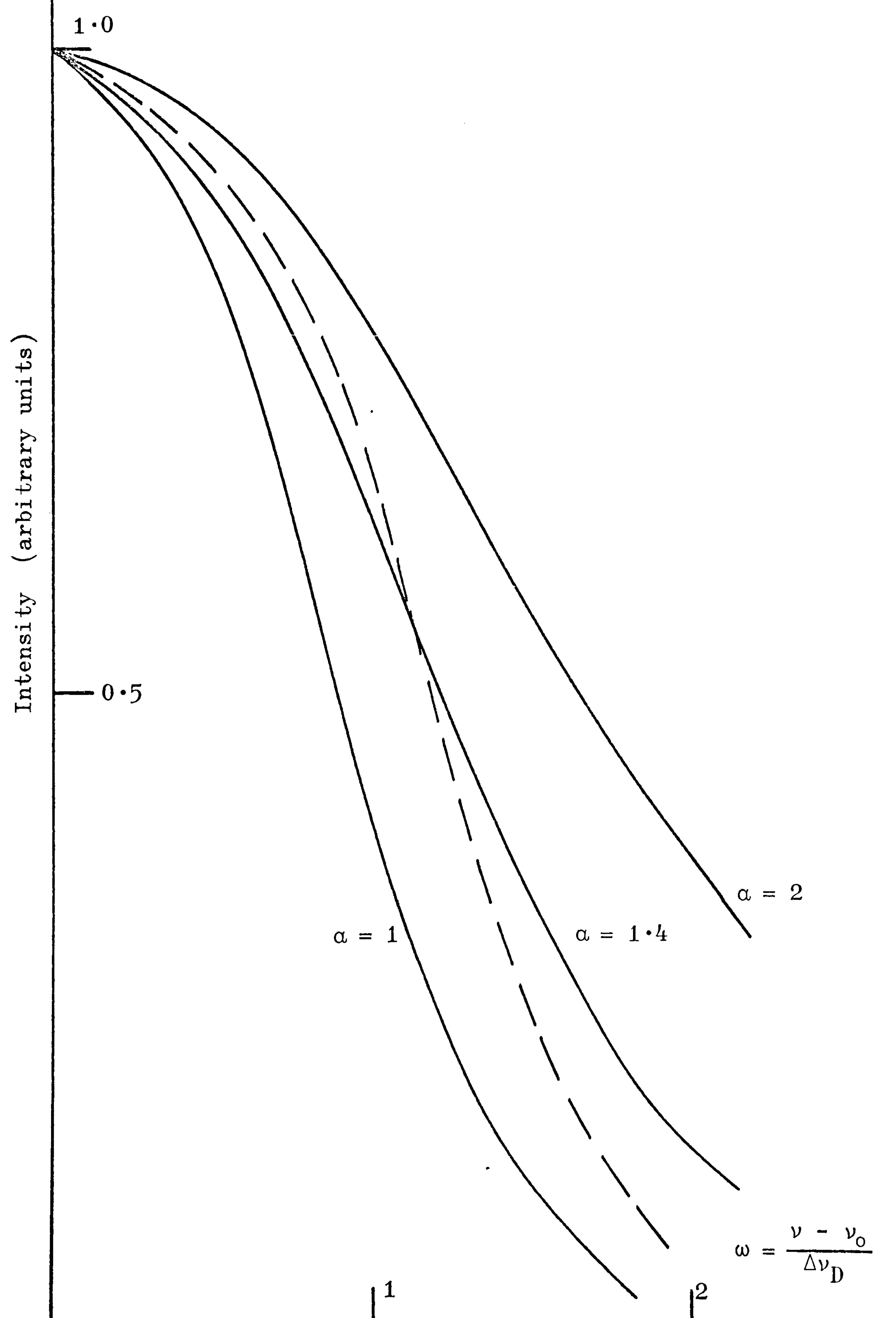

only emitted in the +x or -x direction. Further, assume that neutral density is uniform and that re-emission is frequency re-distributed completely, i.e. the local re-emission is always with a Doppler profile.

The 'first generation photons', i.e. photons originating from electronically excited 6^3P_1 states make a contribution $E_1(\omega)$ to the total emission $E(\omega)$. Thus:

$$E_1(\omega) = \int_0^L 1 \cdot e^{-\omega^2} e^{-0\cdot 2\, k_0 x\, e^{-\omega^2}} dx, \qquad \ldots (8.25)$$

where:

L = is the slab thickness;

$k_0(N_0)$ is the absorption constant;

$1 \cdot e^{-\omega^2}$ is the original local emission in each direction (if n_e is not uniform, then this term becomes:

$$(n_e(x)/n_{eo}) \cdot e^{-\omega^2}$$

where n_{eo} is the density at some reference point).

Re-writing equation (8.25) gives:

$$\frac{\beta}{L} E_1(\omega) = \int_0^\beta e^{-\omega^2} e^{-y e^{-\omega^2}} dy \ , \qquad \ldots (8.26)$$

where $\beta = 0\cdot 2\, k_0 L$, as before.

One can also calculate $C_2(x)\, dx$, the number of first generation photons absorbed in element dx from all other emitting elements. To calculate $C_2(x)$ consider Fig. 47. The contribution of element dx' to element dx is evidently

$$1 \cdot e^{-\omega^2} dx'\, e^{-0\cdot 2\, k_0 (x-x') e^{-\omega^2}} \left(1 - e^{-0\cdot 2\, k_0\, dx\, e^{-\omega^2}}\right) , \qquad \ldots (8.27)$$

or

$$1 \cdot e^{-\omega^2} e^{-0\cdot 2\, k_0 (x-x')\, e^{-\omega^2}} \cdot e^{-\omega^2}\, 0\cdot 2\, k_0\, dx\, dx' \ , \qquad \ldots (8.28)$$

and so in total:

$$C\ (x) = C\ (y) = \int_{-\infty}^{+\infty} \int_0^\beta e^{-2\omega^2} e^{-|y-y'| e^{-\omega^2}} dy'\, d\omega \ , \qquad \ldots (8.29)$$

where:

$$y = 0\cdot 2\, k_0 x\ .$$

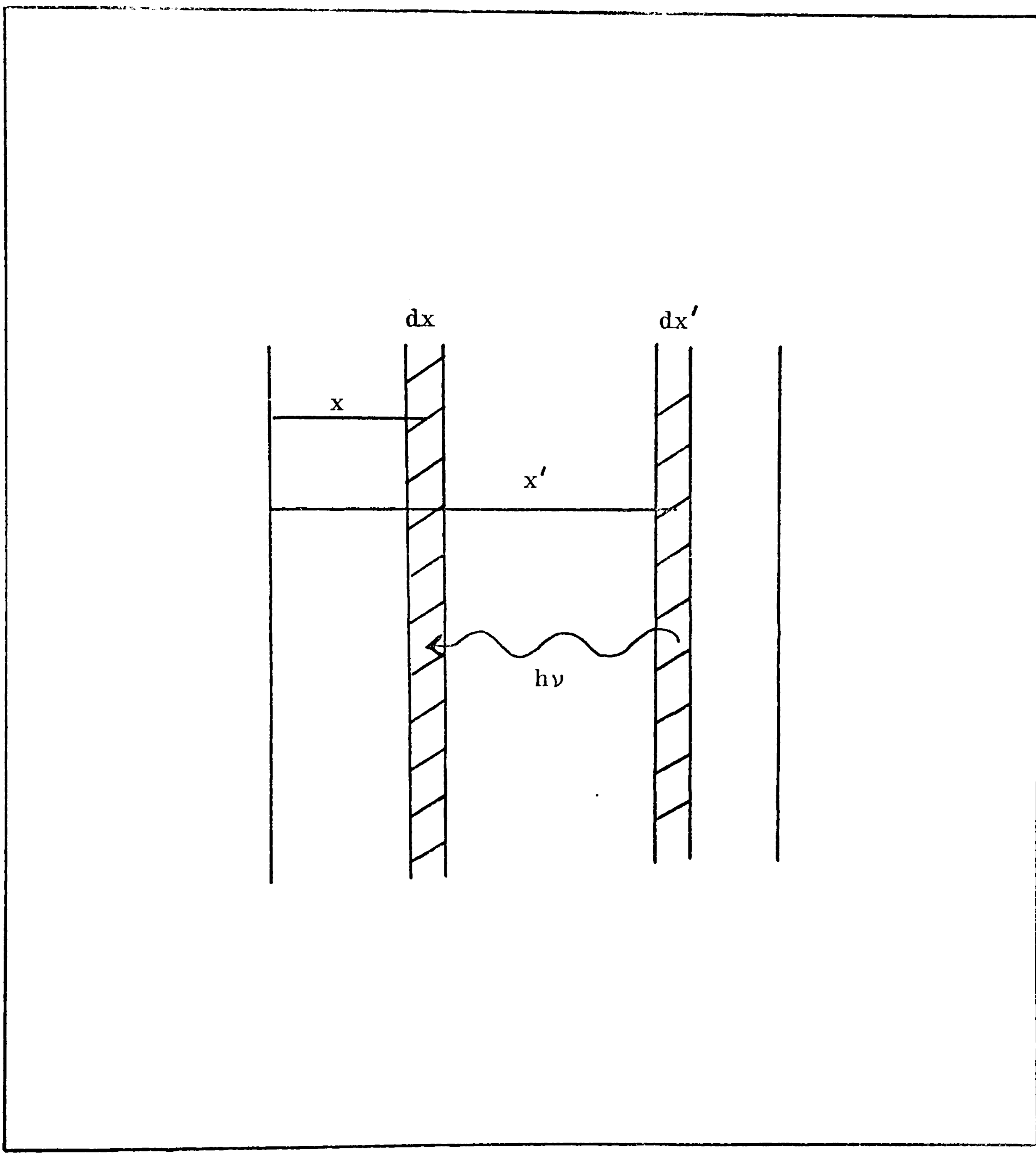

Fig.47
Diagram to illustrate model for lamp emission profile. Photon emitted in dx' is absorbed in dx

Now these absorbed first generation photons will be re-emitted as second generation photons, with the emission profile:

$$C_1(x)\ dx\ \frac{e^{-\omega^2}}{2\sqrt{\pi}}\ , \qquad \ldots (8.30)$$

where the 2 accounts for half the absorbed photons being re-emitted in one direction, and the $\sqrt{\pi}$ accounts for frequency re-distribution, i.e.

$$\int_{-\infty}^{+\infty} e^{-\omega^2}\ d\omega = \sqrt{\pi}\ . \qquad \ldots (8.31)$$

Thus one can calculate $E_2(\omega)$ and similarly all higher contributions:

$$\frac{\beta}{L}\,E_i(\omega) = \int_0^{\beta} \frac{C_i(y)}{2\sqrt{\pi}}\ e^{-\omega^2} e^{-ye^{-\omega^2}}\ dy\ , \qquad \ldots (8.32)$$

and

$$E(\omega) = \sum_i\ E_i(\omega)\ . \qquad \ldots (8.33)$$

By generalizing equation (8.29) one can easily show that:

$$C_{i+1}(y) = \int_{-\infty}^{+\infty}\int_0^{\beta} \frac{C_i(y')}{2\sqrt{\pi}}\ e^{-2\,\omega^2} e^{|y-y'|\,e^{-\omega^2}}\ dy'\,d\omega\ . \qquad \ldots (8.34)$$

The E_i and C_i can actually be obtained analytically, but these recursion formulas make it very convenient for computer calculation. For $\beta = 4$ the various $E_i(\omega)$ are shown in Fig.48 and thus one can see in a direct and intuitive way how the total $E(\omega)$ comes about, see Fig.49 (where the sum has been taken to $i = 10$). One even finds that this simple model gives approximately the same half-width as before, i.e. $\Delta\omega \approx 1{\cdot}35$.

In light of the approximations used to calculate α, it seems advisable to use experimental values where they are obtainable. The theoretical models, however, do confirm that even when an appreciable amount of self-absorption occurs ($\beta \approx 4$), the total emission profile is still nearly Gaussian in confirmation of the experimentally found values of α..

Fig.48
Contributions to calculated lamp emission profile. $\beta = 4$

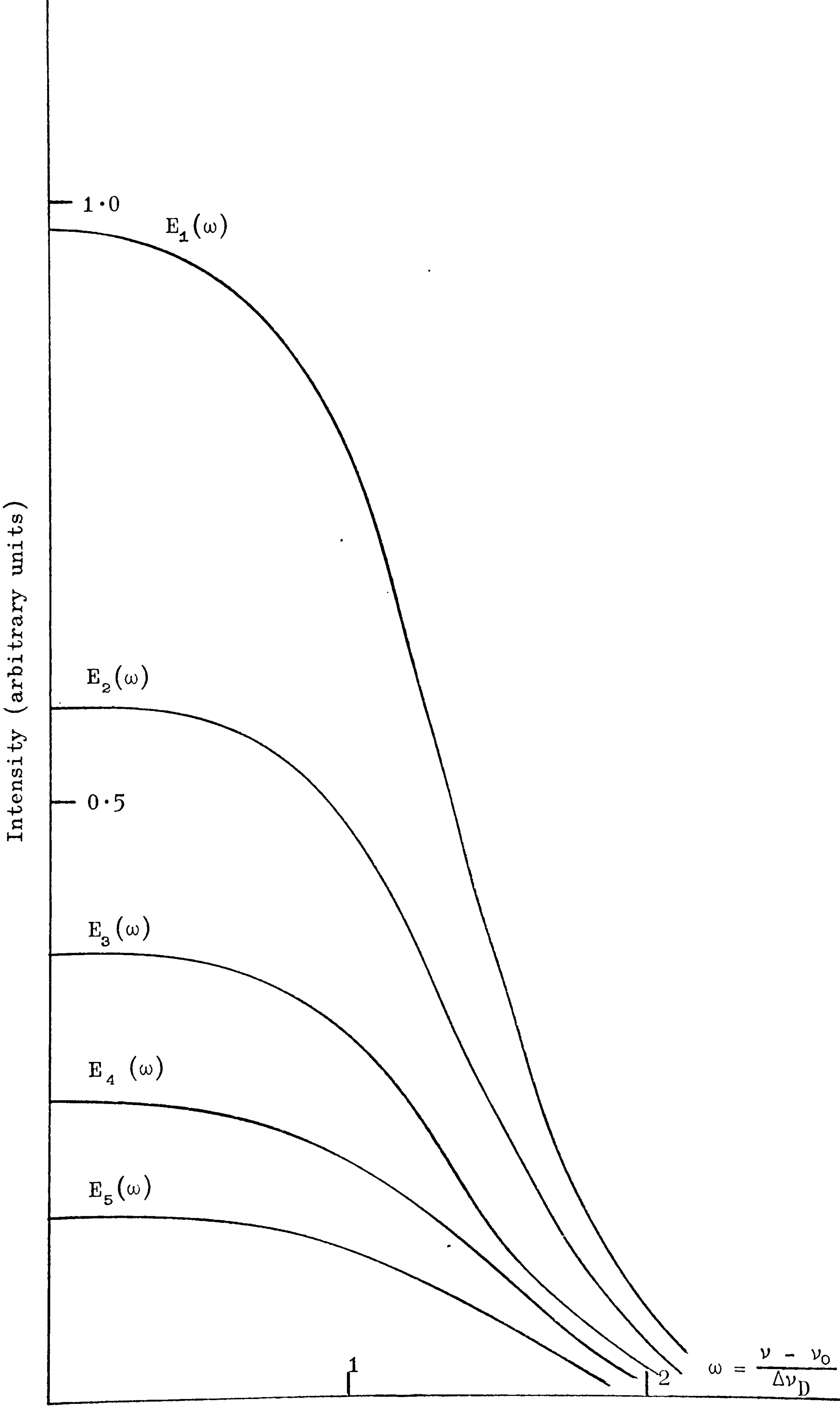

Fig.49

Calculated lamp emission profile for two values of total optical thickness, β. $E(\omega) = \sum_i E_i(\omega)$

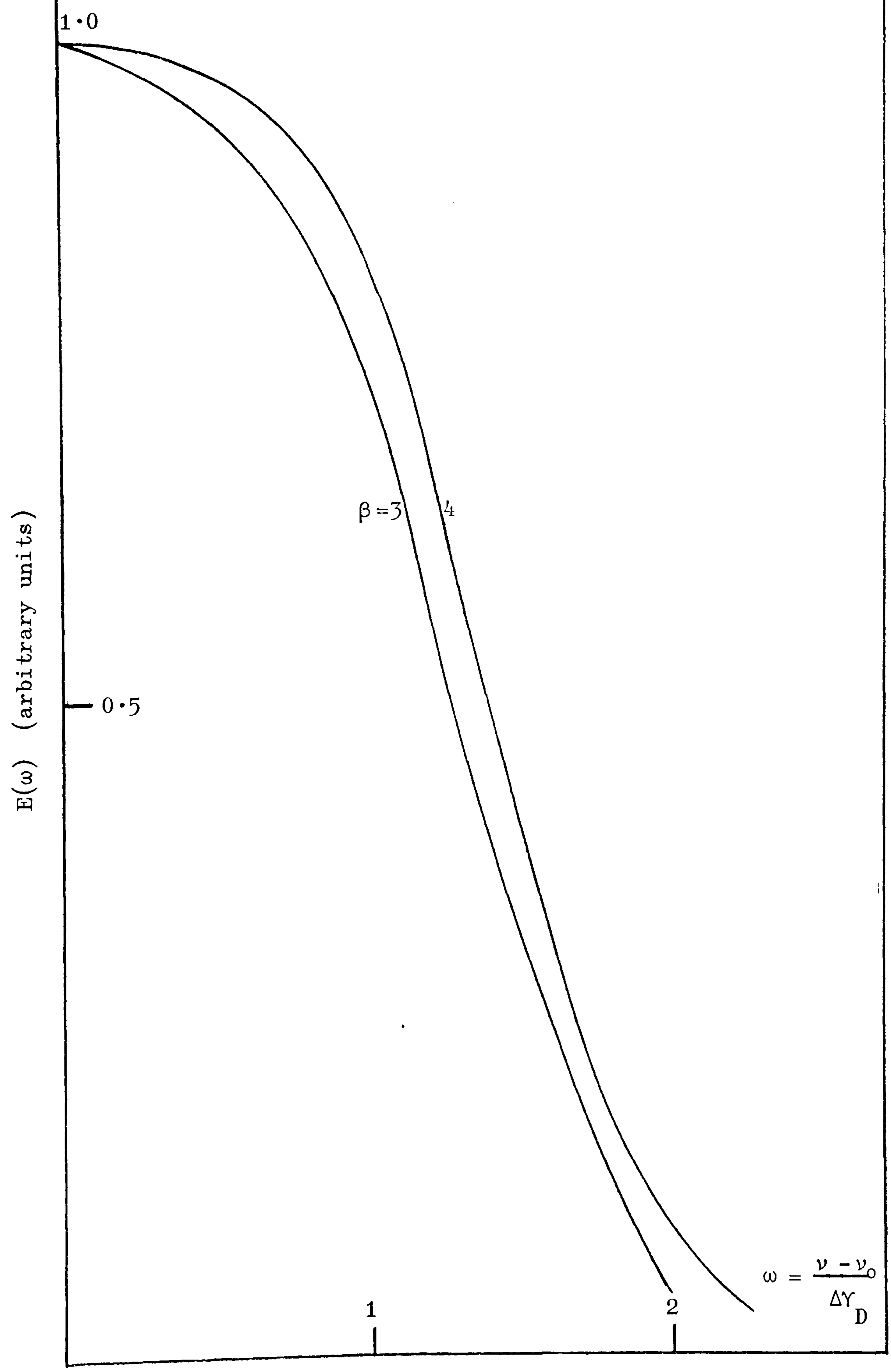

8.4 NEUTRAL DENSITY MEASUREMENTS

8.4.1 Method and Results

Rather than depend on uncertainties in estimating the lamp α , it was decided to simply calibrate the transmission vs known neutral density i.e. with the discharge switched off, the neutral density N was varied via T_{bath}, and the transmission plotted against N, see Fig.50. The curve of Fig.50 is consistent with a value of $\alpha \simeq 1{\cdot}4$. The calibration curve is then applied when the discharge is on and the observed change in transmission related to change in N.

Changes in transmission when the current was raised could be observed on the oscilloscope trace, and indicated N decreasing with increasing I, as expected. However, the lamp output was not a clean square wave to begin with, and after transmission through the discharge the signal was very hashy so that taking accurate measurements from the oscilloscope trace would be impossible. The p.s.d. cleaned the signal up, as is its function, and its output was very steady.

Transmission on the calibration run was quite reproducible, but with the discharge on, transmission results had more scatter. This scatter was partly due to experimental technique which finally evolved to the form described below, and partly due to the inherent scatter in the current limit phenomenon, when T_{bath} is only controlled to $\pm 0{\cdot}5^{o}C$. To reduce the effect of scatter, a number of runs were done and average values calculated. The typical experimental run proceeded as follows:

(1) The p.m. voltage was set at a particular value for the entire run.

(2) The height of the adjustable table was set at a particular value for the whole run (h is the height of the transmission pass above or below the diameter chord).

Fig.50

Experimental transmission curve. Path length 25 mm

$T_{Lamp} = +\ 19^{o}C \qquad I_{Lamp} = 10\ mA$

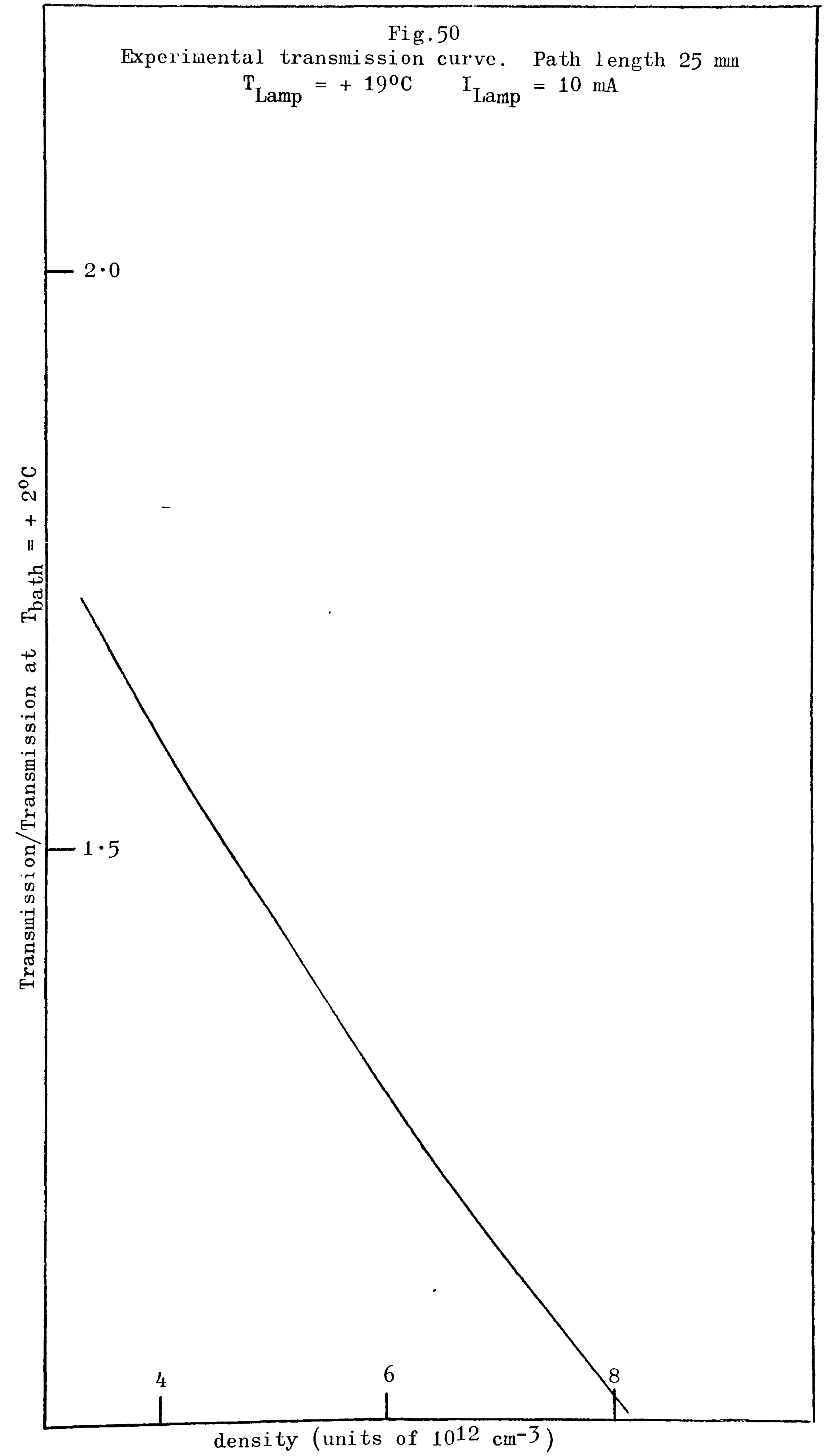

(3) With the discharge off, the neutral density was varied via T_{bath} (say, from + 2°C to - 6°C) and the transmission calibrated against these known densities.

(4) With T_{bath} set at a particular value, say + 2°C, I was varied, say from 1A to 4A, and the transmission noted.

(5) With the discharge off, the calibration procedure was repeated.

(6) The two calibration runs were averaged for a calibration curve, and from this $\bar{N}(h,I,p_0)$ was obtained ($\bar{N}$ is averaged along the line of sight at height h).

The reasons for this procedure which evolved after some experimentation, was as follows:

1. h is set on a particular value for two reasons:

(a) changes in h do not yield completely reproducible results, as the transmission of the quartz is effected by local imperfections and one never obtains precisely the same value of h once having changed it. Thus each new position of h requires a new calibration to be completely safe;

(b) the transmission of the quartz for $h \gtrsim \frac{1}{2} r_0$ falls off rapidly due to absorbed Hg in the quartz (see section 8.4.2) but mainly due to the higher incidence angle between the quartz surface and the beam path. Thus the p.m. voltage has to be increased for $h \geqslant \frac{1}{2} r_0$, however V_{pm} can not be reset with complete accuracy and the p.m. gain is strongly effected by V_{pm}. Thus each new setting of V_{pm} requires another calibration to be safe.

2. Each time I and/or T_{bath} is set at a new value it takes some minutes for the transmission to come to an equilibrium value. As long range (~ 1 hour) drift of the lamp is hard to avoid, frequent calibrations are advisable.

Most of the runs were obtained at 33 cm from the end of the cathode taper. However, by reversing the discharge this became 95 cm, yet the results were essentially the same, confirming that the current limiting effects are occurring with longitudinal homogeneity.

The scatter in results became particularly severe when I was very close to I_L. For this reason, runs were confined to $I \lesssim 0{\cdot}8\ I_L$.

As mentioned above, the quartz transmission for $h \geqslant \frac{1}{2}\ r_0$ fell off quite rapidly and made measurements for $h > \frac{2}{3}\ r_0$ impossible. Thus $\bar{N}(h)$ could not be obtained for the entire range of h, $0 < h < r_0$, which would be necessary to employ an Abel inversion for $N(r)$. This, of course, does not prevent a direct test of the theory, as one can easily obtain theoretical predictions of $\bar{N}(h)$ from the predicted $N(r)$, see Fig. 10 In fact the comparison of theoretical and experimental values of $\bar{N}(h)$ is more satisfactory as this employs the measurements in an unprocessed form and avoids the distortions inherent in Abel inversion.

Runs were done at $T_{bath} = +\ 2^oC$, 0^oC and -2^oC for a range of I, Runs were not done at lower values of T_{bath}, as here the transmission variations are slight even at $I = I_L$. The uncorrected results taken directly from the data via the calibration curves are presented in Fig.51

The points do however effect averaging, ranging from 15 runs-average for $I = 4A$, $T = +\ 2^oC$ to only 1 run for $I = 3A$, $T = +\ 2^oC$.

The theoretical curves for $\bar{N}(h)/N_0$ are obtained from Fig.10 in an obvious way: from T_{bath}, and $r_0 = 12.5$ mm one obtains I_{AT}, equation (3·5); thus I/I_{AT} and from Fig.8, λ/r_0; hence from Fig.10, $N(r)$ and so $\bar{N}(h)$.

The results may be seen to indicate the expected decrease of $\bar{N}$ with increasing I, and without doing the Abel inversion, the increased depletion at the centre of the column may also be noted. The results are generally below the theoretical predictions especially for higher currents. This discrepancy is almost entirely attributable to the non-Gaussian nature

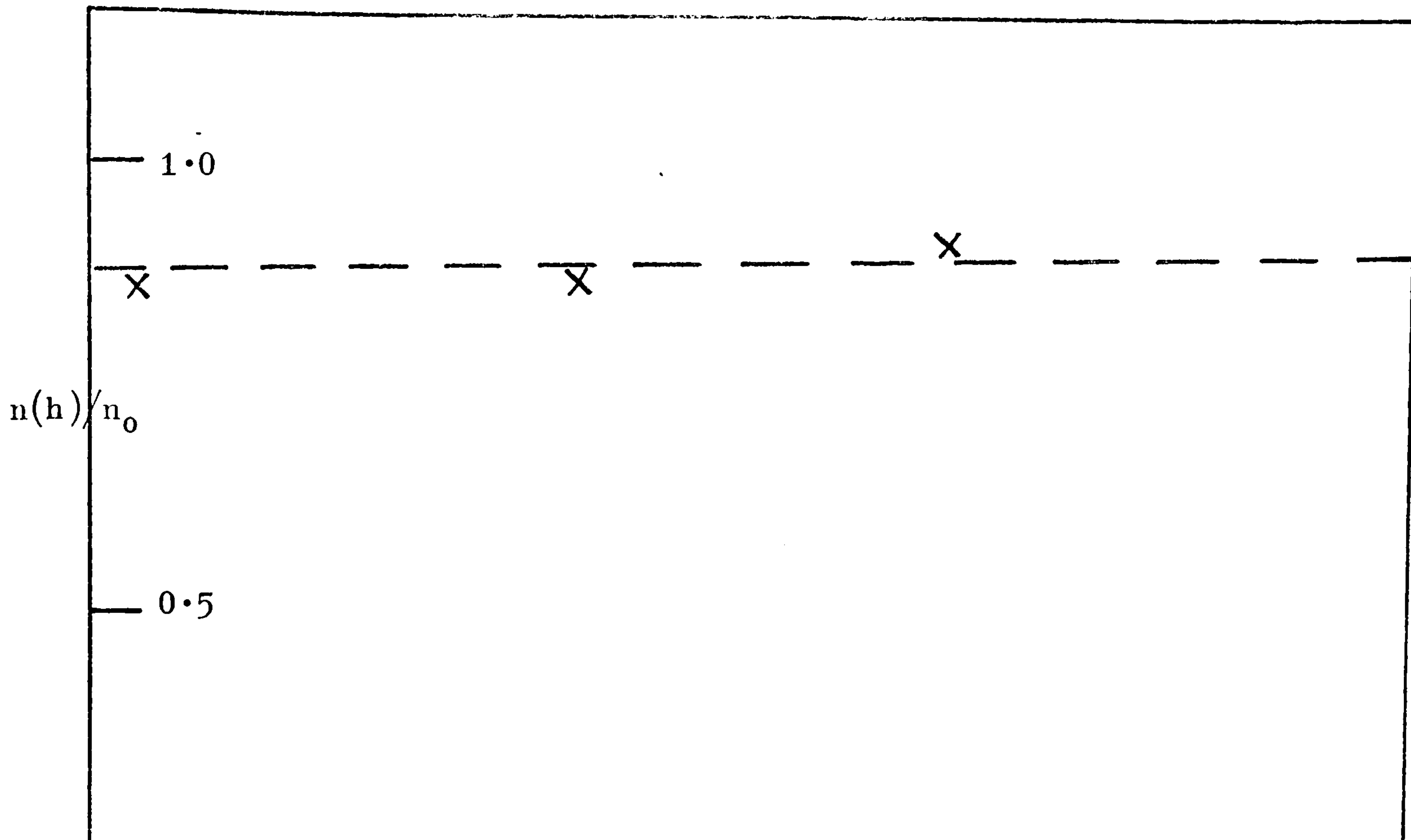

Fig.51a
Measured neutral density as a function of h(height of traversal above the diameter traversal). Broken line gives theoretical values see section 5. $r_o = 1{\cdot}25$ cm. I = 1A. $T_{bath} = -2^oC$

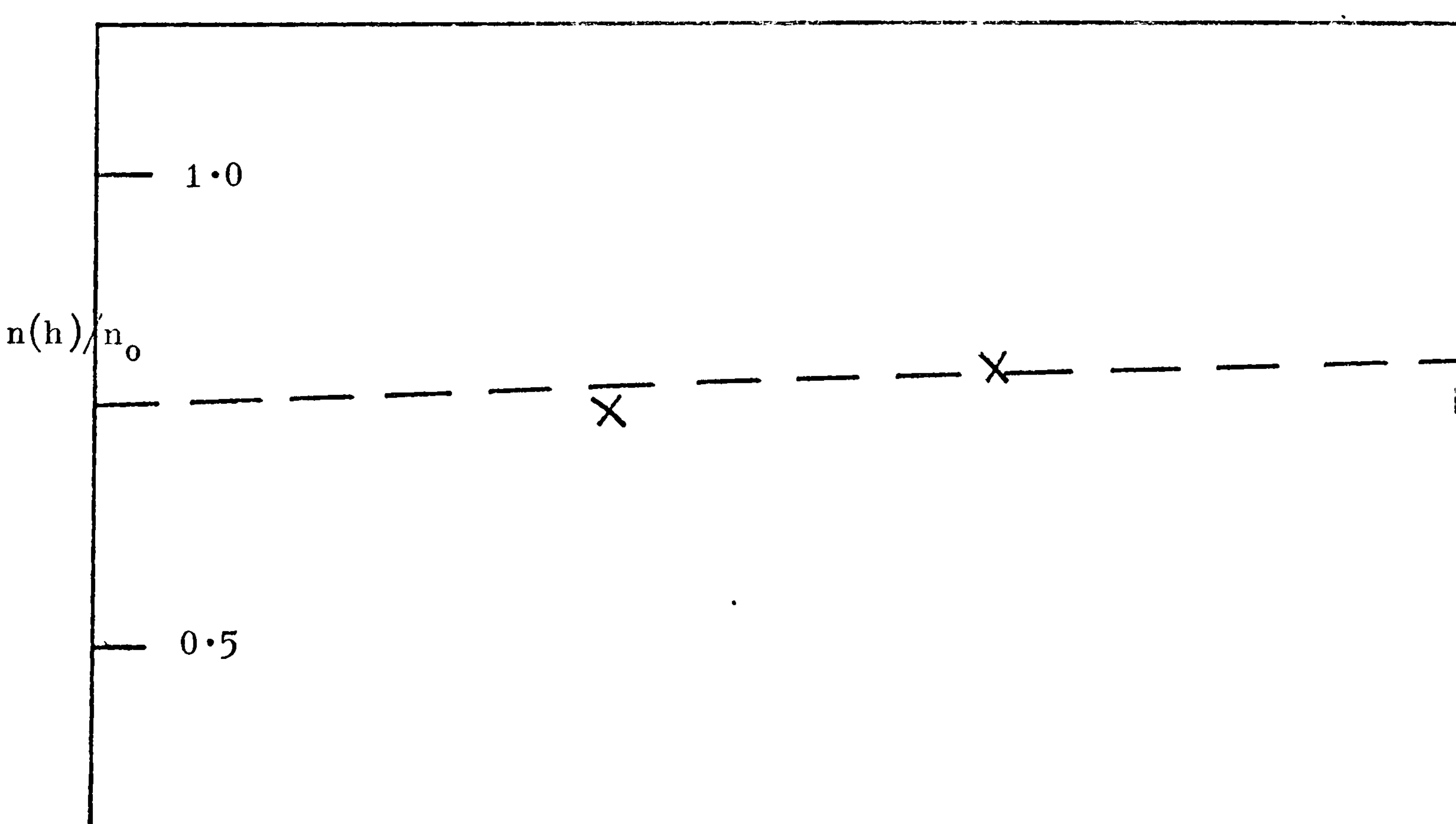

Fig.51b
Measured neutral density as a function of h(height of traversal above the diameter traversal). Broken line gives theoretical values, see section 5. $r_o = 1{\cdot}25$ cm. I = 1·5A, $T_{bath} = -2^oC$

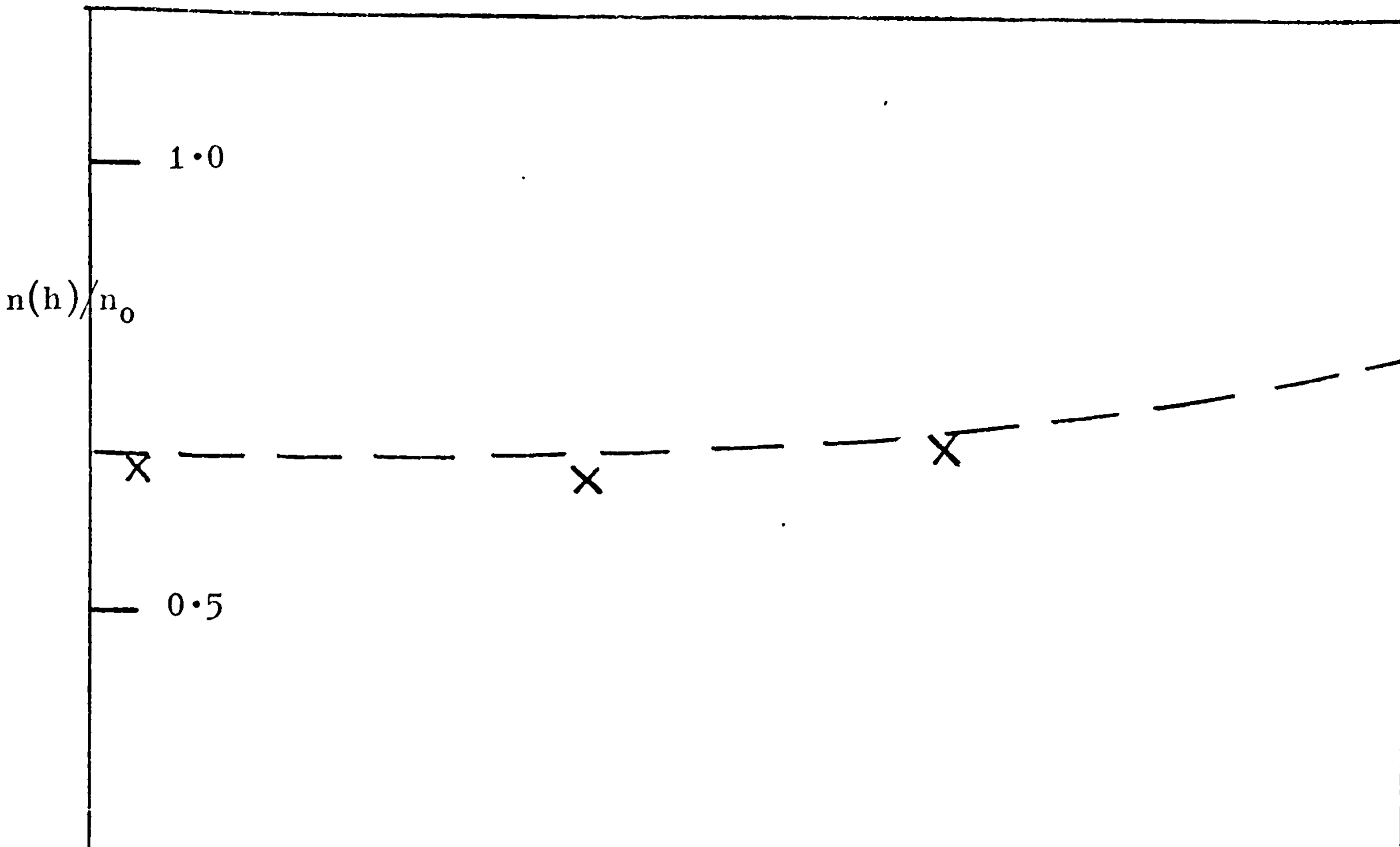

Fig.51c
Measured neutral density as a function of h(height of traversal above the diameter traversal). Broken line gives theoretical values, see section 5. r_0 = 1·25 cm. I= 2·0A. T_{bath}= -2°C

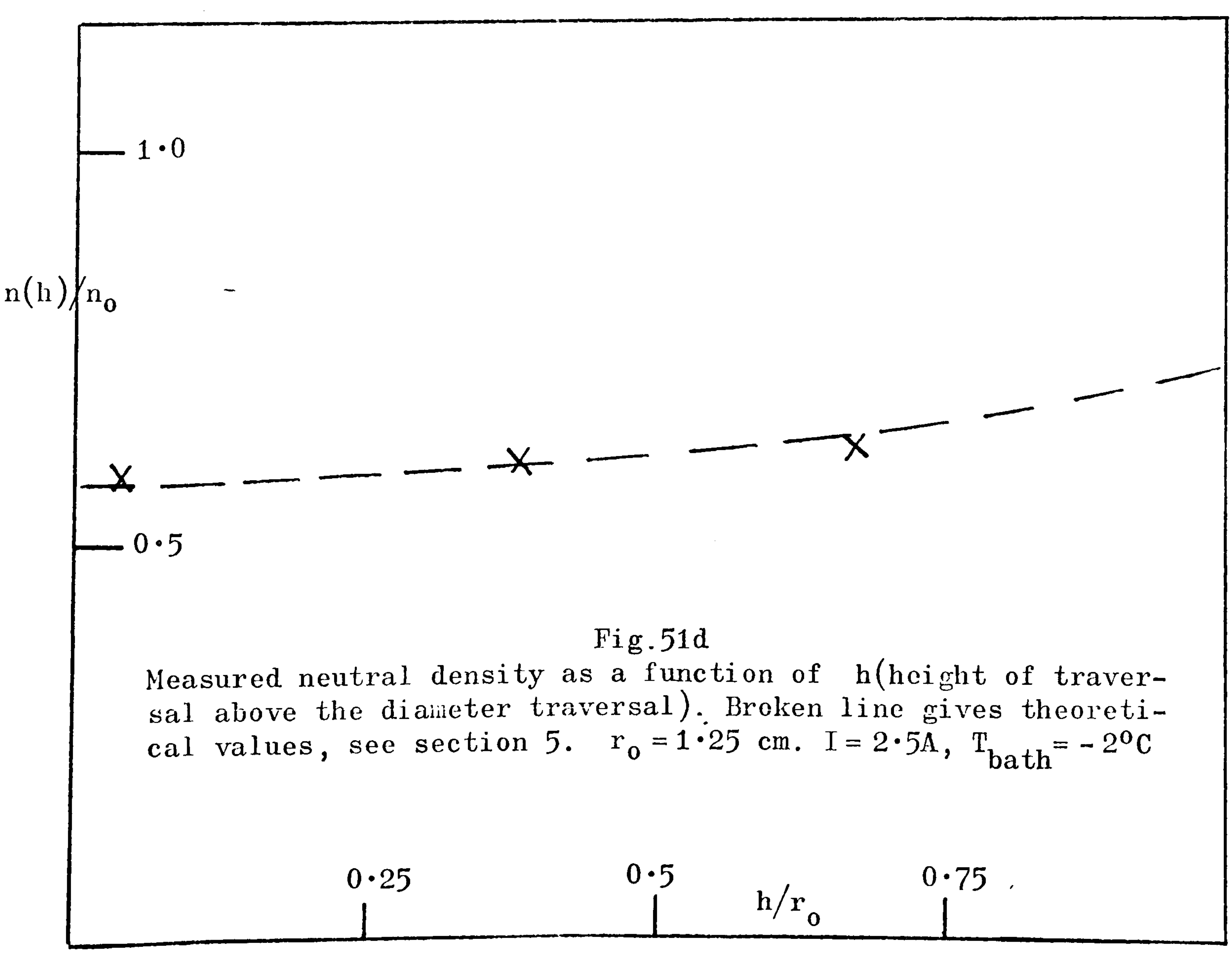

Fig.51d
Measured neutral density as a function of h(height of traversal above the diameter traversal). Broken line gives theoretical values, see section 5. r_0 = 1·25 cm. I = 2·5A, T_{bath} = - 2°C

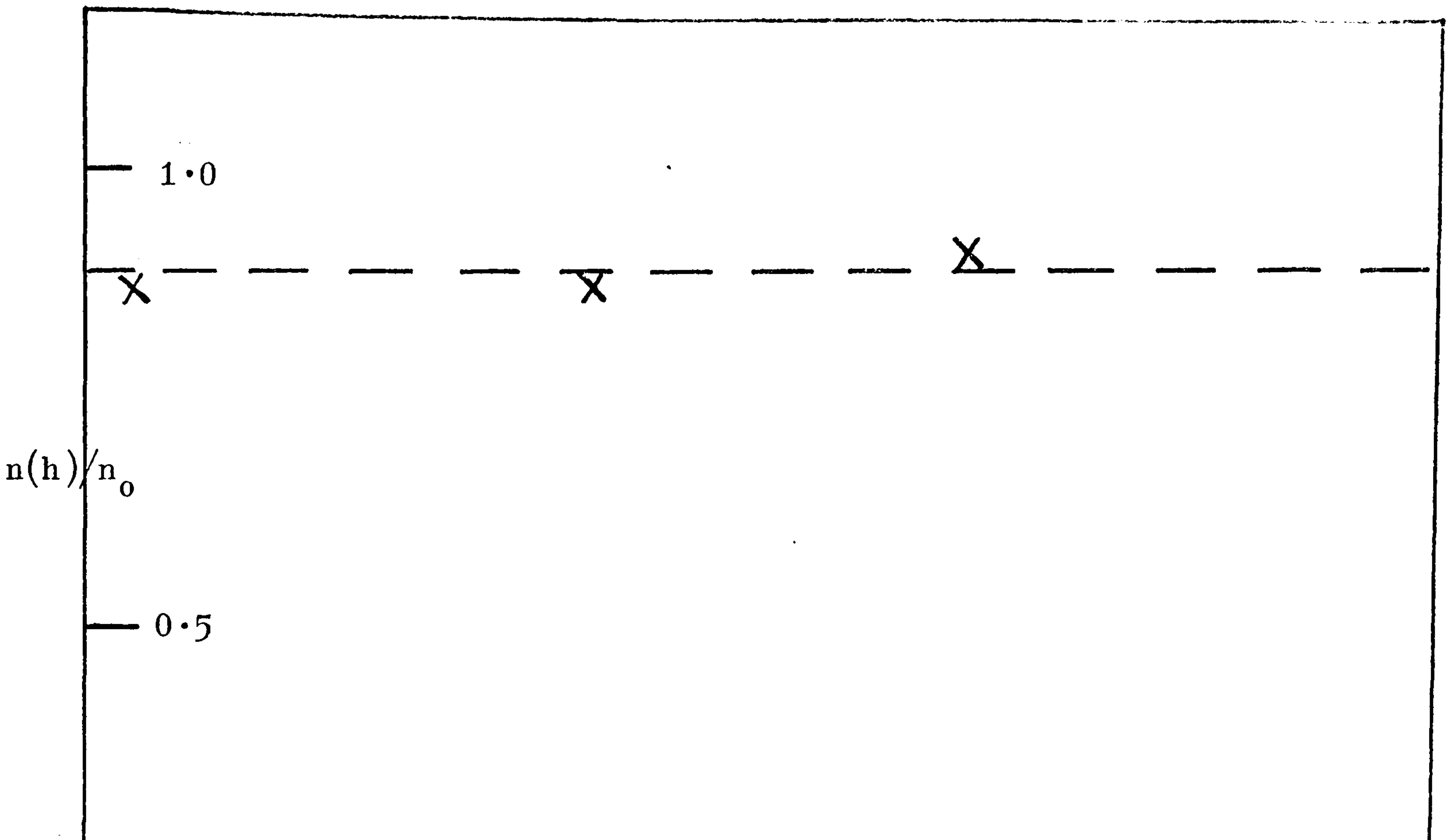

Fig.51e
Measured neutral density as a function of h(height of traversal above the diameter traversal). Broken line gives theoretical values, see section 5. $r_0 = 1{\cdot}25$ cm. I =1A. $T_{bath} = 0^oC$

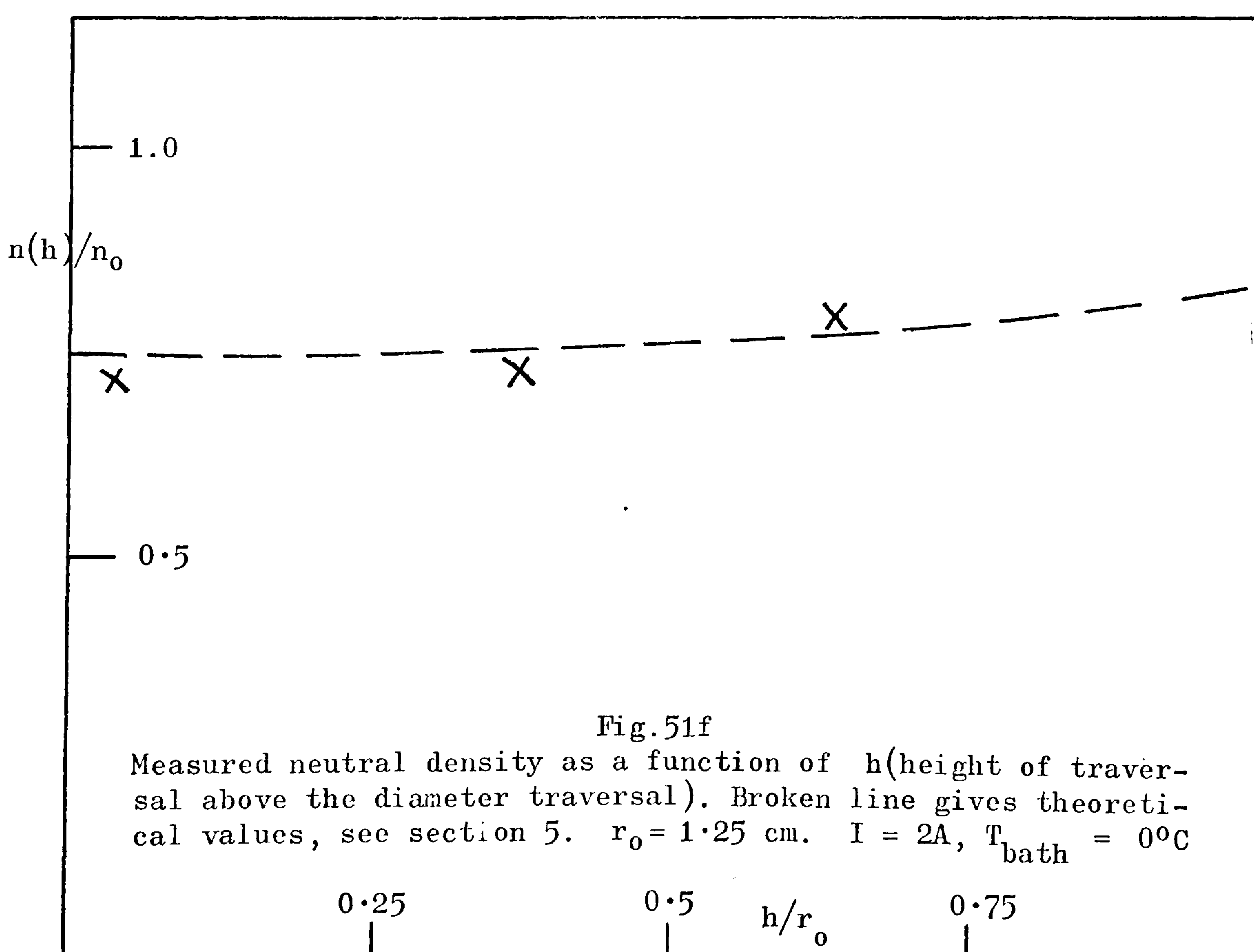

Fig.51f
Measured neutral density as a function of h(height of traversal above the diameter traversal). Broken line gives theoretical values, see section 5. $r_0 = 1{\cdot}25$ cm. I = 2A, $T_{bath} = 0^oC$

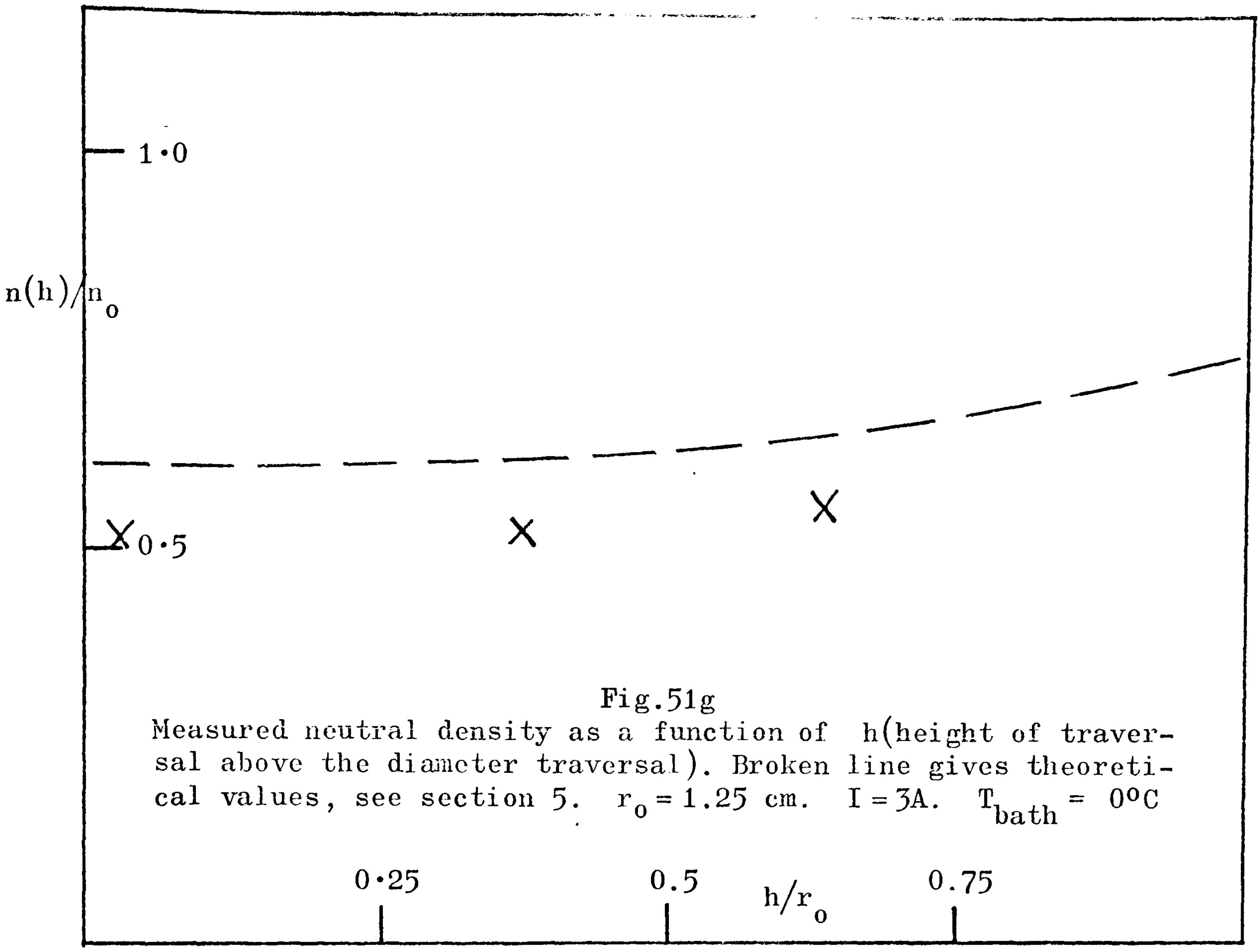

Fig.51g
Measured neutral density as a function of h(height of traversal above the diameter traversal). Broken line gives theoretical values, see section 5. $r_o = 1.25$ cm. $I = 3A$. $T_{bath} = 0^oC$

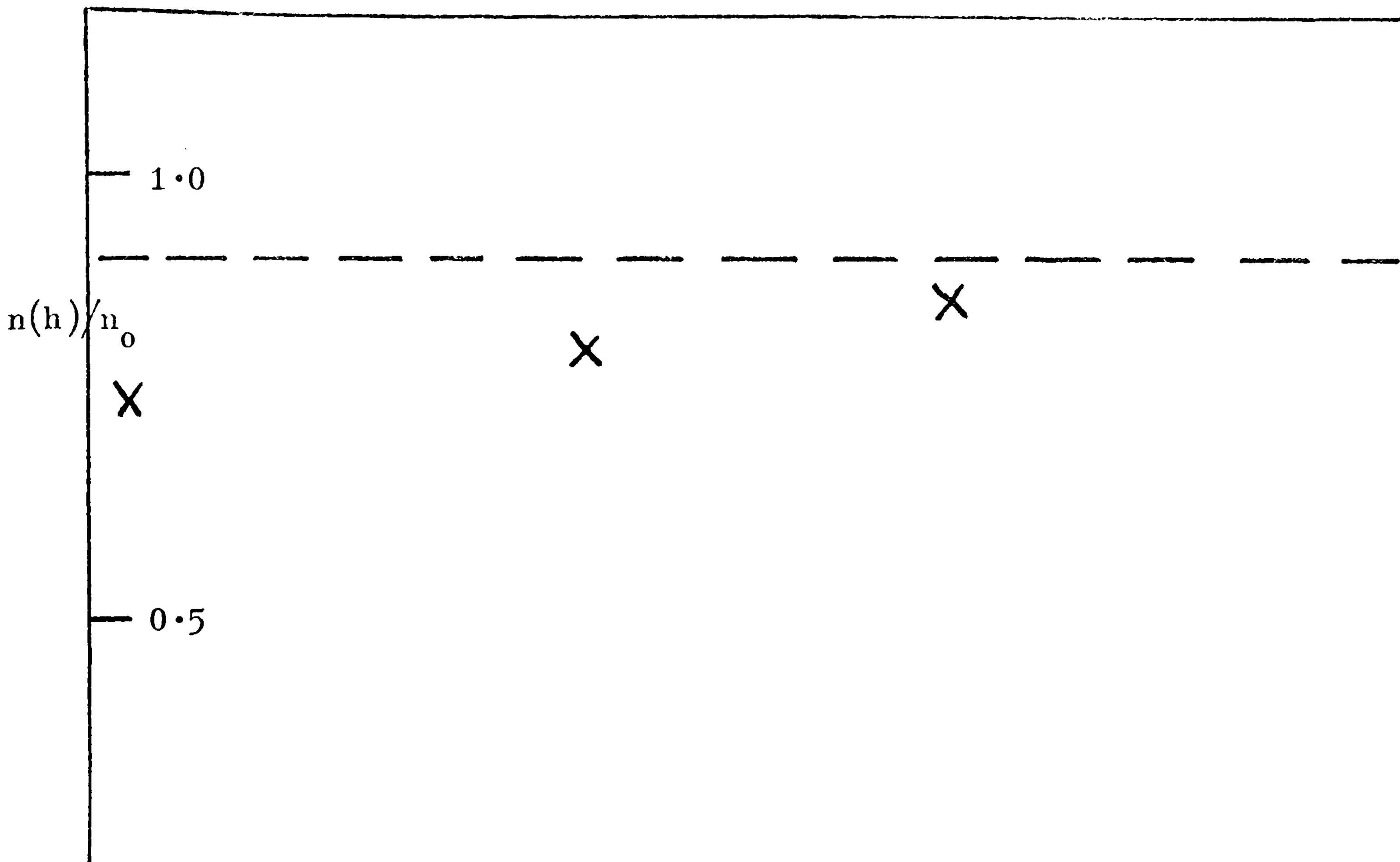

Fig.51h
Measured neutral density as a function of h(height of traversal above the diameter traversal). Broken line gives theoretical values, see section 5. $r_o = 1{\cdot}25$ cm. $I = 1A$, $T_{bath} = +\ 2^oC$

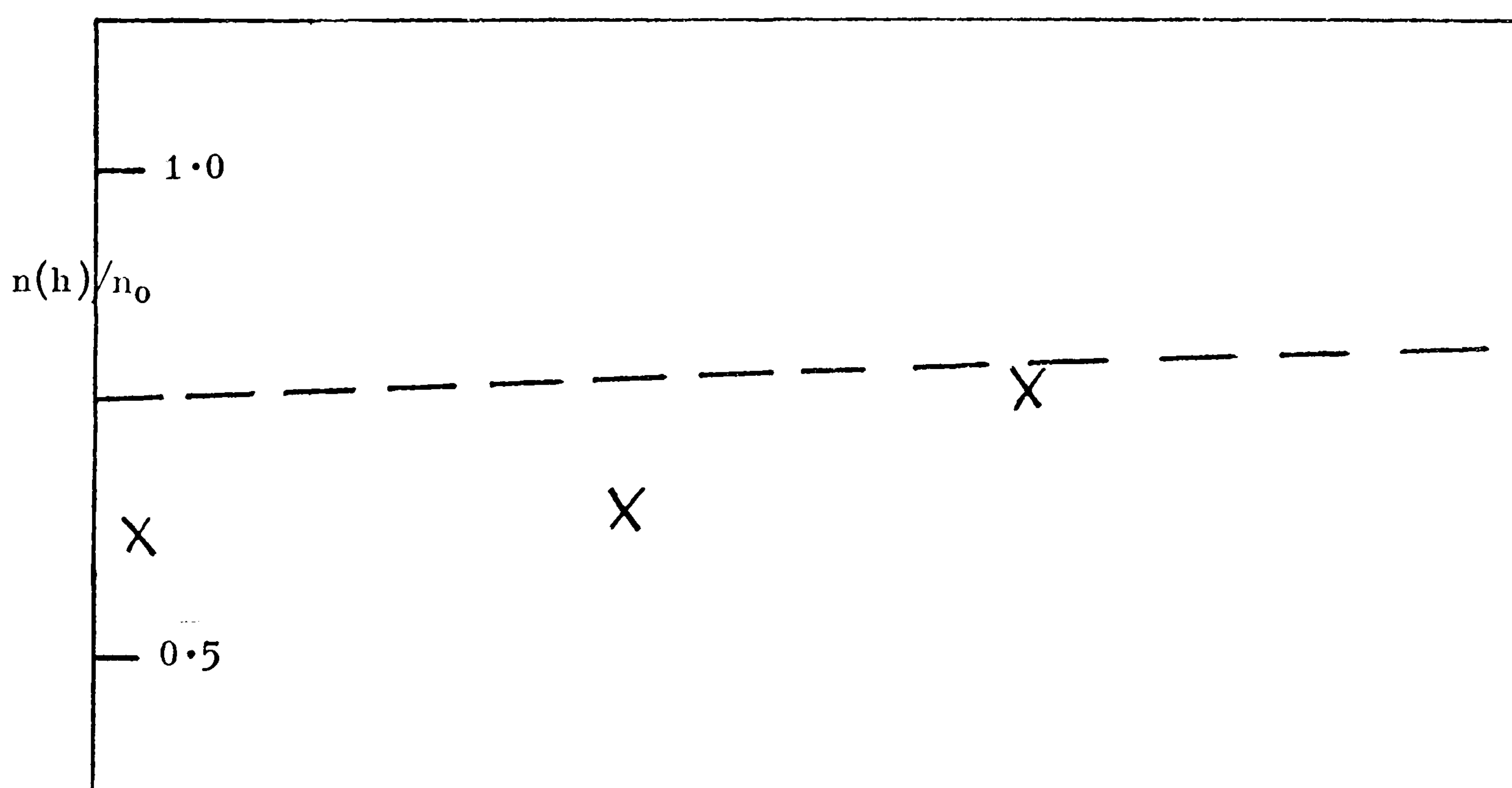

Fig.51i
Measured neutral density as a function of h(height of traversal above the diameter traversal). Broken line gives theoretical values, see section 5. $r_o = 1{\cdot}25$ cm. $I = 2A$, $T_{bath} = +\ 2^oC$

0·25 0·5 0·75

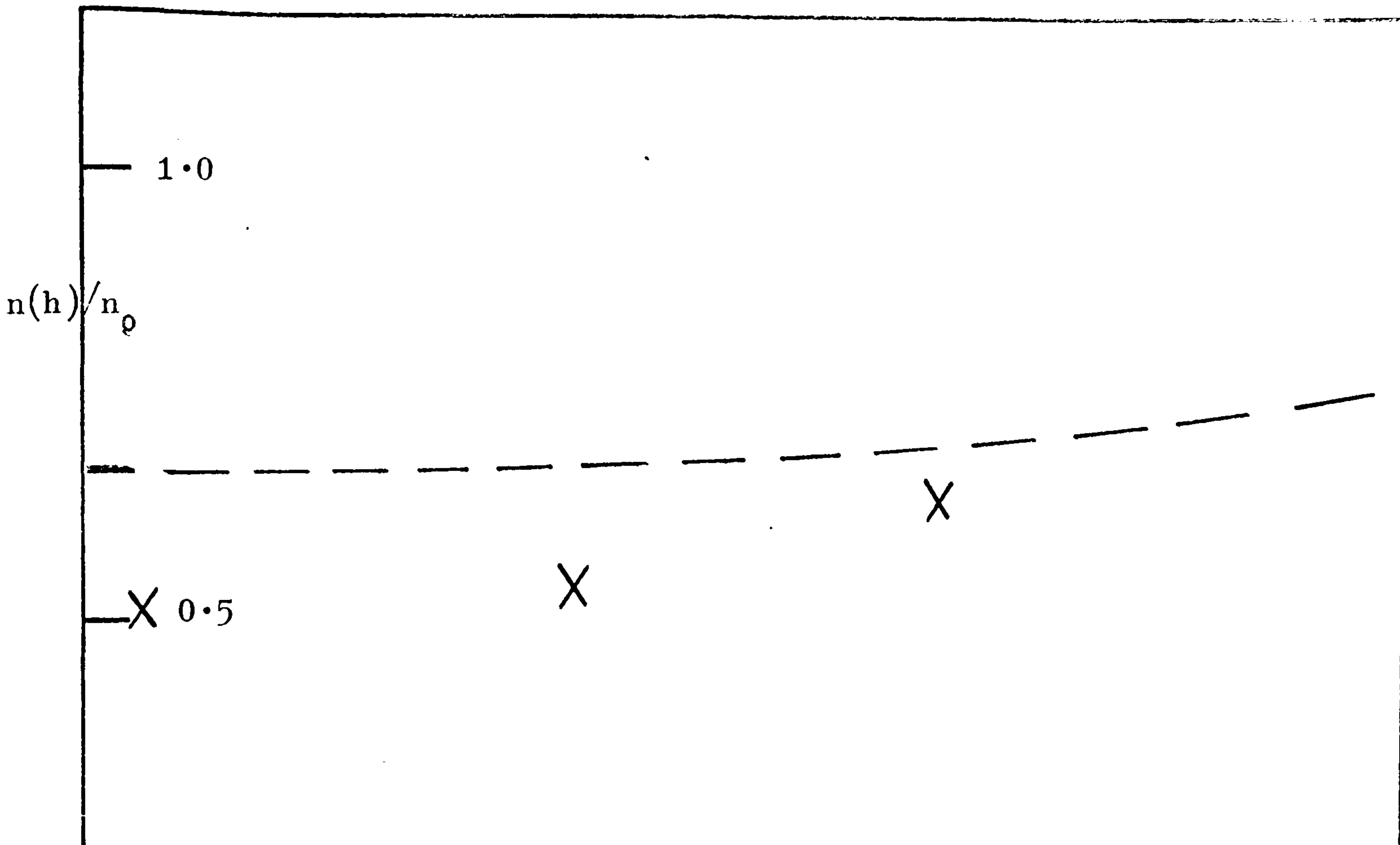

Fig.51j

Measured neutral density as a function of h(height of traversal above the diameter traversal). Broken line gives theoretical values, see section 5. $r_0 = 1{\cdot}25$ cm. $I = 3A$, $T_{bath} = +2^oC$

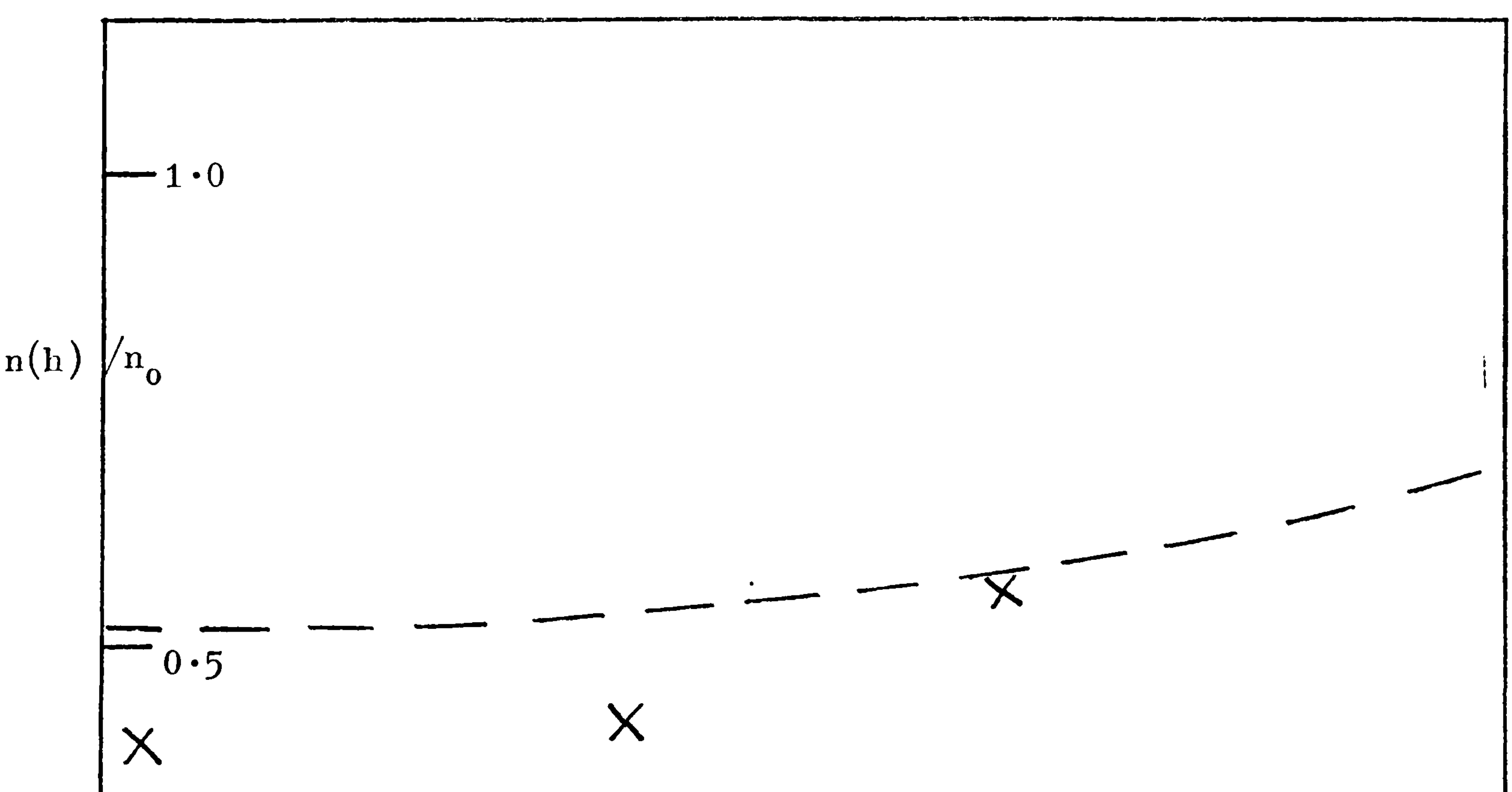

Fig.51k

Measured neutral density as a function of h(height of traversal above the diameter traversal). Broken line gives theoretical values, see section 5. $r_0 = 1{\cdot}25$ cm. $I = 4A$, $T_{bath} = +2^oC$

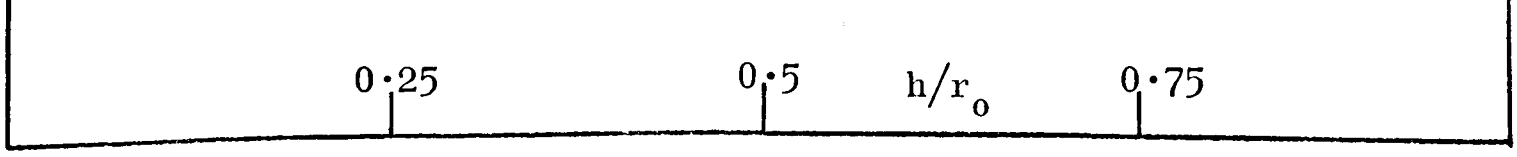

of the absorption profile near current limitation. The calibration runs correspond to Gaussian profiles (the neutrals at $I = 0$ have a Maxwellian distribution), but when I is an appreciable fraction of I_L, the neutrals in the discharge are no longer Maxwellian due to selective ionization, and the calibration curve must be corrected. This correction is calculated in section 8.5 and when applied to the experimental results, indicates that the theory for $N(r,I,p_0)$ has been confirmed to within experimental error. (The chief experimental error is due to $\Delta T_{bath} = \pm 0{\cdot}5^oC$, which corresponds to $\Delta N \approx 5\%$ at $T = 0^oC$).

8.4.2 Hg Wall Population

There is a Hg wall population of two sorts:

(a) adsorbed Hg atoms on the surface of the quartz.

(b) Hg atoms within the quartz lattice which attained this deep penetration when as ions they struck the wall with the energy gained from falling through the wall sheath potential. This process is termed 'atom clean-up' and establishes the lifetime of sealed-off lamps.

The variation and magnitude of these populations with current is of interest for two reasons:

(a) these atoms may play a role in the discharge operation if their population varies during the current run.

(b) these atoms may absorb 2537Å radiation, and if their population varies during the current run, this transmission change will put the results for vapour density variations in error.

Theoretical information on these populations appears to be quite scarce. From the value of the adsorption energy of Hg on silver, Estermann (1925), it seems likely that the adsorption time of Hg on quartz is very short ($< 10^{-7}$ sec?) and that the population of the adsorbed state is so small as to be of no consequence to the problems considered here.

The imbedded neutrals are another matter. Kenty (1938) in doing pulsed work in low pressure discharges found that the wall population of these neutrals varied during the pulse and played a considerable role in the discharge mechanisms.

Of course, imbedded atoms are held with a whole spectrum of binding energies and presumably over a short time only the population of the weakly bound atoms changes appreciably. The majority of the wall population may change only over a very long time period (tens of hours of operation, say). In D/C operation, therefore, it may be that when a new value of I is established, there will be a brief dis-equilibrium as the weakly bound population comes into equilibrium with the new ion wall current (the number of ions pounded into the quartz per sec equals the number knocked out by ion bombardment per sec., Kenty (1938), Torvén (1968)), thereafter, neutral vapour conditions will not be dependent on the wall population.

We therefore wish to establish experimentally whether or not:

(a) the Hg wall population absorbs appreciable 2537Å radiation (as the atomic absorption profile must be very strongly Stark broadened by the local fields in the lattice - the wall population might have to be unrealistically high to cause appreciable absorption);

(b) the bulk of the wall population varies over intermediate time periods (tens of minutes).

The answer to the first question seems almost certainly yes, as after many hours of running, dark Hg stains appear on portions of the quartz of such apparent opacity that it seems unlikely that any wavelength would be transmitted. In addition, the following simple experiment was performed: after a number of current runs, the 2537A transmission through an apparently transparent section of quartz was noted. A hot flame was then applied to the outside of this section (thus decreasing the wall population) and the transmission was observed to double approximately.

To establish whether this wall population absorption was varying between the calibration with $I = 0$ and the finite I of a run, the following experiments were performed: the lamp was run very hot $\sim +120^{o}C$, so that it would put out a self-reversed line. That this line was self-reversed was confirmed by checking that there was essentially no change in transmission as T_{bath} was varied at $I = 0$. Thus, this lamp line is insensitive to changes in the vapour density. However, it should be just as sensitive to changes in the wall density as an unreversed lamp line, since the absorption profile of the wall atoms is quite wide. The transmission of this reversed lamp line was then observed as I changed and it was noted that the transmission was uneffected. This implied that the bulk of the wall population (that was doing the absorption) did not vary appreciably over a few tens of minutes. To confirm that this reversed line was actually sensitive to changes in wall population, a hot flame was again applied to the quartz (thereby reducing the wall population) and the transmission again doubled, approximately.

By way of a further check, the lamp line at ~ 2650Å (probably a combination of HgI 2652, 2654, 2655 Å and NeI 2647Å) was used in the same way as the reversed 2537Å line and with the same results. Of course this ~ 2650Å line is quite insensitive to changes in Hg vapour density, but it appears to detect wall density changes. The Stark broadening of the wall atoms therefore must be hundreds of Angstroms wide, c.f. the isolated atom Doppler width of 10^{-3}Å .

Conclusions: the absorption by wall atoms does not change appreciably in tens of minutes, and the measurements of gas neutral density by absorption are therefore valid if re-calibrations are frequent. With continued use the quartz will gradually become so absorbant as to be useless for further absorption studies (even the application of a hot flame to the quartz eventually becomes ineffective). Transmission for $h \geq \frac{2}{3} r_0$, already poor due to the large incidence angle on the quartz, becomes extremely difficult with build-up of the Hg wall population.

8.5 NON-GAUSSIAN ABSORPTION PROFILE DUE TO SELECTIVE IONIZATION

8.5.1 Theory

In the absence of a discharge the neutral velocity distribution is assumed to be Maxwellian and it may be shown, see below, that this gives rise to a Gaussian absorption profile. In the presence of a discharge, selective ionization distorts the neutral distribution from the Maxwellian, and a non-Gaussian profile results.

The neutral m.f.p. for ionization varies linearly with the neutral speed, so we may write for future convenience $\lambda = \lambda' \frac{v}{\bar{v}}$, where $\bar{v}$ is the r.m.s. neutral speed. The implication of this is that the ionization process will selectively deplete the slow neutrals. Since the neutrals are assumed to follow rectilinear paths in this low pressure regime, see Appendix, that part of the neutral distribution which has had to traverse a large discharge space, will be selectively ionized as well, i.e. particle trajectories almost parallel to the tube axis are longer and these particles have greater probability of being ionized.

Fortunately these effects are fully calculable and the appropriate corrections to the neutral density measurements (which employed a calibration for Gaussian absorption) can be made.

In the absence of a discharge: consider Fig. 11 and the fraction of the particles at the volume point P which reached P via the solid cone at (θ, φ) and in the velocity range v to v + dv. This fraction is:

$$\frac{d^3 N_P(v,\theta,\varphi)}{N_P} = \pi^{-\frac{3}{2}} \left(\frac{m}{2kT} \right)^{\frac{3}{2}} e^{\left(- v^2 / \frac{2kT}{M} \right)} v^2 \sin\theta \; dv \; d\theta \; d\varphi, \quad \ldots (8.35)$$

i.e. the Maxwellian distribution function. Consider, the absorption Doppler shift for such a distribution as viewed along the x-axis. The shift is:

$$\Delta\nu = \frac{\nu_0 v_x}{c} = \frac{\nu_0 v}{c} \sin\theta \cos\varphi \qquad \ldots (8.36)$$

where c is the speed of light. Thus we may write that fraction of the particles at P which arrived via the cone at (θ,φ) and are capable of absorbing radiation at $\Delta\nu = \nu - \nu_0$ as

$$\frac{d^3 N_P(\Delta\nu,\theta,\varphi)}{N_P} = \pi^{-\frac{3}{2}} \left(\frac{M}{2\pi kT}\right)^{\frac{3}{2}} \frac{c}{\nu_0} \exp\left[-\frac{c^2 \Delta\nu^2}{\nu_0^2 \sin^2\theta \cos^2\varphi \; 2kT/M}\right]$$

$$\times \frac{c^2}{\nu_0^2} \Delta\nu^2 \csc^2\theta \sec^3\varphi \, d\Delta\nu \, d\theta \, d\varphi \, . \qquad \ldots (8.37)$$

Thus the fraction of the particles at P capable of absorbing the radiation at $\Delta\nu = \nu - \nu_0$ is:

$$\frac{dN_P(\Delta\nu)}{N_P} = \int_{\varphi=-\pi/2}^{+\pi/2} \int_{\theta=0}^{\pi} \frac{d^3 N_p(\Delta\nu,\theta,\varphi)}{N_P} \qquad \ldots (8.38)$$

where the integral is taken over only half the range of φ, so as not to include those particles which absorb at $\Delta\nu = \nu + \nu_0$. The result may be shown to be:

$$\frac{d\, N_P(\omega)}{N_P} = \frac{c}{\nu_0} \sqrt{\frac{M}{2\pi kT}} \; e^{-\omega^2} \qquad \ldots (8.39)$$

i.e., a Gaussian distribution, where:

$$\omega \equiv \frac{\Delta\nu}{\Delta\nu_D} \quad \text{and} \quad \Delta\nu_D \equiv \frac{\nu_0}{c} \sqrt{\frac{2kT}{M}} \, .$$

(Note that $\Delta\nu_D$ is defined somewhat differently than in section 8.2.)

The absorption profile of course varies as $dN_P(\omega)$, and so we have the usual Gaussian absorption profile.

In the presence of a discharge: by reasoning similar to that in section 5.3.6, each contribution to $d^3 N(v,\theta,\varphi)$ is reduced by the factor:

$$\exp\left\{-\frac{\ell_{PW}(\theta,\varphi)}{\lambda' v/\bar{v}}\right\}, \qquad \ldots (8.40)$$

see Fig. 11 where $\ell_{PW}(\theta,\varphi)$ is the distance from P to the wall at angle (θ,φ): thus:

$$\frac{d^3 N_P(v,\theta,\varphi,\lambda')}{N_P} = \pi^{\frac{3}{2}}\left(\frac{M}{2kT}\right)^{\frac{3}{2}} e^{-\frac{v^2}{2kT/M}} v^2$$

$$\exp\left[-\frac{\ell_{PW}(\theta,\varphi)}{\lambda' v/\bar{v}}\right] \sin\theta \, dv \, d\theta \, d\varphi , \qquad \ldots (8.41)$$

and, as in equation (5·35)

$$\frac{\ell_{PW}(\theta,\varphi)}{r_0} = -\frac{\rho\cos\theta - \sqrt{\rho^2\cos^2\theta - (1-\rho^2)(\sin^2\theta\sin^2\varphi - 1)}}{\sin^2\theta\sin^2\varphi - 1}. \qquad \ldots (8.42)$$

(This equation is only valid for P on a diameter, for P off diameter the equation is very cumbersome), where $\rho = r/r_0$; thus characterizing P by ρ one has

$$\frac{dN(\omega,\rho,\lambda'/r_0)}{N(\rho,\lambda'/r_0)} = \pi^{-\frac{3}{2}}\omega^2 d\omega \int_{\varphi=-\pi/2}^{+\pi/2}\int_{\theta=0}^{\pi} \csc^2\theta \sec^3\varphi$$

$$\times \exp-\left\{\omega^2\csc^2\theta\sec^2\varphi + \frac{\ell_{PW}(\theta,\varphi)\sin\theta\cos\varphi}{\omega(\lambda'/r_0)}\right\} d\theta \, d\varphi. \qquad \ldots (8.43)$$

As before, integrals such as this can only be obtained by numerical integration on a computer. Even so, only values of the integral for $\lambda'/r_0 = 2$ and $\rho = 0,1$ have been computed, as the integrand varies rapidly near $\varphi = \pi/2$ and $\theta = 0$, and a very fine mesh is needed to obtain convergence. Values for $\rho = 0,1$ are somewhat cheaper on computer time as one can take advantage of the symmetries here. The un-normalized absorption profiles at these two points and for $\lambda'/r_0 = 2$ are given in Fig. 53. As one can see the profiles are quite non-Gaussian. Such absorption profiles are rather unusual, although self-reversed emission profiles are common enough. In the latter case, however, the non-Gaussian profile is due to a corporate effect — the result of integrating

Fig.53a
Computed absorption profile for depleted Maxwellian distribution at the centre of the column. $\lambda/r_o = 1$

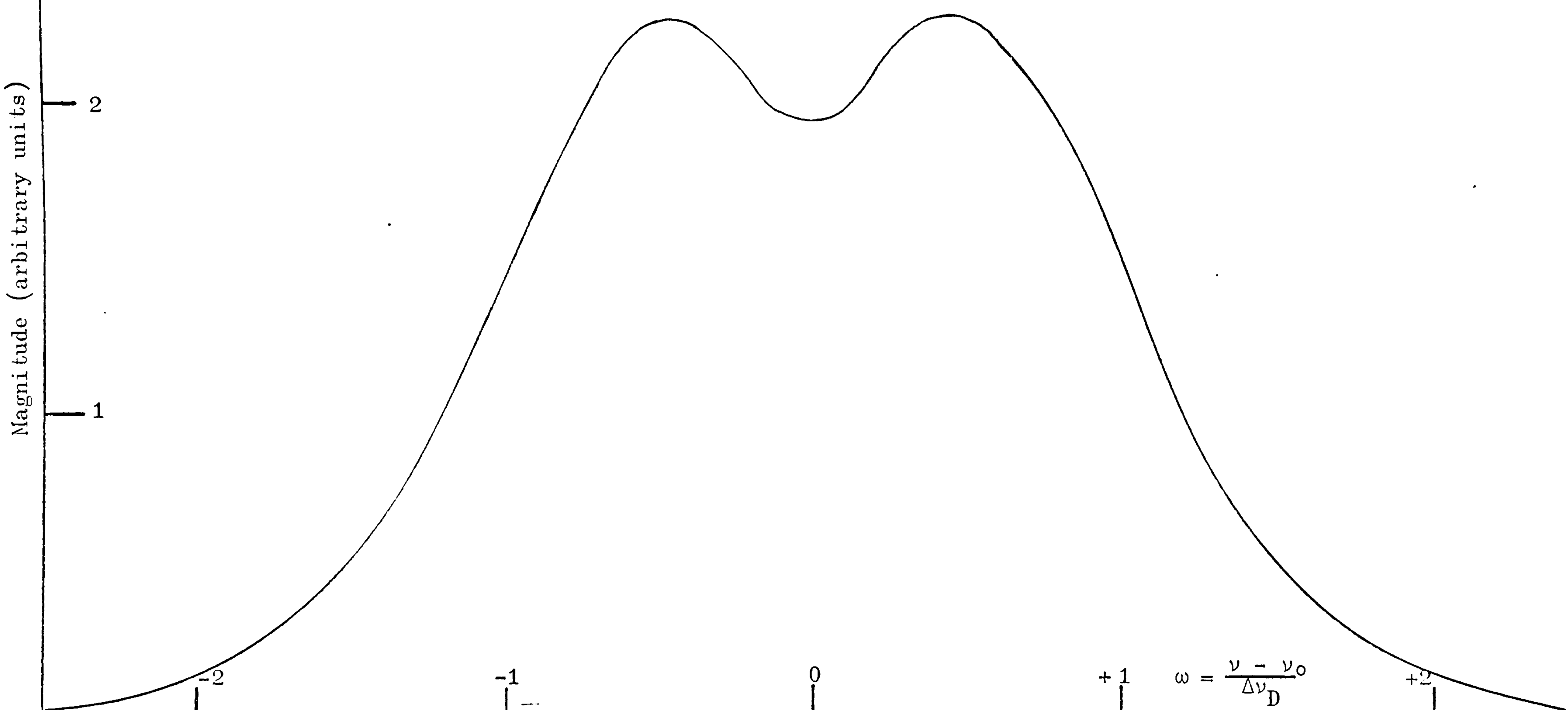

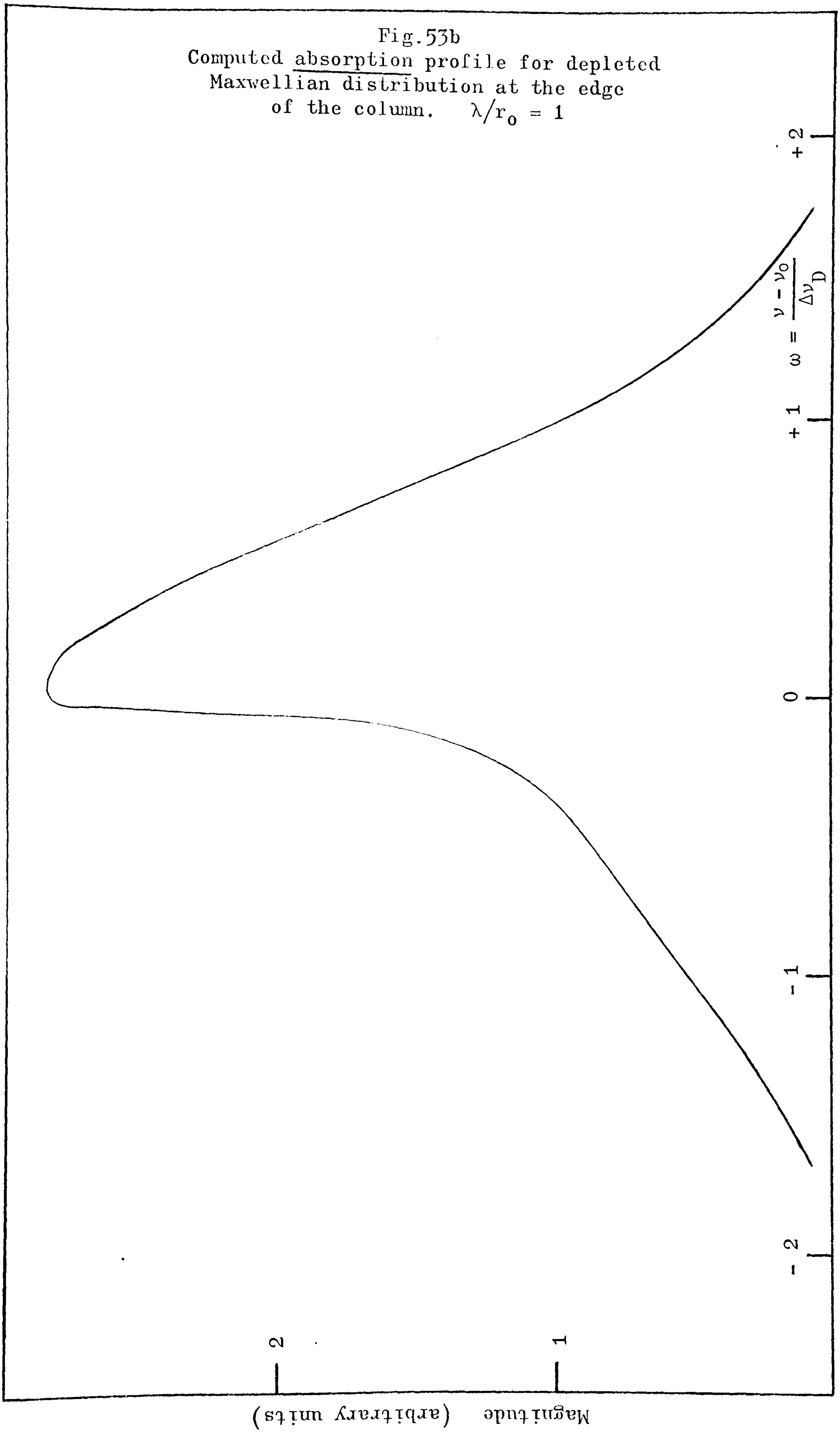

Fig.53b
Computed absorption profile for depleted Maxwellian distribution at the edge of the column. $\lambda/r_0 = 1$

the emissions over a finite depth, whereas this non-Gaussian profile (the local emission profile is the same shape, of course) is due to a distortion in the local distribution.

8.5.2 Correction to Neutral Density Measurements

In theory one can calculate $dN(\omega,\rho,\lambda'/r_0)$ for the whole range $0 < \rho < 1$ (assuming transmission across a diameter) from equation (8.43) and thus obtain the absorption cross-section:

$$k_0(N)\ K(\omega,\rho,\lambda'/r_0)\ , \qquad \ldots\ (8.44)$$

where:

$$K(\omega,\rho,\lambda'/r_0) \propto dN(\omega,\rho,\lambda'/r_0)$$

and K is normalized. Equation (8.44) then replaces the Gaussian cross-section $k_0 e^{-\omega^2}$. The absorption of a lamp line:

$$E_0\ e^{-(\omega/a)^2}\ ,$$

by traversal through such a region will be:

$$A(a,p_0,\lambda'/r_0) = \frac{2\displaystyle\int_{r=0}^{r_0}\int_{\omega=-\infty}^{+\infty} E_0 e^{-(\omega/a)^2} k_0[N(p_0,\lambda'/r_0,r)]K(\omega,r,\lambda'/r_0)}{\displaystyle\int_{-\infty}^{+\infty} E_0\ e^{-(\omega/a)^2}\ d\omega}\ d\omega\ dr \qquad \ldots\ (8.45)$$

For a given I, r_0 and p_0 one may calculate I/I_{AT} and thus obtain λ/r_0 from Fig.8 (one may assume $\lambda'/r_0 \approx \lambda/r_0$, or being completely rigorous, calculate λ'/r_0 vs I/I_{AT} from the velocity-dependent theory of section 5.3.6). With this value of λ/r_0 one may obtain $N(p_0,\lambda'/r_0,r)$ from Fig.10 (or again, being rigorous, compute $N(p_0,\lambda'/r_0,r)$ from the velocity dependent theory of section 5.3.6, and hence $k_0[N]$ from equation (8.22)). As all the functions required have been presented, the full absorption function $A(a,p_0,\lambda'/r_0)$ for any given I, r_0 and p_0 may be calculated in principle and this predicted absorption compared with the experimental value.

Unfortunately, with present computer facilities the numerical evaluation of all the integrals required would be prohibitively expensive. Instead a more modest attempt at estimating the neutral correction will be made as outlined below.

The physical picture of the error is as follows: a non-Gaussian profile, such as Fig.53, transmits more radiation than a Gaussian profile of the same total area, i.e. same neutral density. Thus if one calibrates the transmission with a Gaussian profile, the non-Gaussian profile gives a transmission which appears to indicate a lower density than in fact is present. Thus we observe the general tendency for the experimental points to fall below the theoretical curves in Figs.51

As an example of the correction we shall treat only one point, $I = 2A$, $T = +2^{o}C$. One calculates that for these parameters $\lambda/r_0 \sim 2$ and diameter traversal gives $\bar{N}(h)/N_0 \simeq 0{\cdot}5$ giving an average β across the diameter of $\beta = 1{\cdot}16 \times 10^{-13}\, \bar{N}\, \ell \approx 1$.

From Fig.53 we have the absorption profile, $L_c(\omega)$, at the centre of the discharge for these parameters. If the entire diameter had this absorption profile then the transmission would be:

$$T_c(\alpha,\beta) = \frac{\int_{-\infty}^{+\infty} E_0\, e^{-(\omega/\alpha)^2 - \beta L_c(\omega)}\, d\omega}{\int_{-\infty}^{+\infty} E_0\, e^{-(\omega/\alpha)^2}\, d\omega} \qquad \ldots (8.46)$$

so that:

$$T_c(1{\cdot}5,1{\cdot}0) = \frac{2}{1{\cdot}5\sqrt{\pi}} \int_0^{\infty} e^{-(\omega/1{\cdot}5)^2 - L_c(\omega)}\, d\omega$$

$$= 0{\cdot}807$$

by numerical integration compared with the calibration transmission of a Gaussian profile:

$$T_G(\alpha,\beta) = \frac{\int_{-\infty}^{+\infty} E_o\, e^{(\omega/\alpha)^2 - \beta e^{-\omega^2}}\, d\omega}{\int_{-\infty}^{+\infty} E_o\, e^{-(\omega/\alpha)^2}\, d\omega}$$

so that:

$$T_G(1{\cdot}5, 1{\cdot}0) = 0{\cdot}62 \ .$$

If the entire diameter had the absorption profile, $L_E(\omega)$, at the edge of the column, see Fig.53, then the transmission would be:

$$T_E(1{\cdot}5,1{\cdot}0) = \frac{1}{\alpha\sqrt{\pi}} \int_{-\infty}^{+\infty} e^{-(\omega/1\cdot5)^2 - L_E(\omega)}\, d\omega$$

$$= 0{\cdot}70$$

by numerical integration. To avoid further integrations, let us make the approximation that the transmission in the non-Gaussian case for the entire diameter is simply:

$$T_{NG} = \frac{1}{3}\left(T_c + 2\, T_E \right) = 0{\cdot}74 \ .$$

By examining Fig.41 of $A(\alpha,\beta) = 1 - T(\alpha,\beta)$ for $\alpha = 1{\cdot}5$, $\beta \sim 1$ one can see that an error in transmission from $0{\cdot}62$ to $0{\cdot}74$ implies an error in $\bar{N}$ of about 30%, which is approximately the discrepancy between the theoretical and experimental values for $I = 2A$, $T = +2^oC$, $r_o = 12{\cdot}5$ mm.

8.6 METASTABLE DENSITIES AND CUMULATIVE IONIZATION

8.6.1 Introduction

The upper state of the 2537Å Hg resonance line is the $6\,^3P_1$ state with a lifetime of 10^{-7} sec. There are two nearby metastable levels 6^3P_0 and 6^3P_2 where one might anticipate a population build-up. If this build-up became appreciable then ionization from these metastable states could become comparable to or greater than direct ionization from the ground state $6\,^1S_0$, i.e. cumulative, or step-wise ionization could be important.

The current limitation theory of Chapter V is not directly dependent on the ionization mechanism as one never calculates λ, the neutral

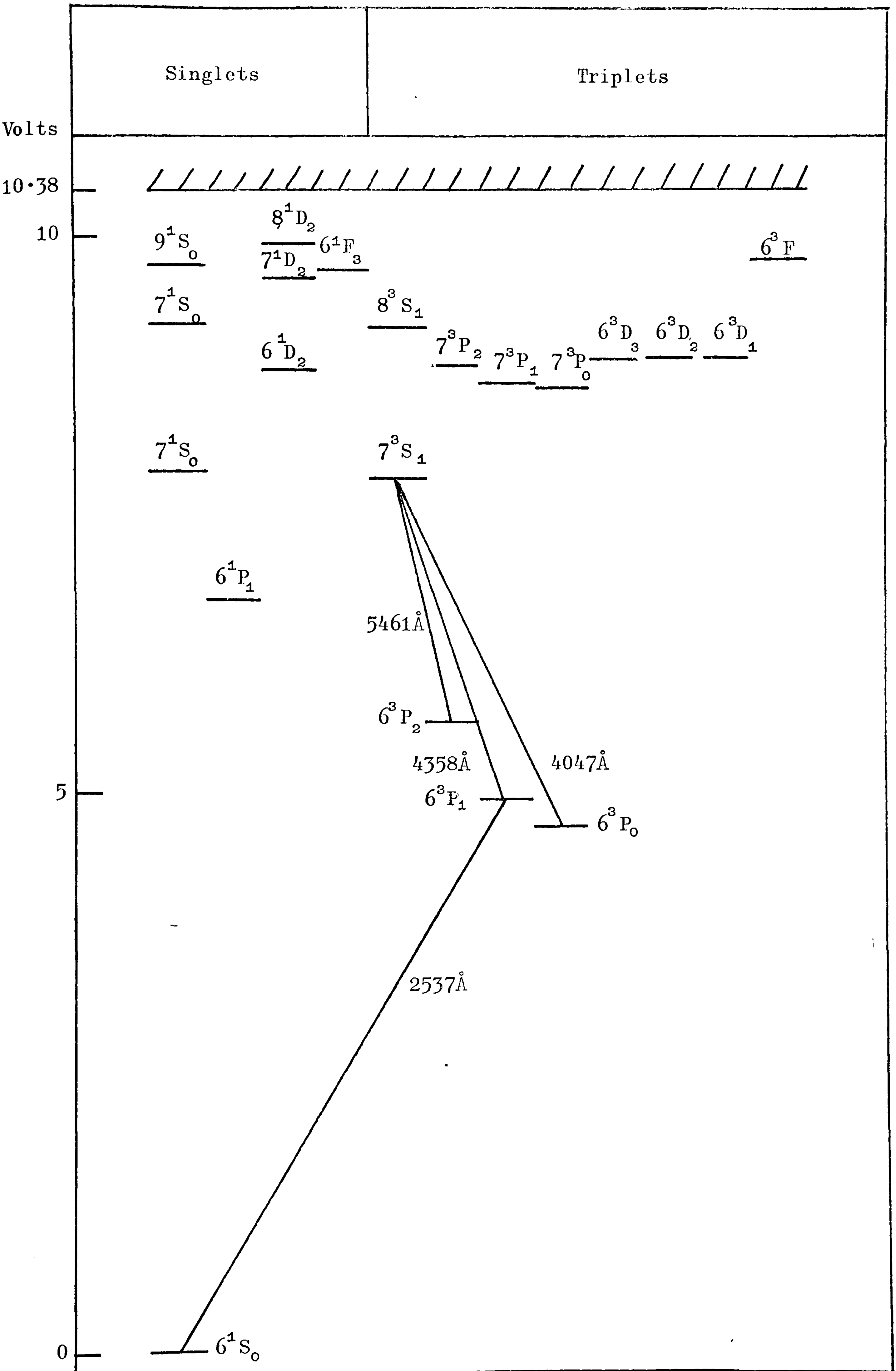

Fig.54 Energy levels of Hg

m.f.p. for ionization. However, the Poletaev prescription <u>is</u> dependent on the ionization mechanism and while it is the Poletaev <u>experimental</u> constant, C_1, that is employed in the theory of Chapter V, there would be some doubt as to the constancy of C_1 if the ionization mechanism varied appreciably over the range of I and p_0 near current limit.

Klarfeld (1941) concludes that for the normal positive column (i.e. far from current limit), cumulative ionization is insignificant for $p_0 < 1$ mTorr. The question remains whether in the extreme conditions near current limit where the current density is high and the neutral density depleted, these conclusions still hold. As any theory calculation of metastable densities is subject to large uncertainties, especially near current limit, it was decided to measure these densities by the absorption technique.

8.6.2 <u>Measurement of Metastable Densities</u>

The experimental arrangement was precisely as for the neutral density measurements. All traversals were across the tube diameter, 2.5 cm.

The metastable densities were measured using the absorption of the 5461Å and 4047Å lines, see energy level diagram Fig.54, put out by the lamp. Of course it is not possible to calibrate the transmission of such lines with known densities of metastables, but fortunately this is unnecessary as these non-resonance lines are unlikely to be self-broadened (especially as the lamp current is so low, 10 mA, and the lamp Hg pressure only ~ 1 mTorr) so that one can directly employ the absorption theory outlined in section 8.2 assuming $\alpha = 1$. For these lines Fabrikant et al (1937), supply the relation for $\beta = 10^{-12} N\ell$.

Curves of the metastable densities as a function of p_0 and I are presented in Fig.55. Some of the results can be compared to the data given by Fabrikant et al (1937), and this is shown in Table 7.

Fig.55a

Number density of the 6^3P_2 metastable state as a function of current. Open circles for $T_{bath} = -3^oC$; closed circles for $T_{bath} = 0^oC$. ($r_o = 1{\cdot}25$ cm)

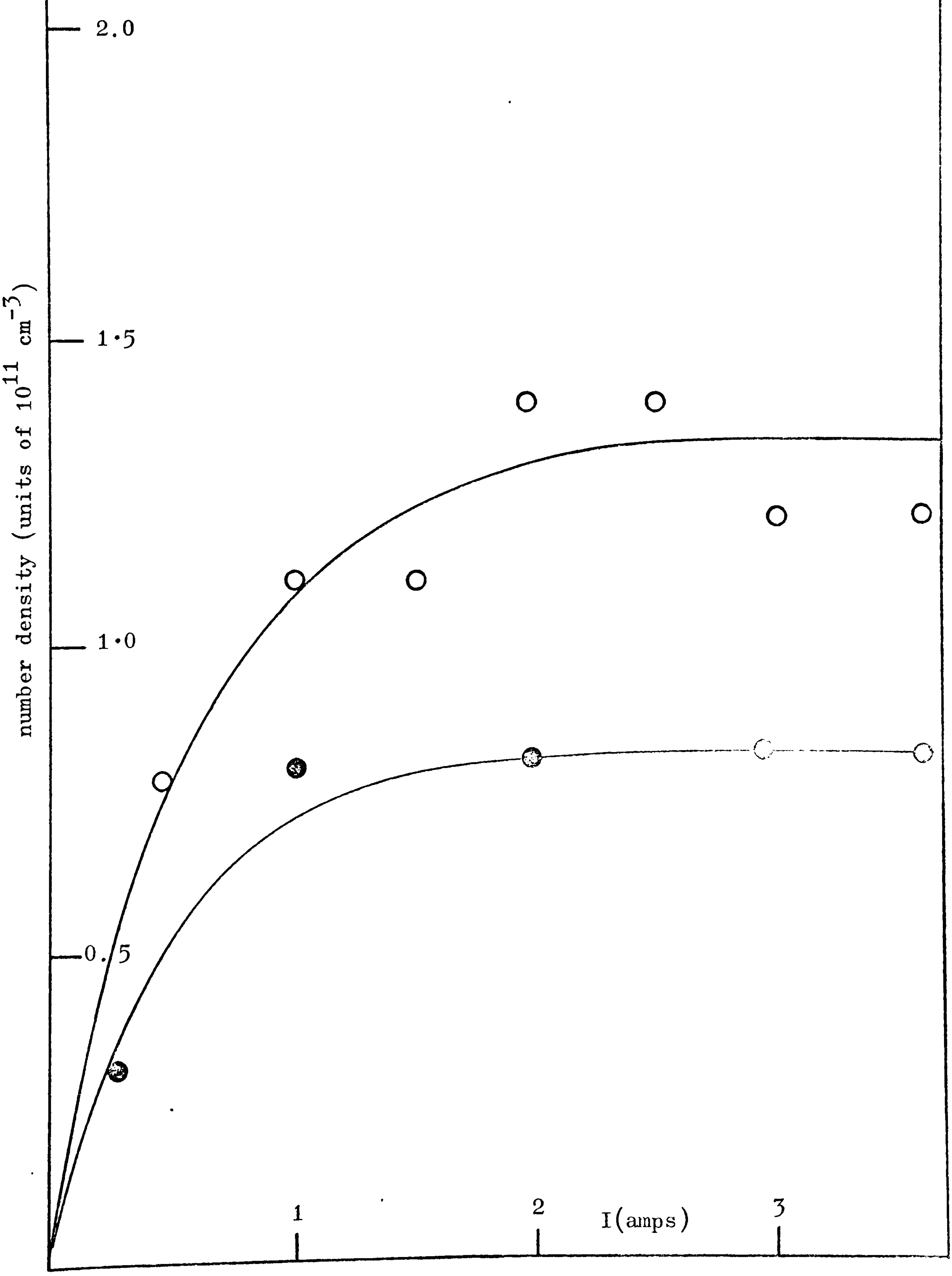

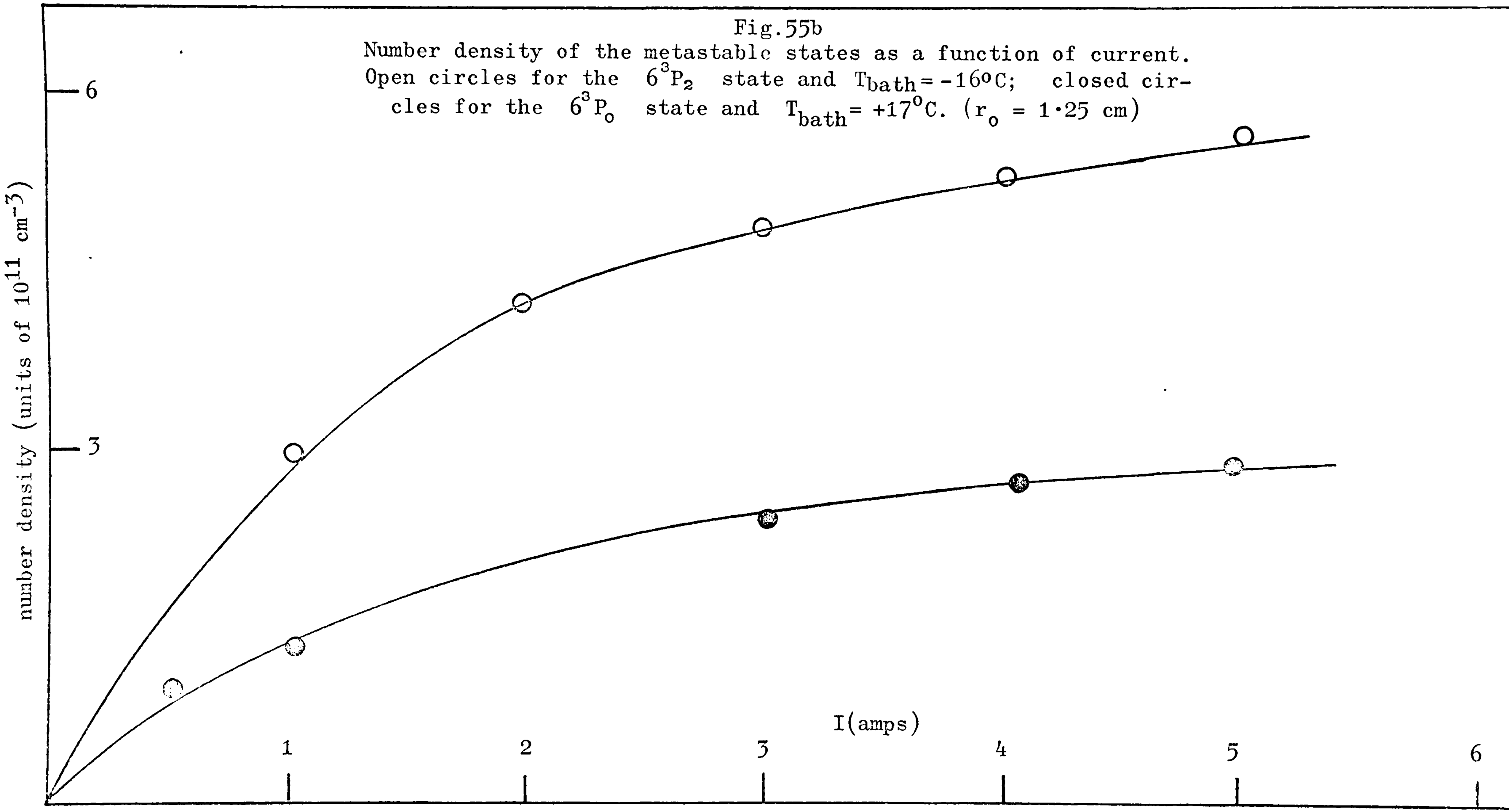

Fig.55b
Number density of the metastable states as a function of current. Open circles for the 6^3P_2 state and $T_{bath} = -16°C$; closed circles for the 6^3P_0 state and $T_{bath} = +17°C$. ($r_o = 1{\cdot}25$ cm)

TABLE 7

METASTABLE CONCENTRATIONS

p_0 in mTorr	density of $6^3P_0 \times 10^{11}$	density of $6^3P_2 \times 10^{11}$
0·25	0·6 (1.2)	1·1 (2·1)
0·90	2·3 (2·5)	4·8 (7·2)

Fabrikants results are shown in brackets. As can be seen, the present results are lower than Fabrikant's which is probably due to the longitudinal density gradient present in Fabrikant's apparatus, i.e. the p_0 at the point of observation in his apparatus is higher than the p_0 given by his bath temperature (which is the value recorded in the first column).

It is of some interest to discover how the metastables are lost - is it loss to the walls, or is it by electron impact in the discharge volume ? (It is assumed that the metastables are not lost by spontaneous decay via an optical transition.)

The metastable creation rate per unit length is:

$$Q(T_e)\ \bar{n}_e\ \bar{N}\pi r_0^2 \qquad \ldots (8.48)$$

where $Q(T_e)$ gives the excitation rate from the ground state, by electron impact, $\bar{N}$ is the average neutral density.

If the loss is primarily to the walls then the loss rate is

$$\tfrac{1}{4}\, n_m\ \bar{c}\ 2\pi\, r_0 \qquad \ldots (8.49)$$

where n_m is the metastable density and it is assumed that the metastables still have the neutral random velocity distribution with average velocity $\bar{c}$.

If the loss is via electron impact then the loss rate is:

$$\pi r_0^2 Q'(T_e)\ \bar{n}_e\ n_m\ , \qquad \ldots (8.50)$$

where $Q'(T_e)$ gives the electron impact loss rate.

Thus we have either:

$$\tfrac{1}{4}\, n_m(I)\ \bar{c}\ 2\pi r_o = \pi r_o^2\ Q(T_e(I))\ \overline{n_e(I)}\ \overline{N(I)}, \qquad \ldots (8.51)$$

or:

$$\pi r_o^2 Q'(T_e(I))\ \overline{n_e(I)}\ n_m(I) = \pi r_o^2 Q(T_e(I))\ \overline{n_e(I)}\ \overline{N(I)}, \qquad \ldots (8.52)$$

giving $n_m(I)$. Unfortunately, as one can see from these equations there are too many ways in which the dependence on I comes in to give any simple picture, and indeed, the experimental curves of $n_m(I)$, Fig.55, are not easily interpretable.

There is however one easily interpretable graph and that is $n_m(I_L)$, the metastable density at $I = I_L$ vs I_L. In this case equation (8.51) becomes:

$$\tfrac{1}{4}\, n_m(I_L)\ \bar{c}\ 2\pi r_o = \pi r_o^2\ Q(T_e(I_L))\overline{n_e(I_L)}\ N(I_L) \qquad \ldots (8.53)$$

and since $\overline{N(I_L)} = C_1/r_o$, and $\overline{n_e(I_L)} \propto I_L$ and $T_e(T_L)$ is the same for all I_L we have the prediction that:

$$n_m(I_L) \propto I_L\ , \qquad \ldots (8.54)$$

i.e. a linear relation.

Similarly equation (8.52) implies that $n_m(I_L)$ is some constant value independent of I_L.

In Fig.56 are presented experimental values for $n_m(I_L)$ and the results appear to be consistent with the model of metastable loss to the walls. This, of course, does not settle the question of the contribution of cumulative ionization, for even though the majority of metastables are lost to the walls, it could be that the small minority which are lost by electron ionization still make a large contribution to the total ionization rate, relative to the rate directly from the ground state.

8.6.3 Cumulative Ionization

The contribution of cumulative ionization to the total ionization has been estimated using the theoretical ionization cross sections for the metastable states given by Vriens (1964).

Fig.56

Number density of the 6^3P_2 metastable state at current limit. ($r_o = 1{\cdot}25$ cm)

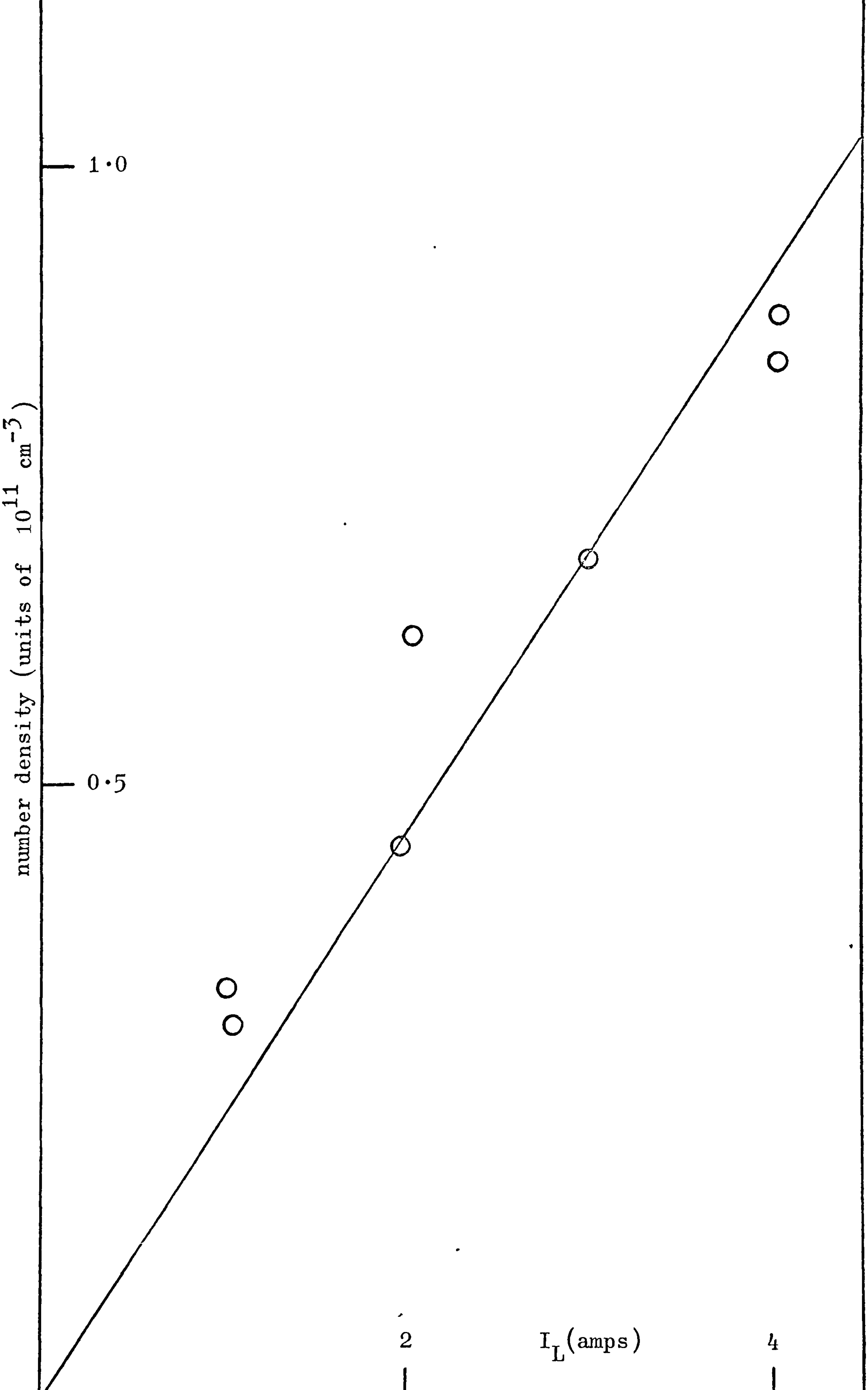

As in section 5.2.3 the ionization rate for a Maxwellian electron distribution is:

$$Z_j \propto n_j \int_{\varepsilon_{Tj}}^{\infty} S_{ej}(\varepsilon)\ \varepsilon\ e^{-\varepsilon/\varepsilon_m}\, d\varepsilon, \qquad \ldots (8.55)$$

where Z_j is the ionization rate from level j of density n_j with threshold ionization ε_{Tj} and ionization efficiency $S_{ej}(\varepsilon)$. For a drift Maxwellian it is:

$$Z_j \propto n_j \int_{\varepsilon_{Tj}}^{\infty} S_{ej}(\varepsilon)\varepsilon^{\frac{1}{2}}\ e^{-\varepsilon/\varepsilon_m - \Gamma} \left\{ e^{2\sqrt{\Gamma\varepsilon/\varepsilon_m}} - e^{-2\sqrt{\Gamma\varepsilon/\varepsilon_m}} \right\} d\varepsilon, \qquad \ldots (8.56)$$

where Γ is the drift parameter as before.

The contributions from the metastables was computed using the experimental measurements of section 8.6.2, giving approximately:

$$\frac{n\ 6^3P_0}{n\ 6^1S_0} = 0\cdot 68\%$$

$$\frac{n\ 6^3P_2}{n\ 6^1S_0} = 1\cdot 2\% \quad .$$

For all values of ε_m from 5 to 40 eV, and Γ from 0 to 1·0, the value of

$$\frac{Z\ 6^3P_0 + Z\ 6^3P_2}{Z\ 6^1S_0} \sim 3\% \quad ,$$

was found to hold.

Thus even near current limit the contribution of cumulative ionization is slight, relative to the contribution from direct ionization. (Some cumulative ionization can occur as a result of collisions between metastables or between a 6^3P_0 metastable and a particle in the 6^3P_1 state. Using the cross sections given by Forrest and Franklin (1969) and the measured populations of these states, it may be shown that these contributions are quite negligible here).

Forrest (1967) and Forrest and Franklin (1969) have calculated the contributions of cumulative ionization in a purely theoretical way, i.e. rather than employ measured densities of excited state, they have calculated these as well. The resultant calculation incorporates a total of 18 processes and hence may be subject to some uncertainties (as cross-sections are often known only approximately, and the errors of assuming a Maxwellian electron distribution may accumulate) at least relative to the present approach where only the three processes of direct interest require computation. A comparison of results should therefore be of interest.

Take for example the data for $T_{bath} = +16{\cdot}5^oC$ and $I = 3A$ where the following data has been found: $r_o = 1{\cdot}25$ cm; $p_o = 0{\cdot}9$ mTorr; $n_e \simeq 4 \times 10^{11}$ cm^{-3}; $n\ 6^3P_0 \simeq 2{\cdot}5 \times 10^{11}$cm^{-3}; $n\ 6^3P_2 \simeq 5 \times 10^{11}$cm^{-3} and $T_e \simeq 3$ eV. Assuming a Maxwellian distribution, the contributions can be calculated and it is found that cumulative ionization constitutes about 8% of the total.

This result is about an order of magnitude below the theoretical predictions given by Forrest and Franklin (1969) but would seem to agree with the estimation of Klarfeld (1941) that cumulative ionization at $p_o = 1$ mTorr is negligible.

8.6.4 2537Å Emission near Current Limit

The discharge emission of 2537Å radiation near current limit was observed across a diameter with the monochromator and photomultiplier. Intensities, in arbitrary units are given in Figs.57 and 58.

The $n\ 6^3P_1$ creation rate is:

$$\pi r_o^2\, Q\, [T_e(I,p_o)]\overline{n_e(I)}\ \ \overline{N(I,p_o)} \qquad \ldots (8.57)$$

where $Q[T_e]$ is the electron excitation rate, while the loss rate is

$$\pi\ r_o^2\ \frac{\overline{n\ 6^3P_1(I,p_o)}}{\tau} \qquad \ldots (8.58)$$

where τ is the radiative lifetime of the 6^3P_1 state, 10^{-7} sec.

Fig.57
Emitted intensity of 2537Å radiation for various currents, as a function of bath temperature (path length 2·5 cm)

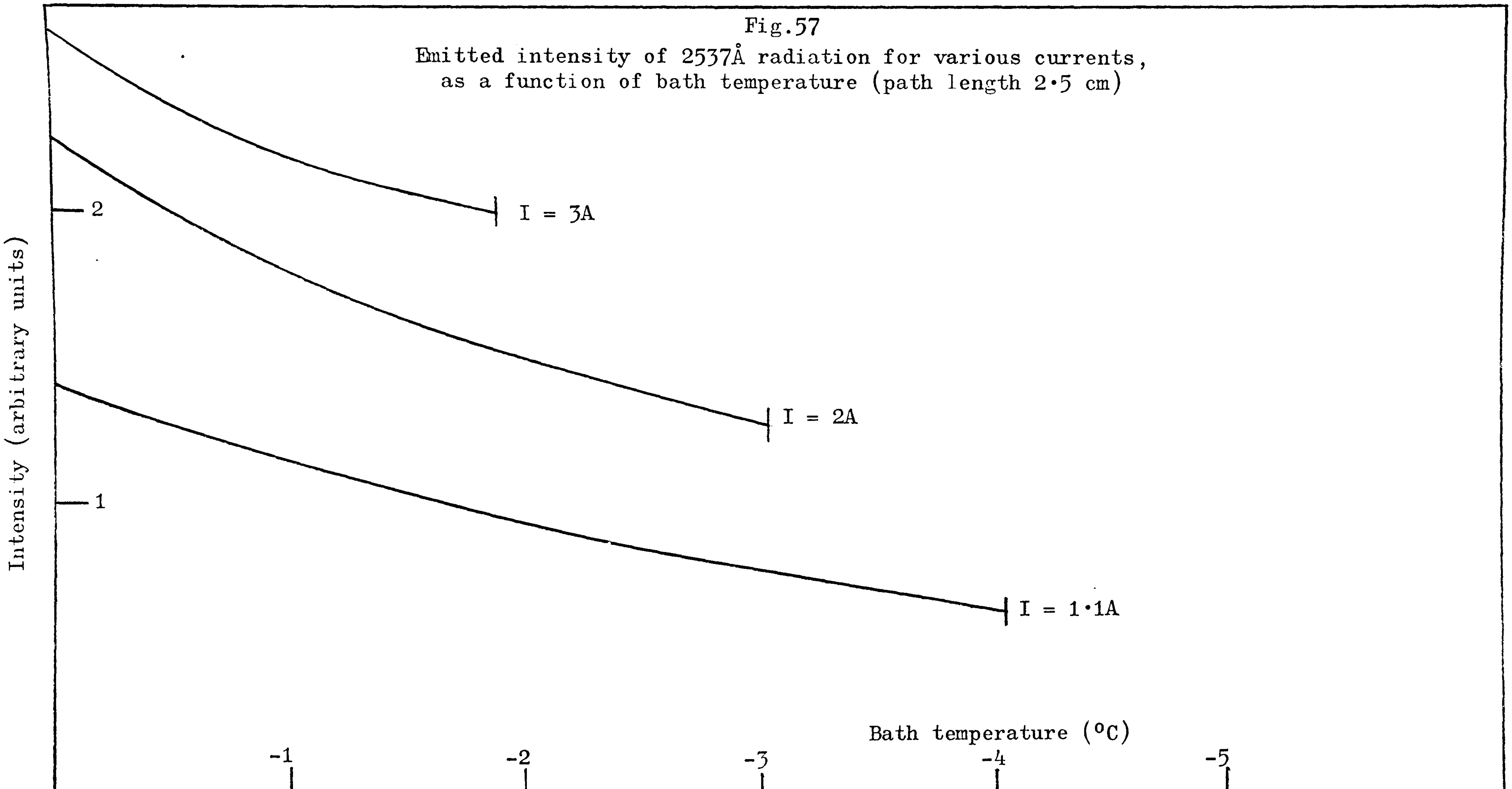

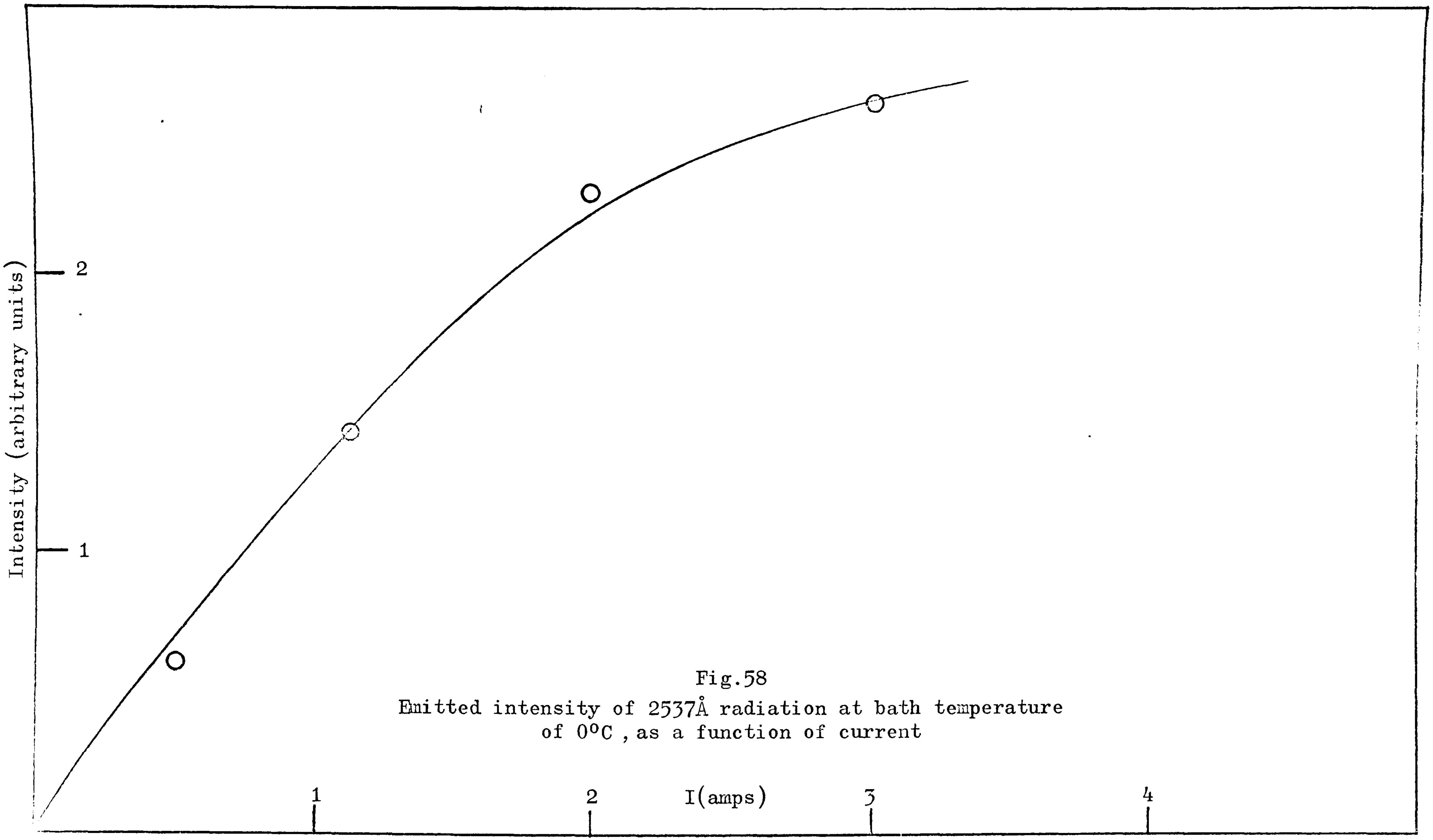

Fig.58
Emitted intensity of 2537Å radiation at bath temperature of 0°C , as a function of current

Thus:

$$n\ 6^3P_1(I,p_0) = \tau\ Q\,[\,T_e(I,p_0)]\ n_e(I)\ \bar{N}(I,p_0)\ , \qquad \ldots (8.59)$$

giving the variation of $n\ 6^3P_1$ with I and p_0 and thus of the 2537Å emission rate.

As in the case of the metastable populations, the variation given by equation (8.59) is quite complicated and as can be seen from the experimental results of Figs.57 and 58 no simple interpretation is evident. However, as before, $\overline{n\ 6^3P_1(I_L)}$ is a simple function.

At current limit T_e always has the same value, $\overline{N(I_L)} = C_1/p_0$ and as $n_e(I) \propto I$ then:

$$n\ 6^3P_1(I_L) \propto I_L\ ,$$

i.e. a linear function.

In Fig.59 experimental results for 2537Å output at I_L vs I_L are given and confirm the predicted linear relation.

This experimental evidence may be taken as further confirmation that at current limitation the electron distribution always attains the same limiting form, and that C_1 is indeed a constant.

Fig.59
Emitted intensity of 2537Å radiation of current limit as a function of the current limit

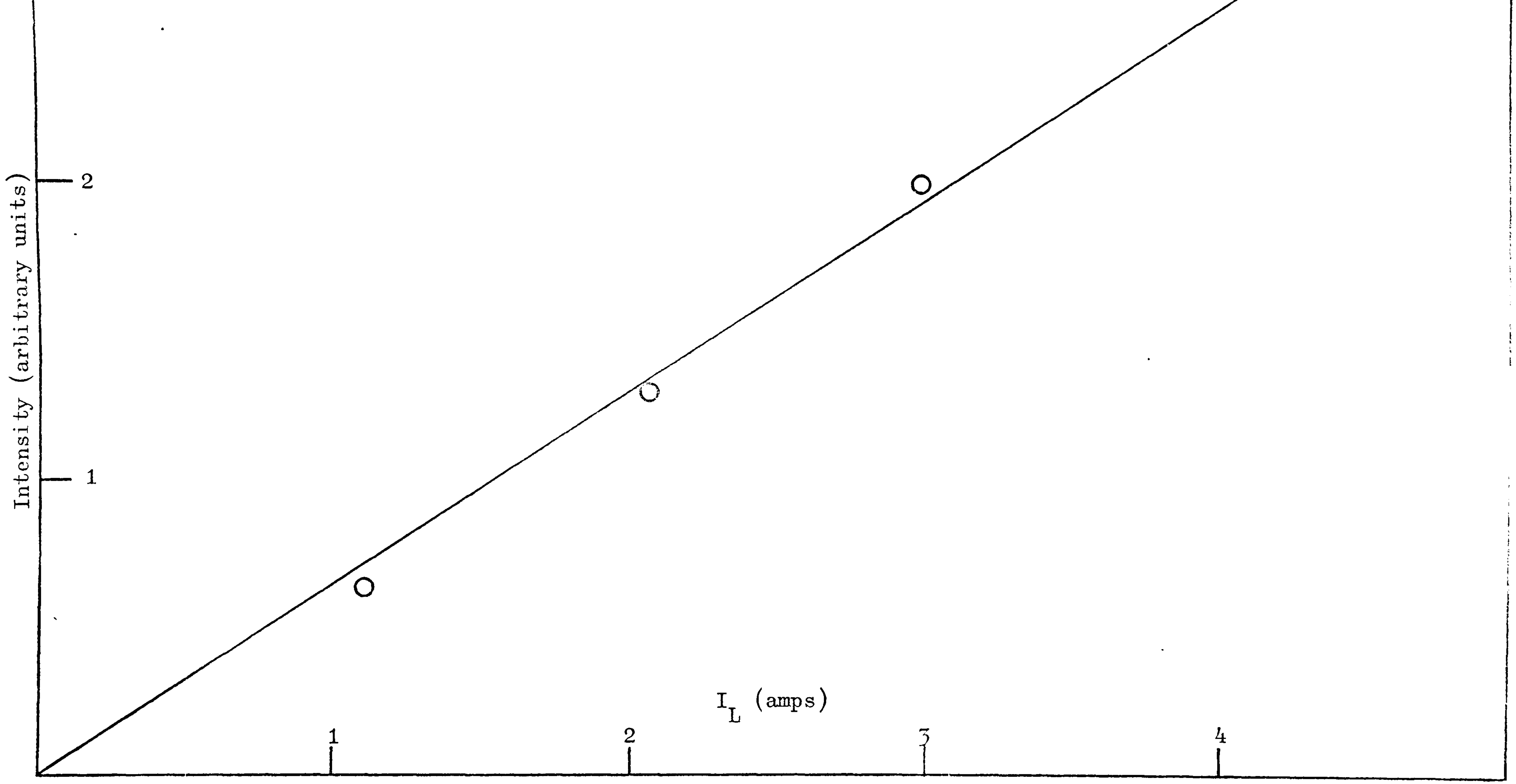

CHAPTER IX

CONCLUSIONS

A new theory has been presented predicting the current limits of a low pressure Hg arc discharge in terms of the discharge parameters, p_0 and r_0. Arc existence is only possible for a restricted region in (I, p_0, r_0) - space.

This theory has been confirmed by experimental work, employing a specially constructed discharge tube in which discharge conditions, especially vapour conditions, are subject to very careful control.

Theoretical predictions of the radial variation of neutral atoms in the discharge have been provided for all values of (I, p_0, r_0) and these predicted variations have been confirmed by experimental measurements of neutral density, using a resonance radiation absorption technique.

Experimental measurements using Langmuir probes have confirmed various aspects of this new current limit theory as pertains to the charged particle behaviour: ion wall current as a function of arc current, electron temperature as a function of I, p_0, r_0 etc.

Experimental measurements of total heavy particle wall flux, using ionization gauges, have verified related aspects of the new theory and shed light on the phenomenon of current sustained pressure effects.

The non-Gaussian resonance radiation absorption profile of neutrals in a high current discharge has been computed and experimental results are shown to be consistent with these calculations.

A simple theory of the resonance radiation emission profile of an optically thick plasma is presented and experimental results using a Hg resonance radiation lamp are in broad agreement with this simple theory.

Measurements of Hg metastable densities in a low pressure arc are presented and related calculations indicate the region of onset of cumulative ionization.

The Bohm criterion for the formation of a wall sheath is generalized to incorporate several complicating factors, including that of oblique ion motion relative to the plasma-sheath boundary.

The double sheath which forms at an abrupt diameter constriction in a low pressure Hg arc has been considered and the various dependent and independent variables are related in a comprehensive and consistent way.

The possibility is considered of Hg sputtering by ion bombardment in a low pressure arc and a potential application to Hg valve technology is indicated. An experimental estimate of the sputtering rate of Hg^+ on Hg liquid is presented.

APPENDIX I

VALIDITY OF FREE FALL MODEL FOR NEUTRALS IN THE CURRENT LIMIT REGIME

I.1 CHARGE TRANSFER

An ion in the discharge may collide with a neutral, transferring its charge. As this process has a large cross-section, $q \approx 5\times 10^{-14}\,\text{cm}^2$, Kovar (1964), this could constitute a distortion from purely rectilinear neutral motion. In the present work the neutral density n is such that $p_0 \leqslant 0{\cdot}2$ mTorr for the $r_0 = 1{\cdot}25$ cm tube and $p_0 \leqslant 0{\cdot}5$ mTorr for $r_0 = 0{\cdot}5$ cm. The m.f.p. for charge transfer is

$$\lambda = \frac{1}{nq} \qquad \text{... (A.1)}$$

hence for: $r = 1{\cdot}25$ cm , $\lambda \geqslant 2{\cdot}8$ cm

for: $r = 0.5$ cm , $\lambda \geqslant 1{\cdot}1$ cm.

As one can see the effect may not be negligible. The rate at which this process occurs is:

$$\text{rate} = q\, v_i\, n_i\, n \qquad \text{cm}^{-3}\text{sec}^{-1} \qquad \text{... (A.2)}$$

taking:

$$v_i = 10^5\ \text{cm sec}^{-1} \qquad (T_e \approx 3\ \text{eV})$$
$$n_i = 4\times 10^{10}\ \text{cm}^{-3} \qquad (I \sim 2\text{A})$$
$$n = 0{\cdot}2\times 3{\cdot}56\times 10^{13}\ \text{cm}^{-3}$$

Thus:

$$\text{rate} = 1{\cdot}4\times 10^{15}\ \text{cm}^{-3}\ \text{sec}^{-1}$$

This should be compared to the sort of neutral flux which normally flows through one cm^3, i.e.

$$\tfrac{1}{4}\, n\, \bar{c}\ , \qquad \text{... (A.3)}$$

which in this case is $3{\cdot}6\times 10^{16}\ \text{cm}^{-2}\ \text{sec}^{-1}$.

It is evident that while this effect is small, $\sim 4\%$, it is not completely negligible and one should like to know what effect this process will have on the current limit calculations of section 5.3. By considering Fig.60 , one can conclude that this effect will introduce less than 4% error in the calculations of section 5.3. These calculations depend

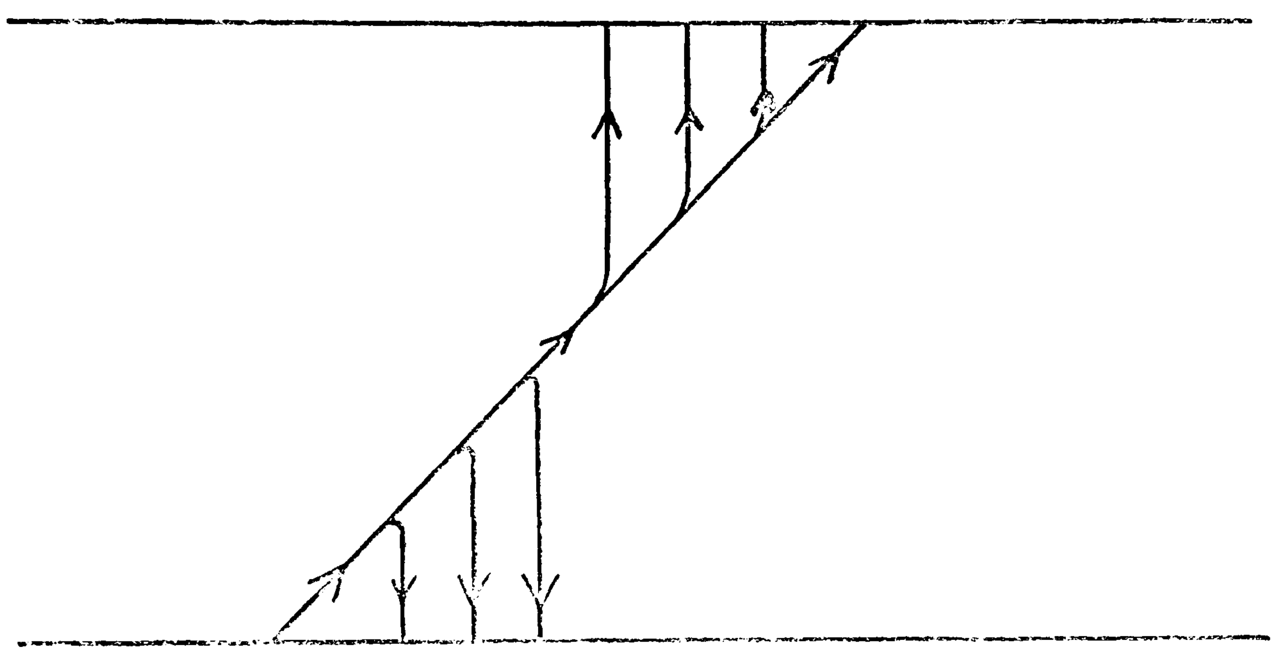

Fig.60
Effect of charge transfer collisions
on neutral trajectories

essentially on the length of the neutral paths, and as shown in Fig.60 the effect of charge transfer is to shorten a neutral path, but only by something like 25% on average.

It is concluded therefore that for the present operating range of n_e and p_o, charge transfer effects may be safely neglected.

I.2 MOMENTUM TRANSFER FROM ELECTRONS

While electron momentum is much less than neutral momentum:

$$\frac{m\,\bar{v}_e}{M\bar{c}} \approx 0\cdot02 \qquad \ldots \text{(A.4)}$$

the elastic collision rate is high and momentum transfer is efficient. For anisotropic electron distribution the net effect on the neutral trajectory (provided there are only $\lesssim 10^2$ collisions per traversal) will be negligible, but near current limit the electron distribution has a strong drift component, and the net transfer of anode-directed momentum to the neutrals may become appreciable.

Using the electron-neutral collision cross-sections for Hg given in Torvén (1965), and assuming a drift Maxwellian distribution, one may estimate this effect as follows ("estimate", because the distribution is likely to be distorted even from a drift Maxwellian).

From, e.g. Forrest (1967), one has the drift Maxwellian distribution:

$$d^2n(v,\theta) = n_e\left(\frac{m}{2\pi\,kT}\right)^{\frac{3}{2}} e^{-m(v^2+u^2)/2kT}\, e^{mu\,v\,\cos\theta/kT}\, v^2 2\pi\sin\theta\, d\theta\, dv\,, \qquad \ldots \text{(A.5)}$$

where u is the drift speed in the cathode direction,

$d^2n(v,\theta)$ is the number of electrons with total velocity v between v and $v+dv$ directed into the cone at θ, where θ is measured relative to the drift direction.

These d^2n electrons have:

$$d^2n\; v\,\sigma\,(v) \qquad \ldots \text{(A.6)}$$

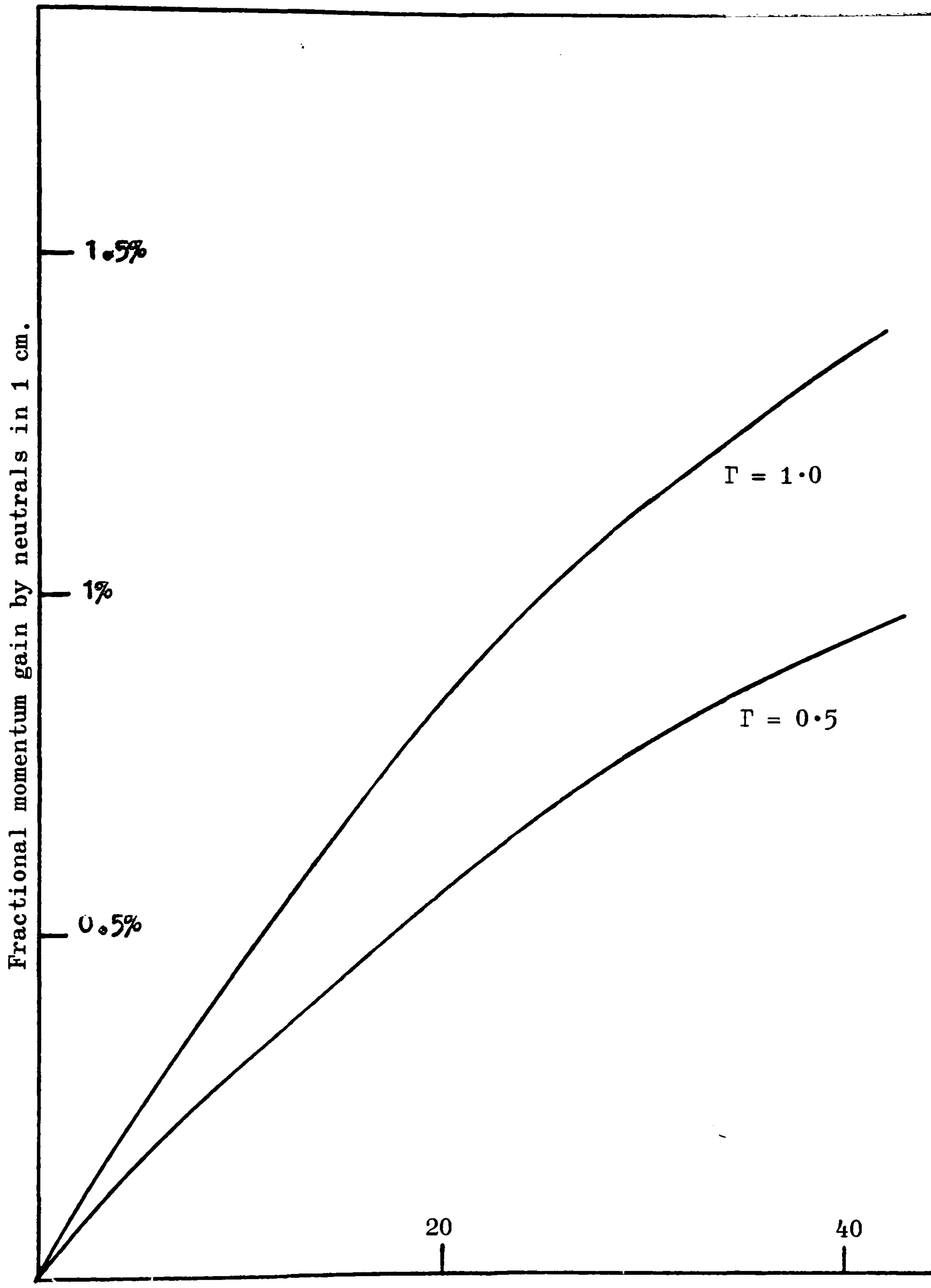

Figs.61 and 62

Fractional momentum gain by neutrals in travelling 1 cm through an electron density of $n_e = 10^{10}$ cm^{-3}, as a function of electron temperature and electron drift. Gain for $n_e = 10^{11}$ cm^{-3} is ten times greater etc.

collisions per second with a given neutral atom, where $\sigma(v)$ is the momentum transfer cross-section. Thus the rate of transfer of cathode directed momentum is:

$$d^2n \; v \; \sigma(v) \; m \; v \cos\theta \; , \qquad \ldots (A.7)$$

and the total transfer rate is:

$$\frac{d(M\,v_N)}{dt} = n_e \; 2\pi m \left(\frac{m}{2\pi\, kT}\right)^{\frac{3}{2}} \int_{\theta=0}^{\pi} \int_{v=0}^{\infty}$$

$$v^4 \cos\theta \sin\theta \, \sigma(v) \; e^{-m(v^2+u^2)/2kT} \; e^{m\,uv\cos\theta/kT} \; , \qquad \ldots (A.8)$$

where one can perform the θ integration and transforming to $\varepsilon = \frac{1}{2} mv^2$, $\varepsilon_D = \frac{1}{2} mu^2$, $\varepsilon_m = kT$, $\Gamma = \varepsilon_D/\varepsilon_m$;

$$\frac{d(M\,v_N)}{dt} = \frac{n_e}{2\sqrt{\pi}} \; \frac{1}{\Gamma} \int_0^{\infty} \left(\frac{\varepsilon}{\varepsilon_m}\right)^{\frac{1}{2}} \sigma(\varepsilon) \; d\varepsilon \; e^{-\varepsilon/\varepsilon_m - \Gamma}$$

$$\left\{ 2\sqrt{\frac{\Gamma\varepsilon}{\varepsilon_m}} \left(e^{2\sqrt{\Gamma\varepsilon/\varepsilon_m}} + e^{-2\sqrt{\Gamma\varepsilon/\varepsilon_m}} \right) - \left(e^{2\sqrt{\Gamma\varepsilon/\varepsilon_m}} - e^{-2\sqrt{\Gamma\varepsilon/\varepsilon_m}} \right) \right\} \qquad \ldots (A.9)$$

where:

$$\frac{d(M\,v_N)}{dt} \rightarrow 0 \quad \text{for} \quad \Gamma \rightarrow 0$$

as required.

Integral equation (A.9) has been obtained numerically and is shown in Figs.61 and 62. The method of presentation has been as follows: the neutrals are assumed to be at 300°K $\therefore$ $\bar{c} = 1{\cdot}8 \times 10^4$ cm sec. and neutral momentum

$$M\bar{c} = 6 \times 10^{-18} \quad \text{gm cm sec}^{-1} \; . \qquad \ldots (A.10)$$

At $\bar{c}$, the time of traversal of 1 cm is 5.6×10^{-5} sec, and the collisional momentum gained in this time is obtained from the rate given in equation (A.9). This momentum gain in traversing one cm. is compared to the momentum of equation (A.10) and it is this fraction which appears in Figs. 61 and 62.

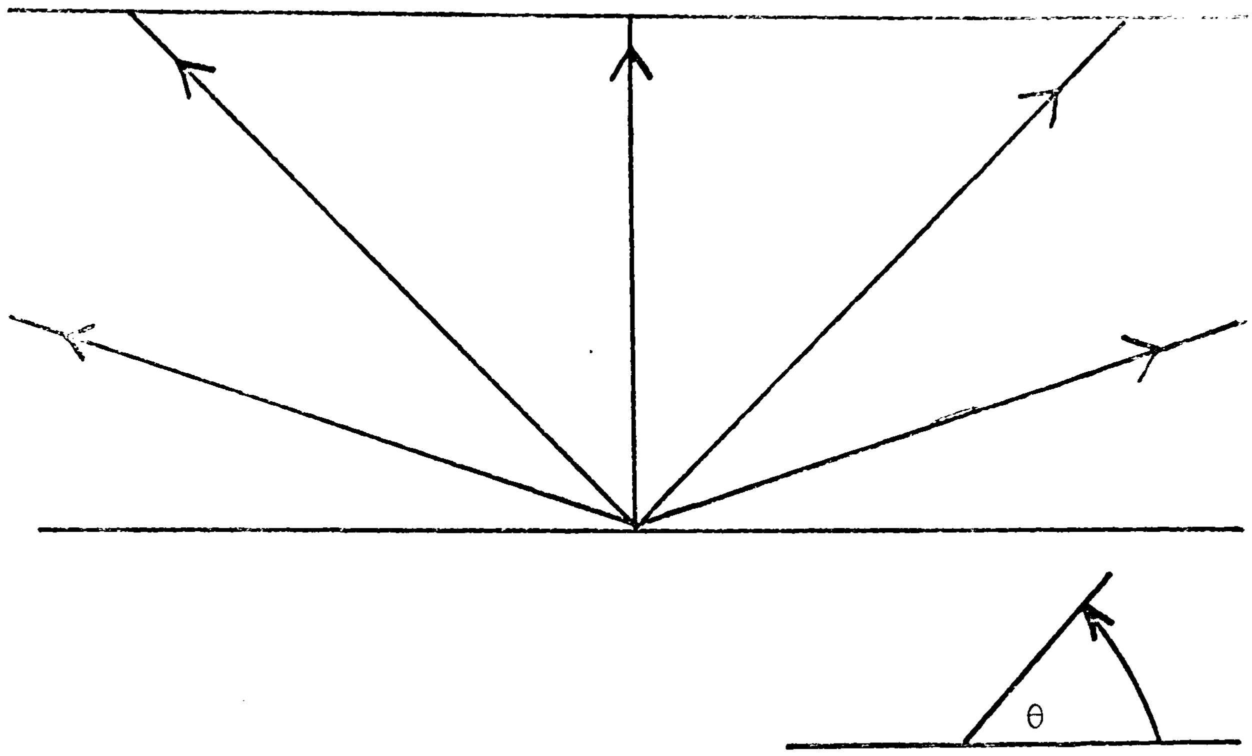

Fig.63a
In the absence of momentum transfer from electrons to neutrals, the neutral trajectories are distributed as shown

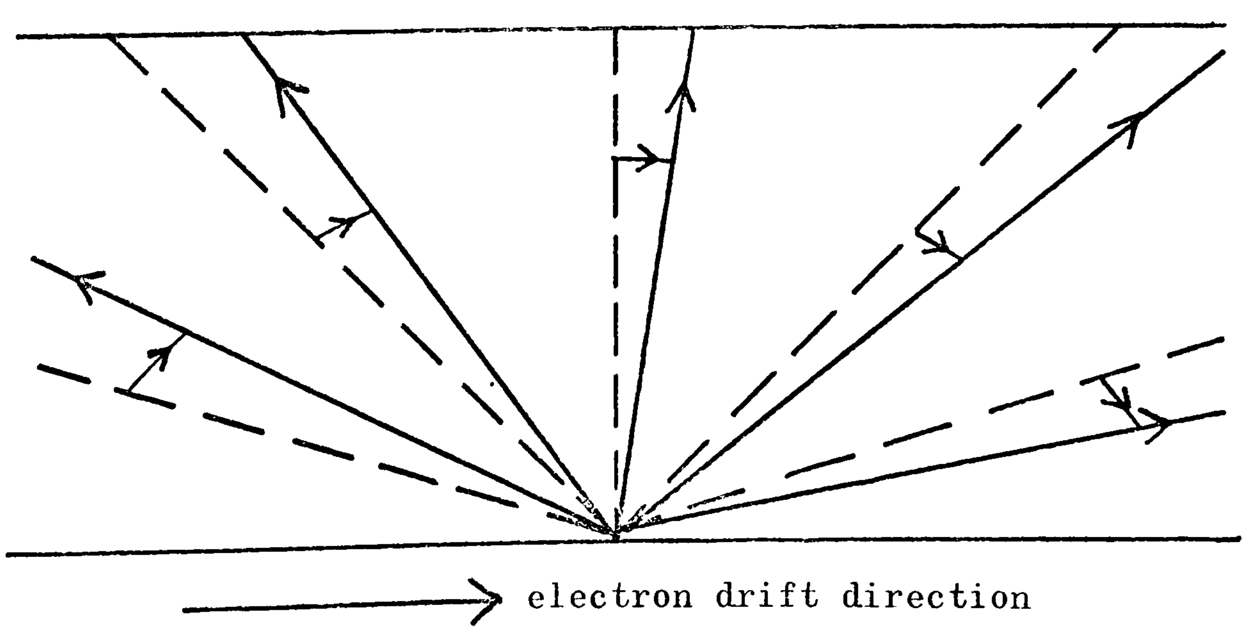

Fig.63b
Net electron momentum transfer to neutrals causes distortions to the neutral trajectories, very approximately as shown

Now n_e is given approximately by equation (5.65) thus:

$$n_e = 2{\cdot}4 \times 10^{10} \text{ I} \quad \text{cm}^{-3} \qquad \ldots \text{(A.11)}$$

and so for the range of I studied here, $I \leqslant 5A$, one can see that, as in the case of charge transfer, the effect is small but not negligible (probe evidence indicates $0{\cdot}5 < \Gamma < 1$ near current limit and $T_{eL} \simeq 10\text{-}20$ eV). However, once again the net effect on the current limit calculations of section 5.3 is even smaller than these fractions would indicate. Consider Fig. 63 where one notes that the approximate effect of a modest momentum transfer is to lengthen the trajectories originally emitted into $0 < \theta < \pi/2$ and shorten the ones in $\pi/2 < \theta < \pi$. The net result is cancellation although some second order effects may give rise to a net change.

The conclusion therefore is that for the ranges of current studied here, the net electron-neutral momentum transfer effect can safely be neglected for purposes of the current limit calculations of section 5.3.

R E F E R E N C E S

AITKEN, J.E. and SANDER, K.F., 1968, Electronics Letters, vol.4, p.426.

ALLEN, J.E. and THONEMANN, P.C., 1954, Proc. Phys. Soc.B, vol.67, p.768.

ALLEN, J.E. and COVILLE, C., 1961, Proc. 5th Int. Conf. Ion. in Gases, Munich, Conference Proceedings, p.278.

ALLEN, J.E., BOSCHI, A. and MAGISTRELLI, F., 1963, Nuovo Cimento, vol.27, p.674.

ANDERSSON, D., BABIĆ, M., SANDAHL, S. and TORVÉN, S. 1969. Proc. 9th Int. Conf. Ion. in Gases, Bucharest, p.142.

ANDREWS, J.G., 1968, private communication.

ANDREWS, J.G., 1969, Thesis, (Oxford University)

ANDREWS, J.G. and VAREY, R.H., 1970a, Nature, vol.225, p.270.

ANDREWS, J.G. and VAREY, R.H., 1970b, J. Phys. A: Gen. Phys., vol.3, p.413.

ANDREWS, J.G. and STANGEBY, P.C., 1970, J. Phys. A : Gen. Phys., vol.3, p.L39.

ANDREWS, J.G., 1970, J. Plasma Phys., vol.4, p.603.

ANDREWS, J.G. and ALLEN, J.E., 1970, Proc. Roy. Soc., in the press.

ARDENNE, von M., 1962, Tabellen zur angewandten Physik., Berlin.

ASKEROV, Sh.G. and SENA, L.A., 1969, Sov. Phys. - Solid State, vol.11, 1288.

AUER, P.L., 1961, Nuovo Cimento, vol.22, p.548.

BERTOTTI, B. and CAVALIERE, A., 1965, Nuovo Cimento, vol.35, p.1244.

BICKERTON, R.J. and von ENGEL, A., 1956, Proc. Phys. Soc. vol.69B, p.468.

BLAMONT, J.E., 1957, Ann. Phys. (Paris), vol.2, p.551.

BLANK, J.L., 1968, Phys. Fluids, vol.11, 1686.

BLEAKNEY, B., 1930, Phys. Rev., vol.35, p.139.

BLEEKRODE, R., 1967, Proc. 8th Int. Conf. Ion. in Gases, p.150.

BOHM, D., 1949, 'Char. of Elect. Disch. in Mag. Fields' (ed. A. Guthrie and R.K. Wakerling, New York,) Chapter 3.

BRESLIN, A.C. and EMELEUS· K.G., 1967, Int. J. Electronics, vol.22, p.429.

CARLQUIST, P., and JACOBSEN, C. 1964, Icarus, vol.3, p.270.

CARUSO, A. and CAVALIERE, A., 1962, Nuovo Cimento, vol.26, p.1389.

CARUSO, A. and CAVALIERE, A. 1964, Brit. J. Appl. Phys.. vol.15, p.1021.

CLARK, K.C., and FAIRCHILD, C.E., 1964, 'Atomic Collision Processes' (ed. McDowell, M.R.C.), Amsterdam, p.581.

COHEN, I.M. and KRUSKAL, M.D., 1965, Phys. Fluids, vol.8, p.920.

COULTER, A.G., LECKEY, R.C.G., HIGGINSON, G.S., 1963, Proc. 6th Int. Conf. Ion. Gases, vol.2, p.161.

COURANT, R. and FRIEDRICHS, K.O., 1948, 'Supersonic Flow and Shock Waves', New York, Interscience.

CRAWFORD, F.W. and KINO, G.S., 1961, Proc. I.R.E., vol.49, p.1767.

CRAWFORD, F.W. and FREESTON, I.L., 1963, Proc. 6th Int. Conf. Ion. in Gases, vol.3, p.461.

CRAWFORD, F.W. and SELF, S.A., 1965, Int. J. Electronics, vol.18, p.569.

DAVIES, D.R., 1966, Thesis, (Oxford University).

DEMIRKHANOV, R.A., FREULICH, H., KURSANOV, U.V. and GUTKIN, T.I., 1962, Brookhaven National Laboratory Bulletin, 767C 36.

EGOROV, V.S., SHREBOV, V.N. and SHUKHTIN, A.M., 1965, Opt. and Spec. vol.20, p.211.

von ENGEL, A., 1965, 'Ionized Gases', Oxford U.P., 2nd edition.

ESTERMANN, I., 1925, Z. fur Elektrochemie, vol.31, p.441; Z. fur Phys., vol.33, p.320.

FABRIKANT, W., BUTAEWA, F., and ZIRG, I., 1937. Phys. Zeit. der Sowj., vol.11, p.576.

FABRIKANT, W., BUTAEWA, F., and ZIRG, I., 1938, Phys. Zeit. der Sowj., vol.13, p.23.

FETZ, H., 1940, Ann. Phys., vol.37, p.1.

FETZ, H., and HAUG, A., 1950, Z. angew. Phys., vol.2, p.150.

FORREST, J.R. and FRANKLIN, R.N., 1966, Brit. J. Appl. Phys., vol.17, p.1569.

FORREST, J.R., 1967, Thesis (Oxford Univeristy).

FORREST, J.R. and FRANKLIN, R.N., 1968, Brit. J. Appl. Phys., vol.1, p.1357.

FORREST, J.R., and FRANKLIN, R.N., 1969, J. Phys. B. (Atom. Mole. Phys.) vol.2, p.471.

FOSTER, E.W., 1964, Rep. Prog. Phys., vol.27.

FRANKLIN, R.N., 1970, private communication.

FRANCIS, G., 1960, 'Ionization Phenomena in Gases' London : Buttersworth

FRANKLIN, R.N. and OCKENDON, J.R., 1970, J. Plasma Phys., vol.4, p.371.

FRAZER, D.A., GOWAR, J. and WHELDON, R.J., 1965, Brit. J. Appl. Phys., vol.16, p.211.

FRIEDMAN, H.W., 1967, Phys. Fluids, vol.10, p.2053.

FRIEDMAN, H.W. and LEVI, E., 1967, Phys. Fluids, vol.10, p.1499.

FRIEDMAN, H.W., amd LEVI, E., 1970, Phys. Fluids, vol.13, p.1049.

GABOR, D., 1952, Proc. Roy. Soc. A, vol.213, p.73.

GIBBS, H.M. and HULL, R.J., 1967, Phys. Rev., vol.153, p.132.

GOLDAN, P.D., 1970, Phys. Fluids, vol.13, p.1055.

GRANOVSKII, B.L. and SUETIN, T., 1954, C.R. Dokl., vol.49, p.410.

GRANOVSKII, B.L. and SUETIN, T., 1946, J. Tech. Phys., vol.16, p.1023.

GRANOVSKII, B.L., and BYKHOVSKAYA, L., 1946, J. Phys. USSR, vol.10, p.351.

GRANOVSKII, B.L. and SUETIN, T., 1947, J. Tech. Phys., vol.17, p.291.

HALL, L.S., 1962, Proc. Phys. Soc., vol.80, p.309,

HAMBERGER, S., 1961. Proc. 5th Int. Conf. Ion, Gases, vol.2, p.1919.

HAMBERGER, S., 1966, Thesis, (London University).

HARRISON, E.R. and THOMPSON, W.B., 1959, Proc. Phys. Soc. B., vol.74, p.145.

HARRISON, F.R., KAPP, L.B., QUIGLEY, M.B.C. and SWIFT-HOOK, D.T., 1965, Proc. 7th Int. Conf. Ion. in Gases, vol.3, p.396.

HEARN, A.G., 1963, Proc. Phys. Soc., vol.81, p.648.

HEARN, A.G, 1964, Proc. Phys. Soc., vol.84, p.11.

HINDMARSH, W.R., 1967, 'Atomic Spectra' Oxford U.P.

HOWE, R.H., 1953, J. Appl. Phys., vol.24, p.881.

HOYAUX, M.F. and GANS, P., 1959, Proc. 4th Int. Conf. Ion. in Gases, p.364.

HOYAUX, M.F., 1965, Gen. El. Review, vol.74, p.669.

HOYAUX, M.F. and WILLIAMS, E.M., 1967, J. Appl. Phys., vol.38, p.3630.

HOYAUX, M.F. and KETTANI, M.A., 1968, Onde Elect. (France) vol.48, p.251.

HOYAUX, M.F., 1968, 'Arc Physics', Springer, New York.

HULL, A.W., 1934, Electrical Engineering, vol.53, p.1435.

HULL, A.W. and ELDER, F.R., 1942, J. Appl. Phys., vol.13, p.372.

IRISH, R.T. and BRYANT, G.H., 1964, Proc. Phys. Soc., vol.84, p.975.

KENTY, C., 1938, J. Appl. Phys., vol.9, p.765.

KILLIAN, T., 1930, Phys. Rev., vol.35, p.1238.

KINO, G.S., and SHAW, E.K., 1966, Phys. Fluids, vol.9, p.587.

KISTEMAKER, J., ROL, P.K., and POLITICK, J., 1965, Nucl. Inst. amd Meth. vol.38, p.1.

KLARFELD, B., 1937, Tech. Phys. USSR, vol.4, p.44,

KLARFELD, B. and POLETAEV, I.A., 1939, C.R. DOKl., vol.23, p.465.

KLARFELD, B., 1941, J. Phys., vol.5, p.155.

KOEDAM, M., and KRUITHOFF, A.A., 1962, 1963, Physica, vol.28, p.80 and vol.29, p.565.

KOVAR, F.R., 1964, Phys. Rev., vol.133, p.A681.

KREYE, W.C., 1967, Proc. 8th Int. Conf. Ion. in Gases, p.100.

LANGMUIR, I. and MOTT-SMITH, H., 1924, Gen. El. Rev., vol.27, p.449, p.810.

LANGMUIR, I., 1929, Phys. Rev., vol.33, p.954.

LANGMUIR, I., 1932, J. Am. Chem. Soc., vol.54, p.2798.

MARLOW, W.C., 1965, Lockheed Report.

MEROZ, I., 1960, 'Optical Transition Probabilities', U.S. Dept. of Commerce.

MITCHELL, P.M. and TWIDDY, N.D., 1967, Proc. 8th Int. Conf. Ion. in Gases, p.102.

MITCHELL, A.C.G. and ZEMANSKY, M.W., 1961, 'Resonance Radiation and Excited Atoms', Cambridge U.P., 2nd ed.

NODWELL, R.A. and ROBINSON, A.M., 1965, Proc. 7th Int. Conf. Ion. Gases, vol.1, p.368.

NOTTINGHAM, W.B., 1939, Phys. Rev., vol.55, p.203.

PARKER, J.V., 1963, Phys. Fluids, vol.67, p.1657.

PERSSON, K.B., 1962, Phys. Fluids, vol.5, p.1625.

POLETAEV, I.A., 1951, Zh. Tekn. Fiz., vol.21, p.1021.

QUIGLEY, M.B.C., Thesis, (London University).

RAYMENT, S.W. and TWIDDY, N.D., 1968, Proc. Roy. Soc., vol.A340, p.87.

RILEY, J.R. and HALL, D.S., 1967, Proc. 8th Int. Conf. Ion in Gases, p.135.

ROSA, R.M.V.N. and ALLEN, J.E., 1970, J. Phys. D : Appl. Phys. vol.3, p.184.

ROZHDESTVENSKII, D.S., 1912, Ann Phys. vol.39, p.307.

SCHÖNHUBER, M.J., 1957, Proc. 5th Int. Conf. Ion. in Gases, p.930.

SCHÖNHUBER, M.J., 1963, Z. angew Phys., vol.15, p.454.

SCHOTTKY, W., 1924, Z. fur Phys., vol.31, p.163.

SELF, S.A., 1963, Phys. Fluids, vol.6, p.1762.

SELF, S.A., 1965, J. Appl. Phys., vol.36, p.456.

SELF, S.A. and EWALD, H.N., 1966, Phys. Fluids, 9, 2486.

SENA, L.A. and TAUBE, N.S., 1956, J.E.T.P., vol.3, p.168.

STANGEBY, P.C., 1968, Diploma Thesis (Oxford University)

STANGEBY, P.C. and ALLEN, J.E., 1970a, J. Phys. A : Gen. Phys., vol.3, p.304.

STANGEBY, P.C., and ALLEN, J.E., 1970b, Proc. Conf. Gas Discharges, London.

STANGEBY, P.C. and ALLEN, J.E., 1971a, J. Phys. A : General Phys. (in press).

STANGEBY, P.C. and ALLEN, J.E., 1971b, (to be published)

STEINER, H.C. and STRECKER, R.W., 1960, A.I.E.E. Trans. vol.79, p.139.

THONEMANN, P.C., 1955, Appl. Sci. Res., vol.B5, p.237.

TIMOFEYEV, G.G., 1955, 1956, Z.E.T.Fiz. vol.28, p.378, and vol.30, p.477.

TIMOFEYEV, G.G., 1957, Tech. Phys., vol.2, p.2480.

TIMOFEYER, G.G., 1959, Proc. 4th Int. Conf. Ion. Gases, p.343.

TIMOFEYEV, G.G., 1964, 'Int. El. Dis in Gases', (ed.Klarfeld, B) Pergamon Press, Oxford.

TONKS, L., 1937, Am. El. Soc. Trans, vol.72, p.167.

TONKS, L. and LANGMUIR, I., 1929, Phys. Rev., vol.34, p.876.

TORVÉN, S., 1965, Arkiv. for Fys., vol.29, p.533.

TORVÉN, S., 1968, Arkiv. for Fys., vol.35, p.513.

TORVÉN, S., 1969, Royal Inst. of Tech Report no.69-19, Stockholm.

VAREY, R.H., 1970, J. Phys. D : Appl. Phys., vol.3, p.601.

VILLIERS de, J.N., 1968, Thesis, (Cambridge University)

VILLIERS de, J.N. and SANDER, K.F., 1970, Proc. I.E.E., vol.117, p.295.

VRIENS, L., 1964, Phys. Lett., vol.8, p.260.

WARE, A.A., FAULKNER, J.E., and WOODIE, W.L., 1967, Proc. 8th Int. Conf. Ion in Gases, p.142.

WASSERRAB, T., 1950, Z. Phys., vol.128, p.575.

WASSERRAB, T., 1963, Z. angew. Phys., vol.16, p.441.

WOODS, L.C., 1961, 'The Theory of Subsonic Plane Flow', Cambridge U.P.

WOODS, L.C., 1965, J. Fluid Mech., vol.23, p.315.

YOKOYAMA, M., 1959, Sci. of Light, Japan, vol.8, p.59.